

**MODELING HYPERVELOCITY IMPACT FOR KILL ENHANCEMENT OF
BALLISTIC MISSILE WARHEADS**

by

Cesar Carrasco
Roberto Osegueda
Octavio Melchor-Lucero
and
Luis A. Espino

FAST Center for Structural Integrity of Aerospace Systems
The University of Texas at El Paso
El Paso, Texas 79968

A final report

Grant No. F49620-02-1-0076

DISTRIBUTION STATEMENT A
Approved for Public Release
Distribution Unlimited

Submitted to

Missile Defense Agency
7100 Defense Pentagon
Washington, DC 20301-7100

and US Air Force Office of Scientific Research
AFOSR/NM
801 North Randolph St.
Arlington, VA 22203-1977

This Document Contains
Missing Page/s That Are
Unavailable In The
Original Document

October 2004

BEST AVAILABLE COPY

20041129 038

REPORT DOCUMENTATION PAGE

AFRL-SR-AR-TR-04-

0595

The public reporting burden for this collection of information is estimated to average 1 hour per response, including the time for reviewing gathering and maintaining the data needed, and completing and reviewing the collection of information. Send comments regarding this burden e information, including suggestions for reducing the burden, to Department of Defense, Washington Headquarters Services, Directorate for Inf 1215 Jefferson Davis Highway, Suite 1204, Arlington, VA 22202-4302. Respondents should be aware that notwithstanding any other prov penalty for failing to comply with a collection of information if it does not display a currently valid OMB control number.

PLEASE DO NOT RETURN YOUR FORM TO THE ABOVE ADDRESS.

1. REPORT DATE (DD-MM-YYYY)		2. REPORT TYPE Final		3. DATES COVERED (From - To) 1 Jan 2002 - 30 Jun 2004	
4. TITLE AND SUBTITLE Modeling Hypervelocity Impact for Kill Enhancement of Ballistic Missile Warheads				5a. CONTRACT NUMBER	
				5b. GRANT NUMBER F49620-02-1-0076	
				5c. PROGRAM ELEMENT NUMBER	
				5d. PROJECT NUMBER	
6. AUTHOR(S) Dr. Cesar Carrasco				5e. TASK NUMBER	
				5f. WORK UNIT NUMBER	
7. PERFORMING ORGANIZATION NAME(S) AND ADDRESS(ES) Fast Center for Structural Integrity of Aerospace Systems The University of Texas at El Paso El Paso, TX 79968				8. PERFORMING ORGANIZATION REPORT NUMBER	
9. SPONSORING/MONITORING AGENCY NAME(S) AND ADDRESS(ES) Air Force Office of Scientific Research 4015 Wilson Blvd Mail Room 713 Arlington, VA 22203 NM				10. SPONSOR/MONITOR'S ACRONYM(S) AFOSR	
				11. SPONSOR/MONITOR'S REPORT NUMBER(S)	
12. DISTRIBUTION/AVAILABILITY STATEMENT Distribution Statement A. Approved for public release; distribution is unlimited.					
13. SUPPLEMENTARY NOTES					
14. ABSTRACT Scope of work: A computer code was developed to model various "endgame" encounter configuration scenarios between the EKV and the IBM to quantify and characterize single impacts in the TBM warhead. Numerical simulations using a commercial hydro-code were conducted to model specific single impact scenarios. A damage index directly calculated from simulation results based on the penetration of the projectile and the displacement of the target was developed to quantify the damage inflicted by each impact. The quantified damage of each single case scenario represents a measure of the lethality for each configuration. An Artificial Neural Network (ANN) was developed as a rapid solution model to predict damage indices for a wide range of single impact configurations as a result of the Endgame encounters.					
15. SUBJECT TERMS					
16. SECURITY CLASSIFICATION OF:			17. LIMITATION OF ABSTRACT UU	18. NUMBER OF PAGES	19a. NAME OF RESPONSIBLE PERSON Cesar Carrasco
a. REPORT U	b. ABSTRACT U	c. THIS PAGE U			19b. TELEPHONE NUMBER (Include area code)

Standard Form 298 (Rev. 8/98)
Prescribed by ANSI Std. Z39.18

BEST AVAILABLE COPY

ACKNOWLEDGEMENTS

Effort sponsored by the Missile Defense Agency and the Air Force Office of Scientific Research, under Grant No. F49620-02-1-0076. The U.S. Government is authorized to reproduce and distribute copies of the report for governmental purposes notwithstanding any copyright notation thereon. The program manager for this work was Dr. Arje Nachman, AFOSR. The technical assistance from Larry Libersky in relation to the use of the MAGI code is greatly appreciated. Our expression of gratitude to Ms. Laura Barnum for her experience, patience and assistance in issues related to the administration of the grant.

TABLE OF CONTENTS

PREFACE.....	iv
ACKNOWLEDGEMENTS	v
TABLE OF CONTENTS.....	vi
LIST OF TABLES.....	ix
LIST OF FIGURES	xvii
CHAPTER 1 INTRODUCTION	1
1.1 Introduction.....	1
1.2 Background.....	1
1.3 Objectives	3
1.4 Scope of Work	4
CHAPTER 2 BALLISTIC MISSILE OVERVIEW	7
2.1 Introduction.....	7
2.2 TBM Description	7
2.3 EKV Description.....	10
2.4 Kinetic Energy Rod Warheads Physics	10
2.5 Projectiles Description	13
2.6 Summary	14
CHAPTER 3 ENDGAME SIMULATIONS	15
3.1 Introduction.....	15
3.2 Near-Miss Encounter Configuration.....	15
3.3 EKV Modeling.....	17
3.3.1 Projectile Modeling.....	18
3.3.2 Projectile Ejection Velocity	20
3.3.3 Projectile Tumbling	20
3.3.4 Jellyroll Warhead Design.....	22
3.4 TBM Modeling	24
3.5 Endgame Kinematics Analysis	25
3.6 Impact Characterization	32
3.7 Endgame Simulations	34
3.8 Endgame Simulation Results	36
3.8.1 Impact Quantification per Encounter Configuration	36
3.8.2 Impact Characterization per Encounter Configuration	47
3.9 Impact Quantification per Impact Characterization.....	56
3.10 Significance of Impact Characterization.....	66
3.11 Summary	66
CHAPTER 4 NUMERICAL SIMULATIONS.....	67
4.1 Introduction.....	67

4.2	Smoothed Particles Hydrodynamics	67
4.2.1	Artificial Viscosity	72
4.2.2	Equations of State	72
4.2.3	Kernel Interpolation Function.....	73
4.3	Impact Modeling.....	73
4.4	Preliminary simulation results	76
4.5	Damage Index Development.....	78
4.6	SIDI Results	80
4.7	Lethality comparison between cylinders and spheres.....	104
4.8	Summary	107
CHAPTER 5 ARTIFICIAL NEURAL NETWORKS MODEL.....		108
5.1	Introduction.....	108
5.2	Artificial Neural Networks	108
5.3	Development of the Artificial Neural Network Model.....	110
5.4	Final ANN Architecture.....	113
5.5	Lethality comparison between cylinders and spheres using ANNs.....	118
5.6	Summary	122
CHAPTER 6 ENDGAME DAMAGE QUANTIFICATION ANALYSIS		123
6.1	Introduction.....	123
6.2	Total Damage Quantification per Encounter Configuration.....	124
6.3	Total Damage Ratio per Encounter Configuration	143
6.4	Total Damage Quantification per Impact Characterization	153
6.5	Damage Analysis per Impact Characterization.....	163
6.6	Damage Analysis per Near-Miss Encounter Configuration parameters.....	164
6.6.1	Early Bird Time	164
6.6.2	Crossing Angle and Miss Distance	164
6.7	Damage Analysis per Deployment Conditions.....	173
6.7.1	Tumbling.....	174
6.7.2	Radial Ejection Velocity Variability.....	179
6.8	Damage Analysis per Projectile Geometry/Size.....	188
6.8.1	Impact Configuration	188
6.8.2	Encounter Configuration.....	188
CHAPTER 7 SUMMARY, CONCLUSIONS, AND RECOMMENDATIONS .		189
7.1	Introduction.....	189
7.2	Summary	189
7.3	Conclusions.....	189
7.4	Recommendations.....	191
REFERENCES.....		192
APPENDIX A IMPACT DISTRIBUTION TABLES		198

APPENDIX B	YAW ANGLE STATISTICS CHARTS	203
APPENDIX C	YAW ANGLE FREQUENCY DISTRIBUTION CHARTS.....	213
APPENDIX D	SIDI VALUES DATABASE	220

LIST OF TABLES

Table 3.1.	Encounter Configuration Parameters.....	17
Table 3.2.	Projectile descriptive parameters	20
Table 3.3.	Limit values for optimization code for EKV design variables.	23
Table 3.4.	Final descriptive parameters of EKV design.	24
Table 3.5.	TBM descriptive parameters.....	25
Table 3.6.	Endgame Simulations Configurations.	34
Table 3.7.	Impact Distribution per Encounter Configuration for a Cylindrical Projectile with $L/D = 4$ @ $EBt = -0.006$ sec. Without Tumbling Effects and Without V_{rp} Variability.	39
Table 3.8.	Impact Distribution per Encounter Configuration for a Cylindrical Projectile with $L/D = 1$ @ $EBt = -0.006$ sec. Without Tumbling Effects and Without V_{rp} Variability.	40
Table 3.9.	Impact Distribution per Encounter Configuration for a Spherical Projectile @ $EBt = -0.006$ sec. Without V_{rp} Variability.....	40
Table 3.10.	Impact Frequency Criterion.	41
Table 3.11.	Impact Distribution Trends per Encounter Configuration for a Cylindrical Projectile with $L/D = 4$ @ $EBt = -0.006$ sec. Without Tumbling Effects and Without V_{rp} Variability.	42
Table 3.12.	Impact Distribution Trends per Encounter Configuration for a Cylindrical Projectile with $L/D = 4$ @ $EBt = -0.006$ sec. With Tumbling Effects and Without V_{rp} Variability.	42
Table 3.13.	Impact Distribution Trends per Encounter Configuration for a Cylindrical Projectile with $L/D = 4$ @ $EBt = -0.006$ sec. Without Tumbling Effects and With a COV V_{rp} of 25%.	42
Table 3.14.	Impact Distribution Trends per Encounter Configuration for a Cylindrical Projectile with $L/D = 4$ @ $EBt = -0.006$ sec. With Tumbling Effects and With a COV V_{rp} of 25%.	43
Table 3.15.	Impact Quantification Matrix for a Cylindrical Projectile with $L/D = 4$ Without Tumbling Effects per Encounter Configuration	45
Table 3.16.	Impact Distribution per Encounter Configuration for a Cylindrical Projectile with $L/D = 4$ @ $EBt = -0.003$ sec. Without Tumbling Effects and Without V_{rp} Variability.....	46

Table 3.17. Impact Characterization Parameter Statistics.	47
Table 3.18. Predefined Impact Characterization Parameter Ranges.....	56
Table 3.19. Impact Quantification per Impact Configuration for Cylindrical Projectiles $L/D = 4$ Without Radial Ejection Velocity Variability and Without Tumbling.....	58
Table 3.20. Impact Quantification per Impact Configuration for Cylindrical Projectiles $L/D = 2$ Without Radial Ejection Velocity Variability and Without Tumbling.....	58
Table 3.21. Impact Quantification per Impact Configuration for Cylindrical Projectiles $L/D = 1$ Without Radial Ejection Velocity Variability and Without Tumbling.....	58
Table 3.22. Yaw Angle Ranges per Impact Configuration Range.....	61
Table 3.23. Yaw Angle Distribution for Cylindrical $L/D = 4$ Impacts Without Radial Ejection Velocity Variability and Without Tumbling.	61
Table 3.24. Yaw Angle Distribution for Cylindrical $L/D = 4$ Impacts Without Radial Ejection Velocity Variability and With Tumbling.....	61
Table 3.25. Impact Quantification per Impact Configuration for a Cylindrical Projectile $L/D = 4$	63
Table 3.26. Impact Quantification Matrix for a Cylindrical Projectile with $L/D = 4$ Without Tumbling Effects per Impact Configuration.....	65
Table 3.27. Impact Quantification Matrix for a Cylindrical Projectile with $L/D = 4$ With Tumbling Effects per Impact Configuration.....	65
Table 4.1. Bumper plate dimensions and material properties.....	75
Table 4.2. Material Parameters for Steel.....	75
Table 4.3. Material Parameters for Tungsten.....	76
Table 4.4. Color Description for Ratios of Cylinder/Sphere.	104
Table 5.1. Ranges of parameters used in ANN database.....	111
Table 5.2. Case comparison of actual SIDI and predicted SIDI.....	116
Table 6.1. Total Damage Quantification per Encounter Configuration for a Cylindrical Projectile with $L/D = 4$ @ $EBt = -0.006$ sec. Without Tumbling Effects and Without V_{rp} Variability.	125
Table 6.2. Total Damage Quantification per Encounter Configuration for a Cylindrical Projectile with $L/D = 2$ @ $EBt = -0.006$ sec. Without Tumbling Effects and Without V_{rp} Variability.	125

Table 6.3.	Total Damage Quantification per Encounter Configuration for a Cylindrical Projectile with $L/D = 1$ @ $EBt = -0.006$ sec. Without Tumbling Effects and Without V_{rp} Variability.	125
Table 6.4.	Total Damage Quantification per Encounter Configuration for a Spherical Projectile @ $EBt = -0.006$ sec. Without V_{rp} Variability.....	126
Table 6.5.	Total Damage Comparison among Projectile Geometry/Sizes of the Same Mass Without Tumbling Effects and Without V_{rp} Variability.	128
Table 6.6.	Total Damage Quantification per Encounter Configuration for a Cylindrical Projectile with $L/D = 4$ @ $EBt = -0.006$ sec. With Tumbling Effects and Without V_{rp} Variability.	129
Table 6.7.	Total Damage Quantification per Encounter Configuration for a Cylindrical Projectile with $L/D = 2$ @ $EBt = -0.006$ sec. With Tumbling Effects and Without V_{rp} Variability.	129
Table 6.8.	Total Damage Quantification per Encounter Configuration for a Cylindrical Projectile with $L/D = 1$ @ $EBt = -0.006$ sec. With Tumbling Effects and Without V_{rp} Variability.	130
Table 6.9.	Total Damage Comparison among Projectile Geometry/Sizes of the Same Mass With Tumbling Effects and Without V_{rp} Variability.	130
Table 6.10.	Impact Configuration Comparison for Cylindrical Projectile with $L/D = 4$ With and Without Tumbling Effects and Without V_{rp} Variability for Encounter Scenario 2.	131
Table 6.11.	Impact Configuration Comparison for a Cylindrical Projectile with $L/D = 1$ With and Without Tumbling Effects and Without V_{rp} Variability for Encounter Scenario 2.	132
Table 6.12.	Total Damage Quantification per Encounter Configuration for a Cylindrical Projectile with $L/D = 4$ @ $EBt -0.006$ sec. Without Tumbling Effects and With a $COV V_{rp}$ of 25%.	132
Table 6.13.	Total Damage Quantification per Encounter Configuration for a Cylindrical Projectile with $L/D = 4$ @ $EBt -0.006$ sec. With Tumbling Effects and With a $COV V_{rp}$ of 25%.	133
Table 6.14.	Total Damage Level Criterion.	133

Table 6.15. Total Damage Quantification Trends per Encounter Configuration for a Cylindrical Projectile with $L/D = 4$ @ $EBt = -0.006$ sec. Without Tumbling Effects and Without $COVV_{rp}$	134
Table 6.16. Total Damage Quantification Trends per Encounter Configuration for a Cylindrical Projectile with $L/D = 4$ @ $EBt = -0.006$ sec. With Tumbling Effects and With a $COVV_{rp}$ of 75%.....	134
Table 6.17. Total Damage Quantification Matrix for a Cylindrical Projectile with $L/D = 4$ Without Tumbling Effects	136
Table 6.18. Total Damage Quantification Matrix for a Cylindrical Projectile with $L/D = 2$ Without Tumbling Effects	137
Table 6.19. Total Damage Quantification Matrix for a Cylindrical Projectile with $L/D = 1$ Without Tumbling Effects	138
Table 6.20. Total Damage Quantification Matrix for a Spherical Projectile.....	139
Table 6.21. Total Damage Quantification Matrix for a Cylindrical Projectile with $L/D = 4$ With Tumbling Effects	140
Table 6.22. Total Damage Quantification Matrix for a Cylindrical Projectile with $L/D = 2$ With Tumbling Effects	141
Table 6.23. Total Damage Quantification Matrix for a Cylindrical Projectile with $L/D = 1$ With Tumbling Effects	142
Table 6.24. Total Damage-Ratio per Encounter Configuration between a Cylindrical Projectile with $L/D = 4$ and a Sphere @ $EBt = -0.006$ sec. Without Tumbling Effects and Without $COVV_{rp}$	144
Table 6.25. Damage-Ratio Level Criterion.....	145
Table 6.26. Damage-Ratio Levels per Encounter Configuration between a Cylindrical Projectile with $L/D = 4$ and a Sphere @ $EBt = -0.006$ sec. Without Tumbling Effects and Without $COVV_{rp}$	145
Table 6.27. Damage-Ratio Levels per Encounter Configuration between a Cylindrical Projectile with $L/D = 4$ and a Sphere @ $EBt = -0.006$ sec. Without Tumbling Effects and With a $COVV_{rp}$ of 75%.....	146
Table 6.28. Matrix of Damage-Ratio Levels for a Cylindrical Projectile with $L/D = 4$ Without Tumbling Effects	147
Table 6.29. Matrix of Damage-Ratio Levels for a Cylindrical Projectile with $L/D = 2$ Without Tumbling Effects	148

Table 6.30.	Matrix of Damage-Ratio Levels for a Cylindrical Projectile with $L/D = 1$ Without Tumbling Effects	149
Table 6.31.	Matrix of Damage-Ratio Levels for a Cylindrical Projectile with $L/D = 4$ With Tumbling Effects	150
Table 6.32.	Matrix of Damage-Ratio Levels for a Cylindrical Projectile with $L/D = 2$ With Tumbling Effects	151
Table 6.33.	Matrix of Damage-Ratio Levels for a Cylindrical Projectile with $L/D = 1$ With Tumbling Effects	152
Table 6.34.	Total Damage Quantification per Impact Configuration for Cylindrical Projectiles $L/D = 4$ Without Radial Ejection Velocity and Without Tumbling	155
Table 6.35.	Total Damage Quantification per Impact Configuration for Cylindrical Projectiles $L/D = 2$ Without Radial Ejection Velocity and Without Tumbling	155
Table 6.36.	Total Damage Quantification per Impact Configuration for Cylindrical Projectiles $L/D = 1$ Without Radial Ejection Velocity and Without Tumbling	155
Table 6.37.	Total Damage Quantification per Impact Configuration for Cylindrical Projectiles $L/D = 4$	156
Table 6.38.	Total Damage Quantification per Impact Configuration for Cylindrical Projectiles $L/D = 2$	157
Table 6.39.	Total Damage Quantification per Impact Configuration for Cylindrical Projectiles $L/D = 1$	158
Table 6.40.	Total Damage Quantification Matrix for a Cylindrical Projectile with $L/D = 4$ Without Tumbling Effects per Impact Configuration.....	160
Table 6.41.	Total Damage Quantification Matrix for a Cylindrical Projectile with $L/D = 4$ With Tumbling Effects per Impact Configuration.....	160
Table 6.42.	Total Damage Quantification Matrix for a Cylindrical Projectile with $L/D = 2$ Without Tumbling Effects per Impact Configuration.....	161
Table 6.43.	Total Damage Quantification Matrix for a Cylindrical Projectile with $L/D = 2$ With Tumbling Effects per Impact Configuration.....	161
Table 6.44.	Total Damage Quantification Matrix for a Cylindrical Projectile with $L/D = 1$ Without Tumbling Effects per Impact Configuration.....	162
Table 6.45.	Total Damage Quantification Matrix for a Cylindrical Projectile with $L/D = 1$ With Tumbling Effects per Impact Configuration.....	162
Table 6.46.	Selected Encounter Scenarios for Damage Tendencies.....	165

Table 6.47.	Impact Quantification per Impact Configuration for Encounter Scenario 1 Without Tumbling Effects.	166
Table 6.48.	Impact Quantification per Impact Configuration for Encounter Scenario 2 Without Tumbling Effects.	166
Table 6.49.	Impact Quantification per Impact Configuration for Encounter Scenario 3 Without Tumbling Effects.	167
Table 6.50.	Impact Quantification per Impact Configuration for Encounter Scenario 4 Without Tumbling Effects.	167
Table 6.51.	Impact Quantification per Impact Configuration for Encounter Scenario 5 Without Tumbling Effects.	168
Table 6.52.	Impact Quantification per Impact Configuration for Encounter Scenario 6 Without Tumbling Effects.	168
Table 6.53.	Total Damage Quantification per Impact Configuration for Encounter Scenario 1 Without Tumbling Effects.	170
Table 6.54.	Total Damage Quantification per Impact Configuration for Encounter Scenario 2 Without Tumbling Effects.	170
Table 6.55.	Total Damage Quantification per Impact Configuration for Encounter Scenario 3 Without Tumbling Effects.	171
Table 6.56.	Total Damage Quantification per Impact Configuration for Encounter Scenario 4 Without Tumbling Effects.	171
Table 6.57.	Total Damage Quantification per Impact Configuration for Encounter Scenario 5 Without Tumbling Effects.	172
Table 6.58.	Total Damage Quantification per Impact Configuration for Encounter Scenario 6 Without Tumbling Effects.	172
Table 6.59.	Impact Quantification per Impact Configuration for Encounter Scenario 2 With Tumbling Effects.	175
Table 6.60.	Impact Quantification per Impact Configuration for Encounter Scenario 3 With Tumbling Effects.	175
Table 6.61.	Impact Quantification per Impact Configuration for Encounter Scenario 4 With Tumbling Effects.	176
Table 6.62.	Impact Quantification per Impact Configuration for Encounter Scenario 6 With Tumbling Effects.	176
Table 6.63.	Total Damage Quantification per Impact Configuration for Encounter Scenario 2 With Tumbling Effects.	177

Table 6.64.	Total Damage Quantification per Impact Configuration for Encounter Scenario 3 With Tumbling Effects.	177
Table 6.65.	Total Damage Quantification per Impact Configuration for Encounter Scenario 4 With Tumbling Effects.	178
Table 6.66.	Total Damage Quantification per Impact Configuration for Encounter Scenario 6 With Tumbling Effects.	178
Table 6.67.	Impact Quantification per Impact Configuration for Encounter Scenario 2 With 25% Variability Without Tumbling Effects.....	181
Table 6.68.	Impact Quantification per Impact Configuration for Encounter Scenario 2 With 75% Variability Without Tumbling Effects.....	181
Table 6.69.	Impact Quantification per Impact Configuration for Encounter Scenario 4 With 25% Variability Without Tumbling Effects.....	182
Table 6.70.	Impact Quantification per Impact Configuration for Encounter Scenario 4 With 75% Variability Without Tumbling Effects.....	182
Table 6.71.	Impact Quantification per Impact Configuration for Encounter Scenario 6 With 25% Variability Without Tumbling Effects.....	183
Table 6.72.	Impact Quantification per Impact Configuration for Encounter Scenario 6 With 75% Variability Without Tumbling Effects.....	183
Table 6.73.	Total Damage Quantification per Impact Configuration for Encounter Scenario 2 With 25% Variability Without Tumbling Effects.....	185
Table 6.74.	Total Damage Quantification per Impact Configuration for Encounter Scenario 2 With 75% Variability Without Tumbling Effects.....	185
Table 6.75.	Total Damage Quantification per Impact Configuration for Encounter Scenario 4 With 25% Variability Without Tumbling Effects.....	186
Table 6.76.	Total Damage Quantification per Impact Configuration for Encounter Scenario 4 With 75% Variability Without Tumbling Effects.....	186
Table 6.77.	Total Damage Quantification per Impact Configuration for Encounter Scenario 6 With 25% Variability Without Tumbling Effects.....	187
Table 6.78.	Total Damage Quantification per Impact Configuration for Encounter Scenario 6 With 75% Variability Without Tumbling Effects.....	187
Table A.1.	Impact Distribution per Encounter Configuration for a Spherical Projectile Without Radial Ejection Velocity Variability @ <i>EBt</i> -0.0012.....	199
Table A.2.	Impact Distribution per Encounter Configuration for a Spherical Projectile Without Radial Ejection Velocity Variability @ <i>EBt</i> -0.009	199

Table A.3.	Impact Distribution per Encounter Configuration for a Spherical Projectile Without Radial Ejection Velocity Variability @ EBt 0.000.....	200
Table A.4.	Impact Distribution per Encounter Configuration for a Spherical Projectile Without Radial Ejection Velocity Variability @ EBt +0.003.....	200
Table A.5.	Impact Distribution per Encounter Configuration for a Spherical Projectile Without Radial Ejection Velocity Variability @ EBt +0.006.....	201
Table A.6.	Impact Distribution per Encounter Configuration for a Spherical Projectile Without Radial Ejection Velocity Variability @ EBt +0.009.....	201
Table A.7.	Impact Distribution per Encounter Configuration for a Spherical Projectile Without Radial Ejection Velocity Variability @ EBt +0.012.....	202
Table D.2.	SIDI values for cylindrical projectile with $L/D = 1$ for all velocities.	223
Table D.3.	SIDI values for cylindrical projectile with $L/D = 2$ for all velocities	239
Table D.4.	SIDI values for cylindrical projectile with $L/D = 4$ for all velocities.	255
Table D.5.	SIDI Values of verification cases used for ANN.....	271

LIST OF FIGURES

Figure 2.1.	TBM's Attack system (BMDO Fact Sheet (1998)).....	7
Figure 2.2.	Different types of Payloads carried by TBMs (Lloyd R. M. (2000))	8
Figure 2.3.	Schematic of major components of a Russian Tochka-U TBM (Redman (2000)).....	8
Figure 2.4.	Tochka ballistic missile with its actual components. (Lloyd R. M. (2000))..	9
Figure 2.5.	Tactical Ballistic Missile Comparison (BMDO Fact Sheet (1998)).....	10
Figure 2.6.	Schematic of KE rod warheads (Lloyd R. M. (1998)).....	11
Figure 2.7.	Schematic of Aimed KE rod warhead mechanism (Lloyd R. M. (1998)) ...	12
Figure 2.8.	Jellyroll and Center Core KE rod warheads concepts (Lloyd R. M. (1998))	13
Figure 2.9.	Projectile Shapes and Geometries (Lloyd R. M. (2000)).....	14
Figure 3.1.	Schematic of a Near Miss Encounter Configuration Crossing Angle and Miss.....	16
Figure 3.2.	Schematic of a Near Miss Encounter Configuration: Early/Late Bird time	17
Figure 3.3.	Isotropic Jellyroll configuration of KE-rod warheads. (Lloyd R. M. (1998))	18
Figure 3.4.	Used projectile sizes and shapes.	19
Figure 3.5.	Rod deployment demonstrating tumbling after ejection. (Lloyd R. M. (2000)).....	21
Figure 3.6.	Schematic of tumbling rotating vector.....	21
Figure 3.7.	Design parameters of an Isotropic Jellyroll warhead (Lloyd R. M. (1998))	22
Figure 3.8.	TBM representation in Endgame Simulations.....	24
Figure 3.9.	Schematic of geometric surfaces used to model the TBM sections.....	25
Figure 3.10.	Terminal Encounter Kinematic Analysis.....	26
Figure 3.11.	Encounter analysis with scalar values included.....	29
Figure 3.12.	Projectile visualization in E system of Coordinates.	30
Figure 3.13.	Method for optimizing the number of impacts on the TBM.....	31
Figure 3.14.	Definition of strike and spatial orientation angles	33
Figure 3.15.	Endgame simulation flowchart.	35

Figure 3.16. Visualization of Endgame simulation results for Encounter Configuration with $CA = 120^\circ$, $EBt = 0.006$ s, and $MD = 4.0$.	36
Figure 3.17. Impact Frequencies vs Miss Distance.	37
Figure 3.18. Impact Frequencies vs. Crossing Angle.	38
Figure 3.19. Relative Frequency Distributions of Impact Characterization Parameters for Spherical Projectiles over the Entire Range of Encounter Configuration Scenarios, Without Radial Ejection Velocity Variability	48
Figure 3.20. Relative Frequency Distributions of Impact Characterization Parameters for Spherical Projectiles over the Entire Range of Encounter Configuration Scenarios, With 75% Radial Ejection Velocity Variability	48
Figure 3.21. Relative Frequency Distributions of Impact Characterization Parameters for Cylindrical Projectiles $L/D=4$ over the Entire Range of Encounter Configuration Scenarios, Without V_{rp} Variability, and Without Tumbling	49
Figure 3.22. Relative Frequency Distributions of Impact Characterization Parameters for Cylindrical Projectiles $L/D=4$ over the Entire Range of Encounter Configuration Scenarios, Without V_{rp} Variability, and With Tumbling	49
Figure 3.23. Relative Frequency Distributions of Impact Characterization Parameters for Cylindrical Projectiles $L/D=4$ over the Entire Range of Encounter Configuration Scenarios, With 75 V_{rp} Variability, and Without Tumbling	50
Figure 3.24. Relative Frequency Distributions of Impact Characterization Parameters for Cylindrical Projectiles $L/D=4$ over the Entire Range of Encounter Configuration Scenarios, With 75% V_{rp} Variability, and With Tumbling.	50
Figure 3.25. Typical Cylindrical Impacts.	51
Figure 3.26. Yaw Angle Definition for Cylindrical Projectiles.	52
Figure 3.27. Yaw Angle Statistics for Cylindrical Projectiles $L/D = 4$ vs. Crossing Angle at Selected Miss Distance Scenarios Without Radial Ejection Velocity Variability, and Without Tumbling.	53
Figure 3.28. Relative Frequency of Tail Impacts at Low Crossing Angles.	54
Figure 3.29. Relative Impact Velocity vs. Crossing Angle for Cylindrical Projectiles $L/D = 4$ Without Radial Ejection Velocity Variability.	55
Figure 3.30. Relative Impact Velocity vs. Crossing Angle for Cylindrical Projectiles $L/D = 4$ With 75% Radial Ejection Velocity Variability.	55
Figure 3.31. Yaw Angle Frequency Distribution per Impact Velocity Range for Cylindrical Projectiles $L/D = 4$, Without Radial Ejection Velocity Variability.	60

Figure 4.1. Neighboring particles calculation	70
Figure 4.2. Neighboring particles according to selected smoothing distance.....	70
Figure 4.3. Schematic of idealized model of impact.....	74
Figure 4.4. Visualization of simulation results in Enight 7.0.	77
Figure 4.5. Typical time-history plot of Kinetic Energy for projectile $L/D = 4$ with velocity = 2.15 km/s and angles $\alpha = 45, \beta = 0, \phi = 0$	78
Figure 4.6. Comparison of impacts for SIDI development	79
Figure 4.7. Damage Index values for projectile velocity of 2.15 km/s for cylindrical projectiles with $L/D = 4$ and sphere.	80
Figure 4.8. Impact Simulations for $LD = 4$ and $\alpha = 90$ at ϕ angles of 0, 15, 30, 45, 60, 75 (a, b, c, d, e, f respectively) at final time step.	82
Figure 4.9. Impact Simulations for $LD = 4$ and $\alpha = 75$ at ϕ angles of 0, 15, 30, 45, 60, 75 (a, b, c, d, e, f respectively) at final time step.	83
Figure 4.10. Impact Simulations for $LD = 4$ and $\alpha = 60$ at ϕ angles of 0, 15, 30, 45, 60, 75 (a, b, c, d, e, f respectively) at final time step.	84
Figure 4.11. Impact Simulations for $LD = 4$ and $\alpha = 45$ at ϕ angles of 0, 15, 30, 45, 60, 75 (a, b, c, d, e, f respectively) at final time step.	85
Figure 4.12. Impact Simulations for $LD = 4$ and $\alpha = 30$ at ϕ angles of 0, 15, 30, 45, 60, 75 (a, b, c, d, e, f respectively) at final time step.	86
Figure 4.13. Impact Simulations for $LD = 4$ and $\alpha = 15$ at ϕ angles of 0, 15, 30, 45, 60, 75 (a, b, c, d, e, f respectively) at final time step.	87
Figure 4.14. Impact Simulations for $LD = 4$ and $\alpha = 0$ at ϕ angles of 0, 15, 30, 45, 60, 75 (a, b, c, d, e, f respectively) at final time step.	88
Figure 4.15. Impact Simulations for $LD = 4$ and $\alpha = -15$ at ϕ angles of 0, 15, 30, 45, 60, 75 (a, b, c, d, e, f respectively) at final time step.	89
Figure 4.16. Impact Simulations for $LD = 4$ and $\alpha = -30$ at ϕ angles of 0, 15, 30, 45, 60, 75 (a, b, c, d, e, f respectively) at final time step.	90
Figure 4.17. Impact Simulations for $LD = 4$ and $\alpha = -45$ at ϕ angles of 0, 15, 30, 45, 60, 75 (a, b, c, d, e, f respectively) at final time step.	91
Figure 4.18. Impact Simulations for $LD = 4$ and $\alpha = -60$ at ϕ angles of 0, 15, 30, 45, 60, 75 (a, b, c, d, e, f respectively) at final time step.	92
Figure 4.19. Impact Simulations for $LD = 4$ and $\alpha = -75$ at ϕ angles of 0, 15, 30, 45, 60, 75 (a, b, c, d, e, f respectively) at final time step.	93

Figure 4.20. Impact Simulations for sphere projectile at α angles of 0, 15, 30, 45, 60, 75 (a, b, c, d, e, f respectively) at final time step.	94
Figure 4.21. Case 1: Cylinder Impact $L/D = 4$, vel = 2.15, $\alpha = 90$, $\phi = 75$	95
Figure 4.22. Case 2: Cylinder Impact $L/D = 4$, vel = 2.15, $\alpha = 45$, $\phi = 30$	95
Figure 4.23. Case 3: Cylinder Impact $L/D = 4$, vel = 2.15, $\alpha = 15$, $\phi = 0$	95
Figure 4.24. Case 4: Cylinder Impact $L/D = 4$, vel = 2.15, $\alpha = -30$, $\phi = 15$	96
Figure 4.25. Case 5: Cylinder Impact $L/D = 4$, vel = 2.15, $\alpha = -60$, $\phi = 60$	96
Figure 4.26. Case 6: Sphere Impact vel = 2.15, $\alpha = 90$	96
Figure 4.27. Comparison between L/D 's and sphere.	97
Figure 4.28. $L/D = 1$, vel = 2.15, $\alpha = 0$, $\phi = 15$	98
Figure 4.29. $L/D = 2$, vel = 2.15, $\alpha = 0$, $\phi = 15$	98
Figure 4.30. $L/D = 4$, vel = 2.15, $\alpha = 0$, $\phi = 15$	98
Figure 4.31. SIDI projectile material comparison with $h = 0.15$, $L/D = 4$ and Sphere, velocity = 02.15 km/s, $\alpha = 0, 45, 90$, and $\phi = 0, 45$, and 75.	99
Figure 4.32. Copper projectile impact with mass of 15 gr, $L/D = 4$, vel = 2.15 km/s, $\alpha = 0$, $\phi = 0$	100
Figure 4.33. Tungsten projectile impact with mass of 15 gr, $L/D = 4$, vel = 2.15 km/s, $\alpha = 0$, $\phi = 0$	100
Figure 4.34. SIDI projectile mass comparison with $h = 0.15$, $L/D = 4$ and Sphere, velocity = 02.15 km/s, $\alpha = 0, 45, 90$, and $\phi = 0, 45$, and 75.	101
Figure 4.35. Tungsten projectile impact with mass of 60 gr, $L/D = 4$, vel = 2.15 km/s, $\alpha = 0$, $\phi = 0$	101
Figure 4.36. Dual impact comparison.	102
Figure 4.37. Single projectile impact with mass 15 gr, $L/D = 4$, vel = 2.15 km/s, $\alpha = 0$, $\phi = 0$	103
Figure 4.38. Dual projectile impact with mass 15 gr, $L/D = 4$, vel = 2.15 km/s, $\alpha = 0$, $\phi = 0$ at relative distance of 0 diameters.	103
Figure 4.39. Dual projectile impact with mass 15 gr, $L/D = 4$, vel = 2.15 km/s, $\alpha = 0$, $\phi = 0$ at relative distance of 10 diameters.	103
Figure 4.40. Table for $L/D = 4$ and Vel = 1.80 km/s and Sphere.	104
Figure 4.41. Table for ratio of SIDI Cylinder/Sphere for $L/D = 4$ and velocity of 1.80 km/s.	105

Figure 4.42. Colored table for ratio of SIDI Cylinder/Sphere for $L/D = 4$ and velocity of 1.80 km/s.....	105
Figure 4.43. Tables of SIDI ratios Cylinder/ Sphere for $L/D = 4$ and all velocities.	106
Figure 4.44. Tables of SIDI ratios Cylinder/Sphere for velocity 1.80 km/s and all L/D 's.	107
Figure 5.1. Schematic of a Processing Element.....	109
Figure 5.2. General structure of an Artificial Neural Network	110
Figure 5.3. Matlab Code flowchart for optimum ANN architecture.....	112
Figure 5.4. Final ANN Architecture.....	113
Figure 5.5. Transfer functions used on ANN hidden layers.....	114
Figure 5.6. Results of ANN predicted DI values from training file.....	115
Figure 5.7. Results of ANN predicted DI values from training file.....	115
Figure 5.8. Results of ANN predicted DI values from validation cases	117
Figure 5.9. Results of ANN predicted DI values from validation cases	117
Figure 5.10. Curve comparison between the actual and predicted values	118
Figure 5.11. Table for ANN predicted values of LD = 4 and Vel = 1.80 km/s and Sphere.	118
Figure 5.12. Colored table for predicted ratio of SIDI Cylinder/Sphere for LD = 4 and velocity of 1.80 km/s.....	119
Figure 5.13. Tables of predicted SID ratios Cylinder/Sphere for LD = 1 and all new velocities.	120
Figure 5.14. Tables of predicted SID ratios Cylinder/Sphere for LD = 2 and all new velocities.	121
Figure 5.15. Tables of predicted SID ratios Cylinder/Sphere for LD = 4 and all new velocities.	122
Figure 6.1. Damage Prediction and Quantification Sequence in an Endgame Simulation.	124
Figure 6.2. Cylinder L/D of 4 Total Damage vs. Crossing Angle @ EBt of -0.012 sec.	127
Figure 6.3. Cylinder L/D of 4 Total Damage vs. Crossing Angle @ EBt of -0.006 sec.	127
Figure 6.4. Cylinder L/D of 4 Total Damage vs. Crossing Angle @ EBt of 0.012 sec.	128

Figure 6.5. Most Frequent Strike Angle Ranges Under a Certain Impact Velocity Range.	163
Figure 6.6. Impact Frequencies at Various Variability Levels.....	180
Figure B.1. Yaw Angle Statistics for Cylindrical Projectiles $L/D = 1$ vs. Crossing Angle at miss distances of 1m, 1.5m, 2m, 2.5m (a, b, c, d, respectively)	204
Figure B.2. Yaw Angle Statistics for Cylindrical Projectiles $L/D = 1$ vs. Crossing Angle at miss distances of 3m, 3.5m, 4m, 4.5m (a, b, c, d, respectively)	205
Figure B. 3. Yaw Angle Statistics for Cylindrical Projectiles $L/D = 1$ vs. Crossing Angle at miss distances of 5m, 5.5m, 6m (a, b, c, respectively)	206
Figure B.4. Yaw Angle Statistics for Cylindrical Projectiles $L/D = 2$ vs. Crossing Angle at miss distances of 1m, 1.5m, 2m, 2.5m (a, b, c, d, respectively)	207
Figure B.5 Yaw Angle Statistics for Cylindrical Projectiles $L/D = 2$ vs. Crossing Angle at miss distances of 3m, 3.5m, 4m, 4.5m (a, b, c, d, respectively)	208
Figure B.6. Yaw Angle Statistics for Cylindrical Projectiles $L/D = 2$ vs. Crossing Angle at miss distances of 5m, 5.5m, 6m (a, b, c, respectively)	209
Figure B.7. Yaw Angle Statistics for Cylindrical Projectiles $L/D = 4$ vs. Crossing Angle at miss distances of 1m, 1.5m, 2m, 2.5m (a, b, c, d, respectively)	210
Figure B.8. Yaw Angle Statistics for Cylindrical Projectiles $L/D = 4$ vs. Crossing Angle at miss distances of 3m, 3.5m, 4m, 4.5m (a, b, c, d, respectively)	211
Figure B.9. Yaw Angle Statistics for Cylindrical Projectiles $L/D = 4$ vs. Crossing Angle at miss distances of 5m, 5.5m, 6m (a, b, c, respectively)	212
Figure C.1. Yaw Angle Frequency Distribution per Impact Velocity Ranges of 0-0.3075 km/s, 0.3075-0.615 km/s, 0.615-0.9225 km/s, 0.9225-1.23 km/s (a, b, c, d respectively) for Cylindrical Projectiles $L/D = 1$, Without Radial Ejection Velocity Variability.	214
Figure C.2. Yaw Angle Frequency Distribution per Impact Velocity Ranges of 1.23-1.5375 km/s, 1.5375-1.845 km/s, 1.845-up km/s (a, b, c respectively) for Cylindrical Projectiles $L/D = 1$, Without Radial Ejection Velocity Variability	215
Figure C. 3. Yaw Angle Frequency Distribution per Impact Velocity Ranges of 0-0.3075 km/s, 0.3075-0.615 km/s, 0.615-0.9225 km/s, 0.9225-1.23 km/s (a, b, c, d respectively) for Cylindrical Projectiles $L/D = 2$, Without Radial Ejection Velocity Variability.	216
Figure C.4. Yaw Angle Frequency Distribution per Impact Velocity Ranges of 1.23-1.5375 km/s, 1.5375-1.845 km/s, 1.845-up km/s (a, b, c respectively) for Cylindrical Projectiles $L/D = 2$, Without Radial Ejection Velocity Variability	217

- Figure C.5. Yaw Angle Frequency Distribution per Impact Velocity Ranges of 0-0.3075 km/s, 0.3075-0.615 km/s, 0.615-0.9225 km/s, 0.9225-1.23 km/s (a, b, c, d respectively) for Cylindrical Projectiles $L/D = 4$, Without Radial Ejection Velocity Variability 218
- Figure C.6. Yaw Angle Frequency Distribution per Impact Velocity Ranges of 1.23-1.5375 km/s, 1.5375-1.845 km/s, 1.845-up km/s (a, b, c respectively) for Cylindrical Projectiles $L/D = 4$, Without Radial Ejection Velocity Variability 219

CHAPTER 1

INTRODUCTION

1.1 Introduction

National defense missile systems that are capable of deviating or destroying incoming ballistic missiles have acquired notoriety and importance in the last few decades. The increasing threat of rogue nations developing new technology for ballistic missiles capable of reaching long distances have made these defense systems focus on counteracting the possible effects of biological, chemical or nuclear missiles. Such systems have recently focused on direct impact between a guided missile interceptor (Exo-atmospheric Kill Vehicle, EKV) and an incoming tactical ballistic missile (TBM).

The high relative closing velocities expected in the hypervelocity range of 2 to 15 km/s and the development of countermeasures (i.e. deployment of decoys or concealment of the warhead within several metal coated balloons) represent an increase in difficulty beyond the additional challenge inherent to the problem of impacting an incoming missile. Although the development of infrared target discrimination, communications and guidance systems that would recognize, if decoys of the incoming missile are deployed, and track the missile's trajectory would enable direct impact of the EKV on the TBM, which leaves little room for malfunction or error of the operational systems of the EKV.

Current efforts are being made in developing a new system of missiles combining EKV guidance technology with a guided-ejection system that can fire a cluster of projectiles with near-uniform spray density directed towards the target. The ultimate goal of the current national defense missile systems is to maximize the probability of kill, either by direct impact or using this array of very high-speed projectiles, to completely disable the targeted TBM warhead.

1.2 Background

The defense missile systems being developed now are required to provide high standards of reliability and a maximum probability of kill in their missions for obvious reasons. The new generation of missiles in the design process, such as the Theater High Altitude Area Defense System, is based on a direct-hit concept that utilizes guidance systems. However, due to high relative closing velocities and possible countermeasures, a direct-hit of a TBM decreases the reliability of such missiles. In order to improve the probability of kill, new systems capable of ejecting a cluster of projectiles in the direction of the TBM are in the developing phase. This cluster of projectiles/penetrators increases the projected impact area and the reliability of these missiles. It is reasonable to assume that if a direct-hit is not accomplished, this cloud of projectiles would inflict some damage to the TBM. If this array of projectiles/penetrators reaches the TBM, it is desired that they cause the maximum damage to the TBM warhead in order to disable it. The achievement of such a goal requires the study of the interplay of different factors influencing the inflicted damage to the TBM. Therefore, the design parameters of these guided-ejection systems, such as projectile shape, size, and velocity as well as the spray

pattern of the projectiles' cloud, becomes essential to maximize the chances of disabling or destroying the TBM. The optimum design parameters can be obtained by setting the encounter configuration of the projectiles and the TBM in laboratories equipped with two-stage light gas guns capable of firing projectiles at the hypervelocity range. Conducting such tests increase the cost and are extremely time-consuming; moreover, set up of the desired encounter configuration between the projectiles and the TBM is difficult to achieve. As an alternative to this high-cost procedure, numerical simulations can be used to study the interaction of the encounter parameters and projectile characteristics that inflict more damage.

Researchers have studied lethality of projectile impacts and missile physics using numerical simulations for several years. Furthermore, the simulations have provided a strong insight as to how the missile system is going to behave in mission. However, most information is maintained confidential. Although research about this subject is extensive, limited work has been published. Lloyd R. M. (1998 and 2000) provides an extensive study related to the lethality and design of missiles and rod warheads. He presents the theory and physics behind the Kinetic Energy (KE) rod warhead systems, which is the missile system firing a cluster of projectiles/penetrators towards the TBM. His studies cover the rod penetration mechanics of projectiles considering the trade-offs when varying the shape, yaw angle, and the ratio between the length and the diameter of cylindrical projectiles (L/D ratio). He performed numerical simulations of rod impacts using hydrocodes in order to predict the behavior of the impact and to compare it with the theoretical results. His method of investigating the lethality of such warheads was different depending on the payload the TBM contained. However, the damage criterion was mainly based on the number of projectiles impacting the TBM. Dickinson D. L. *et al.* (1997), Allahdadi F. A. *et al.* (1998), and Lloyd R. M. (2000) defined damage as the capacity of the warheads to initiate a high order explosion in the TBM. They used Jacobs' equation to model a higher order explosion. Jacobs' equation is defined by

$$V_c = \frac{A}{\sqrt{D \cos \theta}} (1 + B) \left(1 + \frac{CT}{D} \right) \quad (1.1)$$

where V_c is the critical impact speed required to produce a detonation (mm/ μ s), A is the constant defining the explosive sensitivity (mm^{3/2}/ μ s), D is the critical dimension of the fragment (mm), θ is the impact obliquity (deg), B is the fragment shape factor, C is the cover plate protection coefficient, and T is the cover plate thickness (mm). This equation relates the threshold impact speed for detonation as a function of impact orientation, to investigate fragment damage to high explosive payloads. Research about rod impact mechanics and its effects on the target is more extensive. Swift H. F. (1982) exposed an extensive review of the mechanics of hypervelocity impacts. He considers both long and short rod impacts into very thick targets, intermediate thickness targets, and thin targets. Segletes S. B. *et al.* (2003) presented a study where he gives improved and simplified forms of long-rod penetration equations leading to exact solutions. His improvements to the equations permitted him to add computational efficiency to the calculations. Jolly W. H. *et al.* (1993), Hörz F. *et al.* (1995), Dvorak B. D. (1999), and Cour-Palais B.G. (2001)

performed several lab experiments with two-stage light gas guns and hypervelocity launchers to study the effect of different shapes of projectiles. Bjerke T. W. *et al.* (1992), Johnson G. R. *et al.* (1993), Anderson C. E. *et al.* (1996), Hayhurst C. J. *et al.* (1998), Dickinson D. L. *et al.* (1999), Rosenberg Z. *et al.* (2000), Gee D. J. *et al.* (2001), and Zukas J. A. *et al.* (2001) used numerical simulations to study the L/D ratio, impact velocity, obliquity and yaw angle impact effects of cylindrical projectiles. Li K. *et al.* (1996 and 1997) presented an experimental study where he assessed the effects of projectiles impacts with induced tumbling into different materials. He concluded that an increase of impact angle can reduce the penetration capability of the projectile.

Studies that adequately quantify damage caused by different projectile shapes, sizes, and incidence angles of impacts are not available in the literature. There has been extensive analysis of the penetration characteristics of spherical projectiles for different impact velocities, obliquity angles and for different types of materials. Also, studies of the different penetration mechanics of cylindrical projectiles of different materials, different L/D ratios, impact velocities and obliquities and for a range of yaw angles are extensively available in the literature. However, there has been very little work done to compare the lethality of both geometries and determine under which conditions one geometry is more lethal than the other.

First attempts to study cylindrical projectile penetration used the steady-state hydrodynamic theory were made by Birkhoff G. *et al.* (1948) and Tate A. (1967 and 1969). This work completely ignored the effects of strength based on the understanding that at high velocities the shear stresses developed in the target and projectile were much larger than the yield stresses of the material. More recent work by Anderson C.E. *et al.* (1999) and Rosenberg Z. *et al.* (2000) showed, by comparing experimental data with numerical simulations, that the yielding characteristics of the target and the projectile has to be considered if accurate predictions of penetration depth are required. Tate A. (1986), Anderson C. E. *et al.* (1999) and Rosenberg Z. *et al.* (2000) modified the original hydrodynamic model to account for the yield stress effect. An issue not included in the first modified hydrodynamic models is the relation between the L/D ratio and the penetration depth. Work done by Chocron S. *et al.* (2003), Anderson C. E. *et al.* (1996), Walker J. D. *et al.* (1995) and Rosenberg Z. *et al.* (1994) included the effect of the L/D ratio in the penetration models. In particular, the work done by Anderson C. E. *et al.* (1996) recognized that numerical simulations tend to be in very good agreement with experimental data. Most of the work previously mentioned only considered normal impacts on semi-infinite plates, the effect of the obliquity and orientation angles were not considered. Although the research done by Johnson *et al.* (1993) and Gee D. J. *et al.* (2001) demonstrated that numerical simulations provide reasonably accurate results for impact problems involving rods at various obliquities, yaw angles and velocities, it covered only a very limited range of obliquity and yaw angles.

1.3 Objectives

The main objective of this study is to provide answers/recommendations that would enable the design of the EKV in terms of inflicting more damage to the TBM. In

order to achieve the main objective, several tasks have been identified to arrive to satisfactory conclusions.

The tasks of this research are:

- (1) Perform a terminal encounter kinematics study of the trajectories between the EKV and the TBM.
- (2) Develop a damage quantification index calculated directly from each single impact simulation results.
- (3) Develop a rapid solution model capable of interpolate damage indexes of impact configurations different from the ones numerically simulated.
- (4) Study the existing trade-offs of varying the parameters influencing the impact of the rod warheads.

1.4 Scope of work

A computer code was developed to model various "endgame" encounter configuration scenarios between the EKV and the TBM to quantify and characterize single impacts in the TBM warhead. Numerical simulations using a commercial hydrocode were conducted to model specific single impact scenarios. A damage index directly calculated from simulation results based on the penetration of the projectile and the displacement of the target was developed to quantify the damage inflicted by each impact. The quantified damage of each single case scenario represents a measure of the lethality for each configuration. An Artificial Neural Network (ANN) was developed as a rapid solution model to predict damage indices for a wide range of single impact configurations as a result of the Endgame encounters. The individual damage indices were then aggregated to obtain a global damage index that characterizes each TBM-EKV encounter configuration.

BALLISTIC MISSILE OVERVIEW

2.1 Introduction

Defense missile systems developed nowadays employ guided missiles using KE-rod warheads to counteract the possible destructive effects of tactical ballistic missiles (TBM). Design, simulation, and modeling efforts of these systems require a complete knowledge of both the TBM and EKV physical dimensions and characteristics in addition to a basic understanding of the theory behind the KE-rod warheads. A description of the TBM and EKV missile characteristics, and a discussion of the physics of KE-rod warheads are presented in this chapter.

2.2 TBM Description

The trend among military forces for acquisition or development of theater missiles has expanded with the growth of regional rivalries and the strategy of using long-range strike capability. This trend currently poses a threat that is only regional in character due to the range capacity of the missiles (BMDO Fact Sheet (1998)). However, the trend is clearly in the direction of increasing range, lethality, accuracy, and system's sophistication. The TBMs employ a high-atmosphere or exo-atmospheric ballistic trajectory to reach the target as depicted in Figure 2.1. Their long range, short flight time, relatively low cost and ability to carry a variety of warheads provide a military advantage for the nation that possesses them. Many countries import, develop, or ingeniously modify missiles to deliver nuclear, chemical or biological payloads. Typical payload warheads carried by TBMs are shown in Figure 2.2.

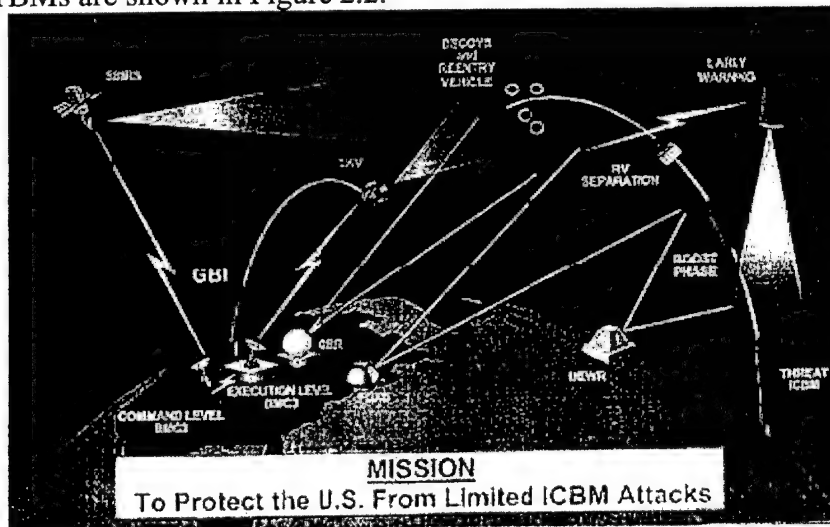


Figure 2.1. TBM's Attack system (BMDO Fact Sheet (1998))

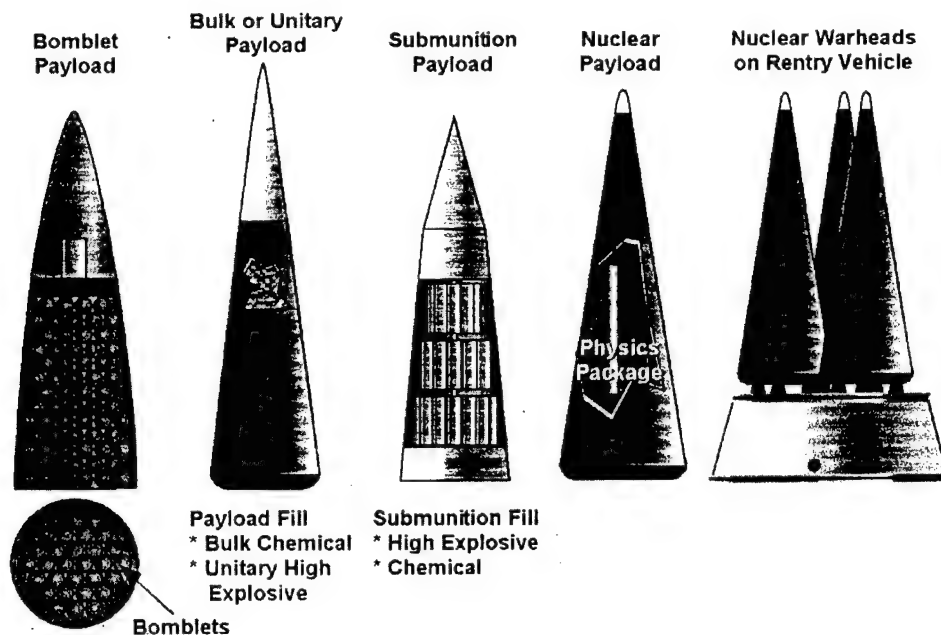


Figure 2.2. Different types of Payloads carried by TBMs (Lloyd R. M. (2000))

Figure 2.3 illustrates the cross section of a typical TBM missile (the Russian Tochka-U) with its major components.

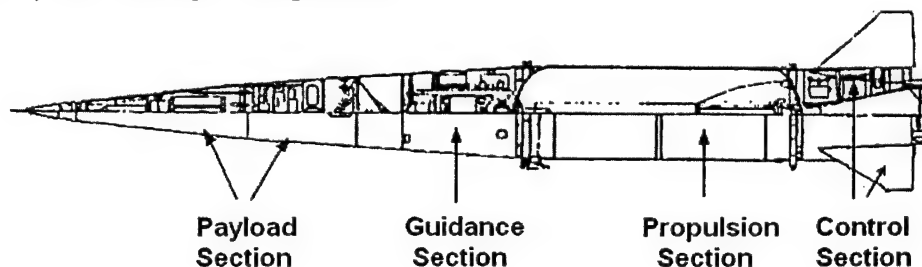


Figure 2.3. Schematic of major components of a Russian Tochka-U TBM (Redman (2000))

It is important to emphasize that the components could be located at different sections within the missile as a countermeasure. For example, Figure 2.4 shows a cutaway of a Russian Tochka-U missile where the warhead is placed in the middle section of the missile. This arrangement allows the TBM to be hit in its nose section without damaging its payload.

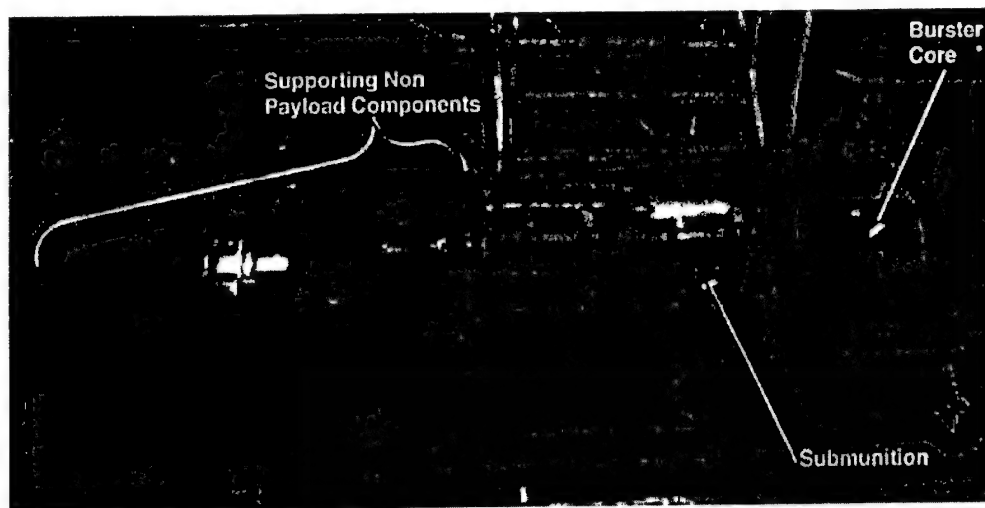


Figure 2.4. Tochka ballistic missile with its actual components. (Lloyd R. M. (2000))

TBM missiles are generally classified according to their range. Missiles that travel from 0 to 1,000 kilometers are classified as Short-Range ballistic missiles (SRBM). Medium-Range ballistic missiles (MRBM) can travel from 1,001 to 3,000 kilometers. Intermediate-range ballistic missiles (IRBM) travel from 3,001 to 5,500 kilometers. Figure 2.5 shows a comparison of different missile sizes, ranges, warheads that can carry, and countries developing them (BMDO Fact Sheet (1998)). Travel velocities of TBMs are from 5 to 10 km/s.

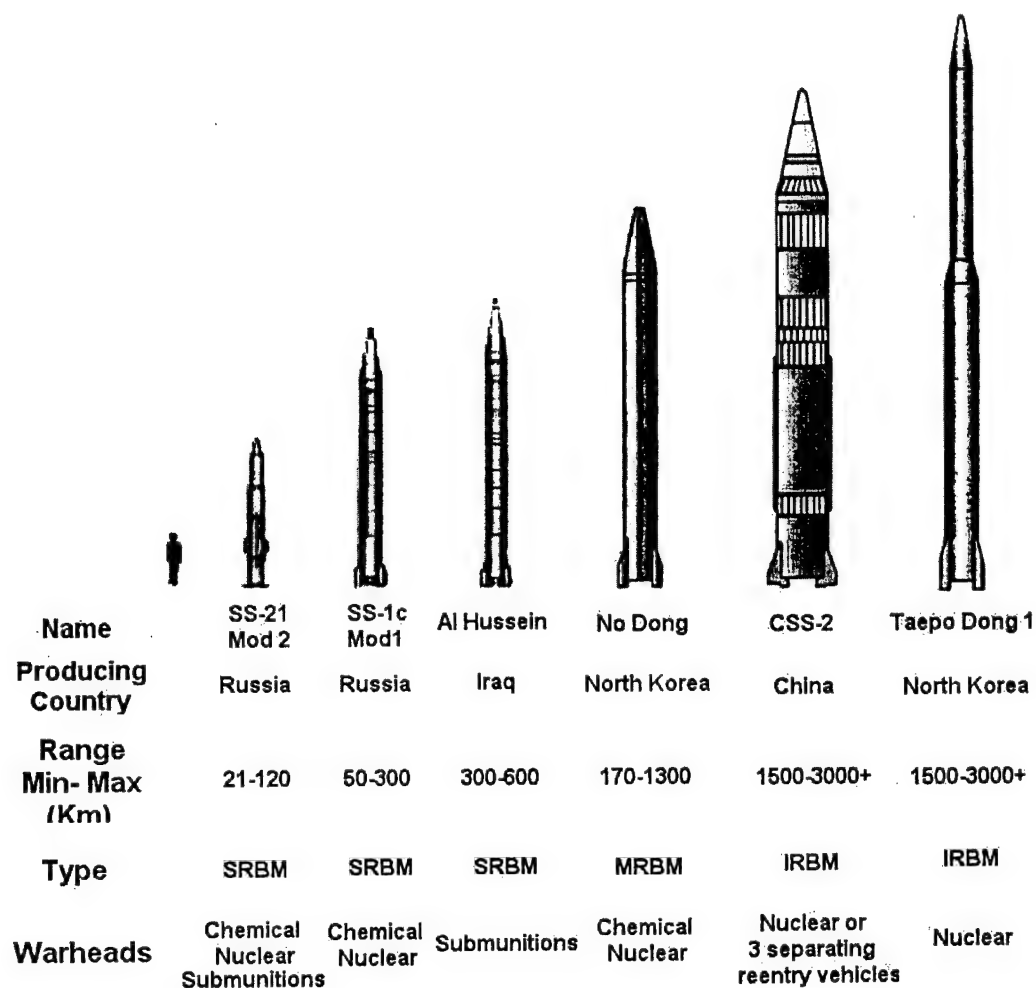


Figure 2.5. Tactical Ballistic Missile Comparison (BMDO Fact Sheet (1998))

2.3 EKV Description

A critical element of defense missile systems is the Exoatmospheric Kill Vehicle (EKV). The EKV must perform a variety of complicated tasks as the interceptor vehicle. The EKV will detect, track and destroy incoming TBMs while they are still in the midcourse of their trajectories, outside the Earth's atmosphere. The primary mission of the EKV is to eliminate the TBM through a hit-to-kill collision or by using Kinetic Energy rod warheads. Travel velocities of the EKV vary from 4 to 8 km/s (BMDO Fact Sheet (1998)).

2.4 Kinetic Energy Rod Warheads Physics

Kinetic Energy rod warhead technology is a new method to destroy ballistic missiles when a hit-to-kill collision is difficult to achieve (near-miss encounter). This

type of warhead deploys high-density rods towards the TBM creating a tightly spaced cloud of metal projectiles as depicted in figure 2.6.

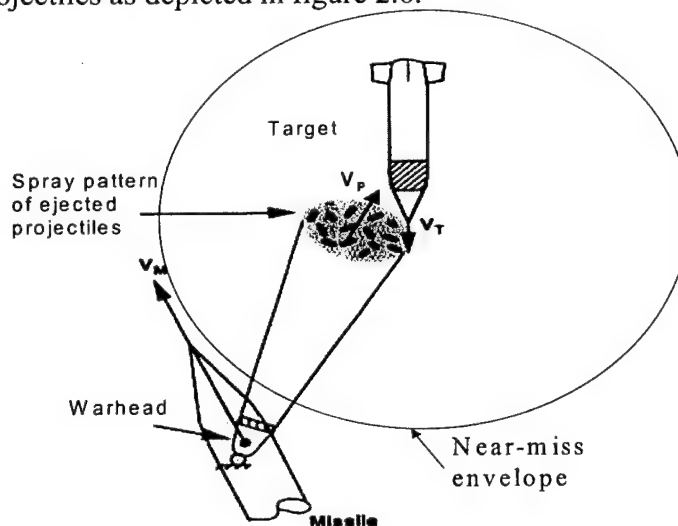


Figure 2.6. Schematic of KE rod warheads (Lloyd R. M. (1998)).

This new technology delivers more mass towards the TBM than current missiles using blast fragmentation. The explosive charge to metal mass ratio (C/M ratio) of usual blast fragmentation interceptor missiles is generally of 1.0. A KE rod warhead configuration usually has C/M ratios from 0.1 to 0.3 (Lloyd R. M. (1998)). The KE rod warhead permits to carry more warhead weight than a blast fragmentation missile. As an example, a blast fragmentation missile with a C/M ratio of 1.0 and a combined weight of explosive charge plus mass warhead of 160 lb allocates 80 lb of explosive charge and an equal weight of metal core. A KE rod warhead with the same combined weight of 160 lb but with a C/M ratio of 0.2 contains 128 lb of metal deployed in the target direction. The metal mass ejected by KE rod warhead configurations can be as high as 16 times the mass weight ejected by blast fragmentation (Lloyd R. M. (1998)). This is considerably more metal deployed towards the TBM than a typical blast fragmentation.

Two categories of KE rod warhead systems can be identified depending on the deployment scheme: aimed ejection mode and isotropic ejection mode. Aimed KE rod warhead is a mass focusing mechanism that permits to deploy its entire warhead mass towards the target direction. This is achieved by placing a center core and an outer ring of explosive charge surrounding the projectiles of the EKV as illustrated in Figure 2.7. Detonation of certain arc lengths of the outer explosive ring ejects the rods towards the required predetermined location of the TBM.

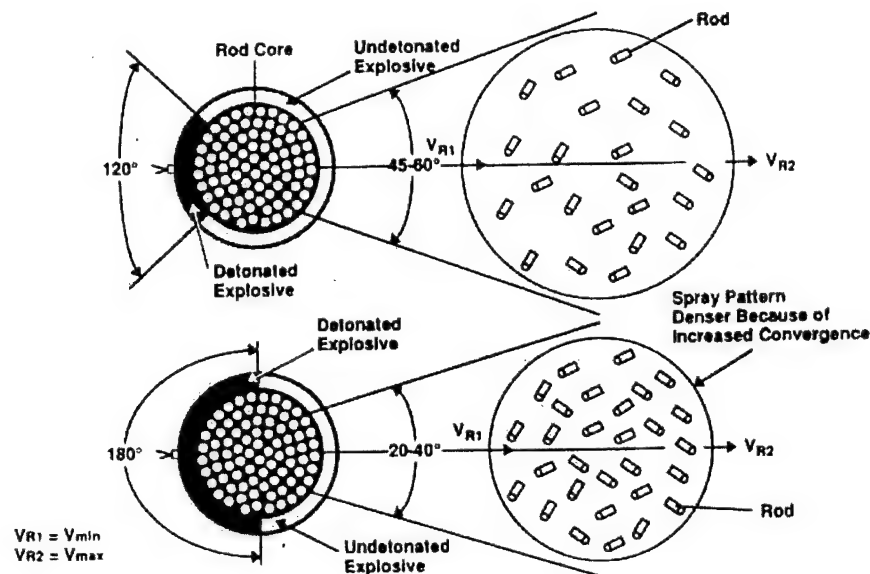


Figure 2.7. Schematic of Aimed KE rod warhead mechanism (Lloyd R. M. (1998))

Isotropic KE rod warheads deploy its warhead mass in an expansive 360 deg cloud about the missile's axis. The two main categories of isotropic rod warhead mechanisms are the center core and the jellyroll concepts. The center core configuration contains a center explosive surrounded by projectiles on its circumference and a ring of foam buffer between the explosive and the projectiles. The buffer is made of a low sound speed material which absorbs explosive shock and prevents rods from shattering or fracturing. A jellyroll configuration contains a thin layer of explosive, foam buffer, and rods arranged in alternating circular layers. A jellyroll arrangement permits to deploy the warheads in a thin disk shaped pattern about the missiles axis. Figure 2.8 illustrates a schematic of both center core and jellyroll rod warhead mechanisms.

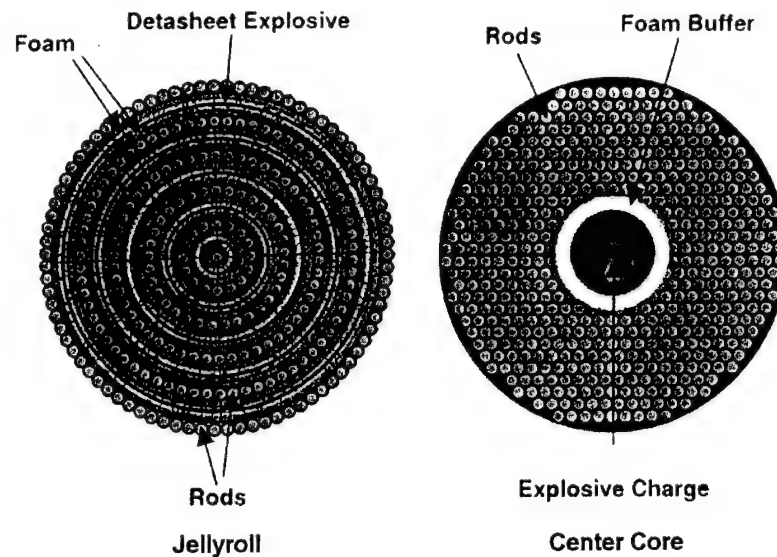


Figure 2.8. Jellyroll and Center Core KE rod warheads concepts (Lloyd R. M. (1998))

The deployment velocity of the rod warheads is strongly related to the C/M ratio. The higher the explosive mass, the higher the ejection velocity of the rods. Prediction of rod velocity for isotropic center core deployment is modeled by the Gurney equation as

$$V = \sqrt{2E} \sqrt{\frac{C/M}{\left(1 + \frac{R_e}{L}\right)\left(1 + \frac{C}{2M}\right)}} \quad (2.1)$$

where V is the peak rod velocity, C is the explosive mass, M is the rod total mass, L is the rod length, R_e is the radius of the center core explosive, and $2E$ is a Gurney velocity constant. Equations for aimed and jellyroll isotropic mechanisms have to be derived from the Gurney equation to appropriately model the rod deployment velocities. After a short period of time of deployment from the EKV, rod warheads will begin to separate and tumble at random directions. Tumbling effects will influence the angular velocity and the angular acceleration of the projectiles causing misalignments with its relative velocity vector. The tumbling effect could decrease the damage inflicted of each single rod and it will be discussed in the next chapter.

2.5 Projectiles Description

KE Rod Warheads projectiles could be selected from a variety of sizes and geometries, as shown in Figure 2.9.

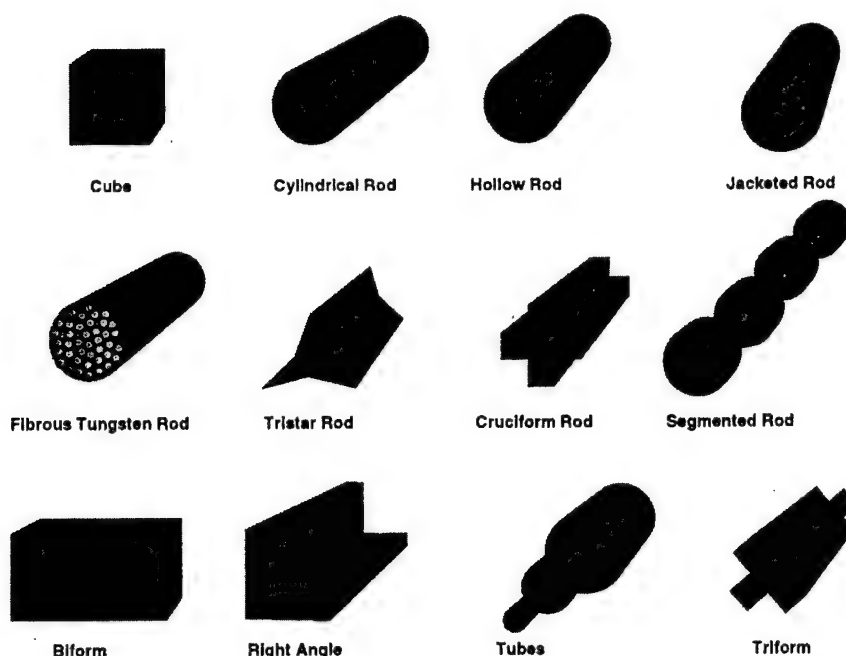


Figure 2.9. Projectile Shapes and Geometries (Lloyd R. M. (2000))

Common rod warhead geometries are cylinders and spheres. A cylindrical rod is characterized by the ratio between its length and diameter (L/D ratio). Several researchers (Bjerke T. W. *et al.* (1992), Johnson G. R. *et al.* (1993), Anderson C. E. *et al.* (1996), Hayhurst C. J. *et al.* (1998), Dickinson D. L. *et al.* (1999), Rosenberg Z. *et al.* (2000), Gee D. J. *et al.* (2001), and Zukas J. A. *et al.* (2001)) have performed extensive experiments, both actual and numerical, to study the effects of the L/D ratio of cylindrical projectiles impacting bumper plates.

The material of these projectiles plays an important role in inflicting damage to a target. High-density materials capable of penetrating thick or hardened payloads are used to cause maximum damage. Dense materials such as tungsten (17.6 gr/cc), copper (8.93 gr/cc), or steel (7.9 gr/cc) can be selected to fabricate rod warheads. Moreover, a denser material permits to deliver more mass using the same amount of projectiles towards the TBM than materials with low densities.

2.6 Summary

A general description of the ballistic missiles used today has been presented. Current TBM's can carry different kinds of payloads at different locations within the missile. The EKV's must intercept the TBM to counteract its possible effects. An overview of the theory and physics of KE rod warheads was explained in this chapter. KE rod warheads are used to maximize the overall damage to ballistic missiles when near miss scenarios are presented. Rod warhead damage inflicted to the TBM is strongly related to the material, size, and geometry of the projectiles.

CHAPTER 3

ENDGAME SIMULATIONS

3.1 Introduction

Overall damage inflicted by projectiles ejected from the EKV on the TBM is strongly influenced by the near miss encounter configuration variables. A near miss encounter between a TBM and an EKV is a scenario where the EKV does not achieve a hit-to-kill collision; however, it passes sufficiently close to the TBM so KE rod warheads can be employed. Such scenario has three important variables: the crossing angle, the miss distance, and the ejection time of the rods. Each variable influences the velocity and angle in which the ejected rods strike the TBM as well as the number of projectiles impacting the TBM. Several studies have demonstrated (Bjerke T. W. *et al.* (1992), Christiansen E. L. *et al.* (1993) Johnson G. R. *et al.* (1993), Dickinson D. L. *et al.* (1999), Gee D. J. *et al.* (2001)) that the depth of penetration and damage caused by cylindrical projectiles on bumper plates is strongly related to the yaw angle and the velocity of projectiles at impact. Overall quantification of damage of KE-rod warheads requires a study where both the EKV and the TBM missile designs have to be taken into account as well as the terminal engagement encounter. Missile design is referred in this work to the arrangement of the KE-rod warheads inside the EKV and the shape and size of the TBM. This chapter describes the details employed for modeling the terminal encounter between the EKV and the TBM more commonly referred in the missile designer community as "Endgame Simulations."

3.2 Near Miss Encounter Configuration

A near miss encounter occurs when the EKV does not achieve a hit-to kill collision although it passes sufficiently close to the TBM so KE-rod warheads can be employed as depicted in Figure 3.1. The EKV/TBM encounter configuration is defined by the crossing angle, the miss distance and whether the encounter is an early or later bird. The crossing angle (CA) is the angle formed by the projections of the TBM and EKV trajectories. The miss distance, from now on referred as MD , is the perpendicular distance (shortest distance) between the projections of the TBM and EKV trajectories.

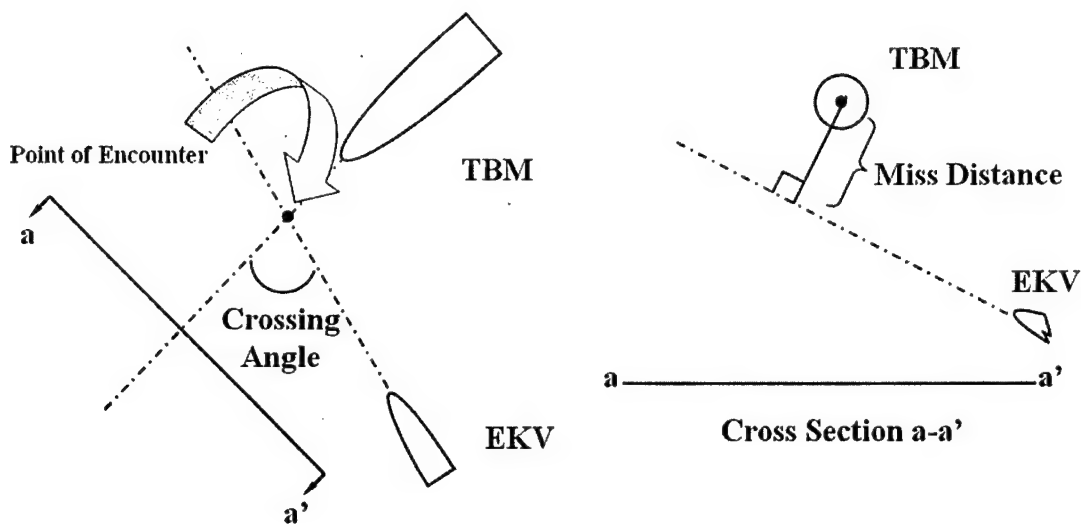


Figure 3.1. Schematic of a Near Miss Encounter Configuration Crossing Angle and Miss

The Early/Late Bird time is based on which missile, either the TBM or the EKV, arrives first to the point of encounter of the two trajectories. Figure 3.2 is used to explain this variable in detail. It is considered a Late Bird time if the TBM arrives first to the point of intersection of the trajectory of both projectiles. On the other hand, if the EKV arrives to the point of encounter before than the TBM, then the time is considered an Early Bird. For this research purposes, both Early/Late Bird times would be referred as an Early Bird time (*EBt*). A Late Bird time will be considered as negative whereas an Early Bird time will be taken as a positive *EBt*.

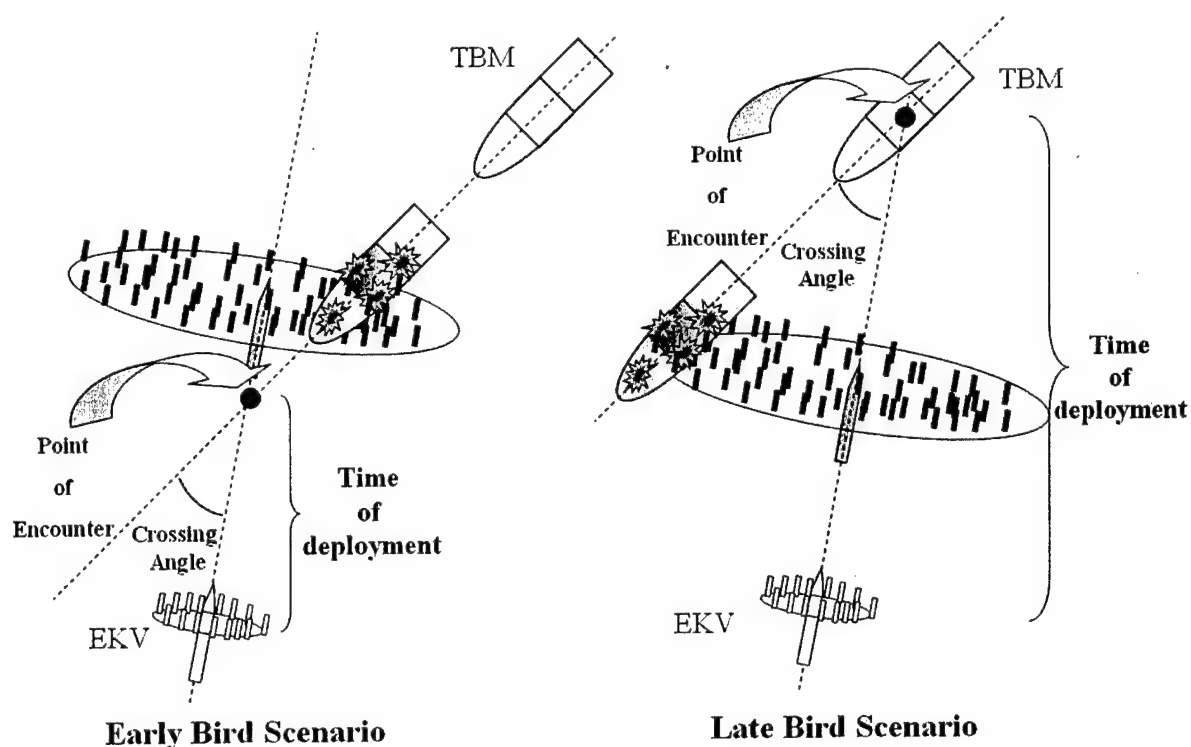


Figure 3.2. Schematic of a Near Miss Encounter Configuration: Early/Late Bird time

The Endgame Simulations were run for a comprehensive range of the near-miss variables, *EBt*, *CA*, and *MD*. A single encounter configuration contains only one value of each near-miss variable. Table 3.1 shows the values used for the *EBt*, *CA*, and *MD*.

Table 3.1. Encounter Configuration Parameters.

Encounter Configuration Variables	Minimum Value	Increment	Maximum Value
<i>EBt</i> (Early Bird Time) (Seconds)	-0.012	0.003	0.012
<i>CA</i> (Crossing Angle) (degrees)	0	15	165
<i>MD</i> (Miss Distance) (meters)	1.0	0.5	6.0

3.3 EKV Modeling

The EKV missile is modeled using an isotropic jellyroll warhead configuration. This configuration was selected because it can be modeled with ease as compared to an aimed or an isotropic center core configuration. Both aimed and center core designs would require a more complex modeling of the projectile deployment mechanics from the

EKV than a jellyroll configuration. A front and side view of a two bay isotropic jellyroll warhead configuration is depicted in Figure 3.3. A bay is a complete transversal array of alternating rings of explosive, buffer, and projectiles.

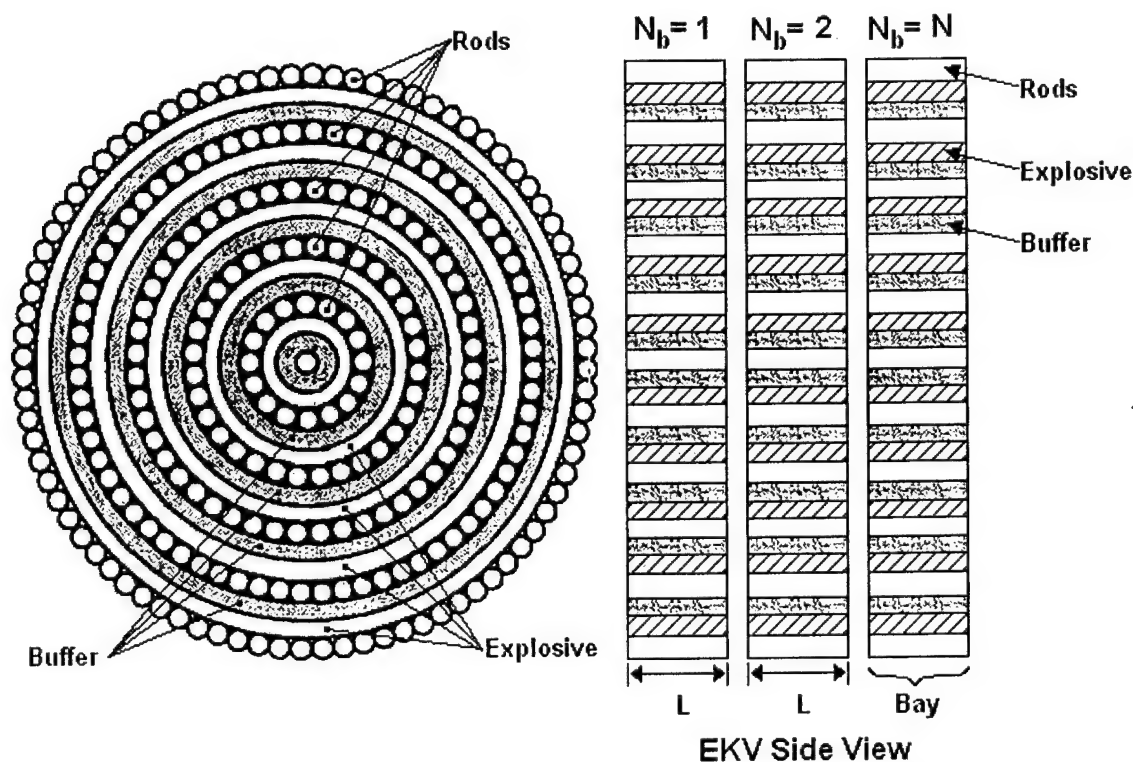


Figure 3.3. Isotropic Jellyroll configuration of KE-rod warheads. (Lloyd R. M. (1998))

3.3.1 Projectile Modeling

Modeling of projectiles in this research was narrowed to only two geometric shapes: cylindrical and spherical rod warheads as illustrated in Figure 3.4.

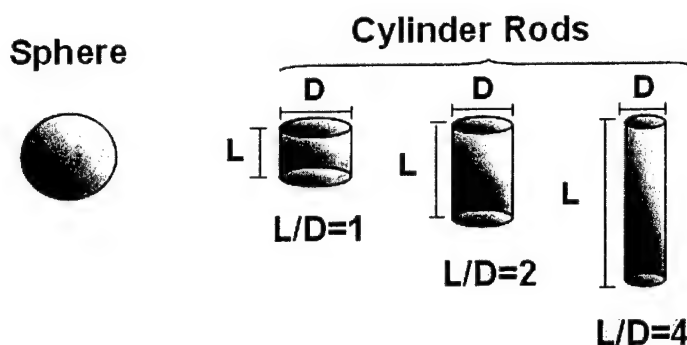


Figure 3.4. Used projectile sizes and shapes.

A constant projectile mass is selected for both a sphere and a cylinder because it permits to compare how inflicted damage at the TBM changes at different projectile shapes. Using a constant projectile mass, m , and the density of the material selected, ρ , the dimensions for both the cylinders and spheres are calculated. The mass and the density are related to the volume by $V = m/\rho$. The volume for a sphere and a cylinder is calculated using $V = 4/3\pi r^3$ and $V = \pi r^2 h$ respectively. Equating the definition of the volume in terms of the mass and density to the equation of the volume for sphere and solving for the radius yields

$$r_s = \left(\frac{3m}{4\pi\rho} \right)^{\frac{1}{3}} \quad (3.1)$$

Using the same procedure, the equation for the cylinder radius is obtained introducing into the equation the L/D ratio of the cylinder. Substituting the diameter for the radius yields $L = 2rL/D$. Inserting L in place of h in the cylinder equation and solving for the radius yields

$$r_c = \left(\frac{m}{2\pi\rho L/D} \right)^{\frac{1}{3}} \quad (3.2)$$

The length of the cylinder is calculated by multiplying the L/D ratio by $2r_c$.

A high-density projectile made of tungsten with mass of 15 gr with L/D ratios of 1, 2, and 4 for the cylinder was selected to perform the simulations. Tungsten was the material selected because its density is high as compared with other materials such as steel or copper and permits the delivery of more mass towards the TBM. Formulas (3.1-3.2) were used to calculate the parameters of the projectile geometry for each shape and size. Listed in Table 3.2 are the descriptive parameters used for the selected projectile shapes and material.

Table 3.2. Projectile descriptive parameters

Geometry	Parameters		
	<i>L/D</i>	Diameter (cm)	Length (cm)
Sphere	N/A	1.176300	N/A
	1	1.027613	1.027613
Cylinder	2	0.815717	1.631234
	4	0.647355	2.589422
Material: Tungsten			
Density: 17.6 (gr/cm ³), Mass: 15 gr			

3.3.2 Projectile Ejection Velocity

Initial radial ejection velocity of projectiles for an isotropic jellyroll configuration is predicted using a modified version of the Gurney's equation for isotropic center core configurations (see Equation (2.1)). This modified equation is expressed as a function of the layer radius where the projectile is located and assumes a constant velocity for each projectile located in the same layer.

$$V_{rp} = \sqrt{2E} \left[\frac{C/M}{\frac{1}{2} \left(1 + \frac{C}{M} \right)} \right]^{\frac{1}{2}} \left(\frac{r_a}{R_o} \right) \quad (3.3)$$

where the value of the Gurney constant, $\sqrt{2E}$, was taken as 7200 ft/s based on an estimate given by (Lloyd R. M. (1998)). This equation assumes perfect dimensions of the buffer and explosive thicknesses as well as the diameter of the rods throughout the EKV, which is not always the case. The "Endgame Simulations" were run assuming coefficients of variation of 0.0, 0.10, 0.25, 0.50, and 0.75 in the radial ejection velocity to take into account the imperfections that appear in the EKV fabrication.

3.3.3 Projectile Tumbling

After the projectiles have been deployed from the EKV, they start to tumble in different directions, as shown in actual experiments (Lloyd R. M. (2000)) in Figure 3.5.

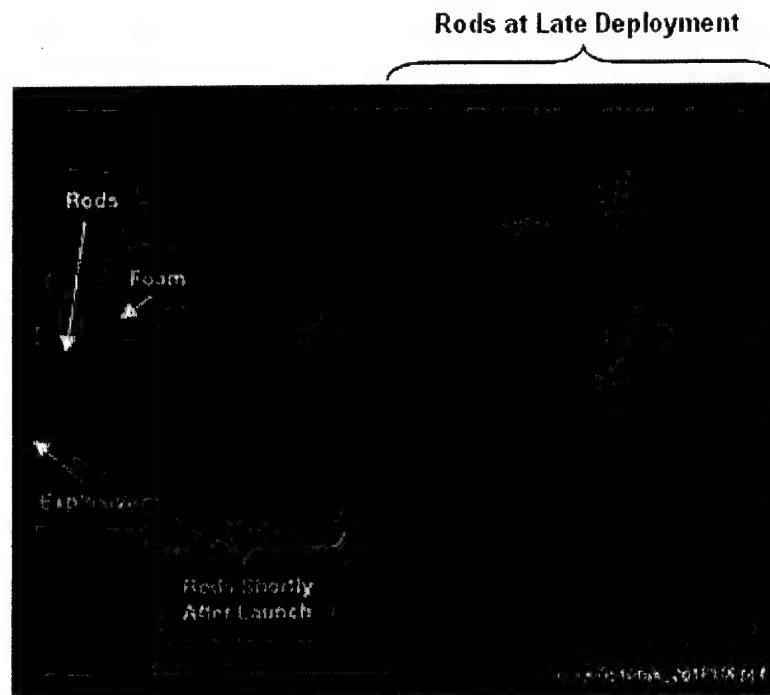


Figure 3.5. Rod deployment demonstrating tumbling after ejection. (Lloyd R. M. (2000))

The projectile tumbling makes the projectiles impact the TBM in angles that are not aligned with the velocity vector. This phenomenon decreases the penetration potential of the projectiles (Li K. *et al.* (1996) and Li K. *et al.* (1997)) and, consequently, the damage inflicted on the TBM. Tumbling effects are modeled using a deployment angular velocity, ω , that rotates the projectile about a vector as shown in Figure 3.6.

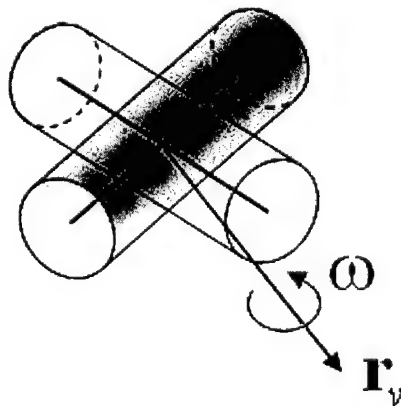


Figure 3.6. Schematic of tumbling rotating vector

In order to randomize projectile tumbling in all directions, a random value using a normal distribution is generated for the deployment angular velocity and the direction cosines of the rotation vector for each projectile. The "Endgame Simulations" in this work were run in two configurations: with projectile tumbling and without projectile tumbling. It is important to note that tumbling effects are not necessary for spherical projectiles. Tumbling effects were assumed with a mean angular velocity, ω , of 200 rad/s only for cylindrical projectiles.

3.3.4 Jellyroll Warhead Design

In order to make a comparison between different projectile sizes and shapes, such as L/D s of 1, 2, and 4 or spheres, the amount of total warhead mass has to be maintained constant. This will provide a benchmark to compare spheres against cylinders or different sizes of cylinders. From a constant mass warhead, the number of warhead layers per bay (a layer consists of two rings of buffer, one ring of explosive material between the two rings of buffer, and a ring of rods), N_w , the number of bays, N_b , the buffer thickness, t_b , and the warhead outer radius, R_o , are calculated to fit the number of rods inside the EKV as the shape and size of the projectiles changes using an optimization function with limit values for each variable shown in Table 3.3. Figure 3.7 shows the design parameters of a jellyroll warhead.

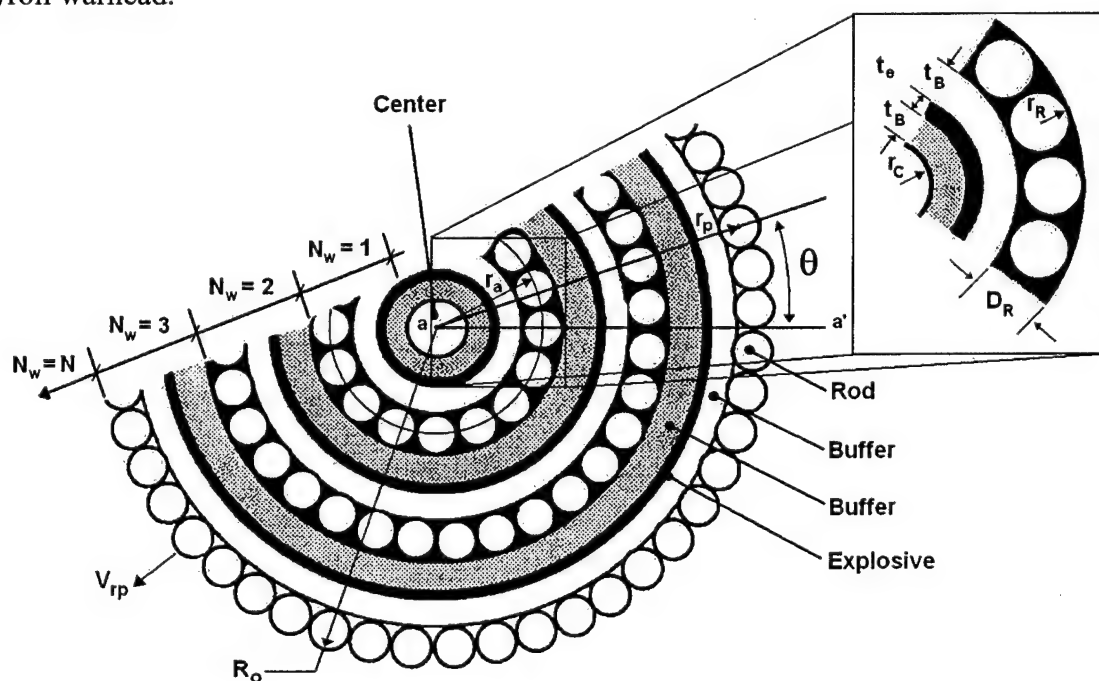


Figure 3.7. Design parameters of an Isotropic Jellyroll warhead (Lloyd R. M. (1998))

Table 3.3. Limit values for optimization code for EKV design variables.

Parameter	Value		Description
	Minimum Value	Maximum Value	
N_w	1	20	Number of layer per bay
N_b	1	4	Number of bays in EKV
t_B	0.001 cm	0.1 cm	Buffer thickness
R_o	0.1 cm	0.5 cm	EKV outer radius

After the four variables mentioned above have been estimated, the explosive thickness, t_e , is calculated using the following equation.

$$t_e = \frac{R_o - [(N_w + 0.5)D_R]}{N_w} - (2t_B) \quad (3.4)$$

The total number of rods, N_R , is approximated by dividing the circumference of a layer, C_w , with radius r_a by the diameter of rods D_r . The number of rods as a function of the warhead layer radius is

$$N_R(r_A) = \frac{C_w}{D_R} = \frac{2\pi r_A}{D_R} \quad (3.5)$$

where the radius of each concentric layer defined as a function of layer number is

$$r_A(N_w) = [r_C + (N_w - 1)(t_B + t_E + t_B + D_R) + (t_B + t_E + t_B)] \quad (3.6)$$

Substituting Equation (3.6) in (3.5) yields the number of rods as a function of layer number.

$$N_R(N_w) = \frac{2\pi}{D_R} [r_C + (N_w - 1)(t_B + t_E + t_B + D_R) + (t_B + t_E + t_B)] \quad (3.7)$$

The total number of rods is simply the summation of the rods calculated for each warhead layer in the EKV. In this manner, the total number or projectiles is a function of the number or layers which was estimated from a constant warhead mass defined as

$$N_R(N_w) = \sum_{N_w=1}^N \frac{2\pi}{D_R} [r_C + (N_w - 1)(t_B + t_E + t_B + D_R) + (t_B + t_E + t_B)] \quad (3.8)$$

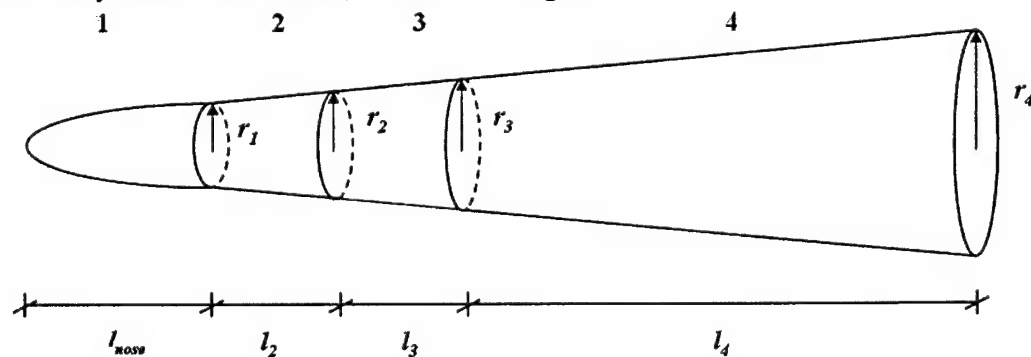
Each projectile location inside the EKV array will be defined by its distance from the EKV center r_p and angle θ , measured always from line segment a-a' (see Figure 3.7). The EKV design parameters, listed in Table 3.4, were arbitrarily chosen since there is no public domain information of typical EKV warheads.

Table 3.4. Final descriptive parameters of EKV design.

Parameter	Value				Description
M	30 Kg				Total warhead mass
C/M	0.01				Explosive charge to mass ratio
ρ_e	1.7 gr/cm ³				Explosive density
	Sphere	LD = 1	LD = 2	LD = 4	
N _w	10	10	10	10	Number of layer per bay
N _b	2	2	2	2	Number of bays in EKV
t _B (cm)	1.07875	0.92705	0.73580	0.58401	Buffer thickness
t _e (cm)	0.07014	0.09191	0.07295	0.05790	Explosive thickness
R _o (cm)	0.34627	0.30250	0.24009	0.19056	EKV outer radius

3.4 TBM Modeling

Different geometric shapes in three dimensions can be used to model actual TBMs as the ones presented in Figures 2.2, 2.3, 2.4, and 2.5. The TBM was divided into four segments with a geometric shape assigned to each one. This allows placing the warhead of the TBM in one of the sections. Two different shapes were selected to model the TBM. The missile nose section is modeled using an ellipsoid and the following sections are modeled using cylinders acting as truncated cones if the radiuses of each section vary across the missile, as shown in Figure 3.8.

**Figure 3.8.** TBM representation in Endgame Simulations.

The TBM sections are modeled as using the quadric surface formulas for the ellipse and truncated cone

$$\frac{(x_1)^2}{r^2} + \frac{(x_2)^2}{r^2} + \frac{(x_3 - l_{nose})^2}{l_{nose}^2} = 1 \quad (3.9)$$

where l_{nose} and r are the length and the radius of the nose section of the TBM and

$$(x_1)^2 + (x_2)^2 = \left[m(x_3 - x_3')^2 + r'^2 \right] \quad (3.10)$$

where x_3^I and r^I are the location and radius of the first circle and m is the slope between the two circles of the truncated cone.

A schematic of these two surfaces with its parameters is illustrated in Figure 3.9.

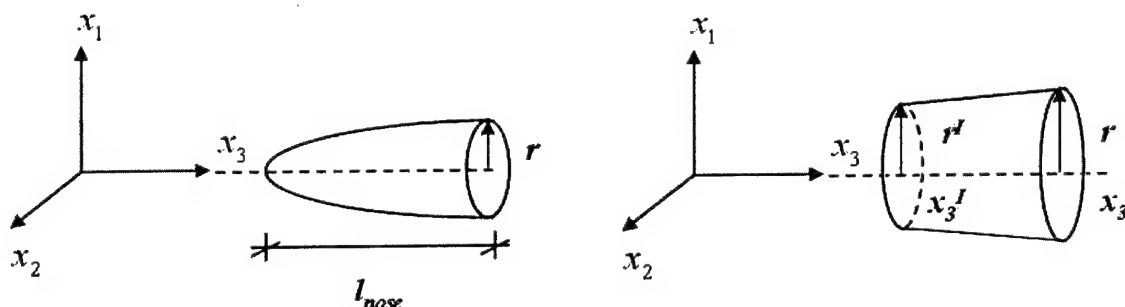


Figure 3.9. Schematic of geometric surfaces used to model the TBM sections

Table 3.5 lists the parameters used to model the TBM surface along with the shape used in each section and the section where the warhead was located.

Table 3.5. TBM descriptive parameters.

Section Number	Section	Shape-Type	Length (m)	Radii at end of section (m)
1	Nose	Ellipsoid	2.0	0.500
2	--	Truncated Cone	1.5	0.546
3	Warhead	Truncated Cone	1.5	0.592
4	Aft	Truncated Cone	5.0	0.750

3.5 Endgame Kinematics Analysis

Studies of KE-rod warhead lethality require a geometric analysis of the terminal encounter trajectories between the EKV and TBM missiles in space in order to find the optimum values of the near miss variables where the different projectile shapes inflict more damage. Consider the EKV/TBM encounter configuration depicted in Figure 3.10 at time $t=0$ at the instant when the EKV projectiles are ejected. The EKV and TBM missile trajectories represented as dashed lines, with local independent fixed right handed coordinate systems **E** and **T** have their origins at the EKV and TBM missile noses respectively. The systems **E** and **T** do not move with the missiles but are fixed in space at the position they had at time $t=0$.

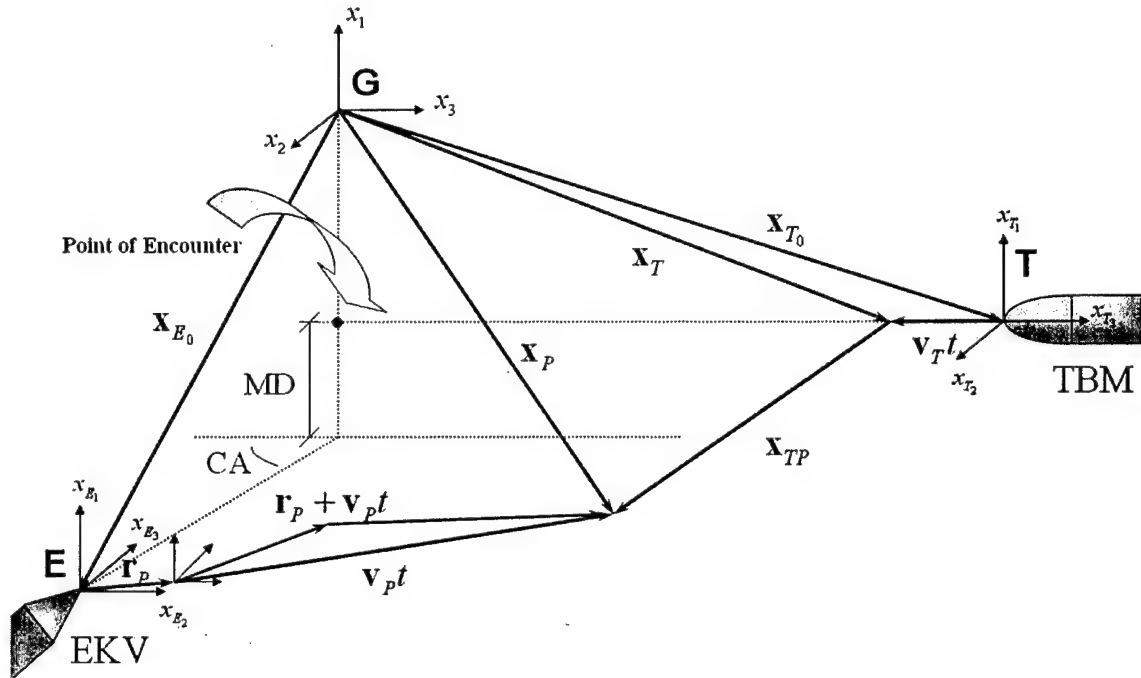


Figure 3.10. Terminal Encounter Kinematic Analysis

From fixed global right handed coordinate system \mathbf{G} located at an arbitrary fixed point, vectors \mathbf{x}_{E_0} and \mathbf{x}_{T_0} define the position of the coordinate systems \mathbf{E} and \mathbf{T} . In other words, vectors \mathbf{x}_{E_0} and \mathbf{x}_{T_0} are the position vectors of the nose of both missiles at time $t=0$ (at the instant when the projectiles in the EKV are ejected). With respect to system of coordinates \mathbf{E} , vectors \mathbf{r}_p and $\mathbf{v}_p t$ are used to specify the position of each projectile ejected from the EKV. Position vector \mathbf{r}_p describes the position of the projectile inside the EKV before it is ejected. Vector \mathbf{v}_p is the projectile velocity vector and is the resultant of the EKV and ejection velocity vectors. In the same manner, vector $\mathbf{v}_T t$ is the TBM velocity vector multiplied by the time to define its position in coordinate system \mathbf{T} . Position vectors \mathbf{x}_p and \mathbf{x}_T specify the trajectories of the projectiles and the TBM respectively in the global system of coordinates \mathbf{G} as a function of time and are defined as

$$\mathbf{x}_p = \mathbf{x}_{E_0} + \mathbf{R}_{E/G} \{ \mathbf{r}_p + \mathbf{v}_p t \} \quad (3.11)$$

$$\mathbf{x}_T = \mathbf{x}_{T_0} + \mathbf{R}_{T/G} \{ \mathbf{v}_T t \} \quad (3.12)$$

where $\mathbf{R}_{E/G}$ and $\mathbf{R}_{T/G}$ are the transformation matrices from local systems of coordinates \mathbf{E} and \mathbf{T} to global system of coordinates \mathbf{G} . The position vector of the projectile with

respect to the TBM in global coordinates, designated as \mathbf{x}_{TP} , is $\mathbf{x}_{TP} = \mathbf{x}_P - \mathbf{x}_T$. Substituting equations (3.11) and (3.12) into vector \mathbf{x}_{TP} yields

$$\mathbf{x}_{TP} = \mathbf{x}_P - \mathbf{x}_T = \mathbf{x}_{E_0} - \mathbf{x}_{T_0} + \mathbf{R}_{E/G} \{ \mathbf{r}_P + \mathbf{v}_P t \} - \mathbf{R}_{T/G} \{ \mathbf{v}_T t \} \quad (3.13)$$

The vector defining the position of the projectiles in TBM local coordinates \mathbf{T} is simply $\mathbf{x}_{TP/T} = \mathbf{R}_{G/T} \mathbf{x}_{TP}$. Substituting equation (3.13) into $\mathbf{x}_{TP/T} = \mathbf{R}_{G/T} \mathbf{x}_{TP}$ yields

$$\mathbf{x}_{TP/T} = \mathbf{R}_{G/T} \mathbf{x}_{TP} = \mathbf{R}_{G/T} \{ \mathbf{x}_{E_0} - \mathbf{x}_{T_0} \} + \mathbf{R}_{G/T} \mathbf{R}_{E/G} \{ \mathbf{r}_P + \mathbf{v}_P t \} - \mathbf{v}_T t \quad (3.14)$$

where $\mathbf{R}_{G/T}$ is the transformation matrix from global system \mathbf{G} to local system \mathbf{T} . Expanding and rearranging the terms of equation (3.14) yields the following equations,

$$\mathbf{x}_{TP/T} = \mathbf{R}_{G/T} \mathbf{x}_{TP} = \mathbf{R}_{G/T} \{ \mathbf{x}_{E_0} - \mathbf{x}_{T_0} \} + \mathbf{R}_{E/T} \{ \mathbf{r}_P + \mathbf{v}_P t \} - \mathbf{v}_T t \quad (3.15)$$

$$\mathbf{x}_{TP/T} = \mathbf{R}_{G/T} \{ \mathbf{x}_{E_0} - \mathbf{x}_{T_0} \} + \mathbf{R}_{E/T} \mathbf{r}_P + \{ \mathbf{R}_{E/T} \mathbf{v}_P - \mathbf{v}_T \} t \quad (3.16)$$

If we let,

$$\mathbf{x}_o = \mathbf{R}_{G/T} \{ \mathbf{x}_{E_0} - \mathbf{x}_{T_0} \} + \mathbf{R}_{E/T} \mathbf{r}_P \quad (3.17)$$

and

$$\mathbf{a} = \{ \mathbf{R}_{E/T} \mathbf{v}_P - \mathbf{v}_T \}, \quad (3.18)$$

vector $\mathbf{x}_{TP/T}$, which is the projectile's position vector (trajectory) with respect to the TBM, can be expressed in parametric form as

$$\mathbf{x}_{TP/T} = \mathbf{x}_o + \mathbf{a}t \quad (3.19)$$

This equation defines the time-dependent position of each projectile ejected from the EKV with respect to the nose of the TBM. To identify the location at which each projectile impacts the surface of the TBM, the intersection between the projectile position vector and the TBM surface has to be determined.

If we take Equations (3.9-3.10), which models the TBM surface, and substitute the components of the parametric Equation (3.19) yields

$$\frac{(x_{o_1} + a_1 t)^2}{r^2} + \frac{(x_{o_2} + a_2 t)^2}{r^2} + \frac{(x_{o_3} + a_3 t - l_{nose})^2}{l_{nose}^2} = 1 \quad (3.20)$$

$$(x_{o_1} + a_1 t)^2 + (x_{o_2} + a_2 t)^2 = \left[m(x_{o_3} + a_3 t - x_3')^2 + r'^2 \right] \quad (3.21)$$

for the ellipsoidal and the cylindrical surfaces respectively. Expanding and rearranging terms yield the following equations

$$\left[(a_1)^2 + (a_2)^2 + \frac{(a_3)^2 r^2}{l_{nose}^2} \right] t^2 + \left[2x_{o_1} a_1 + 2x_{o_2} a_2 + \frac{2(x_{o_3} - l_{nose}) a_3 r^2}{l_{nose}^2} \right] t + \left[(x_{o_1})^2 + (x_{o_2})^2 + \frac{(x_{o_3} - l_{nose})^2 r^2}{l_{nose}^2} - r^2 \right] = 0 \quad (3.22)$$

$$\left[(a_1)^2 + (a_2)^2 - m^2 (a_3)^2 \right] t^2 + \left[2x_{o_1} a_1 + 2x_{o_2} a_2 - 2m^2 (x_{o_3} - x_3') a_3 - 2ma_3 r' \right] t$$

$$\left[(x_{o_1})^2 + (x_{o_2})^2 - m^2(x_{o_3} - x_3')^2 - 2m(x_{o_3} - x_3')r' - (r')^2 \right] = 0 \quad (3.23)$$

If we let

$$\begin{aligned} C_1 &= \left[(a_1)^2 + (a_2)^2 + \frac{(a_3)^2 r^2}{l_{nose}^2} \right] \\ C_2 &= \left[2x_{o_1}a_1 + 2x_{o_2}a_2 + \frac{2(x_{o_3} - l_{nose})a_3 r^2}{l_{nose}^2} \right] \\ C_3 &= \left[(x_{o_1})^2 + (x_{o_2})^2 + \frac{(x_{o_3} - l_{nose})^2 r^2}{l_{nose}^2} - r^2 \right] \end{aligned}$$

for the ellipsoid equation (Equation 3.22) and

$$\begin{aligned} C_1 &= \left[(a_1)^2 + (a_2)^2 - m^2(a_3)^2 \right] \\ C_2 &= \left[2x_{o_1}a_1 + 2x_{o_2}a_2 - 2m^2(x_{o_3} - x_3')a_3 - 2ma_3 r' \right] \\ C_3 &= \left[(x_{o_1})^2 + (x_{o_2})^2 - m^2(x_{o_3} - x_3')^2 - 2m(x_{o_3} - x_3')r' - (r')^2 \right] \end{aligned}$$

for the cylinder equation (Equation 3.23), both Equations (3.22 and 3.23) can be represented as a quadratic equation of the form $C_1 t^2 + C_2 t + C_3 = 0$. Solving for t yields the time it takes each projectile to intersect the TBM surface (t_i). Then, substituting the time of intersection t_i into Equation (3.19) would define the position at which the projectile impacts the TBM.

$$\mathbf{x}_i = \mathbf{x}_o + \mathbf{a}t_i \quad (3.24)$$

The series of equations, described above, for the kinematics analysis of the projectiles impacting the TBM were developed assuming arbitrary coordinate systems **E**, **T** and **G**. Now, let the origin and orientation of these systems be defined as depicted in Figure 3.11. Distance D_T is the distance from the TBM nose and the origin of coordinate system **G**. Distance D_E is measured from the nose of the EKV to the projection of the origin of **G** onto the $x_{E_2} - x_{E_3}$ plane. Both of these distances are given at the moment the projectiles in the EKV are ejected. Recalling Section 3.2, near miss encounter variables, miss distance and crossing angle, are defined as the perpendicular distance between the two missile trajectory projections (MD) and the angle formed between line segment D_E and the negative axes x_3 from system **G** (CA).

For this configuration the transformation matrices in equations 3.11 and 3.12 become,

$$\mathbf{R}_{E/G} = \begin{bmatrix} 1 & 0 & 0 \\ 0 & \cos(CA) & -\sin(CA) \\ 0 & \sin(CA) & \cos(CA) \end{bmatrix} \quad (3.25)$$

and

distance from axes x_{E_3} , r_p , and angle θ measured always counterclockwise from projection of axes x_{E_2} inside the EKV. Therefore, vectors \mathbf{r}_p and \mathbf{v}_p can be expressed as,

$$\mathbf{r}_p = r_p \sin(\theta) \mathbf{i}_{E_1} + r_p \cos(\theta) \mathbf{i}_{E_2} - D_p \mathbf{i}_{E_3} \quad (3.30)$$

$$\mathbf{v}_p = V_{rp} \sin(\theta) \mathbf{i}_{E_1} + V_{rp} \cos(\theta) \mathbf{i}_{E_2} + V_E \mathbf{i}_{E_3} \quad (3.31)$$

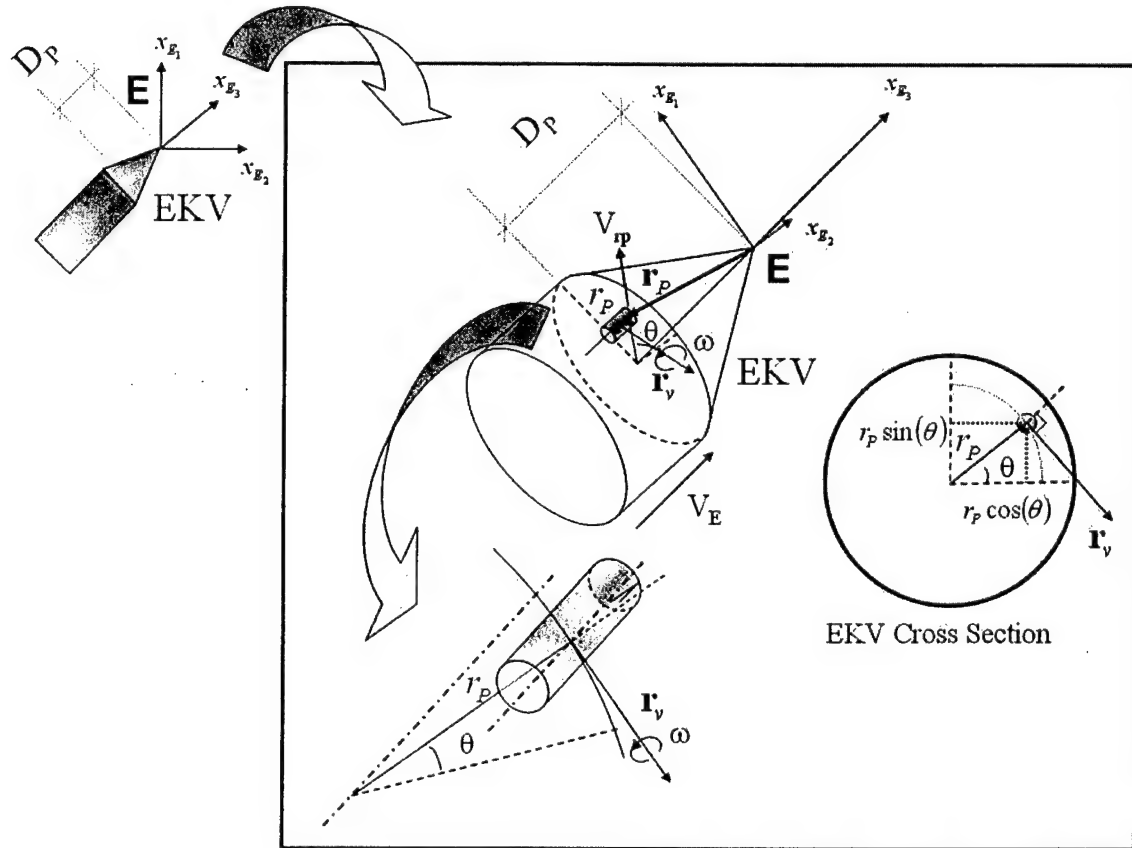


Figure 3.12. Projectile visualization in E system of Coordinates.

The equations described above can be used to identify the point of impact of each one of the EKV projectiles on the TBM surface if the distances D_E and D_T are known. It is expected that the case where both missiles reach the point of intersection of their trajectories at the same time would produce a larger number of projectile impacts than the case where one of the projectiles is ahead of the other. In "Endgame" terminology the case where the EKV is ahead of the TBM is called an "Early Bird Encounter" and is usually characterized in terms of time (see Figure 3.13). Furthermore, the point at which the projectiles are ejected from the EKV has a significant effect on the number of projectiles that will impact the TBM. If the projectiles are not ejected at an appropriate time, the projectiles could completely miss the TBM. The moment at which the

projectiles have to be ejected will be a function of the missiles velocity, crossing angle, miss distance and whether the encounter is an early or late bird. To identify the most appropriate moment of ejection, the distances D_E and D_T need to be expressed in terms of time. Let Δt be defined as the time it would take the TBM to reach the origin of **G** from the moment the projectiles in the EKV are ejected, and EB_t as the early bird time which defines the time the EKV is ahead of the TBM from reaching the intersection of the missiles trajectories at the moment the projectiles are ejected from the EKV, then,

$$D_E = (\Delta t - EB_t)V_E \quad (3.32)$$

$$D_T = \Delta t V_T \quad (3.33)$$

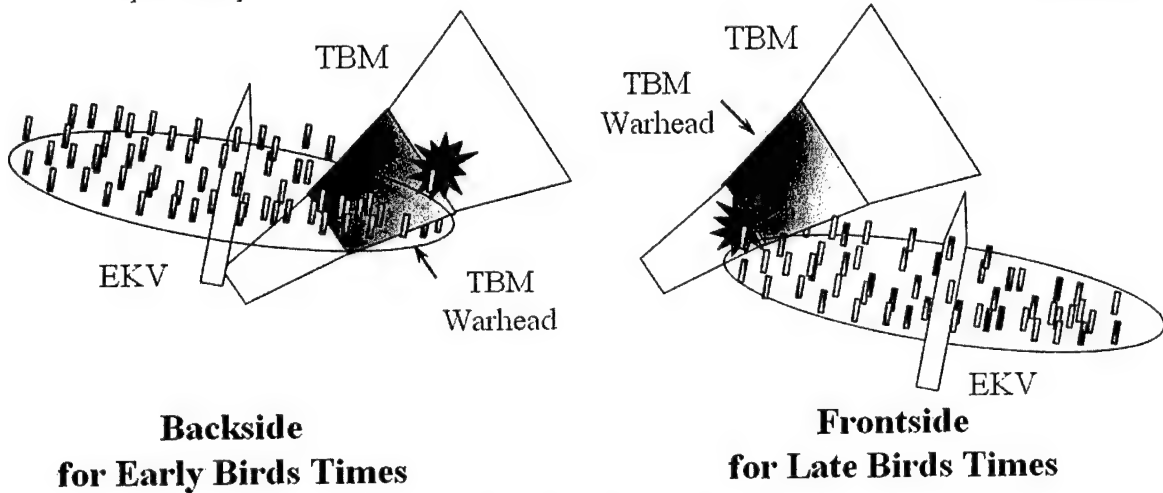


Figure 3.13. Method for optimizing the number of impacts on the TBM.

Substituting equations (3.32-3.33), along with transformations of coordinates (3.25 and 3.26) into equations (3.27 – 3.28) and (3.11-3.12)

$$\mathbf{x}_P = \begin{Bmatrix} -MD \\ (\Delta t - EB_t)V_E \sin(CA) \\ -(\Delta t - EB_t)V_E \cos(CA) \end{Bmatrix} + \begin{Bmatrix} r_p \sin(\theta) + V_{rp} \sin(\theta)t + 0 \\ \left[r_p \cos(\theta) + V_{rp} \cos(\theta)t \right] \cos(CA) - [-D_p + V_E t] \sin(CA) \\ \left[r_p \cos(\theta) + V_{rp} \cos(\theta)t \right] \sin(CA) + [-D_p + V_E t] \cos(CA) \end{Bmatrix} \quad (3.34)$$

$$\mathbf{x}_T = \begin{Bmatrix} 0 \\ 0 \\ V_T(\Delta t - t) \end{Bmatrix} \quad (3.35)$$

These two equations describe the position of a projectile and the TBM nose as a function of time with respect to coordinate system **G**. If we equate these two equations we would obtain a system of three equations and three unknowns (Δt , t and θ) that define

the "aiming parameters" that would produce an impact of a projectile located at a radius r_p on the nose of the TBM. Of course this would be a desired impact if the TBM warhead was located in the nose of the TBM, but this is hardly ever the case. For this reason we need to aim directly at the center of the position of the warhead within the TBM. Let the distance from the nose of the TBM to the center of the warhead be given by D_{tw} , then the position of the warhead as a function of time would be defined by shifting \mathbf{x}_T a distance D_{tw} in the \mathbf{x}_{T3} direction,

$$\mathbf{x}_{TW} = \begin{Bmatrix} 0 \\ 0 \\ V_T(\Delta t - t) + D_{tw} \end{Bmatrix} \quad (3.36)$$

Equating equations (3.34) and (3.36) yields the following three simultaneous equations that can be solved for Δt , t and θ ,

$$-MD + r \sin(\theta) + V_{rp} t \sin(\theta) = 0 \quad (3.37)$$

$$\begin{aligned} (\Delta t - EBt)V_E \sin(CA) + r \cos(\theta) \cos(CA) + V_{rp} t \cos(\theta) \cos(CA) \\ + D_p \sin(CA) - V_E t \sin(CA) = 0 \end{aligned} \quad (3.38)$$

$$\begin{aligned} -(\Delta t - EBt)V_E \cos(CA) + r \cos(\theta) \sin(CA) + V_{rp} t \cos(\theta) \sin(CA) \\ - D_p \cos(CA) + V_E t \cos(CA) - V_T \Delta t + V_T t - D_{tw} = 0 \end{aligned} \quad (3.39)$$

Once Δt is calculated distances D_E and D_T can be determined and the impact location of all projectiles ejected from the EKV onto the TBM can be determined using equation (3.24)

3.6 Impact Characterization

Recognizing that the multiple successful projectiles hit the surface of the TBM at different points of impact (poi), and that the geometry of the TBM surface varies throughout its entire length, an impact characterization was conducted to identify the strike angle of each impact, as well as the spatial orientation of cylindrical projectiles, and the relative impact velocity at which the projectiles hit the TBM surface.

Once the projectile has impacted the TBM, a plane tangent to the point of impact of the projectile in the TBM is defined by calculating the gradient of Equations (3.9-3.10) in function form

$$f(x_1, x_2, x_3) = \frac{(x_1)^2}{r^2} + \frac{(x_2)^2}{r^2} + \frac{(x_3 - l_{nose})^2}{l_{nose}^2} - 1 \quad (3.40)$$

$$f(x_1, x_2, x_3) = (x_{o_1} + a_1 t)^2 + (x_{o_2} + a_2 t)^2 = \left[m(x_{o_3} + a_3 t - x_3')^2 + r'^2 \right]^2 \quad (3.41)$$

and defined by

$$\nabla f(x_1, x_2, x_3) = \frac{2x_1}{r^2} \mathbf{i}_1 + \frac{2x_2}{r^2} \mathbf{i}_2 + \frac{2(x_3 - l_{nose})}{l_{nose}^2} \mathbf{i}_3 \quad (3.42)$$

$$\nabla f(x_1, x_2, x_3) = 2x_1 \mathbf{i}_1 + 2x_2 \mathbf{i}_2 - 2 \left[m(x_3 - x_3')^2 + r'^2 \right] \left[2m(x_3 - x_3') \right] \mathbf{i}_3 \quad (3.43)$$

The origin of this plane is the point of impact defined in Figure 3.14. Two orthogonal planes are defined at the point of impact; 1) a tangent plane (X-Y) to the point of impact, and 2) a normal plane (X-Z) orthogonal to (X-Y) containing a vector normal to the TBM' surface at the point of impact and the resultant relative impact velocity. The X axis is defined in terms of the horizontal projection of the resultant relative impact velocity to the tangent plane (X-Y) with positive sense in the direction of the horizontal component. The Z axis is aligned with the vector normal to the point of impact with positive direction in opposite direction to the vertical component of the resultant relative impact velocity. The Y axis is therefore orthogonal to the aforementioned axis according to the right-hand rule.

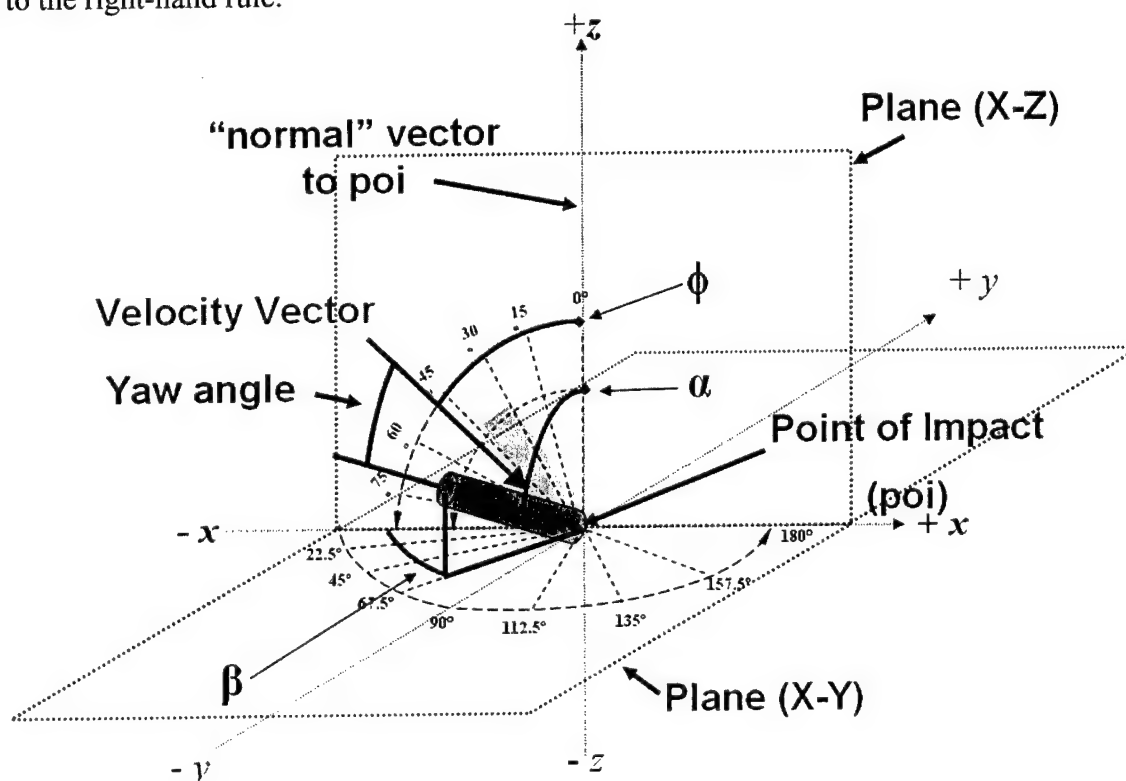


Figure 3.14. Definition of strike and spatial orientation angles

The following are definitions adopted for each characterization parameter. The strike angle (ϕ) is defined as the angle between the resultant relative impact velocity vector and the vector normal to the surface at the point of impact (Z axis) with positive

rotation sense following the right-hand rule. The spatial orientation of a cylindrical projectile is defined by two angles α and β :

- α is the angle between the projectile' longitudinal axis and the positive Z axis, and;
- β is the angle between the projectile' longitudinal axis and the negative $-X$ axis located at the intersection with the normal and tangent planes

The positive rotation of each angle follows the right-hand rule. Since the sphere's geometry is symmetric in every direction, it does not require spatial orientation characterization. The relative impact velocity is the resultant of the velocity vectors between the projectile and the TBM missile. Its magnitude varies depending on the crossing angle between the missiles.

Tumbling effects are modeled by using vector \mathbf{r}_V which is tangent to the arc describing the radius where the projectile is located and rotates following the right hand rule with an angular velocity ω , as depicted in Figure 3.12. This is a unit vector with respect to system \mathbf{E} that is defined by

$$\mathbf{r}_V = -\cos(\theta)\mathbf{i}_{E_1} + \sin(\theta)\mathbf{i}_{E_2} - 0\mathbf{i}_{E_3} \quad (3.44)$$

This added effect does not interfere with the projectile trajectories; therefore, the number of projectiles impacting the TBM remains the same with or without tumbling effects. However, projectile tumbling affects the orientation in which the projectiles impact the TBM and, consequently, the overall damage of a particular encounter configuration.

3.7 Endgame Simulations

The formulas described previously for the EKV and TBM missile designs and the encounter configuration were implemented in a computer code using MatlabTM 6.5 and batch executed in a dual-processor PC workstation with 2.80 GHz each and 3 GMB of RAM. Besides the tumbling considerations, coefficients of variation (COV) for the initial radial ejection velocity, V_{rp} , of 0.00, 0.10, 0.25, 0.50, and 0.75 were assumed for each configuration and tumbling effect. Endgame simulations with coefficient of variation different from zero were run at 30 iterations for each encounter configuration. This is because a single simulation of the encounter configuration with a COV of 0.50 assumes only one sample of the entire population. A population sample of 30 iterations seems enough for this research mainly due to time constraints.

Table 3.6. Endgame Simulations Configurations.

Projectile Tumbling	Shape	V_{rp} COV	Number of Iterations
Tumbling $\omega = 200$ rad/s	Cylinder	0.00	1
		0.10	30
		0.25	30
No Tumbling $\omega = 0$ rad/s	Cylinder	0.50	30
	Sphere	0.75	30

The code performs the simulations based on the data provided in Tables (3.1-3.6) and follows the steps of the flowchart shown in Figure 3.15.

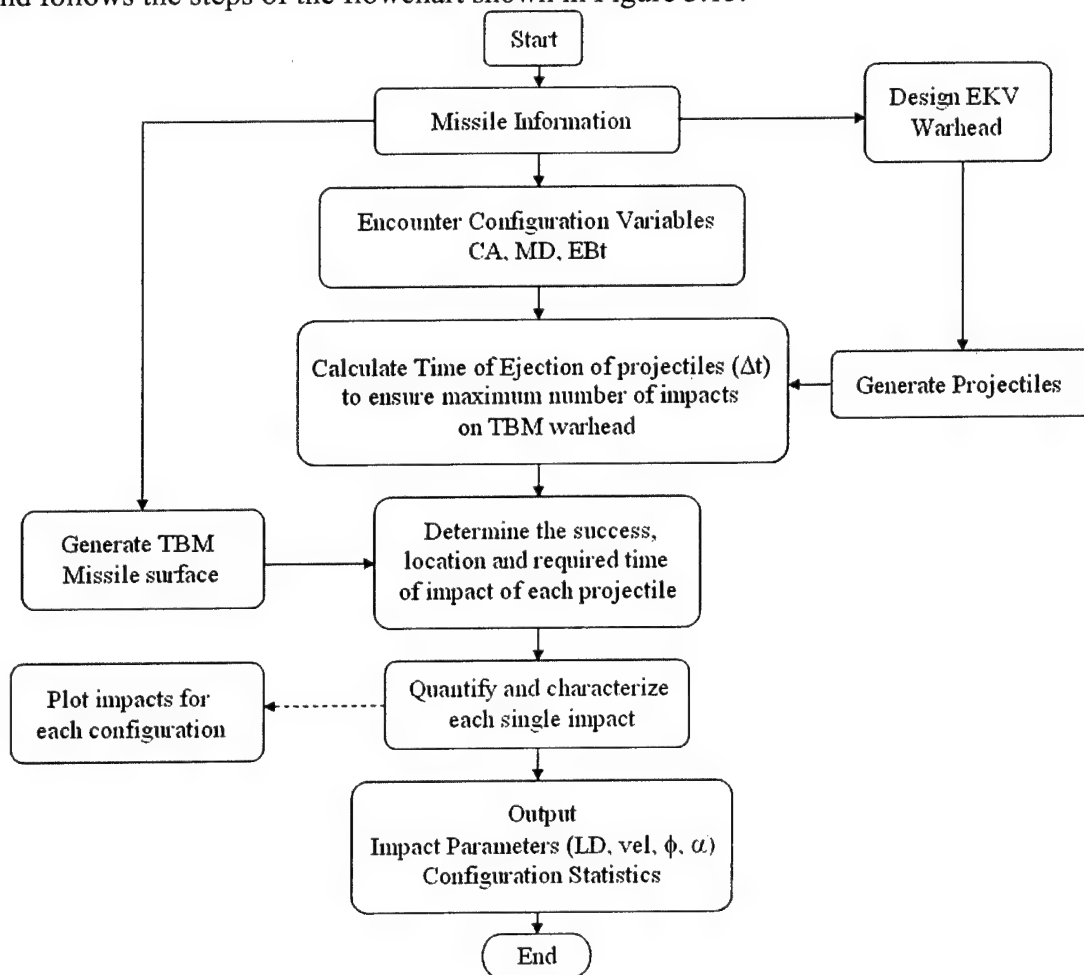


Figure 3.15. Endgame simulation flowchart.

The code is capable to graph three different views of the TBM missile surface with the impact location of each projectile depicting the velocity vector as a ray vector, as illustrated in Figure 3.16.

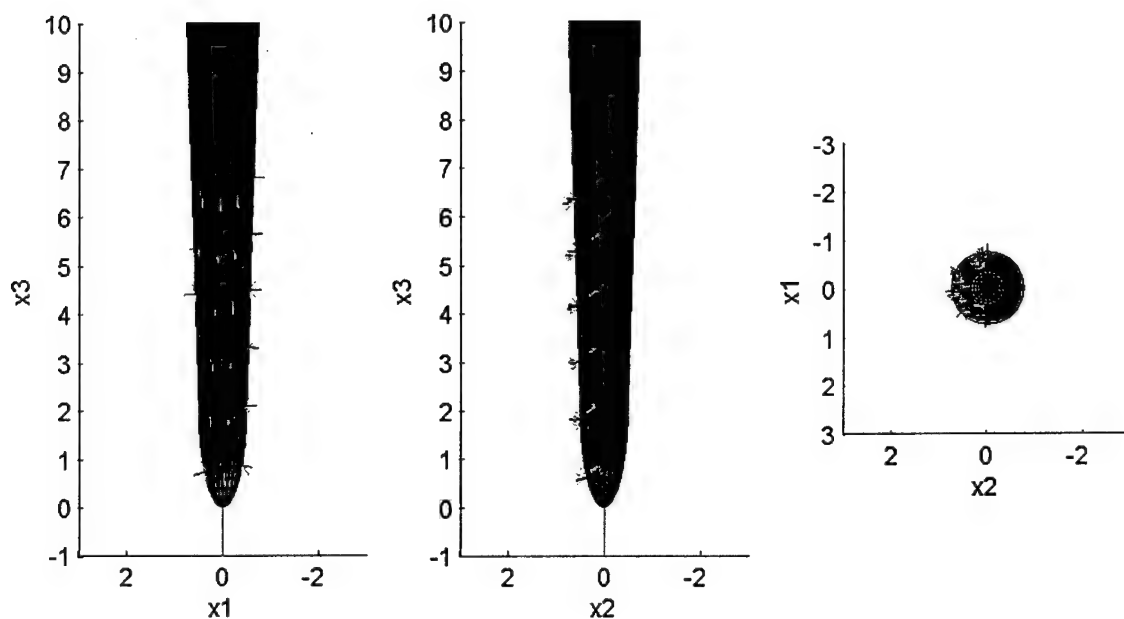


Figure 3.16. Visualization of Endgame simulation results for Encounter Configuration with $CA = 120^\circ$, $EBt = 0.006$ s, and $MD = 4.0$.

3.8 Endgame Simulation Results

The purpose of the endgame simulations is to model the plausible disabling or destruction of the TBM warhead under various specific encounter configuration scenarios with different projectile geometries and sizes, and further recommend endgame conditions or projectile geometry sizes that maximize the lethality of the EKV warhead system. The quantification of impacts on the TBM surface is used as a quantitative measure to assess the effectiveness of the EKV guided-ejection warhead system to some degree. The statistics on the number of projectiles that impact the TBM surface gives some indication of the level of success achieved by the EKV warhead system under a specific encounter configuration scenario for a particular warhead design.

3.8.1 Impact Quantification per Encounter Configuration

Different impact statistics were computed for each encounter configuration scenario, including total number of impacts on the TBM surface as well as number of impacts on the TBM warhead section only. Figure 3.17 is a bar chart that depicts the variation in the frequency of number of impacts along the TBM surface and its warhead section, at a certain encounter configuration scenario of crossing angle and early bird time (CA - EBt) as the miss distance increases.

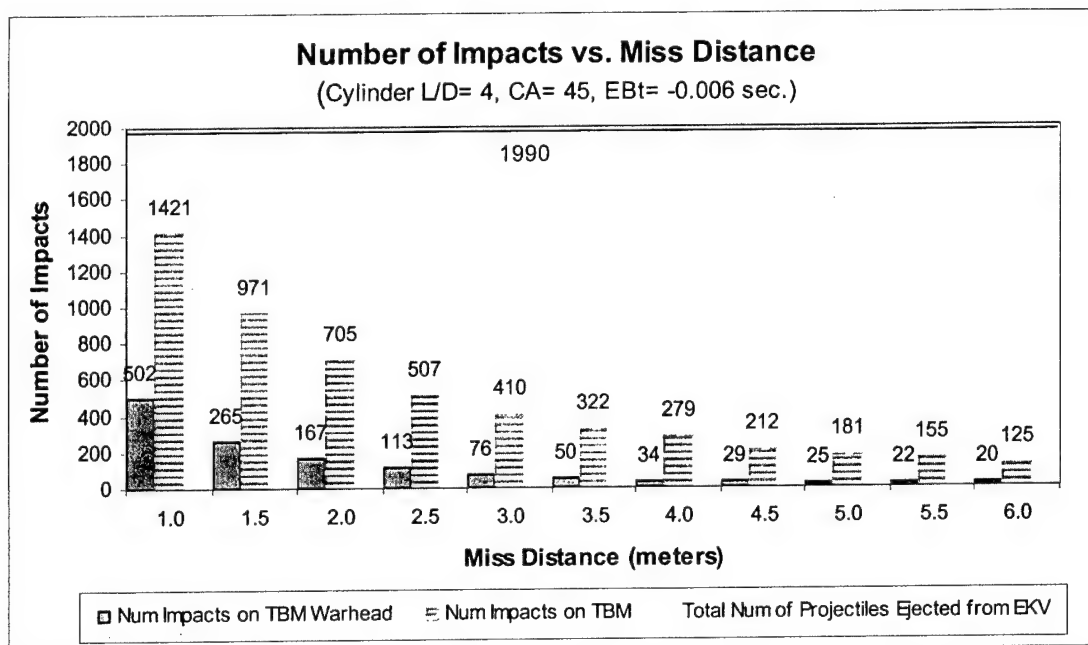


Figure 3.17. Impact Frequencies vs Miss Distance.

From the bar chart it is evident that as the miss distance between the missiles decreases, the number of impacts increases substantially. Similar charts were generated for different encounter configuration scenarios and projectile geometry/sizes, observing similar trends. Another type of chart was generated where the variation in the number of impacts on the TBM warhead is compared against the crossing angle. Figure 3.18 depicts these variations for four miss distances.

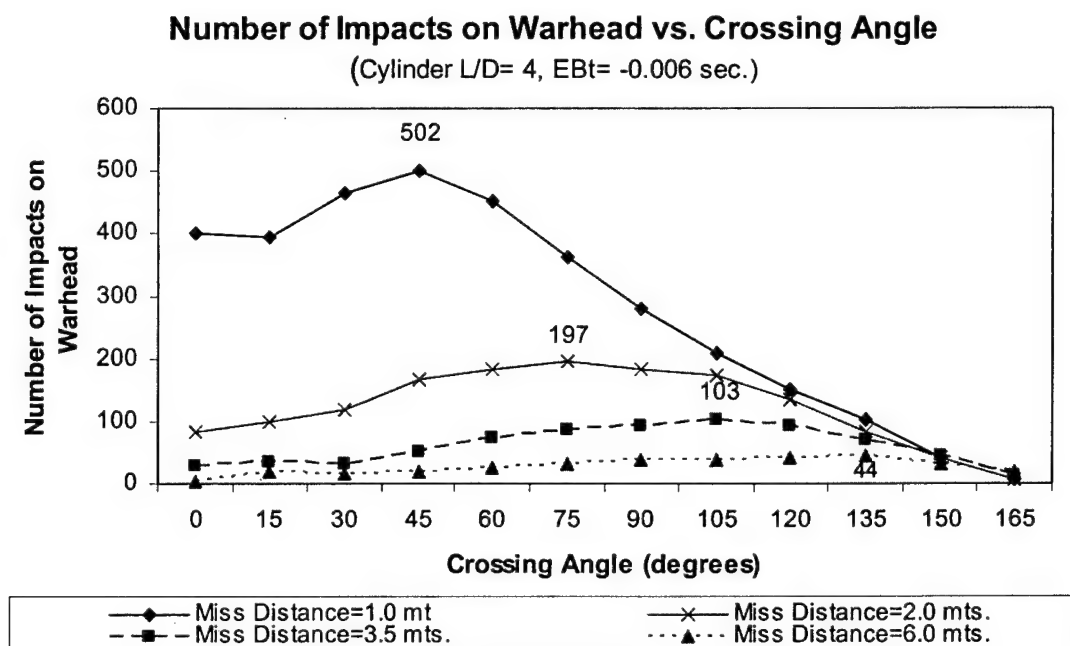


Figure 3.18. Impact Frequencies vs. Crossing Angle.

For the miss distance of 1.0 meter, as the crossing angle increases, the distribution of impacts start at 400 increases to a maximum of 502 at 45° and thereon decreases at an almost constant rate to a minimum occurring at 165°. For the miss distance of 2.0 meters the distribution behaves similarly; however, the maximum of 197 impacts occurs at an angle of 75°. For miss distances of 3.5 and 6.0 meters, the distributions behave similarly, where the maximums of 197 and 44 impacts occur at crossing angles of 105° and 135°, respectively. In every case, the minimum occurs at a crossing angle of 165° with less than 20 impacts. As the miss distance increases from 1.0 to 6.0 meters the parabolic pattern flattens and the peak frequency also shifts towards larger crossing angles. It should be noted that these frequencies correspond to encounter configurations were neither variability in the radial ejection velocity nor tumbling effects were considered.

Similar charts were generated for other early bird scenarios. A similar parabolic pattern was observed in the impact distribution as the crossing angle increases; however, the peak frequencies shift from late bird scenarios to early bird scenarios towards larger crossing angles. At late bird scenarios, the peak occurs between 0° and 45°. At early bird time of -0.003 and 0.000 seconds the peaks occur at 90° and 75°, respectively. In early bird scenarios the highest frequency always occurs at 0°, and then substantially drops. Additional charts were generated for different projectile geometry/sizes, observing similar trends. These charts are not included in this report.

For a comprehensive overview of the distribution of all the impacts on the TBM warhead throughout the entire encounter configuration range, a set of tables were generated for each projectile geometry/size, per encounter configuration parameter.

These set of tables were also generated for projectiles subjected to different deployment conditions, such as different amounts of radial ejection velocity (V_{rp}) variation, as well as with or without tumbling effects. To reduce the number of generated tables per projectile geometry/size, the early-bird time (EBt) parameter was chosen as the first level of classification, resulting in only nine tables per projectile geometry/size/condition. In contrast, selecting any of the other two parameters (CA or MD) would have resulted in twenty to thirty percent more tables per projectile geometry/size/deployment condition.

Table 3.7 shows a typical impact quantification table by encounter configuration consisting of fourteen columns and thirteen rows including the top header row and leftmost header column. From left to right, the table shows the distribution of impacts as the crossing angle (CA) increases from 0° to 165° in increments of 15° . From top to bottom, the tables show the distribution of impacts as the miss distance (MD) increases from 1 to 6 meters in increments of 0.5 meters. The rightmost column shows the total number of impacts per miss distance, and the bottom row shows of the total number of impacts per crossing angle. The sum of sums located at the bottom-right corner is the total number of impacts per early-bird time of that particular projectile geometry/size/deployment condition.

Tables 3.7 through 3.9 illustrate the distribution of impacts throughout the encounter configuration range at an early bird time of -0.006 seconds, for three different projectile geometry/sizes, namely cylindrical projectiles with L/D of 4 and 1 and for a spherical projectile of the same mass. These impact frequencies are obtained from scenarios without tumbling effects and without variability in radial ejection velocity.

The overall tendencies confirm that as the miss distance decreases, the number of impacts increases substantially resembling a direct hit to the TBM warhead.

Table 3.7. Impact Distribution per Encounter Configuration for a Cylindrical Projectile with $L/D = 4$ @ EBt -0.006 sec. Without Tumbling Effects and Without V_{rp} Variability.

L/D=4.00 Early Bird Time=-0.0060														
MD/CA		MD/CA												
		0	15	30	45	60	75	90	105	120	135	150	165 Sum	
1		400	396	466	502	451	364	278	207	151	103	42	6	3366
1.5		166	168	215	265	294	287	246	199	145	101	42	9	2137
2		84	100	119	167	183	197	182	172	135	82	42	8	1471
2.5		52	55	85	113	137	144	155	135	109	74	44	9	1112
3		36	44	57	76	103	112	121	119	102	75	47	10	902
3.5		28	36	32	50	73	87	94	103	92	70	46	12	723
4		20	28	26	34	49	67	75	79	84	68	47	13	590
4.5		16	24	21	29	40	56	58	61	69	66	44	14	498
5		12	20	20	25	35	49	50	51	55	63	42	16	438
5.5		12	20	16	22	28	38	43	46	47	51	40	16	379
6		4	18	16	20	26	31	38	39	42	44	32	18	328
sum		830	909	1073	1303	1419	1432	1340	1211	1031	797	468	131	11944

Table 3.8. Impact Distribution per Encounter Configuration for a Cylindrical Projectile with $L/D = 1$ @ $EBt -0.006$ sec. Without Tumbling Effects and Without Vrp Variability.


L/D=1.00 Early Bird Time=-0.0060														
MD/CA		0	15	30	45	60	75	90	105	120	135	150	165	Sum
1		400	396	464	502	453	367	279	208	151	104	42	6	3372
1.5		168	168	215	263	294	285	247	199	147	101	42	8	2137
2		86	98	118	167	185	198	184	169	136	82	42	8	1473
2.5		52	54	84	112	137	144	157	135	109	74	44	10	1112
3		36	43	57	78	102	112	123	119	102	74	47	10	903
3.5		28	36	32	50	73	88	96	102	93	69	46	12	725
4		20	28	26	34	48	68	76	78	84	68	48	14	592
4.5		16	24	21	28	40	56	58	63	68	66	44	14	498
5		12	20	20	24	34	50	51	51	58	63	42	16	441
5.5		12	20	16	22	29	38	42	46	47	51	40	16	379
6		4	18	16	21	26	31	38	40	42	45	32	18	331
sum		834	905	1069	1301	1421	1437	1351	1210	1037	797	469	132	11963

Table 3.9. Impact Distribution per Encounter Configuration for a Spherical Projectile @ $EBt -0.006$ sec. Without Vrp Variability.

L/D=0		Early Bird Time=-0.0060													
MD/CA		0	15	30	45	60	75	90	105	120	135	150	165	Sum	
1		400	395	464	503	453	367	279	208	151	104	42	6	3372	
1.5		168	168	215	263	295	284	248	199	147	101	42	8	2138	
2		86	98	118	167	184	198	183	170	136	82	42	8	1472	
2.5		52	55	84	112	137	144	157	135	109	74	44	10	1113	
3		36	43	57	78	103	112	121	119	102	74	47	10	902	
3.5		28	35	31	50	74	89	95	102	93	69	46	12	724	
4		20	28	26	34	48	69	76	78	84	68	48	13	592	
4.5		16	24	21	28	40	56	58	63	68	66	44	14	498	
5		12	20	20	24	34	49	51	51	58	63	42	16	440	
5.5		12	20	16	22	29	38	42	46	47	51	40	16	379	
6		4	18	16	20	26	31	38	40	42	45	32	18	330	
sum		834	904	1068	1301	1423	1437	1348	1211	1037	797	469	131	11960	

Similar tables were generated for the remaining early bird times, for cylindrical projectiles with L/D of 2, and for different deployment conditions. However, when comparing the frequency of impacts among the different geometry/sizes under the same encounter configuration scenarios (without tumbling effect and radial ejection variability), it was observed that they are practically the same with minor differences of a few impacts in some cases. These minor differences in number of impacts are related to the different EKV warhead designs per projectile/geometry. These differences consist basically in the different positioning along the jelly-roll pattern due to the different projectile diameters, as well as in the difference in bay positioning due to the different projectile lengths. This recurring pattern made it difficult to differentiate the level of total damage inflicted by each geometry/size, and the fact that at some encounter configuration scenarios have more impacts than others is insufficient evidence to conclude that those scenarios are more lethal. To facilitate the identification of encounter configuration scenarios with similar levels of impacts to the warhead and subsequently identify ranges of encounter configuration scenarios where impacts can be maximized, a five level impact frequency criterion was devised based on the total number of impacts that hit the TBM's warhead. This criterion is shown in Table 3.10.

Table 3.10. Impact Frequency Criterion.

Number of Impacts to the TBM Warhead (niw)	Impact Frequency Descriptor	Associated Color
$niw < 7.5$	Very Low	
$7.5 \leq niw < 16$	Low	
$16 \leq niw < 36$	Moderate	
$36 \leq niw < 73$	High	
$73 \leq niw$	Very High	

Each frequency level is defined by a range of impacts based on a statistical analysis performed on the entire encounter configuration range, and has an associated impact frequency descriptor. To further facilitate the identification on the impact quantification tables, each level can be visually identified with a gray-scale based color. The higher the impact frequency the darker the color associated to that level. After applying the criterion to each cell in the impact frequency tables per encounter configuration, the scenarios of similar level of impact frequency become evident, and the tables are easier to interpret.

Tables 3.11 – 3.12 illustrate trends in the distribution of impacts throughout the encounter configuration range at an early bird time of -0.006 seconds, for a cylindrical projectile with L/D of 4. Tables 3.11 and 3.12 correspond to scenarios without variability in radial ejection velocity of cylindrical projectiles. However, Table 3.11 corresponds to the case without tumbling effects, and Table 3.12 corresponds to the case with tumbling. Both tables are identical since they have exactly the same patterns in levels of impact frequency. Tables 3.13 and 3.14 correspond to scenarios with 25% variability in the radial ejection velocity of the cylindrical projectiles. Table 3.13 corresponds to the case without tumbling effects, and Table 3.14 corresponds to the case with tumbling. Both tables show similar patterns in levels of impact frequencies; however they are not necessarily identical. The reason for these minor differences is that these totals for each scenario correspond to the average of 30 simulations. This exercise was applied when radial ejection variability was considered as it was explained in section 3.7

Table 3.11. Impact Distribution Trends per Encounter Configuration for a Cylindrical Projectile with $L/D = 4$ @ $EBt = -0.006$ sec. Without Tumbling Effects and Without V_{rp} Variability.

L/D=4.00 Early Bird Time=-0.0060														
MD/CA		0	15	30	45	60	75	90	105	120	135	150	165	Sum
1													6	3366
1.5													9	2137
2													8	1471
2.5													9	1112
3													10	902
3.5													12	723
4													13	590
4.5													14	498
5													16	438
5.5													16	379
6													18	328
sum		830	909	1073	1303	1419	1432	1340	1211	1031	797	468	131	11944

Table 3.12. Impact Distribution Trends per Encounter Configuration for a Cylindrical Projectile with $L/D = 4$ @ $EBt = -0.006$ sec. With Tumbling Effects and Without V_{rp} Variability.

L/D=4.00 Early Bird Time=-0.0060														
MD/CA		0	15	30	45	60	75	90	105	120	135	150	165	Sum
1													6	3366
1.5													9	2137
2													8	1471
2.5													9	1112
3													10	902
3.5													12	723
4													13	590
4.5													14	498
5													16	438
5.5													16	379
6													18	328
sum		830	909	1073	1303	1419	1432	1340	1211	1031	797	468	131	11944

Table 3.13. Impact Distribution Trends per Encounter Configuration for a Cylindrical Projectile with $L/D = 4$ @ $EBt = -0.006$ sec. Without Tumbling Effects and With a COV V_{rp} of 25%.

L/D=4.00 Early Bird Time=-0.0060														
MD/CA		0	15	30	45	60	75	90	105	120	135	150	165	Sum
1													2.4	2912.6
1.5													3.3	1661.0
2													3.1	1131.5
2.5													3.4	839.6
3													4.9	657.8
3.5													5.1	530.1
4													6.3	437.8
4.5													6.7	370.7
5													8.3	318.4
5.5													8.3	281.7
6													8.7	247.8
sum		657.3	728.9	923.4	1071.3	1119.2	1100.1	1037.3	936.4	798.4	600.2	356.1	60.4	9389.1

Table 3.14. Impact Distribution Trends per Encounter Configuration for a Cylindrical Projectile with $L/D = 4$ @ $EBt = -0.006$ sec. With Tumbling Effects and With a COV V_{rp} of 25%.

L/D=4.00 Early Bird Time=-0.0060															
MD/CA		0	15	30	45	60	75	90	105	120	135	150	165	Sum	
1														2.1	2904.8
1.5														2.7	1660.1
2														3.1	1136.9
2.5														4.0	842.3
3														4.4	660.2
3.5														5.8	536.4
4														6.8	439.1
4.5		12.1	15.0											6.6	375.7
5		10.2	12.3											7.6	320.6
5.5		7.9	9.8	14.9										6.9	283.5
6		6.4	7.9	13.3										8.6	243.8
		5.6	6.8	10.8	15.0										
sum		661.4	719.9	921.0	1075.9	1123.4	1102.1	1042.4	933.3	794.6	610.9	359.8	58.8		9403.3

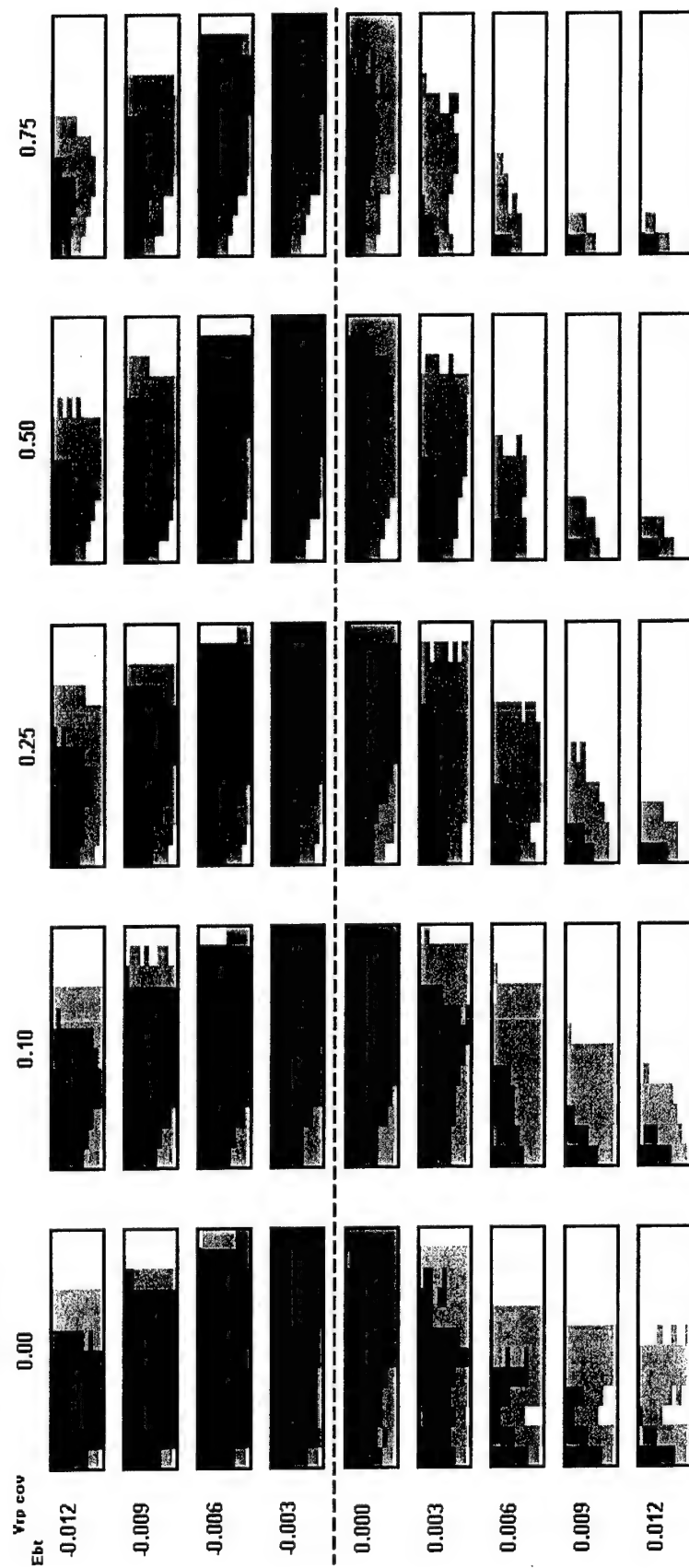
Similarities are noticed in tables prepared for other projectile/sizes and early bird times; thus, concluding that tumbling has no effect on the number of impacts to the TBM. However, when comparing Tables 3.11 and 3.13 (both without tumbling) or when visually inspecting Tables 3.12 and 3.14 (both including tumbling), some differences in number of impacts, and regions of similar levels of impacts are notable. For example, an encounter scenario at a crossing angle of 90° and a miss distance of 4.0 meters without radial ejection velocity variability produces 75 impacts, in comparison to the same scenario including 25% variability which has only 58.1 impacts, represents a reduction of more than 20% in this case. The overall tendency throughout the table indicates a reduction in the number of impacts, except for a few isolated cases where the opposite occurs.

Table 3.15 depicts a typical matrix of impact frequency tables per encounter configuration scenarios, where each cell contains an impact frequency table per early bird time and case of variability in radial ejection velocity. The cell-tables in this matrix contain impact quantifications of cylindrical projectiles of $L/D = 4$ without tumbling.

The matrix consists of six columns and ten rows including the top header row and leftmost header column. From left to right, the cell-tables show impact frequencies calculated with variability in radial ejection velocity (COV V_{rp}) of 0.00, 0.10, 0.25, 0.50, and 0.75. From top to bottom, the matrix shows the cell-tables for which the distribution of impacts was determined as the early bird time (EBt) varies from late bird scenarios to early bird scenarios (-0.012 sec. to +0.012 sec.) in increments of 0.003 seconds. When comparing the cell-tables against the early bird parameter (vertical-wise) under a specific deployment variability case, it is observed that the frequency of impacts is maximized (dark color regions) over a larger scenario of encounter configurations at late-bird times, versus early bird times where the frequencies are minimal (light-color regions) for a large scenario of encounter configurations. The largest encounter configuration scenario range with high frequencies is obtained at -0.003 sec. even when variability in the radial ejection velocity is present. Close to half of the entire encounter configuration range (upper triangle of each cell-table) has high impact frequencies. From the early bird time standpoint, and assuming a miss distance of zero, an early bird time of -0.003 sec. closely

resembles a direct hit to the TBM warhead. As the early bird parameter moves away from this threshold, the encounter is considered a near-miss. A near-miss at a late bird time of -0.006 sec. shows a fairly large reduction in the encounter configuration scenarios with high impact frequencies compared to the threshold of -0.003; specifically up to approximately a crossing angle of 135° and a miss distance of 3.5 meters or less. As the late-bird time increases to -0.009 sec. and -0.012 sec. the high impact regions are limited to crossing angles between 0° and 15° and miss distances close to 1.0 meter.

Table 3.15. Impact Quantification Matrix for a Cylindrical Projectile with $L/D = 4$ Without Tumbling Effects per Encounter



As the early bird time increases (between 0.003 to 0.012 sec.) the regions of very low frequency or no impact increase, and the high impact frequency regions are concentrated around a crossing angle of 0° and miss distance of 1.0 meter, and this is more noticeable as the variability in deployment increases as well.

Very similar patterns almost identical are observed for other projectile geometry/sizes with and without tumbling effects. Thus, these tables are not included in this research work. Therefore, it is concluded that variability in radial ejection velocity does slightly affect the number of impacts in the TBM warhead. The pattern shows that the number of impacts is inversely proportional to the amount of variability. To better understand the patterns observed at a late bird time of -0.003 without variability in ejection velocity, a closer look at the impact frequency distribution is conducted and presented in Table 3.16. When the crossing angle (CA) is 0° , the EKV and TBM are traveling in opposite directions with parallel trajectories; when the distance between them is small the number of impacts is maximized (400 impacts), otherwise, the number of impacts is reduced substantially (4 impacts). In contrast, when the crossing angle is close to 165° the EKV is close by and almost traveling along with the TBM for a longer period of time; therefore, when the EKV's jelly-roll warhead is deployed, a fairly high number of projectiles impact the TBM warhead (between 139 and 94 impacts), even at a miss distance of 6.0 meters. This occurs because the speed of both TBM and EKV is the same and the two warheads are aligned. If the speeds were different, the number of impacts at this large crossing angle might not be as large.

Table 3.16. Impact Distribution per Encounter Configuration for a Cylindrical Projectile with $L/D = 4$ @ $EBt = -0.003$ sec. Without Tumbling Effects and Without V_{rp} Variability.

L/D=4.00 Early Bird Time=-0.0030												
MD/CA	0	15	30	45	60	75	90	105	120	135	150	165 Sum
1	400	260	218	295	371	410	425	418	395	334	249	139
1.5	166	116	133	217	251	303	328	339	338	299	236	133
2	84	78	100	152	168	206	242	273	282	261	220	124
2.5	52	40	74	89	96	145	181	211	232	235	198	132
3	36	34	57	62	82	105	119	168	189	199	182	119
3.5	28	24	34	58	73	92	101	120	163	176	164	115
4	20	22	22	41	65	81	86	95	138	158	148	112
4.5	16	20	20	28	40	69	70	84	113	132	138	111
5	12	18	18	25	34	37	54	70	88	117	129	102
5.5	12	20	16	21	29	26	36	57	77	99	112	99
6	4	16	12	15	14	18	28	40	67	88	104	94
sum	830	648	704	1003	1223	1492	1670	1875	2082	2098	1880	1280
												16785

A final observation from the encounter configuration standpoint is that as the early bird time increases or decreases (late bird time) from -0.003 sec. the number of impacts decreases. This pattern is observed for all projectile/size/conditions. Appendix A includes impact distribution tables per encounter configuration for spherical projectiles at various early bird times, without radial ejection velocity variability.

3.8.2 Impact Characterization per Encounter Configuration

A comprehensive statistical study on each impact characterization parameter was conducted for the entire range of encounter configuration scenarios under the different deployment conditions of tumbling and radial ejection velocity variability. After observing the statistics for the spatial orientation angles, it was decided to simplify the study by: 1) eliminating the β angle from the characterization, since most of its values were very close to either 0° or 180° , and; 2) based on the later, by projecting the longitudinal axis of the cylindrical projectile on to the X-Z plane, and measure the α angle from the positive Z axis to the projected longitudinal axis. Table 3.17 shows combined statistics for all projectile/size, and deployment conditions.

Table 3.17. Impact Characterization Parameter Statistics.

Statistic	Angle α (degrees)		Angle ϕ (degrees)	Relative Impact Velocity Magnitude V (km/s)				
	All COV Without Tumbling	All COV With Tumbling		W & W/O Tumbling for a Radial Ejection Velocity COV of				
				0%	10%	25%	50%	75%
Max	90	90	89.99	2.042	2.065	2.095	2.195	2.33
Mean (approx)	33	-7.5	61	1.5217	1.5177	1.5117	1.5071	1.5134
Min	-90	-90	0.03	0.039	0.036	0.036	0.035	0.036

In addition, Figures 3.19 through 3.24 depict relative frequency distributions for the different impact configuration parameters for spherical and cylindrical projectiles under different conditions of tumbling and radial ejection velocity variability.

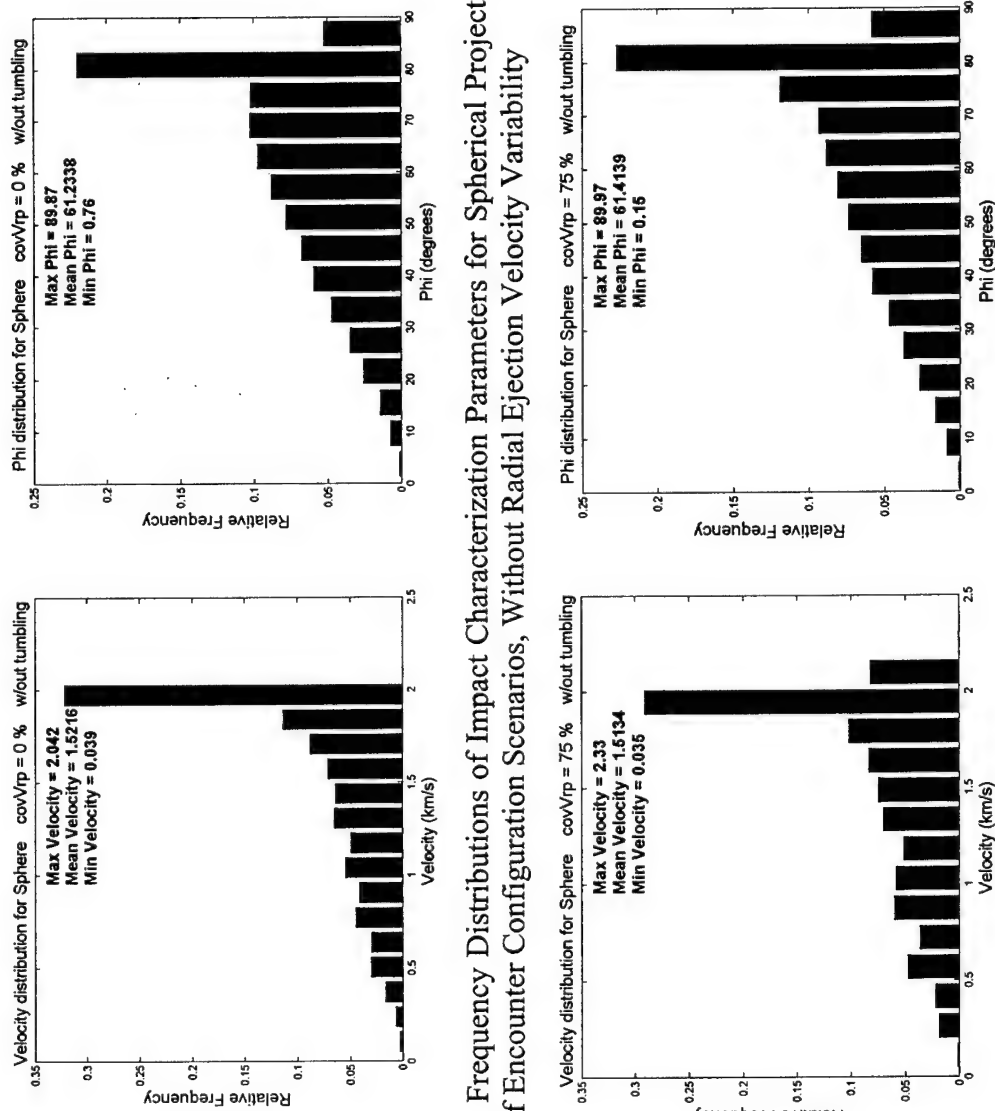


Figure 3.19. Relative Frequency Distributions of Impact Characterization Parameters for Spherical Projectiles over the Entire Range of Encounter Configuration Scenarios, Without Radial Ejection Velocity Variability

Figure 3.20. Relative Frequency Distributions of Impact Characterization Parameters for Spherical Projectiles over the Entire Range of Encounter Configuration Scenarios, With 75% Radial Ejection Velocity Variability

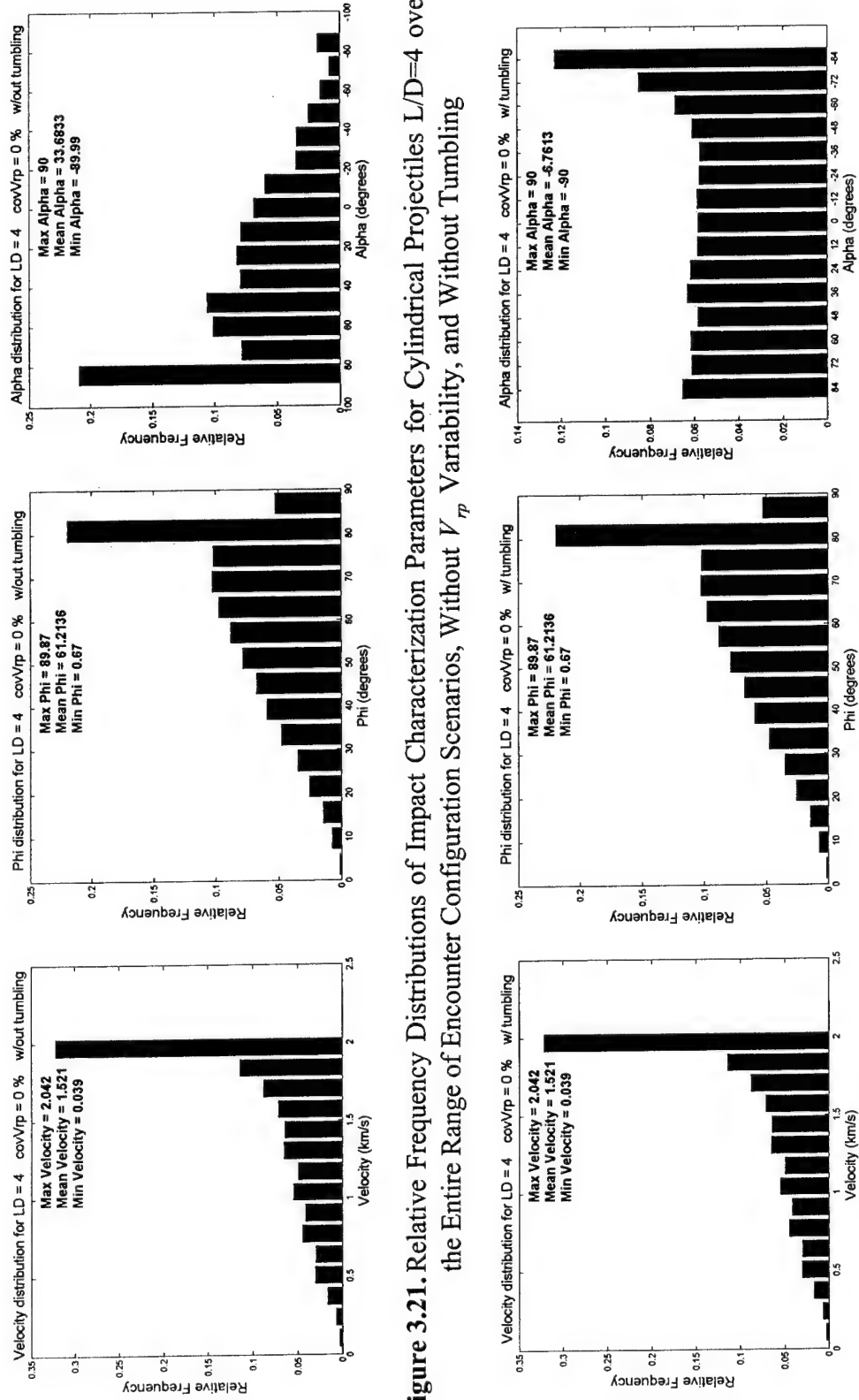


Figure 3.21. Relative Frequency Distributions of Impact Characterization Parameters for Cylindrical Projectiles $L/D=4$ over the Entire Range of Encounter Configuration Scenarios, Without V_{rp} Variability, and Without Tumbling

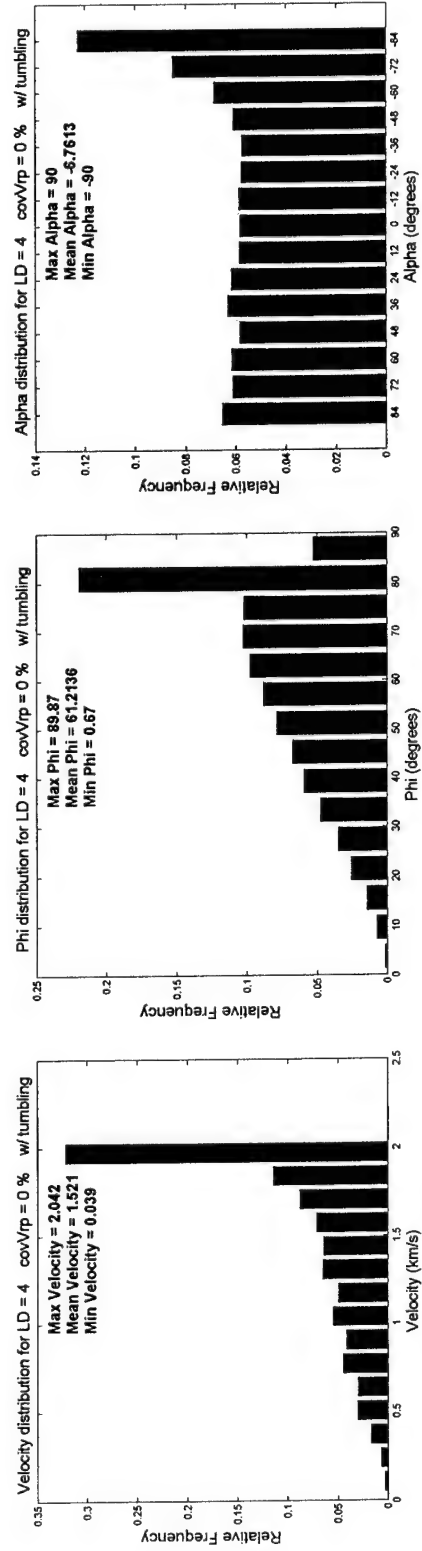


Figure 3.22. Relative Frequency Distributions of Impact Characterization Parameters for Cylindrical Projectiles $L/D=4$ over the Entire Range of Encounter Configuration Scenarios, Without V_{rp} Variability, and With Tumbling

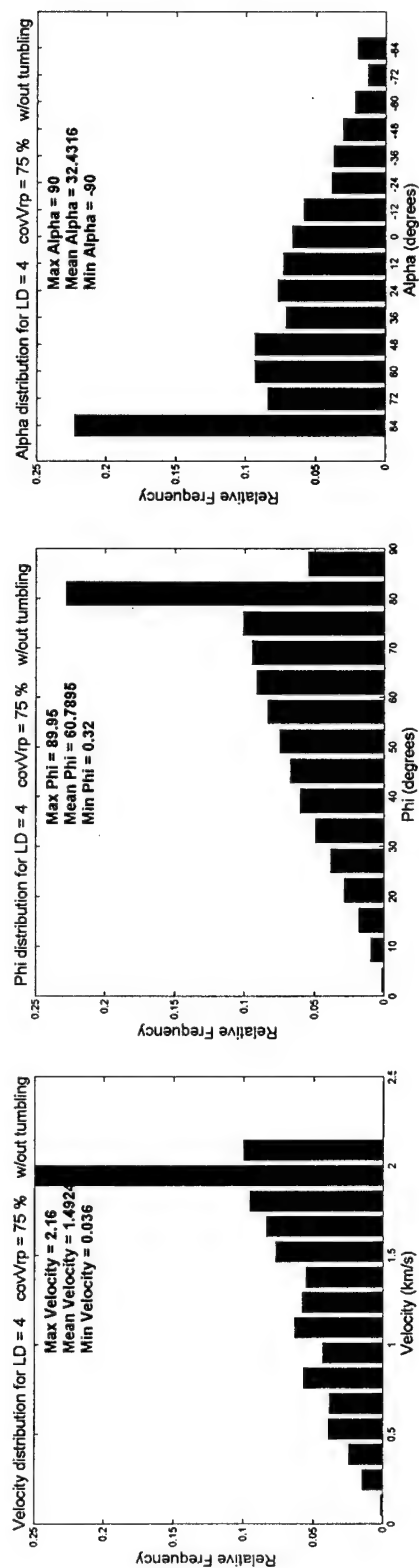


Figure 3.23. Relative Frequency Distributions of Impact Characterization Parameters for Cylindrical Projectiles $L/D=4$ over the Entire Range of Encounter Configuration Scenarios, With 75% V_p Variability, and Without Tumbling

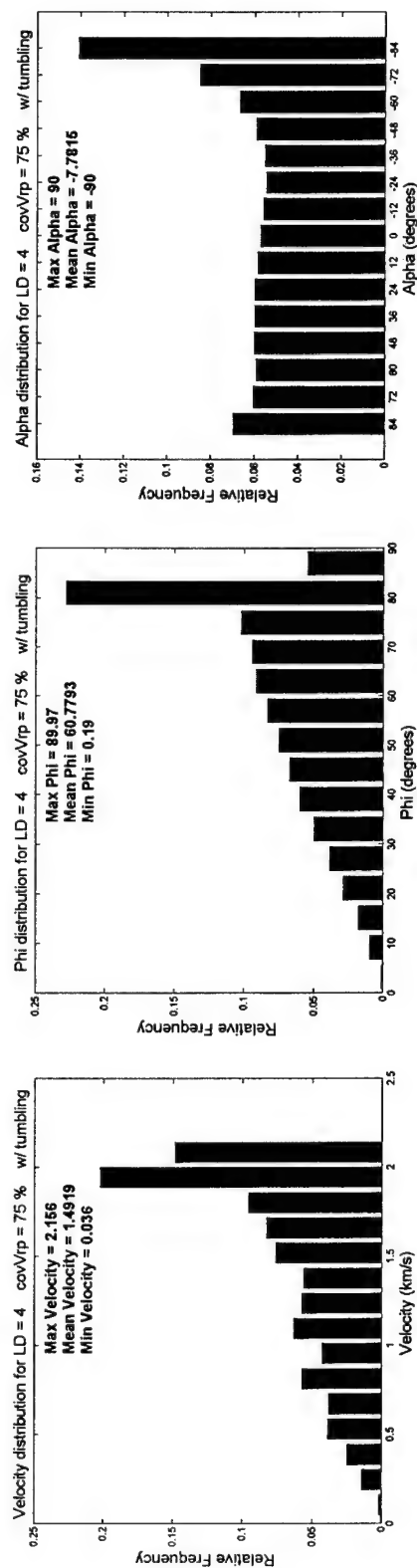


Figure 3.24. Relative Frequency Distributions of Impact Characterization Parameters for Cylindrical Projectiles $L/D=4$ over the Entire Range of Encounter Configuration Scenarios, With 75% V_p Variability, and With Tumbling

Additional relative frequency histograms were generated for the other projectile geometry/size/conditions. These histograms are not included since they look very similar to the ones for $L/D = 4$. As expected, tumbling has an effect on the distribution of spatial orientation angle (α) for cylinders only, by evening out the distribution; however, it has no effect on the distributions of relative velocity magnitude or strike angle (ϕ). On the other hand, variability in radial ejection velocity seems to have a slight effect on the distribution of all the parameters. The possible reason for the minor differences between the distributions is that the histograms with variability in ejection velocity are generated from 30 simulations per encounter configuration scenario. An important parameter in impact mechanics is the yaw angle (ψ) defined as the angle between the spatial orientation angle (α) and the strike angle (ϕ).

$$\psi = \phi - \alpha \quad (3.45)$$

According to the adopted definitions of strike angle and spatial orientation angle, when a cylinder impacts with its tip, its orientation angle always takes a value between 0° and 90° . Conversely, when the cylinder impacts with its tail, α takes negative values between 0° and -90° . The strike angle always takes values between 0° and 90° . Figure 3.25 depicts the two typical cylinder impacts: a) when it impacts with its tip, and b) when it impacts with its tail.

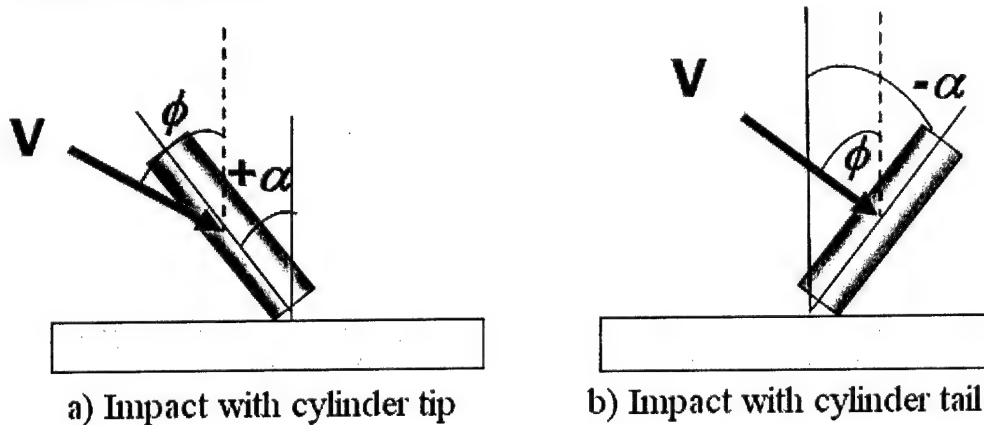


Figure 3.25. Typical Cylindrical Impacts.

Based on these typical cylindrical impact scenarios, when the cylinder impacts with its tip, the resulting yaw angle (ψ) takes values between 0° and 90° . Alternatively, when the cylinder impacts with its tail, the resulting yaw angle (ψ) may take values between 0° and 180° , depending on ϕ and α . Figure 3.26 illustrates a snapshot taken from the graphical output of an endgame simulation where both impact types occur. The frequency at which these cases occur is dependant on the surface of the TBM and the location at which they impact.

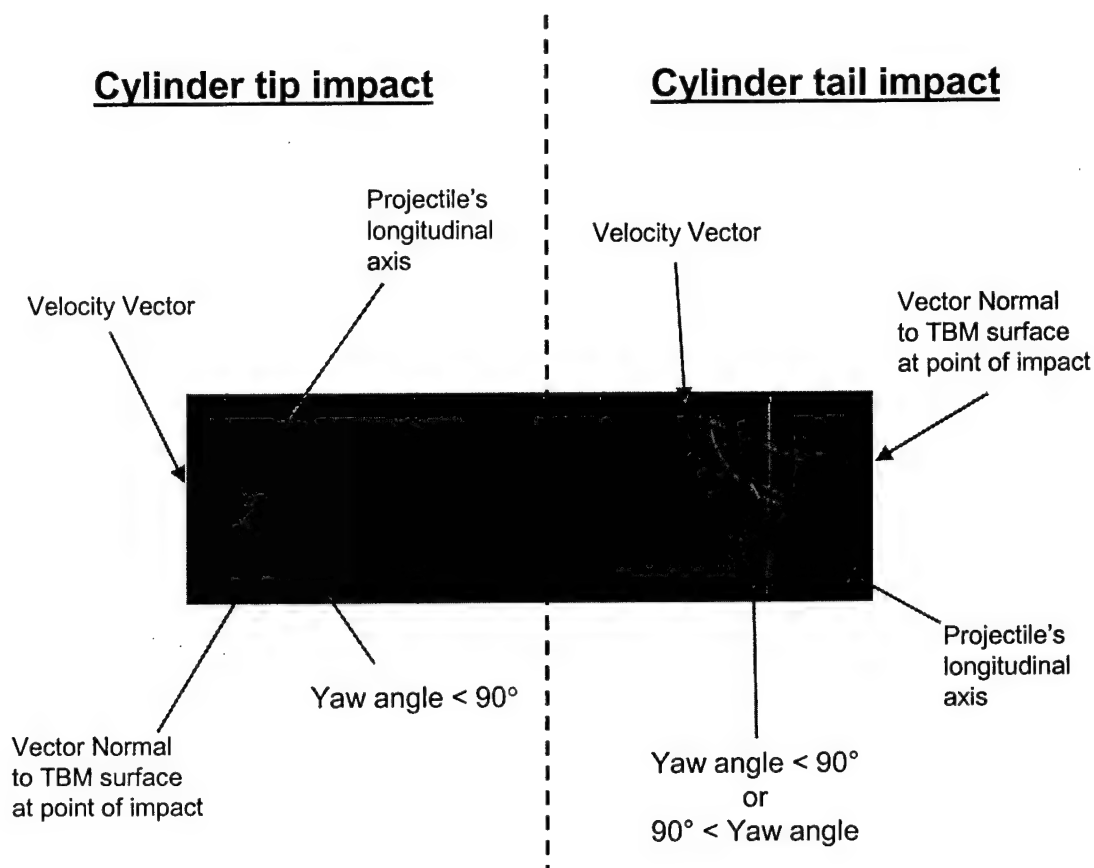


Figure 3.26. Yaw Angle Definition for Cylindrical Projectiles.

A statistical study was conducted to identify the relationship between the yaw angle (ψ) and the encounter configuration scenarios as well as with impact configuration parameters. Figure 3.27 illustrates the variation in the maximum, average and minimum yaw angle at selected miss distances plotted against the crossing angle. The plots were generated for a cylindrical projectile with L/D of 4 without tumbling effects and without variability in radial ejection velocity. These statistics are averages per early bird time.

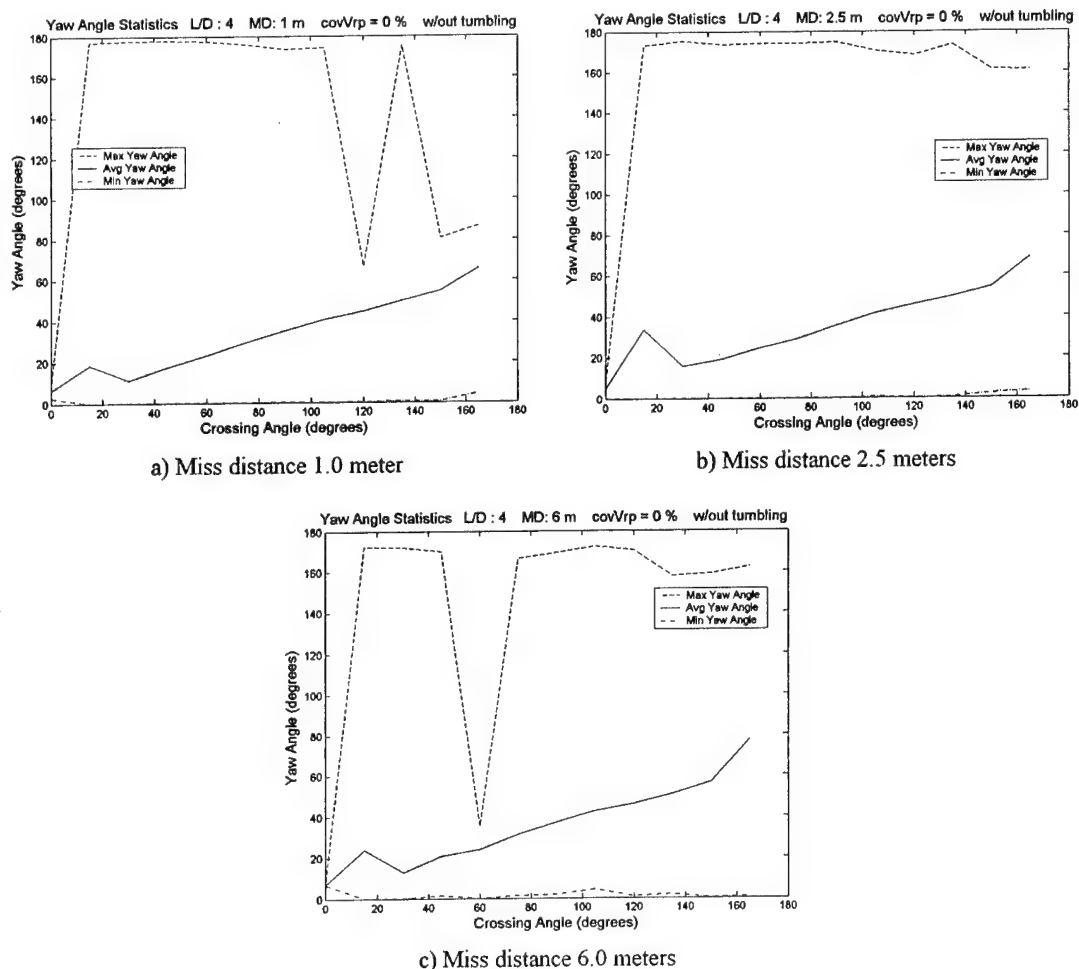


Figure 3.27. Yaw Angle Statistics for Cylindrical Projectiles $L/D = 4$ vs. Crossing Angle at Selected Miss Distance Scenarios Without Radial Ejection Velocity Variability, and Without Tumbling.

Several situations are observed from these plots. The minimum yaw angle remains approximately at less than 5° throughout the entire crossing angle range, regardless of miss distance scenario. The maximum yaw angle jumps from a low value at a crossing angle of 0° to close to 180° at a crossing angle of 15° . Thereon, it generally remains between 160° and 180° , except for a few crossing angle scenarios where it drops substantially and rises back again. These variations occur at different miss distance scenarios for the different projectile geometries/sizes. These sudden variations in the maximum yaw angle are most probably dependent on the impact locations in the warhead section, time of deployment, and the physical characteristics of the different EKV warhead designs.

The average yaw angle increases as the crossing angle varies from 0° to 180° , regardless of the miss distance. This increasing tendency can be explained by the fact that as the crossing angle increases, the number of tail impacts with individual yaw angles larger than 90° also increases, thus raising the average yaw angle for that particular scenario. At a crossing angle of 15° , a unique situation occurs. Even though the number of impacts is practically the same as it is at 0° but less than the number at 30° (see Figure 3.18), the average yaw angle increases. Figure 3.28 is a front view of the impacts on the TBM at crossing angles 0° , 15° and 30° .

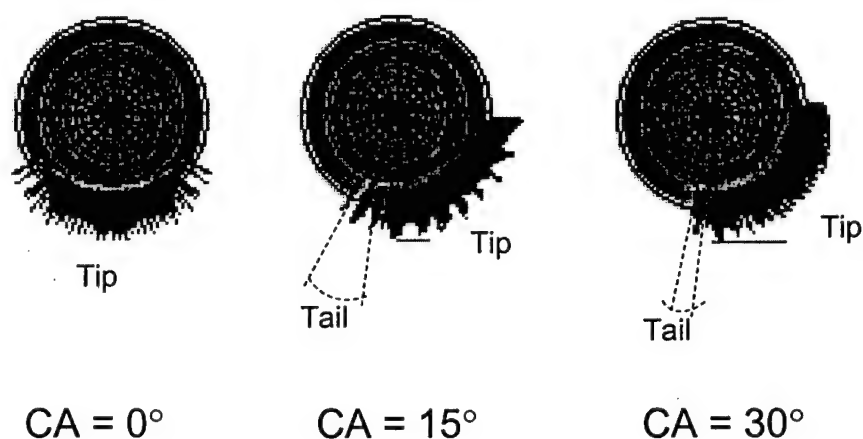


Figure 3.28. Relative Frequency of Tail Impacts at Low Crossing Angles.

At a crossing angle of 0° all cylinders impact with the tip (identified by the cylinder axis colored in magenta). At a crossing angle of 15° the frequency of tail impacts (identified by the cylinder axis colored in black) is greater than at 30° . These tail impacts may also have large yaw angles that raise the average, or the number of tip impacts at a crossing angle of 30° has lower yaw angles than the ones at 15° . Appendix B includes similar charts for other miss distance scenarios and other projectile geometry/sizes.

Finally, the relative impact velocity was also analyzed to identify the relationship with encounter configuration scenarios. Figure 3.29 depicts the variation in the maximum, average and minimum relative impact velocity as the crossing angle increases, for a miss distance of 1.0 meter when variability in radial ejection velocity is not considered. The plots were obtained for cases without and with tumbling effects respectively.

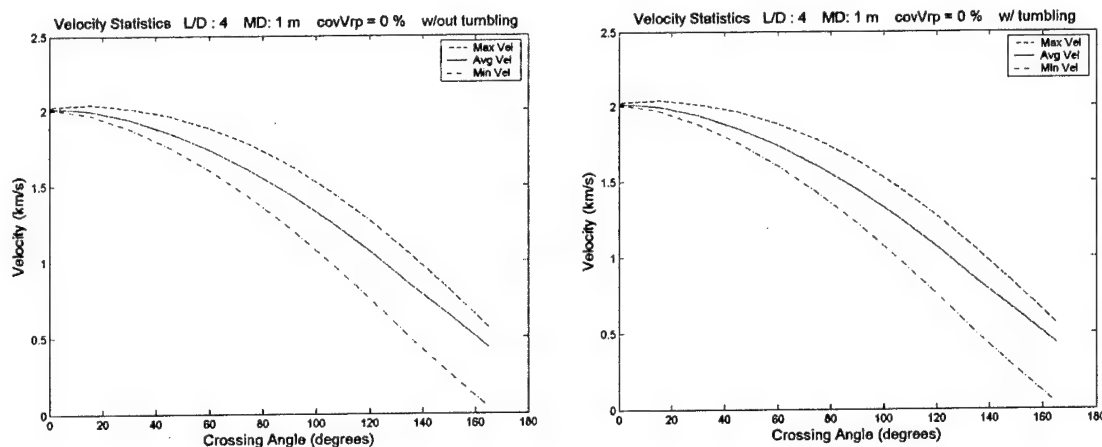


Figure 3.29. Relative Impact Velocity vs. Crossing Angle for Cylindrical Projectiles $L/D = 4$ Without Radial Ejection Velocity Variability.

Both plots illustrate that the relative impact velocity decreases as the crossing angle increases. As the crossing angle increases the resultant relative velocity between missiles reduces from approximately 2.0 km/s to 0.03 km/s. The observed variability (difference between maximum and minimum velocities) is due to the radial ejection velocity of the projectiles, which depends on the physical characteristics of the different warhead design and the crossing angle as well. As observed tumbling has no effect on the impact velocity. The effect that radial ejection velocity variability is depicted in Figure 3.30.

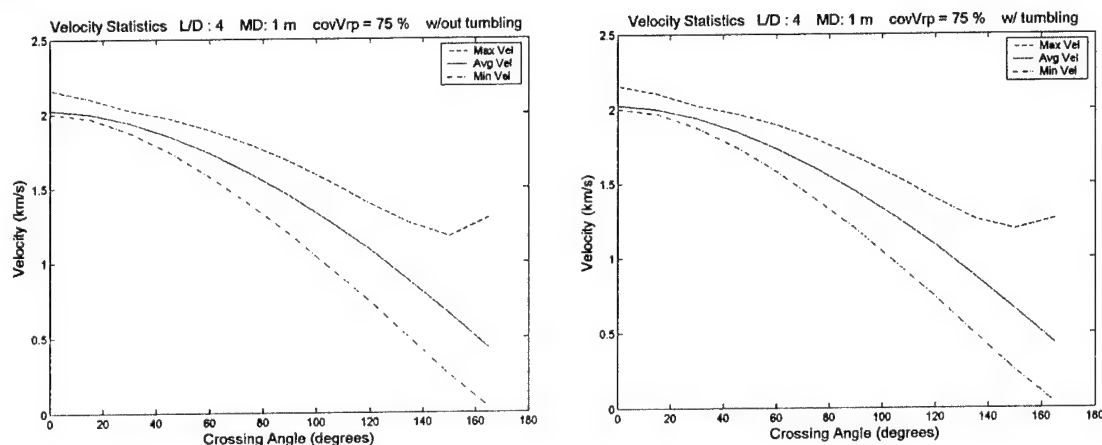


Figure 3.30. Relative Impact Velocity vs. Crossing Angle for Cylindrical Projectiles $L/D = 4$ With 75% Radial Ejection Velocity Variability.

When variability in radial ejection velocity is included, the maximum velocity that can be obtained is higher than the maximum obtained without variability. This

increase is maintained throughout the entire crossing angle range. The increase is more evident for crossing angles close to 0° and above 90° . Again, tumbling does not have any effect on the impact velocity. The plots for other miss distance scenarios and other projectile geometry/sizes were not included in this work because they are practically the same as the ones shown above.

3.9 Impact Quantification per Impact Characterization

Impacts to the warhead were also classified from the impact characterization standpoint for the entire range of encounter configuration scenarios. A new set of tables per projectile geometry/size per deployment conditions was generated. These tables are based on ranges of each impact characterization parameter. Thirteen ranges for spatial orientation angle (α) were defined, along with six ranges for the strike angle, and seven ranges of relative impact velocity. The spatial orientation angle (β) was not taken into account to simplify the study. The corresponding ranges are shown in Table 3.18.

Table 3.18. Predefined Impact Characterization Parameter Ranges.

Range	Orientation angle Alpha (α) (degrees)	Strike angle Phi (ϕ) (degrees)	Velocity Magnitude V (km/s)
1	$90 \geq \alpha > 82.5$	$0.0 \leq \phi < 7.5$	0.0000 – 0.3075
2	$82.5 \geq \alpha > 67.5$	$7.5 \leq \phi < 22.5$	0.3075 – 0.6150
3	$67.5 \geq \alpha > 52.5$	$22.5 \leq \phi < 37.5$	0.6150 – 0.9225
4	$52.5 \geq \alpha > 37.5$	$37.5 \leq \phi < 52.5$	0.9225 – 1.2300
5	$37.5 \geq \alpha > 22.5$	$52.5 \leq \phi < 67.5$	1.2300 – 1.5375
6	$22.5 \geq \alpha > 7.5$	$67.5 \leq \phi < 90$	1.5375 – 1.8450
7	$7.5 \geq \alpha \geq -7.5$		1.8450 –
8	$-7.5 > \alpha \geq -22.5$		
9	$-22.5 > \alpha \geq -37.5$		
10	$-37.5 > \alpha \geq -52.5$		
11	$-52.5 > \alpha \geq -67.5$		
12	$-67.5 > \alpha \geq -82.5$		
13	$-82.5 > \alpha \geq -90$		

The relative impact velocity was selected as first level of classification, followed by velocity strike angle (ϕ), and finally by spatial orientation angle (α). This classification scheme generated seven tables per projectile geometry/size/condition. Table 3.19 shows a typical impact quantification table by impact characterization consisting of sixteen columns and eight rows including the top header row and leftmost header column. From left to right, the table shows the distribution of impacts as the cylinder orientation angle (α) varies from $+90^\circ$ to -90° . From top to bottom, the tables show the distribution of impacts as the velocity strike angle (ϕ) increases from 0° to 90° .

The rightmost columns show the total number of impacts per velocity strike angle range for both the sphere and corresponding cylinder size; the bottom row shows of the total number of impacts per cylinder orientation angle (α) range for the cylinder only. The total number of impacts per relative impact velocity range of each projectile is located under the column of sums per velocity strike angle column respectively.

The table is further subdivided in two sections based on cylinder orientation angles (α):

- a) the left-half section with positive cylinder orientation angles (α) occurring when cylinders impact with their tip, and
- b) the right-half section with negative α , occurring when cylinders impact with their tail.

The table also has a number of reference cells outlined that correspond to $(\phi-\alpha)$ scenarios where a yaw angle (ψ) of 0° is possible. The cells that have at least one impact are light-shaded with a dotted pattern.

Table 3.19. Impact Quantification per Impact Configuration for Cylindrical Projectiles $L/D = 4$ Without Radial Ejection Velocity Variability and Without Tumbling.

L/D=4.00		Velocity= 0.61 50(km/s)- 0.9225(km/s)																SumCyl	
phi/alpha		90°>=a>=82.5		82.5>=a>=67.5		67.5>=a>=52.5		52.5>=a>=37.5		37.5>=a>=22.5		22.5>=a>=7.5		7.5>=a>=0		0>=a>=-7.5		Sphere	
0.0<=phi< 7.5		0	0	0	0	0	0	0	0	0	0	0	0	0	0	0	0	0	0
7.5<=phi<22.5		0	0	0	0	0	0	0	0	0	0	0	0	0	0	0	0	810	811
22.5<=phi<37.5		0	0	0	0	0	0	0	0	0	0	0	0	0	0	0	0	1702	1702
37.5<=phi<52.5		0	0	0	0	0	0	0	0	0	0	0	0	0	0	0	0	1084	1084
52.5<=phi<67.5		0	0	0	0	0	0	0	0	0	0	0	0	0	0	0	0	701	701
67.5<=phi<90.0		0	0	0	0	0	0	0	0	0	0	0	0	0	0	0	0	417	417
sum		37	37	97	168	266	337	431	525	683	812	766	530	33	30	30	30	4703	4715

Table 3.20. Impact Quantification per Impact Configuration for Cylindrical Projectiles $L/D = 2$ Without Radial Ejection Velocity Variability and Without Tumbling.

L/D=2.00		Velocity= 0.61 50(km/s)- 0.9225(km/s)																SumCyl	
phi/alpha		90°>=a>=82.5		82.5>=a>=67.5		67.5>=a>=52.5		52.5>=a>=37.5		37.5>=a>=22.5		22.5>=a>=7.5		7.5>=a>=0		0>=a>=-7.5		Sphere	
0.0<=phi< 7.5		0	0	0	0	0	0	0	0	0	0	0	0	0	0	0	0	0	0
7.5<=phi<22.5		0	0	0	0	0	0	0	0	0	0	0	0	0	0	0	0	810	805
22.5<=phi<37.5		0	0	0	0	0	0	0	0	0	0	0	0	0	0	0	0	1702	1704
37.5<=phi<52.5		0	0	0	0	0	0	0	0	0	0	0	0	0	0	0	0	1072	1076
52.5<=phi<67.5		0	0	0	0	0	0	0	0	0	0	0	0	0	0	0	0	704	707
67.5<=phi<90.0		0	0	0	0	0	0	0	0	0	0	0	0	0	0	0	0	413	413
sum		37	37	99	163	268	334	432	522	680	817	761	530	35	26	26	26	4703	4705

Table 3.21. Impact Quantification per Impact Configuration for Cylindrical Projectiles $L/D = 1$ Without Radial Ejection Velocity Variability and Without Tumbling.

L/D=1.00		Velocity= 0.61 50(km/s)- 0.9225(km/s)																SumCyl	
phi/alpha		90°>=a>=82.5		82.5>=a>=67.5		67.5>=a>=52.5		52.5>=a>=37.5		37.5>=a>=22.5		22.5>=a>=7.5		7.5>=a>=0		0>=a>=-7.5		Sphere	
0.0<=phi< 7.5		0	0	0	0	0	0	0	0	0	0	0	0	0	0	0	0	0	0
7.5<=phi<22.5		0	0	0	0	0	0	0	0	0	0	0	0	0	0	0	0	810	807
22.5<=phi<37.5		0	0	0	0	0	0	0	0	0	0	0	0	0	0	0	0	1702	1704
37.5<=phi<52.5		0	0	0	0	0	0	0	0	0	0	0	0	0	0	0	0	1072	1072
52.5<=phi<67.5		0	0	0	0	0	0	0	0	0	0	0	0	0	0	0	0	704	707
67.5<=phi<90.0		0	0	0	0	0	0	0	0	0	0	0	0	0	0	0	0	414	414
sum		37	37	96	165	269	336	431	522	678	820	758	529	36	27	27	27	4703	4704

Tip impacts

Tail impacts

The distribution of impacts for each cylindrical geometry/size L/D of 1, 2 and 4 was classified in terms of impact characterization at an impact velocity range of 0.615 to 0.9225 km/s and presented in Tables 3.19, 3.20 and 3.21. The frequencies were computed from scenarios without tumbling effects and without variability in radial ejection velocity.

The frequencies per $(\phi-\alpha)$ range scenario as well as the totals per strike angle range and per impact velocity range are practically identical between cylindrical shapes with minor differences. A similar pattern was observed in the quantification tables per encounter configuration, differences are most likely due to the physical characteristics of the different EKV warhead designs per projectile/geometry. At this velocity range it can be observed that the number of tail impacts is approximately 50% larger than the number of tip impacts by adding the corresponding column sums. The largest number of tail impacts occurs when the cylinder orientation (α) is between -22.5° and -37.5° . Also, by observing the number of impacts per strike angle range (ϕ), most of the projectiles impact at a strike angle range between 22.5° and 37.5° .

The distribution of the cylindrical impacts within the range of impact configuration scenarios is certainly correlated to the encounter configuration scenarios. In an effort to understand and roughly explain this correlation, these tables are cross-referenced with plots that relate the encounter configuration scenarios with various impact configuration parameters, such as the velocity versus crossing angle plots. For practical purposes, Table 3.19 is selected for this exercise, since the cylindrical projectile with L/D ratio of 4 has been selected as study case. The correlation will be simplified to crossing angle and yaw angle through the velocity range. From Figure 3.29 the crossing angle range that generated impacts within the velocity range of 0.615 to 0.9225 km/s for a miss distance of 1.0 meter can be identified. Extending two imaginary horizontal lines from the velocity axis for the two boundary values, and intersecting these lines with the maximum and minimum velocity curves accomplished this. At the points where the maximum velocity (0.9225) intersects with the minimum velocity curve, and where the minimum velocity (0.615) intersects with the maximum velocity curve, drop two imaginary vertical lines and intersect the crossing angle axis. These two intersections define a crossing angle interval between 110° and 160° . However, the pre-specified crossing angles that fall within this interval include 120° , 135° and 150° . The same crossing angles are observed for the other miss distance scenarios.

A statistical study was conducted to identify the relationship between the yaw angle (ψ) and the relative impact velocity. Figure 3.31 depicts the frequency distribution of yaw angles for a cylinder L/D of 4 within the 0.615 - 0.9225 km/s velocity range. Plot 3.31a shows the distribution without tumbling and plot 3.31b with tumbling. Similar histograms may be found in Appendix C for other velocity ranges and projectile geometry/sizes without tumbling.

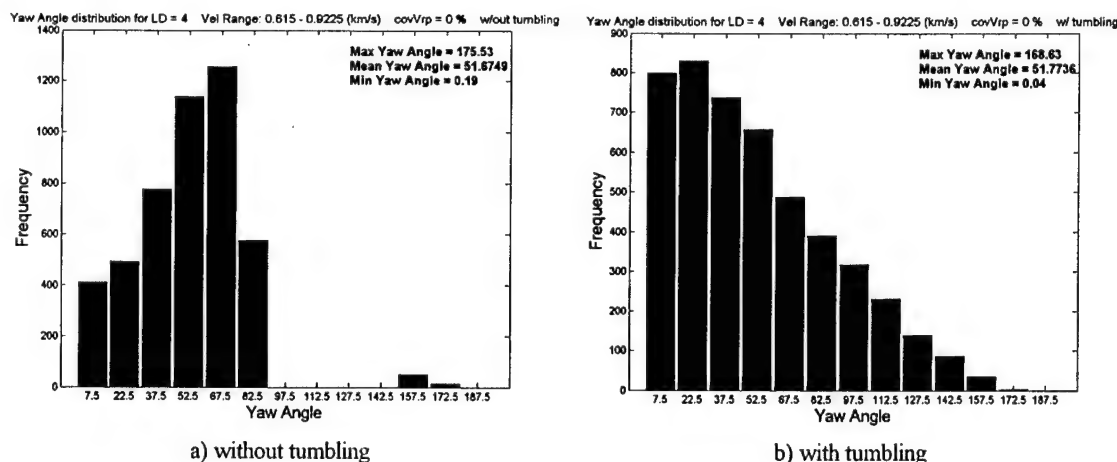


Figure 3.31. Yaw Angle Frequency Distribution per Impact Velocity Range for Cylindrical Projectiles $L/D = 4$, Without Radial Ejection Velocity Variability.

The frequencies and statistics in the histograms are calculated for the entire encounter configuration range of scenarios that generate impacts within that velocity range. The histogram's horizontal axis marks the midclass points for 15° bin-widths. The histogram without tumbling shows a continuous yaw angle range from 0° to 90° where it interrupts to continue with some frequencies between 150° and 180° . The histogram with tumbling shows a continuously decreasing yaw angle range from 0° to 180° . To identify this yaw angle distributions in impact configuration table format, Table 3.22 was generated to show the yaw angle ranges per $(\phi-\alpha)$ range scenario. This table has the reference cells outlined and dark-shadowed, to show the $(\phi-\alpha)$ scenarios where a yaw angle (ψ) of 0° is possible for each strike angle range. As the strike angle range increases (downward direction) the reference scenarios shift to the left in a diagonal pattern. From these reference cells thereon, moving in a horizontal direction, per strike angle range, either to the right or to the left of the reference cells, the yaw angle range varies accordingly with the difference between the (ϕ) ranges and (α) ranges. The maximum yaw angle of 90° occurs to the left in the upper left hand corner, and a maximum of 180° occurs to the right in the lower right hand corner. Table 3.23 is a replica of Table 3.22 with shaded cells that correspond to the range of $(\phi-\alpha)$ scenarios where impacts occurred as shown in table 3.19. The shaded region facilitates the identification of the yaw angle distribution of cylindrical impacts without tumbling. The extreme limits of the shaded areas coincide with histogram 3.31a. Conversely, Table 3.24 shows the range of $(\phi-\alpha)$ scenarios where impacts occurred with tumbling; the impact frequency distribution table for this condition is not included in this report. This table confirms that when tumbling is considered the cylinders impact within the entire range of orientation angles from 0° to 180° . The impact configuration distribution for other velocity ranges and other geometry/sizes can be explained in a similar fashion.

Conversely, Table 3.25 compares the distribution of impacts for cylindrical projectiles $L/D = 4$ per relative impact velocity ranges. The total number of impacts per velocity range increases at higher impact velocity magnitudes. The same pattern observed in Figure 3.31 is replicated in the comparative tables. In contrast, the distribution of impacts per $(\phi-\alpha)$ range scenario narrows down. For the lowest velocity range (0 – 0.3075 km/s), the impacts are distributed throughout the entire range of cylinder orientation angles (α) and the entire strike angle range (ϕ). In contrast, for a high velocity range (1.845 km/s or greater) most impacts concentrate in a range of impact configuration scenarios where the strike angle is shallow ($52.5^\circ < \phi < 90^\circ$) and the orientation angle ranges between $22.5^\circ < \alpha < 90^\circ$, with a few tail impacts ranging between $-67.5^\circ > \alpha > -90^\circ$.

From the yaw angle standpoint, for the lowest velocity range (0 – 0.3075 km/s) the yaw angle distribution ranges between 0° and 165° skipping between 90° and 105° . For the second and third lowest velocity ranges, the yaw angle ranges between 0° and 90° with a few tail impacts hitting between 135° and 180° . For the fourth and fifth high velocity ranges, the yaw angle range slightly decreases between 0° and 75° with just a very few impacts with yaw angles between 150° and 180° . For the second highest velocity range the yaw angle ranges between 0° and 60° , with some tail impacts hitting between 165° and 180° . Finally, in the highest velocity range, the yaw angle range reduces to 0° and 45° , with still a few impacts under a yaw between 165° and 180° .

This pattern may be explained by simultaneously observing the corresponding histograms in Appendix C. These yaw angle ranges may be dependent on both the crossing angle and the radial ejection velocity.

The ratio of tip impacts to tail impacts also varies per velocity range. For the lowest velocity range (0 – 0.3075 km/s) tip impacts are more than twice as much as tail impacts. For the second lowest velocity range (0.3075 – 0.6150 km/s) the ratio inverts. In the third lowest velocity range (0.6150 – 0.9225 km/s) the number of tail impacts is close to 50% larger than tip impacts. For the fourth velocity range (0.9225 – 1.23 km/s) the ratio of tail to tip impacts almost doubles. For the fifth velocity range (1.23 – 1.53 km/s) there is five times more tip impacts are than tail impacts. For the remaining high velocity ranges, the number of tip impacts outnumbers tail impacts by thirteen and almost thirty times, respectively. Similar tables were generated for the remaining relative velocity ranges with similar patterns. The set of tables was completed when tumbling effects were added, as well as different scenarios of radial ejection velocity variability. At this point, the observed patterns do not provide any useful information to assess a level of damage.

Impact configuration regions with similar impact levels were identified after applying the five-level impact frequency criterion described in Table 3.10 to each cell in the table. Tables 3.26 and 3.27 depict matrices of impact quantification tables per impact configuration for a cylindrical projectile with L/D of 4 considering tumbling and not considering tumbling, respectively. From left to right, the cell-tables show impact frequencies calculated with increasing variability in radial ejection velocity ($\text{COV } V_{rp}$) of 0.00, 0.10, 0.25, 0.50, and 0.75. From top to bottom, the matrix shows the cell-tables per relative impact velocity range varying from the lowest range (0.0000- 0.3075 km/s) to the highest (1.845 or greater) in intervals of 0.3075 km/s. The matrix of impact frequencies without tumbling effects shows the diagonal pattern of higher impact frequencies (dark color regions) in every cell table over the range of radial ejection variability. The range of $(\phi-\alpha)$ scenarios is practically the same; however, minor differences are observed in the level of impact frequencies, since these totals correspond to the average of 30 simulations. Therefore, the diagonal pattern diffuses and reduces in intensity with higher variability. When comparing the matrix of tables without tumbling against the matrix with tumbling, a substantial change in the range and number of $(\phi-\alpha)$ scenarios with similar impact frequencies is observed. When tumbling is considered, a wider range of $(\phi-\alpha)$ scenarios is observed, covering the entire range of orientation angles (α) for the same range of strike angles (ϕ) observed in the tables without tumbling. This pattern is consistent even when variability in radial ejection velocity is added. Similar patterns are observed for other projectile geometry/sizes; therefore, these matrices are not included in this work.

Table 3.26. Impact Quantification Matrix for a Cylindrical Projectile with $L/D = 4$ Without Tumbling Effects per Impact Configuration

Vip cov Vel	0.00	0.10	0.25	0.50	0.75
0.0000 - 0.3075					
0.3075 - 0.6150					
0.6150 - 0.9225					
0.9225 - 1.2300					
1.2300 - 1.5375					
1.5375 - 1.8450					
1.8450 -					

Table 3.27. Impact Quantification Matrix for a Cylindrical Projectile with $L/D = 4$ With Tumbling Effects per Impact Configuration

Vip cov Vel	0.00	0.10	0.25	0.50	0.75
0.0000 - 0.3075					
0.3075 - 0.6150					
0.6150 - 0.9225					
0.9225 - 1.2300					
1.2300 - 1.5375					
1.5375 - 1.8450					
1.8450 -					

3.10 Significance of Impact Characterization

The quantification of impacts per impact characterization is insufficient information to assess a level of damage. The statistical study shows that a large range of impact velocities are developed through the entire range of encounter configuration scenarios per projectile geometry/size, as well as a large range of impact orientations. It is well known that the level of projectile impact speeds discussed above generate a large level of damage on the TBM warhead. This damage can be in the form of plastic deformation or even penetration and fragmentation. Since limited numerical and experimental work has been done to quantify the level of damage inflicted by these impacts, non-linear simulations are required to quantitatively measure the level of damage inflicted by a single projectile impact for a wide range of impact conditions. Then by aggregating the single impact damage of each and all the impacts to the TBM warhead, an overall damage to the warhead can be estimated. A comparison of total damage inflicted between encounter configuration scenarios using a specific projectile geometry/size will facilitate an assessment to make recommendations on endgame conditions or projectile geometry/sizes that maximize the lethality of the EKV defense system. Since the total number of single impacts to the TBM warhead of a particular projectile geometry/size exceeds 50,000 in a comprehensive endgame simulation that entails the entire range of all encounter configuration parameters, a rapid solution model to compute single impact damage is required.

3.11 Summary

A thorough explanation of the development of a code for simulating the EKV/TBM terminal encounter was presented. The code, named "Endgame Simulations", was utilized to study the interactions and trade-offs that different values for the near miss variables (*CA*, *MD*, and the *EBt*) and COV for the deployment projectile velocity, and projectile tumbling effects have in the number of projectiles impacting the TBM and how they arrive to the TBM surface. The study of the "Endgame Simulations" results suggest that although the number of the impacts is high, it is not known if the damage inflicted on the TBM is also high. Therefore, a method to calculate the damage inflicted by each single projectile impact is needed.

CHAPTER 4

NUMERICAL SIMULATIONS

4.1 Introduction

The previous chapter described the modeling of the terminal encounter kinematics between the EKV and the TBM. The model was implemented in a computer code capable of quantifying the number of impacts in the TBM payload section and calculates the projectile impact parameters, defined as the directional angles of the longitudinal axis of the cylindrical projectile and velocity vector in which the projectile impacts the TBM surface. However, the sole quantification of impacts and calculation of the impact parameters is not sufficient to assess the damage inflicted on the TBM warhead. This research work proposes a "damage index" to characterize damage based on the quantification of penetration depth and volume of target displaced by each projectile. Several projectile impacts were numerically simulated for a wide range of values of the impact variables and from the numerical results the "damage index" was calculated. Each single impact simulation was identified by the impact parameters which include the projectile's geometry (cylinder or sphere) and size, the magnitude and angle of incidence, ϕ , of the velocity vector and the cylinder orientation angles α and β . A relatively new method called Smoothed Particles Hydrodynamics (SPH) was the selected algorithm to perform the numerical simulations due to its excellent capabilities in the simulation of penetration and fragmentation problems where large plastic deformation occur (Randles P. W. et al. (2000), Campbell J. et al. (2000), Libersky L. D. et al. (1993)). To conduct the numerical simulations the hydrocode *MAGI* was selected because the developers of the code, Libersky L. D. et al. (1993), were willing to cooperate in the project and provided the source code to facilitate its modification to include special output formatting and to calculate the "damage index". This chapter provides an introduction of the SPH method and describes the development of the damage index mentioned above.

4.2 Smoothed Particles Hydrodynamics

Smoothed Particles Hydrodynamics, originally developed by Lucy L. B. (1977), Monaghan J. J. et al. (1983), and Gingold R. A. et al. (1977) to deal with gas dynamics problems in astrophysics and later extended to solid mechanics differences itself from other modeling techniques, such as Lagrangian or Eulerian methods, in that it is a meshless method where the calculation of interactions among neighboring particles is based on their separation alone. These features allow SPH to model problems with large strains and deformations. SPH transforms the governing balance equation of mass, linear momentum, and energy, in partial differential form, into integral equations using an interpolation function, called "kernel", to calculate the field variables at a specific point. The integrals are evaluated as sums over a selected number of neighboring particles because the information is only known at discrete points. The governing balance equations of continuum mechanics for mass, linear momentum, and energy are defined by

$$\frac{\partial \rho}{\partial t} + \mathbf{v} \cdot \nabla \rho + \rho \nabla \cdot \mathbf{v} = 0 \quad (4.1)$$

$$\nabla \mathbf{T} + \rho \mathbf{b} = \rho \frac{d\mathbf{v}}{dt} \quad (4.2)$$

$$\rho \frac{dE}{dt} = \text{tr}(\mathbf{T} \cdot \mathbf{D}) + \rho h - \nabla \cdot \mathbf{q} \quad (4.3)$$

where ρ is the mass density, \mathbf{v} is the velocity vector, \mathbf{T} is the Cauchy stress tensor, \mathbf{b} is the body force per unit mass, \mathbf{D} is the rate of deformation tensor, h is the heat source per unit mass and \mathbf{q} is the heat conduction vector. The term $\partial \rho / \partial t + \mathbf{v} \cdot \nabla \rho$ in Equation (4.1) is the material time rate $\partial \rho / \partial t$. Ignoring the body force \mathbf{b} and assuming that no heat conduction (adiabatic process) and no heat sources are presented Equations (4.1-4.3) become

$$\frac{d\rho}{dt} = -\rho \nabla \cdot \mathbf{v} \quad (4.4)$$

$$\frac{\partial \mathbf{v}}{\partial t} = \frac{1}{\rho} \nabla p \quad (4.5)$$

$$\rho \frac{dE}{dt} = \text{tr}(\boldsymbol{\sigma} \cdot \mathbf{D}) \quad (4.6)$$

To transform the governing equations from a partial differential form to an integral form consider the interpolated approximation of the scalar value function $A(\mathbf{r})$ defined by

$$\langle A(\mathbf{r}) \rangle = \int A(\mathbf{r}') w(\mathbf{r} - \mathbf{r}', h) d\mathbf{r}' \quad (4.7)$$

where

$$w(\mathbf{r} - \mathbf{r}', h) \quad (4.8)$$

is the interpolation kernel function (a two point function with a parameter h called "smoothing distance"), which has the following properties

$$\lim_{h \rightarrow 0} w(\mathbf{r} - \mathbf{r}', h) \rightarrow \delta(\mathbf{r} - \mathbf{r}') \quad (4.9)$$

$$\int w(\mathbf{r} - \mathbf{r}', h) d\mathbf{r} = 1 \quad (4.10)$$

$$w(\mathbf{r} - \mathbf{r}') = 0 \text{ for } |\mathbf{r} - \mathbf{r}'| \geq h \quad (4.11)$$

The first and second properties, Equations (4.9-4.10), assume the kernel function is continuous and differentiable and the volume under the curve of the kernel function has a value of 1. The third property, Equation (4.11), declares that the kernel function is zero if the absolute value of the difference between \mathbf{r} and \mathbf{r}' is greater or equal to the

smoothing distance h . Multiplying and dividing by the density at \mathbf{r}' the summation approximation becomes

$$\langle A(\mathbf{r}) \rangle = \int \frac{A(\mathbf{r}')}{\rho(\mathbf{r}')} w(\mathbf{r} - \mathbf{r}', h) \rho(\mathbf{r}') d\mathbf{r}' \quad (4.12)$$

where

$$\rho(\mathbf{r}') d\mathbf{r}' = m(\mathbf{r}') \quad (4.13)$$

is the mass density. Therefore, substituting Equation (4.13) into Equation (4.12), and letting $\mathbf{r} = \mathbf{r}_i$ and $\mathbf{r}' = \mathbf{r}_j$, and changing the integral to a summation

$$\langle A(\mathbf{r}_i) \rangle = \sum_{j=1}^N \frac{m(\mathbf{r}_j)}{\rho(\mathbf{r}_j)} A(\mathbf{r}_j) w(\mathbf{r}_i - \mathbf{r}_j, h) \quad (4.14)$$

Assume the values of $m(\mathbf{r}_j)$, $\rho(\mathbf{r}_j)$, and $A(\mathbf{r}_j)$ are known at point \mathbf{r}_j (referred to as "particle" j), and write $m(\mathbf{r}_j) = m_j$, $\rho(\mathbf{r}_j) = \rho_j$, and $A(\mathbf{r}_j) = A_j$. Then the interpolated approximation value of A at point i can be determined by the summation

$$\langle A(\mathbf{r}_i) \rangle = \sum_{j=1}^N \frac{m_j}{\rho_j} A_j w(\mathbf{r}_i - \mathbf{r}_j, h) \quad (4.15)$$

Since the interpolation kernel $w(\mathbf{r} - \mathbf{r}', h)$ is continuous and differentiable at any point (particle), so is $A(\mathbf{r}_j)$. The third property of the kernel restricts the number of particles N of the summation to those within the distance $|\mathbf{r} - \mathbf{r}'| \leq h$, the smoothing length, as depicted in the schematic of Figure 4.1.

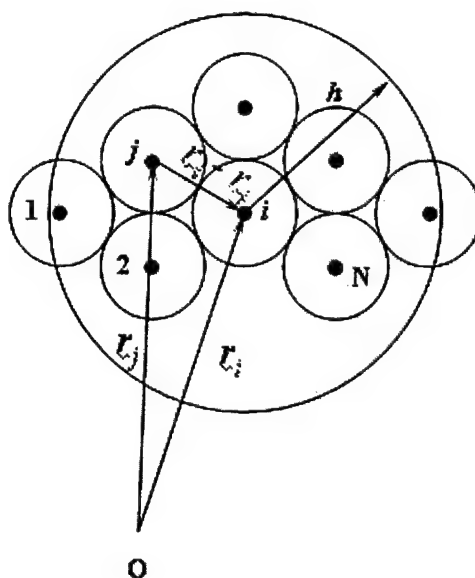


Figure 4.1. Neighboring particles calculation

For example, assuming the interpolation kernel function is the curve shown in Figure 4.2, the resulting value of the field variables at particle i are function of the interactions of particles that occur at a distance less than or equal than a distance h , in this specific example particles $j = 1$ and $j = 2$. The value of the interactions between particles corresponds to the value of the kernel function. The field variable of particle i at each time step is calculated by the sum of all the interactions of the particles within a distance h with particle i . The smoothing distance h is usually chosen by a trial and error process giving the best computational results.

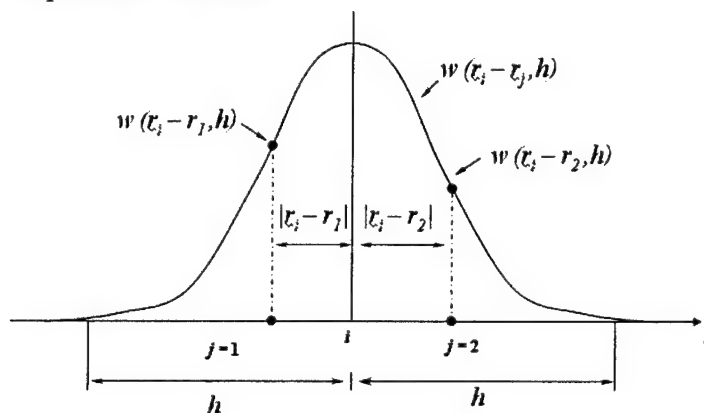


Figure 4.2. Neighboring particles according to selected smoothing distance.

Now, if we let $w(\mathbf{r} - \mathbf{r}', h) = w_{ij}$ equation (4.15) becomes

$$\langle A(\mathbf{r}_i) \rangle = \sum_{j=1}^N \frac{m_j}{\rho_j} A_j w_{ij} \quad (4.16)$$

Substituting $\rho(\mathbf{r}_i)$ for the arbitrary scalar valued function $A(\mathbf{r}_i)$ gives,

$$\langle \rho(\mathbf{r}_i) \rangle = \sum_{j=1}^N m_j w(\mathbf{r}_i - \mathbf{r}_j, h) \quad (4.17)$$

In order to transform the balance Equations (4.4-4.6) into the SPH formulation, the gradient of $A(\mathbf{r}_j)$ and $\rho(\mathbf{r}_i)$, and the divergence of $A(\mathbf{r}_j)$ and the velocity vector with respect to particle i in SPH form is required. Therefore, $\nabla A(\mathbf{r}_i)$, $\nabla \rho(\mathbf{r}_i)$ and $\nabla \cdot \mathbf{A}(\mathbf{r}_i)$ and $\nabla \cdot \mathbf{v}$ operations are defined as

$$\langle \nabla A(\mathbf{r}_i) \rangle = \langle \nabla A \rangle_i = \sum_{j=1}^N \frac{m_j}{\rho_j} A_j \nabla_i w_{ij} \quad (4.18)$$

$$\langle \nabla \rho(\mathbf{r}_i) \rangle = \nabla \langle \rho \rangle_i = \sum_{j=1}^N m_j \nabla_i w_{ij} \quad (4.19)$$

$$\langle \nabla \cdot \mathbf{A}(\mathbf{r}_i) \rangle = \langle \nabla \cdot \mathbf{A} \rangle_i = \sum_{j=1}^N \frac{m_j}{\rho_j} \mathbf{A}_j \cdot \nabla_i w_{ij} \quad (4.20)$$

$$\langle \nabla \cdot \mathbf{v} \rangle_i = \sum_{j=1}^N \frac{m_j}{\rho_j} \mathbf{v}_j \cdot \nabla_i w_{ij} \quad (4.21)$$

Finally, rewriting Equations (4.4-4.6) after performing the gradient and divergence operations described in Equations (4.18-4.21), in SPH form yields

$$\left\langle \frac{\partial \rho}{\partial t} \right\rangle_i = -\langle \rho \nabla \cdot \mathbf{v} \rangle_i = -\sum_{j=1}^N m_j (\mathbf{v}_j - \mathbf{v}_i) \cdot \nabla_i w_{ij} \quad (4.22)$$

$$\left\langle \frac{\partial \mathbf{v}}{\partial t} \right\rangle_i = \left\langle \frac{1}{\rho} \nabla p \right\rangle_i = \sum_{j=1}^N m_j \left(\frac{p_i}{\rho_i^2} + \frac{p_j}{\rho_j^2} \right) \nabla_i w_{ij} \quad (4.23)$$

$$\left\langle \frac{dE}{dt} \right\rangle_i = \sum_{j=1}^N m_j \frac{p_j}{\rho_j^2} (\mathbf{v}_i - \mathbf{v}_j) \cdot \nabla_i w_{ij} \quad (4.24)$$

Equations (4.22-4.24) represent the foundation of the SPH method for calculating the density, mass, velocity, and thermal energy of each particle. The time integration is performed using a central difference scheme in which the time derivatives are replaced by difference equations where the value of the function at the new time step is only a function of the value in the previous step. Various standard methods (e.g. predictor

corrector or second order Runge-Kutta integration) can be used to calculate the time stepping. *MAGI* uses the standard leap-frog algorithm (Libersky L. D. et al. (1993)).

4.2.1 Artificial Viscosity

In order to smooth shocks over a few resolutions lengths and stabilize numerical solutions an artificial viscosity term is added to equations (4.22-4.24). This artificial viscosity term has the dimensions of stress and is added to the pressure or stress term appearing in the SPH summation expression of the equation of motion. For example, Equation (4.23) becomes

$$\left\langle \frac{\partial \mathbf{v}}{\partial t} \right\rangle_i = \sum_{j=1}^N m_j \left\{ \left(\frac{p_i}{\rho_i^2} + \frac{p_j}{\rho_j^2} \right) + \Pi_{ij} \right\} \nabla_i w_{ij} \quad (4.25)$$

where Π_{ij} is the "viscous stress" or viscous pressure". The artificial viscosity is non-zero only for approaching particles (volume expansion) and has the value zero for separating particles (volume compression). The current form of artificial viscosity term Π_{ij} used by most SPH codes (Monaghan, 1992) is

$$\Pi_{ij} = \begin{cases} \frac{\beta \mu_{ij} - \alpha (v^2) (c_i + c_j) \mu_{ij}}{\frac{1}{2} (\rho_i + \rho_j)} & \text{if } (\mathbf{v}_i - \mathbf{v}_j) \cdot (\mathbf{r}_i - \mathbf{r}_j) < 0 \\ 0 & \text{otherwise} \end{cases} \quad (4.26)$$

where

$$\mu_{ij} = \frac{h(\mathbf{v}_i - \mathbf{v}_j) \cdot (\mathbf{r}_i - \mathbf{r}_j)}{(\mathbf{r}_i - \mathbf{r}_j)^2 + \eta^2}$$

given that $(\mathbf{v}_i - \mathbf{v}_j) \cdot (\mathbf{r}_i - \mathbf{r}_j) < 0$, $(\mathbf{v}_i - \mathbf{v}_j) \cdot (\mathbf{r}_i - \mathbf{r}_j) \leq 0$ and parameters $\eta^2 = eh^2$, $\alpha \approx 1$, $\beta \approx 2$, and $e = 0.001$

4.2.2 Equation of State

The Mie-Gruneisen equation of state was used in the simulation work and is defined as

$$P(\rho, E) = \left(1 - \frac{1}{2} \Gamma \eta \right) P_H(\rho) + \Gamma \rho E \quad (4.27)$$

The subscript "H" refers to the Hugoniot curve, while $\eta = \rho/\rho_o - 1$ represents the compression ratio and Γ is the Gruneisen parameter. The Hugoniot pressure is given by

$$P_H = \frac{C^2 \eta (1 + \eta)}{[1 - \eta(S - 1)]} \quad (4.28)$$

where the parameters S and C refer to the slope and bulk sound speed of the linear shock velocity-particle relation $U_s = C + SU_p$.

The plastic flow regime is defined by the von Mises flow stress and requires taking into account thermal softening, strain hardening, and strain rate effects on the equivalent flow stress for metals. A good option is the Johnson-Cook constitutive model (Johnson G. R. *et al.* (1983)), which is implemented in *MAGI*. This model expresses the von Mises flow stress as

$$\sigma = [A + B\varepsilon^n] [1 + C \ln \dot{\varepsilon}^*] [1 - T^{*m}] \quad (4.29)$$

where ε is the equivalent plastic strain, $\dot{\varepsilon}^* = \dot{\varepsilon}/\dot{\varepsilon}_0$ is the dimensionless plastic strain rate for $\dot{\varepsilon}_0 = 1.0s^{-1}$ and T^* is the homologous temperature. The five constants A , B , n , C and m are material parameters. The expressions in the first, second and third brackets represent the effects of strain, strain rate and temperature respectively. A fracture model was not necessary to implement because the SPH method models fragmentation very well (numerical fragmentation).

4.2.3 Kernel Interpolation Function

The interpolation kernel function used for modeling three-dimensional problems in *MAGI* is the cubic spline

$$w(\mathbf{r} - \mathbf{r}', h) = \frac{\sigma}{h^v} \begin{cases} 1 - \frac{3}{2}q^2 + \frac{3}{4}q^3 & \text{if } 0 \leq q \leq 1; \\ \frac{1}{4}(2 - q)^3 & \text{if } 1 \leq q \leq 2; \\ 0 & \text{if otherwise} \end{cases} \quad (4.30)$$

where

$$q = \frac{|\mathbf{r}_i - \mathbf{r}_j|}{h}$$

and v is the number of dimensions used in the problem and σ is the normalization constant with values $\frac{2}{3}$, $\frac{10}{7\pi}$ and $\frac{1}{\pi}$ for one, two, and three dimensions respectively.

4.3 Impact Modeling

In the absence of any information of tactical missiles regarding its design, projectile impacts were modeled using a system of seven bumper steel plates evenly spaced idealizing the TBM skin and internal components. The 0.5 cm thick plates are spaced at 1 cm and the center of gravity of plates 3 through 7 coincides with the projected path of the projectile velocity vector, as illustrated in Figure 4.3. The plate-vector alignment was done to minimize the total number of particles used in the simulation.

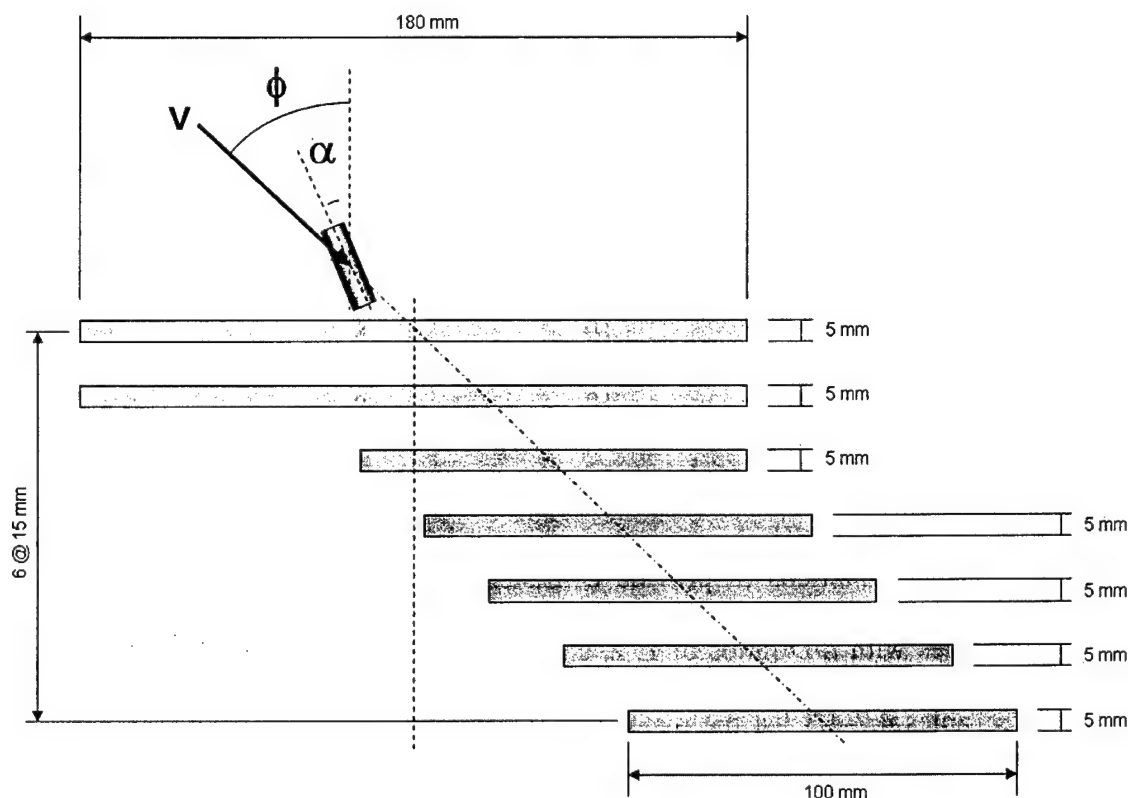


Figure 4.3. Schematic of idealized model of impact

The number of plates used was estimated based on previously performed simulations using the most lethal configuration of projectile impacts. These impact configurations were run using the highest expected projectile velocity at impact and making both the longitudinal axes of the cylindrical projectile and the velocity vector normal to the plate surface. Using a system of seven bumper plates, the projectile stopped in the last plate depleting all its kinetic energy, and in consequence no more penetration occurs. Based on the observation for the most lethal case, the seven-bumper plate system provides a good benchmark to compare the lethality of different impact configurations. The maximum simulation times used for modeling the impacts were set until the kinetic energy of the projectile was depleted before full penetration of the seventh plate. Simulation times range from 120 μ s to 150 μ s depending on the projectile's geometry and orientation. Dimensions of each plate and its material properties are listed in Table 4.1.

Table 4.1. Bumper plate dimensions and material properties.

Plate No.	Dimensions (cm)		
	Length	Width	Thickness
1 st plate	18	8	0.5
2 nd plate	18	10	0.5
3 rd plate	10	10	0.5
4 th plate	10	8	0.5
5 th plate	10	8	0.5
6 th plate	10	8	0.5
7 th plate	10	8	0.5
Material: Steel			
Density: 7.9 (gr/cm ³)			

The projectile shapes and sizes used in this model were the same used in the Endgame simulations to provide consistency throughout this work. As mentioned in section 3.3.1, the projectile mass was kept constant for all the simulations. Cylindrical projectiles with L/D ratios of 1, 2, and 4 were selected for comparison. The parameters describing the material, mass, shape, and sizes used for the projectiles are listed in Table 3.2. Tables 4.2-4.3 list the material parameters for steel and tungsten used in the Mie-Gruneisen and Johnson-Cook constitutive models.

Table 4.2. Material Parameters for Steel.

Parameter	Value	Description
ρ_0	7.90 gr/cm ³	Initial density
C	4.58 km/s	Bulk sound speed
S	1.51	Slope of the shock to particle speed
Γ	2.0	Gruneisen Parameter
T_0	300 °K	Initial temperature
T	1800 °K	Initial melt temperature
A	324 MPa	Yield stress in Johnson-Cook (JC) model
B	114 MPa	Strain hardening constant in JC model
C	0.003	Strain rate hardening constant in JC model
n	0.42	Strain hardening exponent in JC model
m	1.34	Thermal softening constant

Table 4.3. Material Parameters for Tungsten.

Parameter	Value	Description
ρ_0	17.6 gr/cm ³	Initial density
C	4.029 km/s	Bulk sound speed
S	1.237	Slope of the shock to particle speed
Γ	1.54	Gruneisen Parameter
T_0	300 °K	Initial temperature
T	1723 °K	Initial melt temperature
A	1510 MPa	Yield stress in Johnson-Cook (JC) model
B	177 MPa	Strain hardening constant in JC model
C	0.016	Strain rate hardening constant in JC model
n	0.12	Strain hardening exponent in JC model
m	1.00	Thermal softening constant

The simulations for both the cylinder and the sphere were executed with projectile velocities of 0.25, 0.50, 1.00, 1.25, 1.25, 1.80, and 2.15 km/s with obliquity angles ϕ from 0° to 75° with increments of 15° and geometry orientation angle α , only applicable to cylindrical projectiles, from -75° to 90° with increments of 15°.

Early simulation trials were executed using smoothing distances h of 0.25, 0.20, 0.15, 0.12, 0.08, and 0.06 cm. The computational time required to run the simulations grew exponentially as the smoothing distance decreased below values of 0.10 cm. Nevertheless, smaller smoothing distances ($h < 0.10$ cm) give more resolution to the objects besides it gives more accurate results. Although *MAGI* has the option to define different smoothing distances for different objects in the same simulation, equal smoothing distances for all the objects in a single simulation provided more cohesiveness in the visualization of the object particles. A final smoothing distance of 0.1255 cm for both the projectile and plates was selected to run the final simulations.

4.4 Preliminary simulation results

The impact simulations were batch executed on the same PC workstation where the Endgame simulations were run as described in section 3.6. *MAGI* simulation results were given in output files for each field variable at selected time increments in binary form. A special program developed in Delphi™ 6.0 (Pascal Compiler) was used to visualize the simulation results. However, the time it required to read the output files along with some visualization restrictions (the simulations could be only viewed in 2D at the last time step) motivated the search of more powerful software.

Enight™ 7.0 visualization software provided a more powerful tool to visualize the results from *MAGI*. Figure 4.4 shows a 3D visualization of a cylinder impacting the bumper plates with the color-scale representing the variation of the pressure.

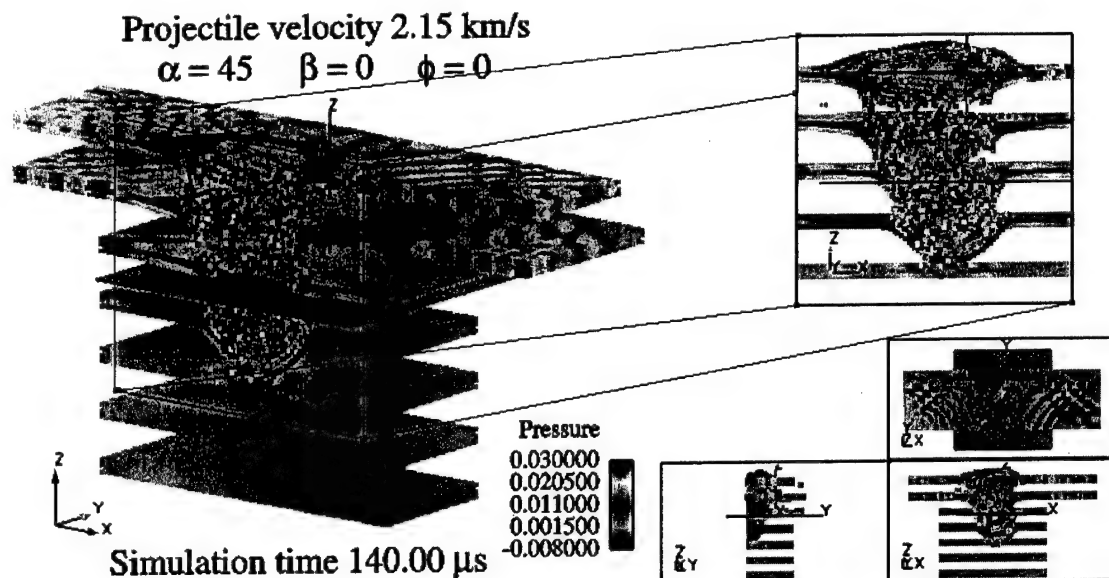


Figure 4.4. Visualization of simulation results in Ensight 7.0.

The program developed in Delphi™ 6.0 was later expanded to analyze several field variables including the density, particle mass, plastic strain, displacement and kinetic energy to visually investigate through time-history plot the possible patterns that interact to cause damage. Figure 4.5 shows a time-history plots for the kinetic energy of a 7 bumper plate system under hypervelocity impact. The curves represent the average of the field variable at each time step per object

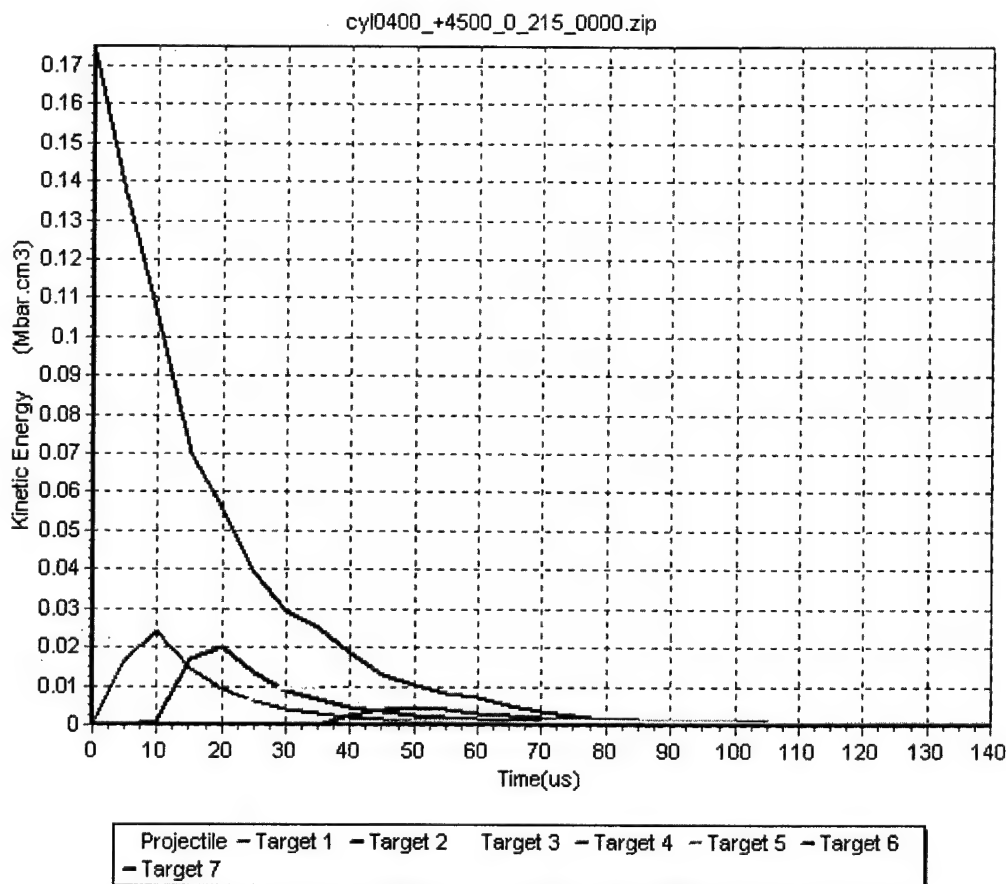


Figure 4.5. Typical time-history plot of Kinetic Energy for projectile $L/D = 4$ with velocity = 2.15 km/s and angles $\alpha = 45$, $\beta = 0$, $\phi = 0$.

4.5 Damage Index Development

Based on the visualizations of early simulation results and time history plots of the field variables, it was observed that the damage generated on the bumper plates could be characterized in terms of the depth of penetration of the projectile and the size of the holes generated on each plate. It can be seen in Figure 4.6 that for small obliquity impact angles the depth of penetration is large while the holes in the plates are kept small. As the obliquity angle increases, the depth of penetration increase but the size of the penetration holes increases.

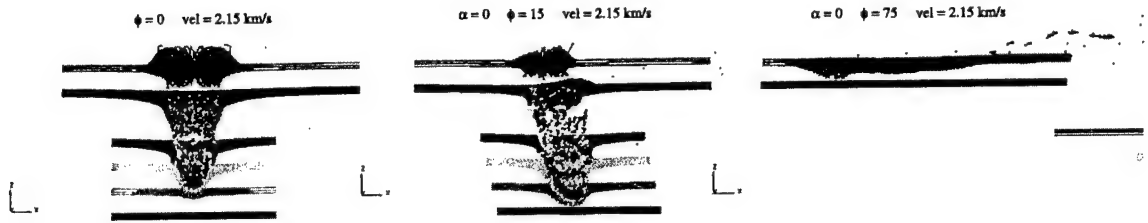


Figure 4.6. Comparison of impacts for SIDI development

Therefore, to quantify damage, both effects (the amount of projectile penetrated and the amount of plate volume displaced) were taken into account. The penetrated volume defined by

$$V_{pen} = \sum_{i=1}^n \left(\frac{z_i}{h_T} \right) \left(\frac{m_i}{\rho_{projectile}} \right) \text{ if } \begin{cases} z_i \leq 0.0 & \frac{z_i}{h_T} = 0 \\ 0.0 < z_i < h_T & \frac{z_i}{h_T} \\ z_i \geq 0.0 & \frac{z_i}{h_T} = 1 \end{cases} \quad (4.31)$$

is the volume of the projectile particles that trespass the top surface of the first bumper plate (particles ejected away from the top plate were not considered). Each particle is weighted in proportion to its penetrated position with respect to the total depth, h_T , of the bumper plate system. The total penetrated volume is the summation of the values of each weighted particle that penetrated the system.

The displaced volume defined by

$$V_{dis} = \sum_{i=1}^n \left(\frac{m_i}{\rho_{plates}} \right) \text{ for } \varepsilon_p \geq 0.75 \quad (4.32)$$

is the volume of the plate particles displaced from its original position which exceeded a minimum plastic strain, ε_p , threshold of 0.75. This threshold was determined by a visual inspection of the results of the preliminary simulations where it was found that particles having a plastic strain larger than 0.75 were already separated from the plate and thus giving an indication of the size of the penetration hole. The calculated displaced volume is multiplied by a factor of 0.05 and added to the penetrated volume. This method permits to scale the displaced volume, whose values range from 6.00 to 15.0 approximately, to the smaller values of the penetrated volume. In addition, it gives more importance to the penetration made by the projectile than the displaced volume of the plates.

The proposed Single Impact Damage Index (SIDI) is calculated by aggregating the weighted displaced and the penetrated volume defined by

$$SIDI = 0.05 V_{dis} + 1.00 V_{pen} \quad (4.33)$$

The formulas defining the damage index were implemented in the program developed previously in Delphi™ 6.0. This program read the field variable output files given by *MAGI* of each simulation. Later, in order to reduce time, the formulas were implemented as a subroutine of *MAGI* and the corresponding SIDI values along with the impact parameters of each simulation were written in a single output data file.

4.6 SIDI Results

Each curve presented in Figure 4.7 represents damage index values per impact scenario for tungsten projectiles with $L/D = 4$ and projectile velocity of 2.15 km/s with projectile orientation angle α fixed and obliquity angle ϕ varying from low values to normal values (75° to 0°) from down to up. Taking advantage of impact symmetry, damage index values of impact scenarios with an angle of $\alpha = -90$, which simulations were not run since they are the same of $\alpha = 90$. It can be seen from this graph that as the angle ϕ approaches zero (normal impact) in each curve, the damage index increases except for cases with $\alpha = 60, 45, 30$ and for sphere where the SIDI slightly decreases at ϕ equal to zero when compared to previous ϕ angle. This could be explained by the fact that a small deviation from normal impact does not significantly decreases the depth of penetration but does increase the size of the penetration holes.

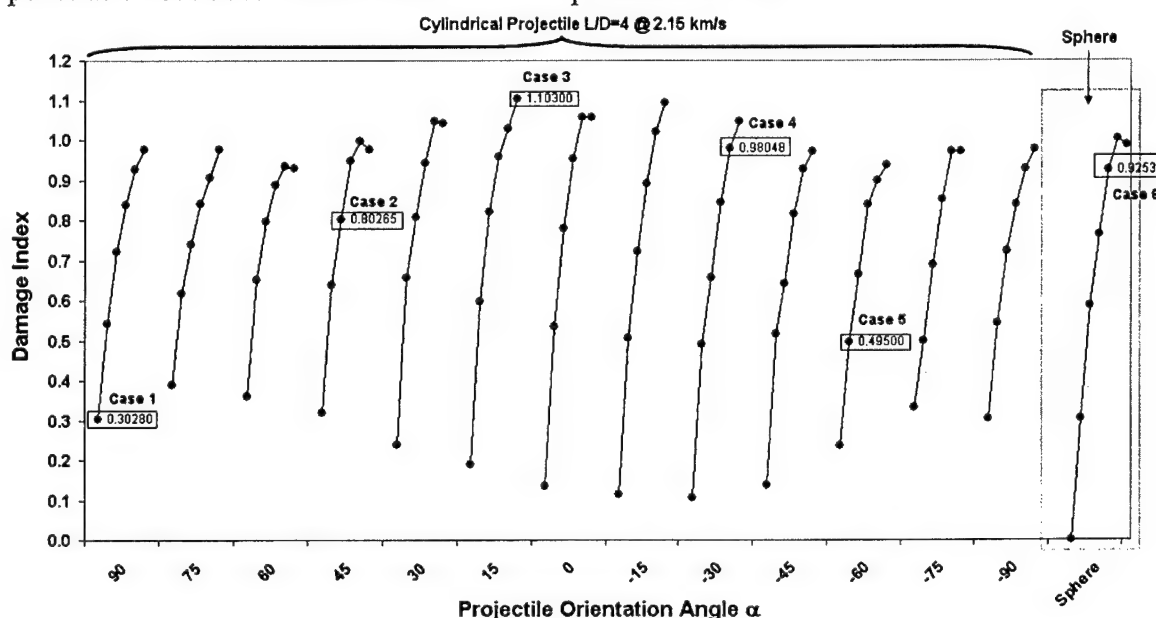


Figure 4.7. Damage Index values for projectile velocity of 2.15 km/s for cylindrical projectiles with $L/D = 4$ and sphere.

Simulations pictures of the last time step of the for all the cases in Figure 4.7 for a $L/D = 4$ and sphere for a projectile velocity of 2.15 km/s per angle α and varying angle ϕ are depicted in Figures 4.8-4.20.

Pictures of the initial and final time steps of the simulations of selected cases 1 through 6 from Figure 4.7 are depicted with its SIDI values in Figures 4.21- 4.26. These figures show that for cases 1 (angles $\alpha = 90$ and $\phi = 75$) and 5 (angles $\alpha = -40$ and $\phi = 60$) its SIDI values are small as compared to cases 2, 3, 4 and 6 where both the obliquity angle ϕ and the orientation angle α approximates to the normal plane with respect to the plate and, consequently, the penetration is deeper than for cases 1 and 5.

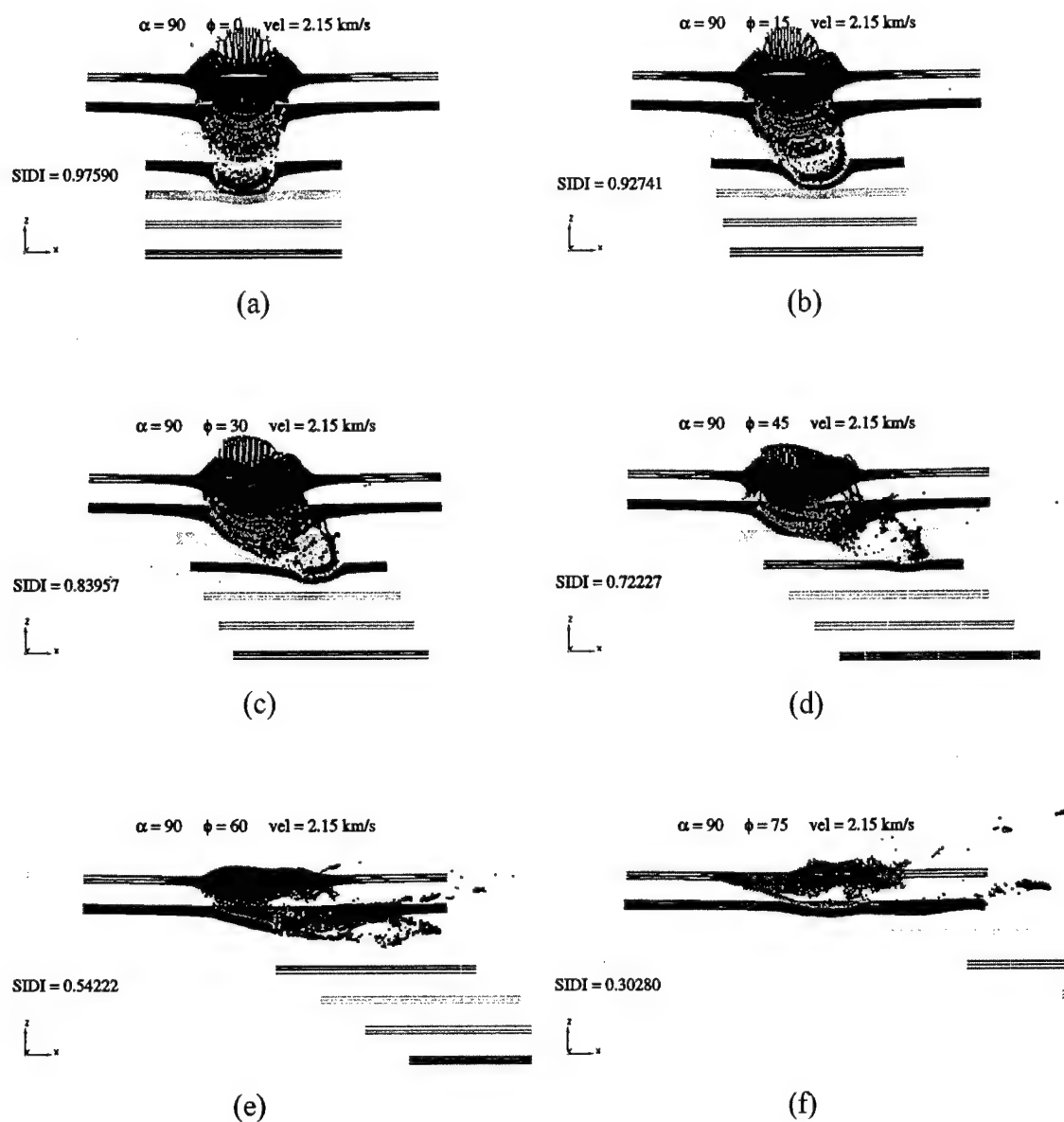


Figure 4.8. Impact Simulations for $LD = 4$ and $\alpha = 90$ at ϕ angles of 0, 15, 30, 45, 60, 75 (a, b, c, d, e, f respectively) at final time step.

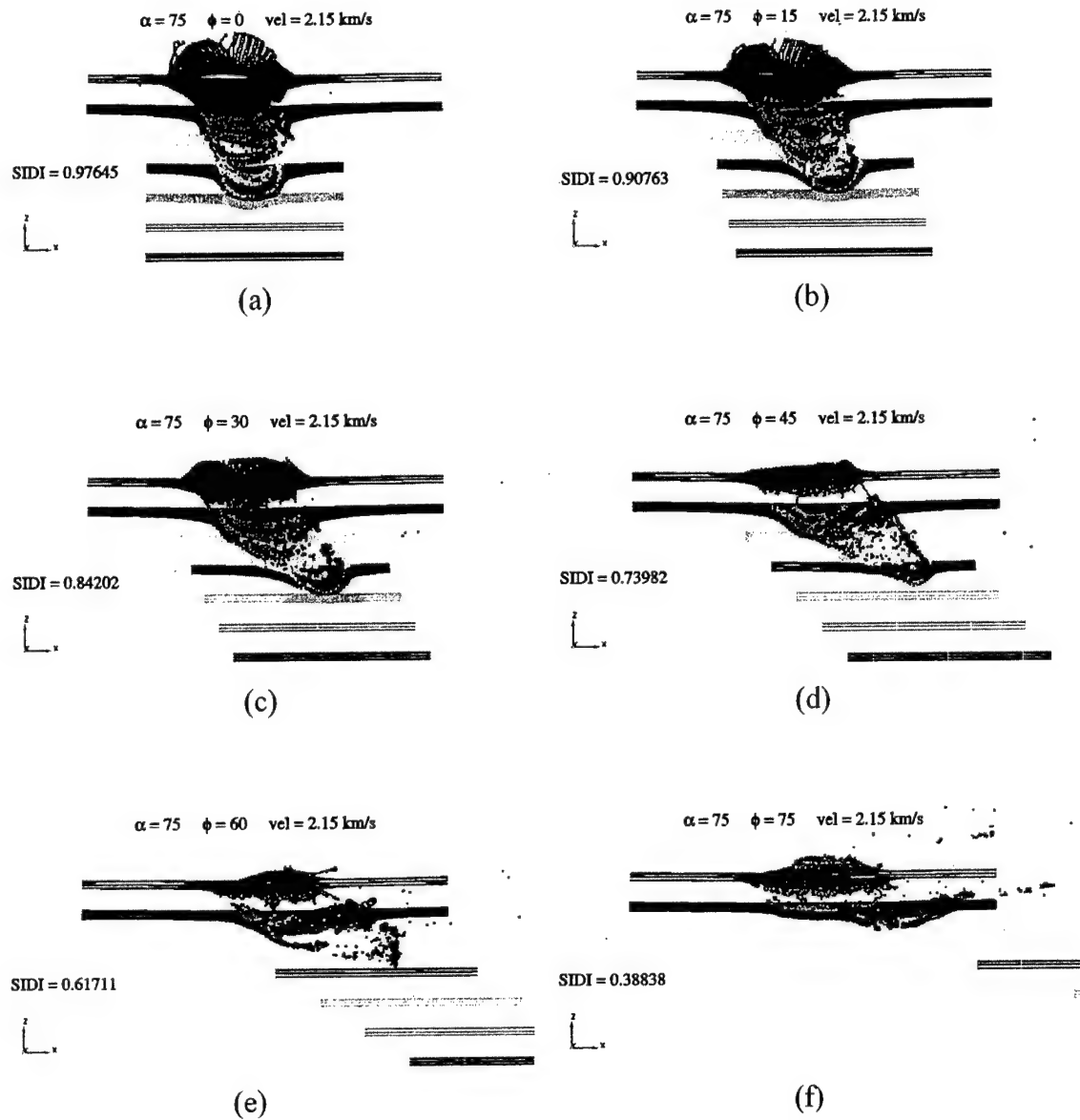


Figure 4.9. Impact Simulations for $LD = 4$ and $\alpha = 75$ at ϕ angles of 0, 15, 30, 45, 60, 75 (a, b, c, d, e, f respectively) at final time step.

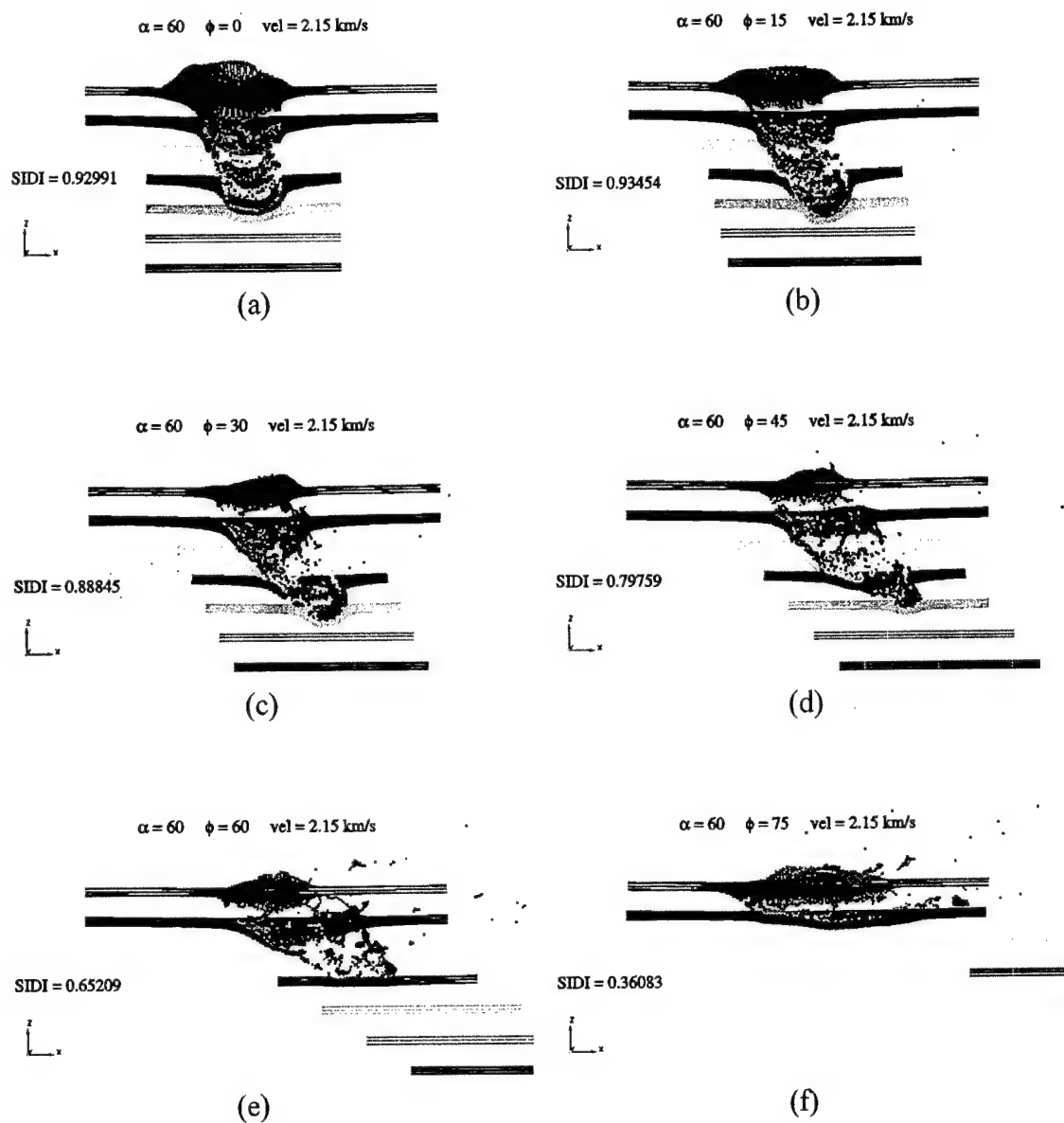


Figure 4.10. Impact Simulations for $LD = 4$ and $\alpha = 60$ at ϕ angles of 0, 15, 30, 45, 60, 75 (a, b, c, d, e, f respectively) at final time step.

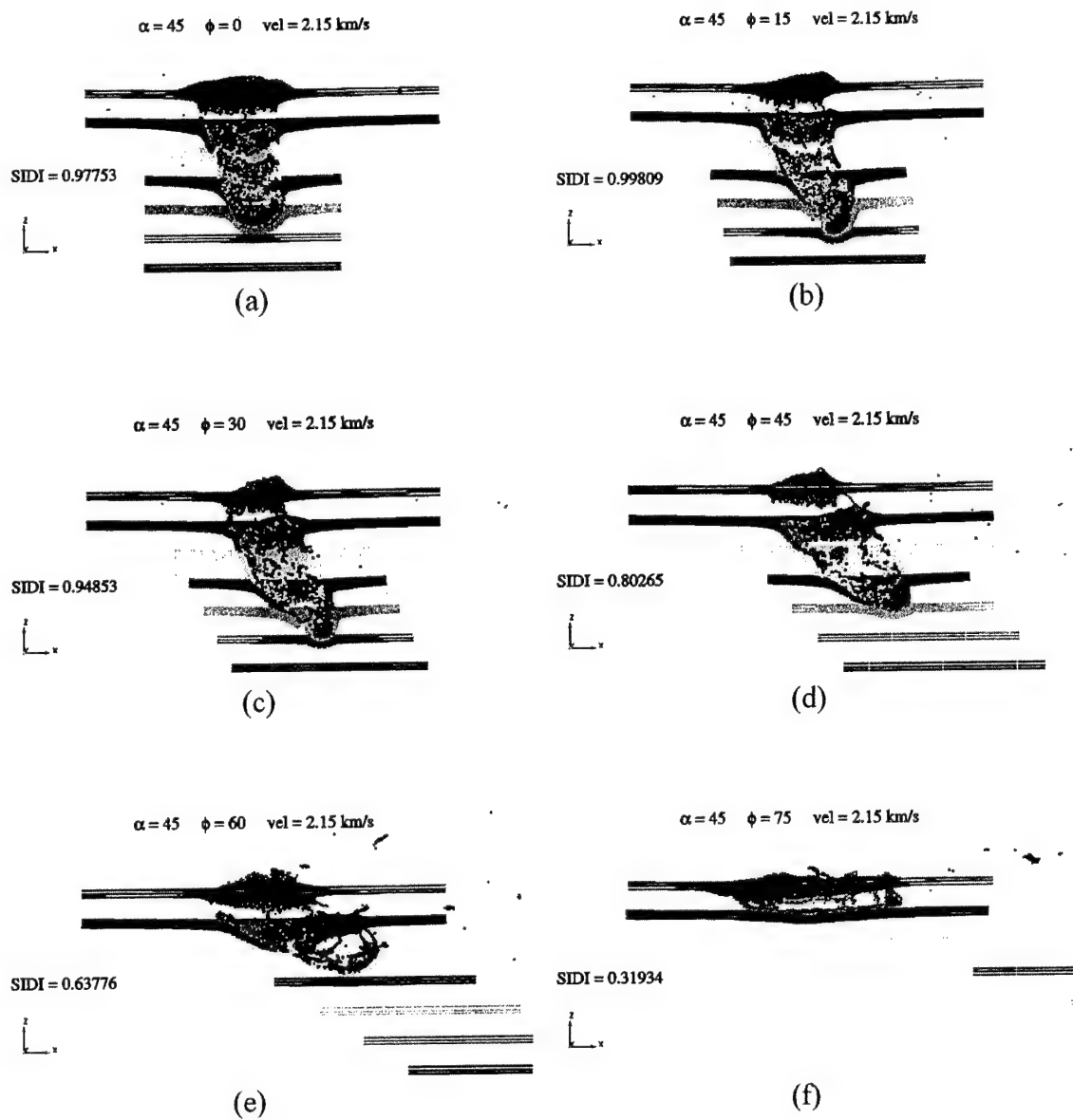


Figure 4.11. Impact Simulations for $LD = 4$ and $\alpha = 45^\circ$ at ϕ angles of 0, 15, 30, 45, 60, 75 (a, b, c, d, e, f respectively) at final time step.

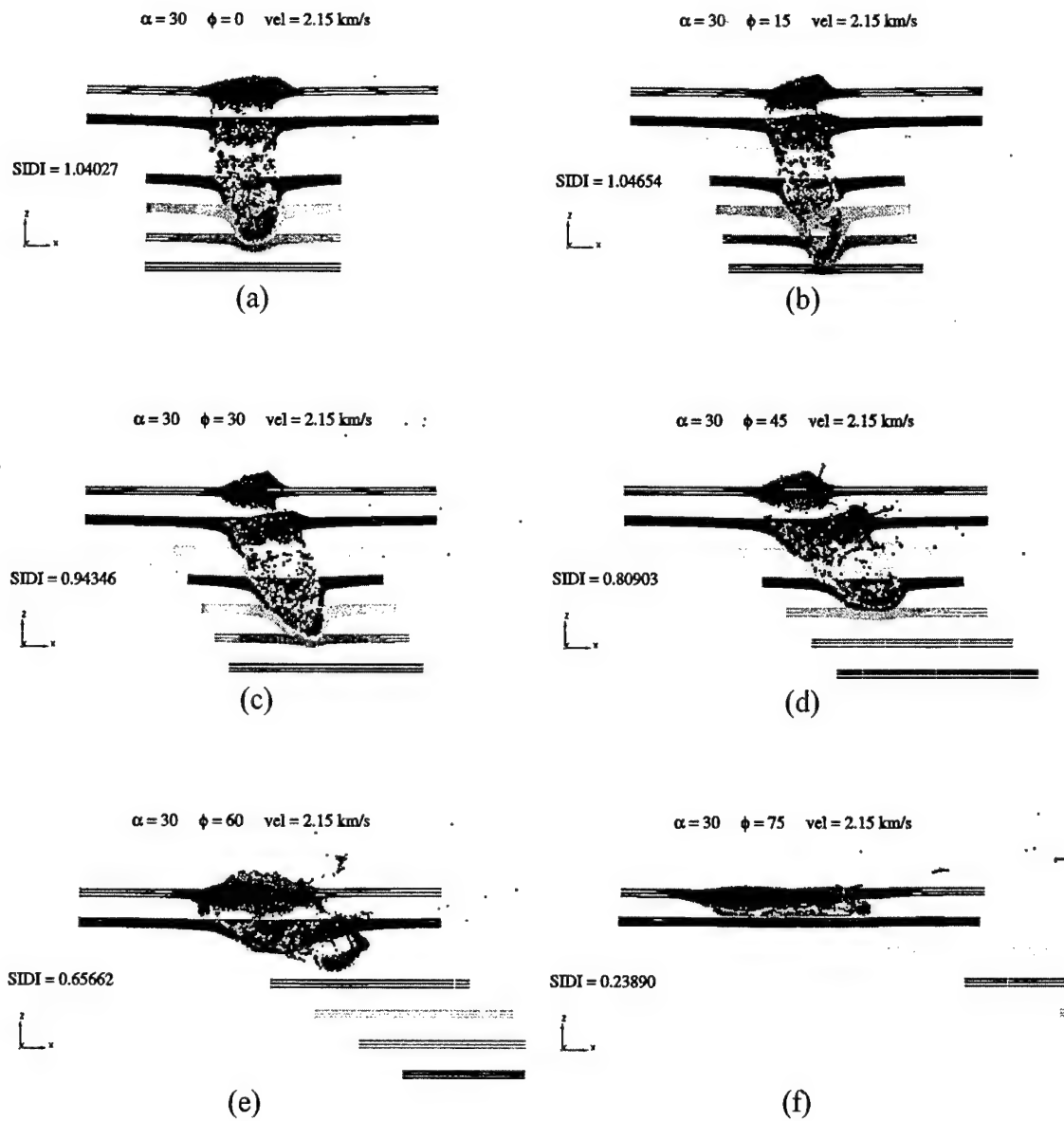


Figure 4.12. Impact Simulations for $LD = 4$ and $\alpha = 30$ at ϕ angles of 0, 15, 30, 45, 60, 75 (a, b, c, d, e, f respectively) at final time step.

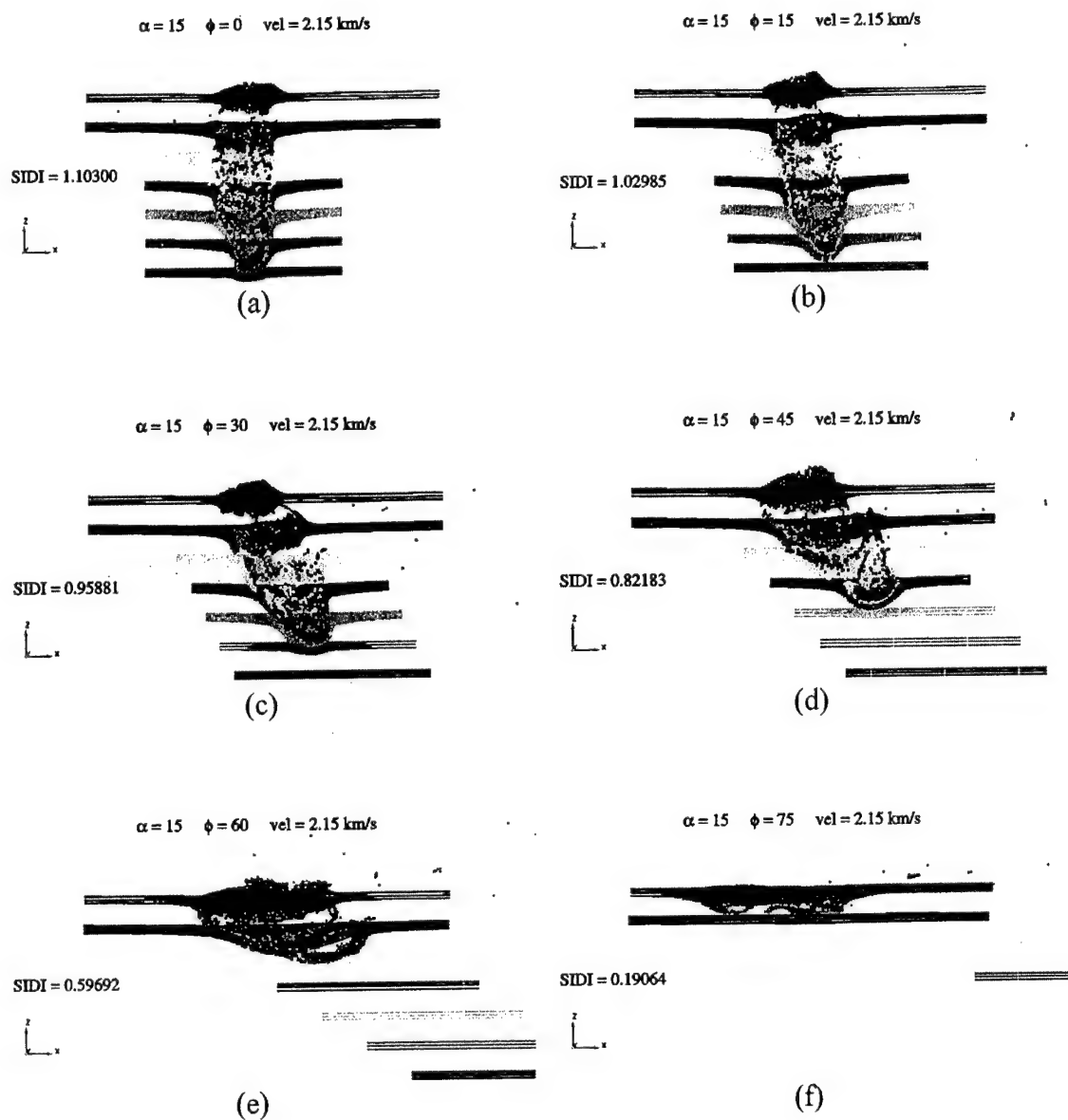


Figure 4.13. Impact Simulations for $LD = 4$ and $\alpha = 15$ at ϕ angles of 0, 15, 30, 45, 60, 75 (a, b, c, d, e, f respectively) at final time step.

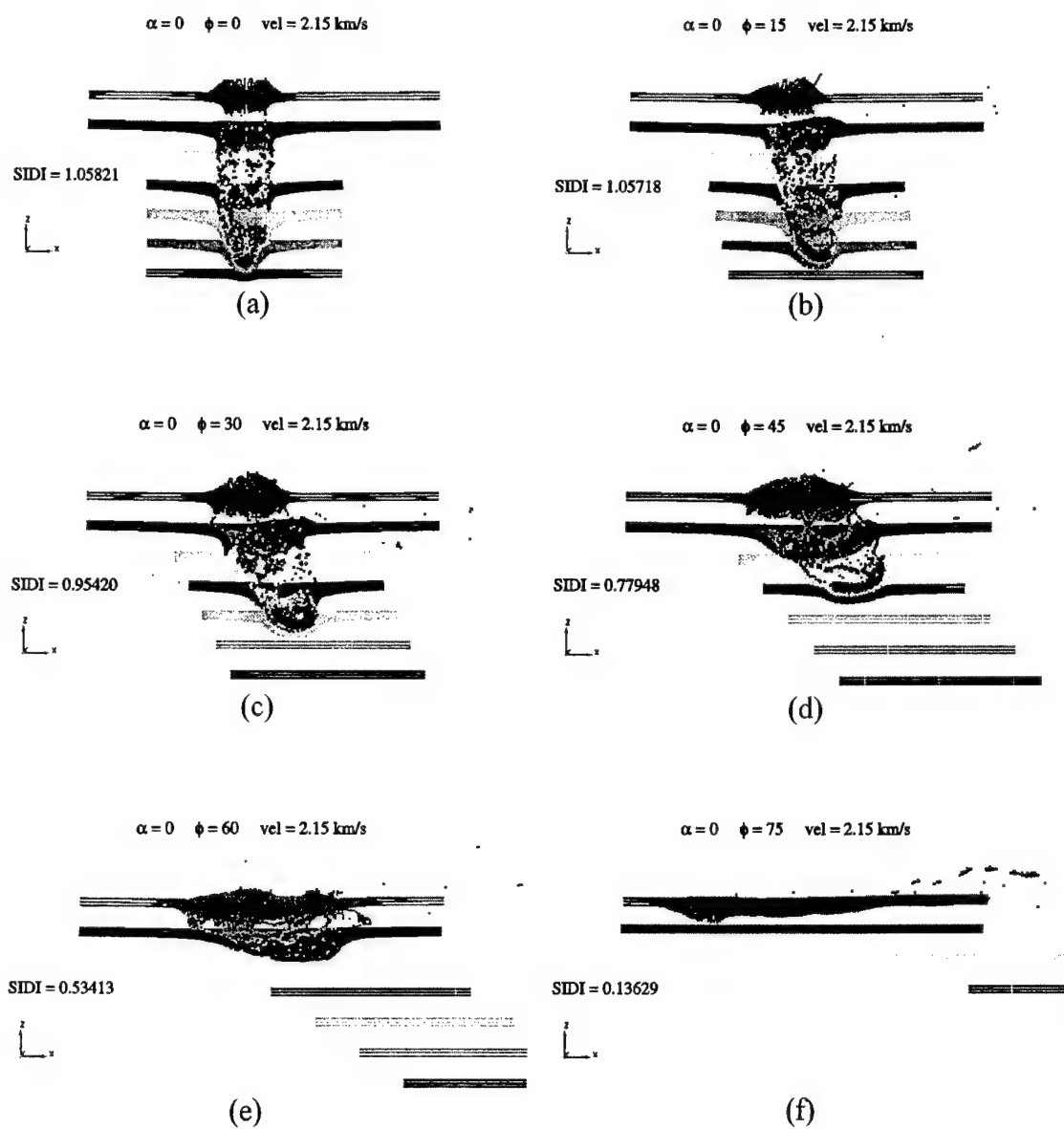


Figure 4.14. Impact Simulations for $LD = 4$ and $\alpha = 0$ at ϕ angles of 0, 15, 30, 45, 60, 75 (a, b, c, d, e, f respectively) at final time step.

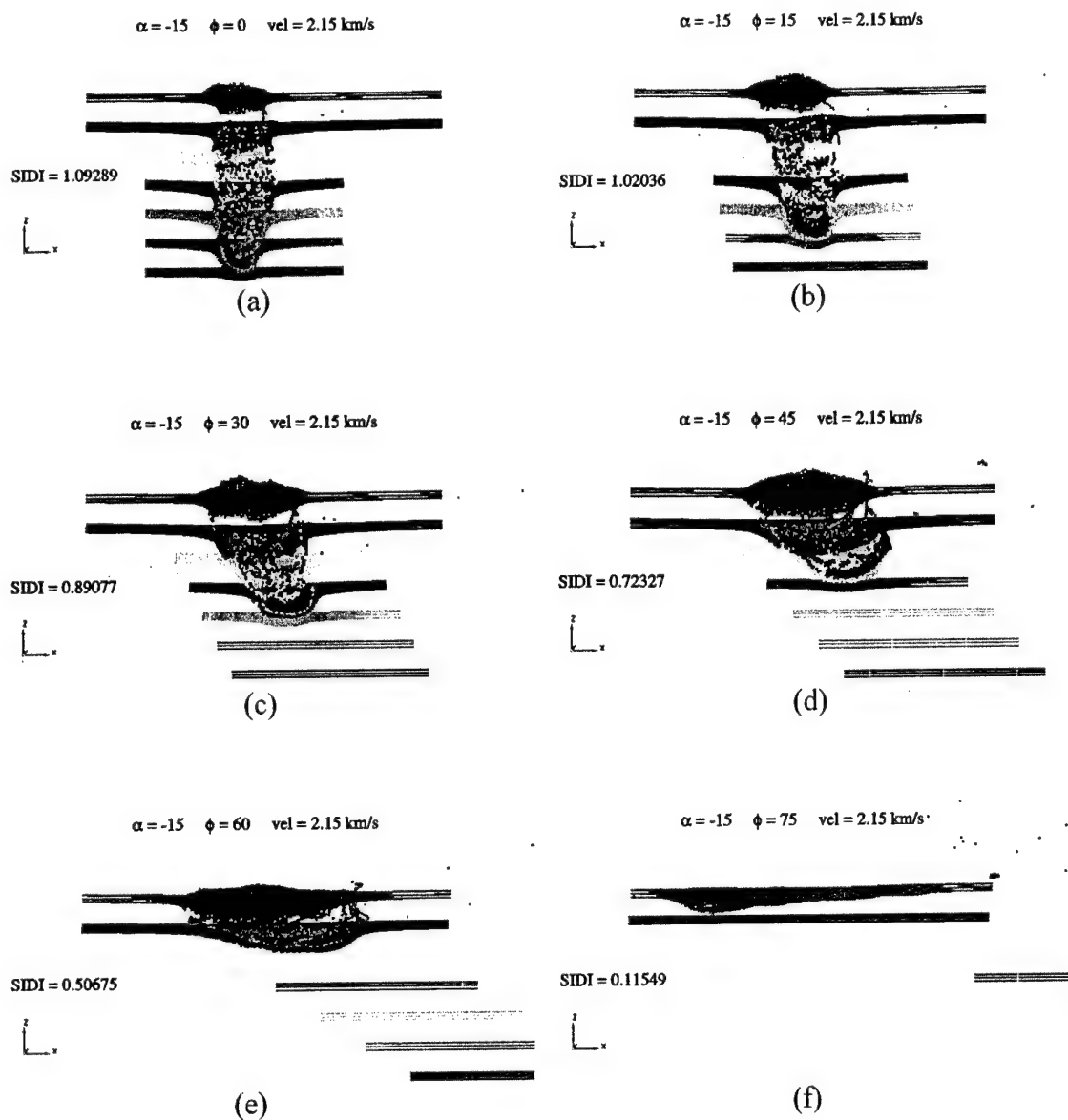


Figure 4.15. Impact Simulations for $LD = 4$ and $\alpha = -15$ at ϕ angles of 0, 15, 30, 45, 60, 75 (a, b, c, d, e, f respectively) at final time step.

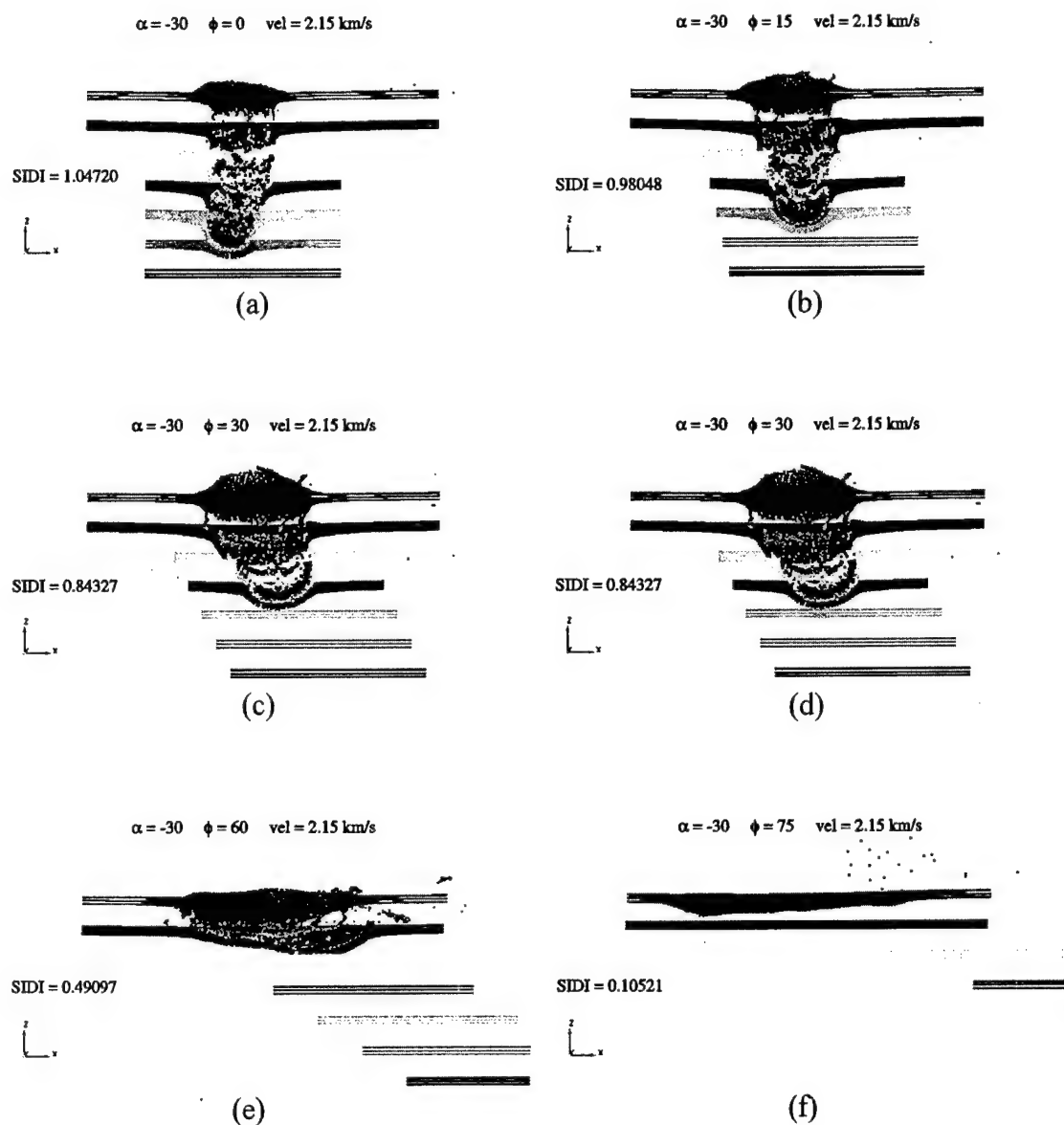


Figure 4.16. Impact Simulations for $LD = 4$ and $\alpha = -30$ at ϕ angles of 0, 15, 30, 45, 60, 75 (a, b, c, d, e, f respectively) at final time step.

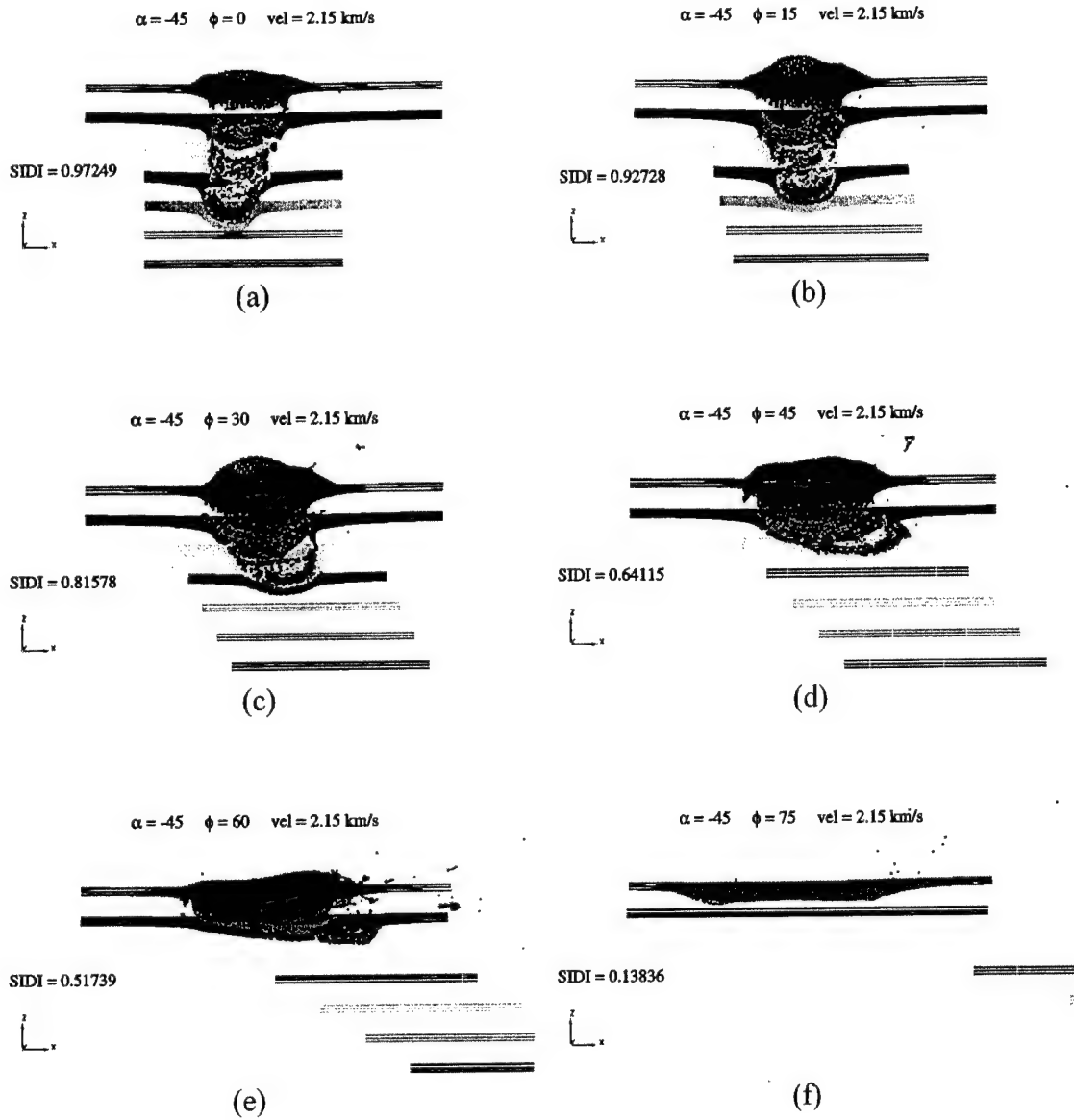


Figure 4.17. Impact Simulations for $LD = 4$ and $\alpha = -45$ at ϕ angles of 0, 15, 30, 45, 60, 75 (a, b, c, d, e, f respectively) at final time step.

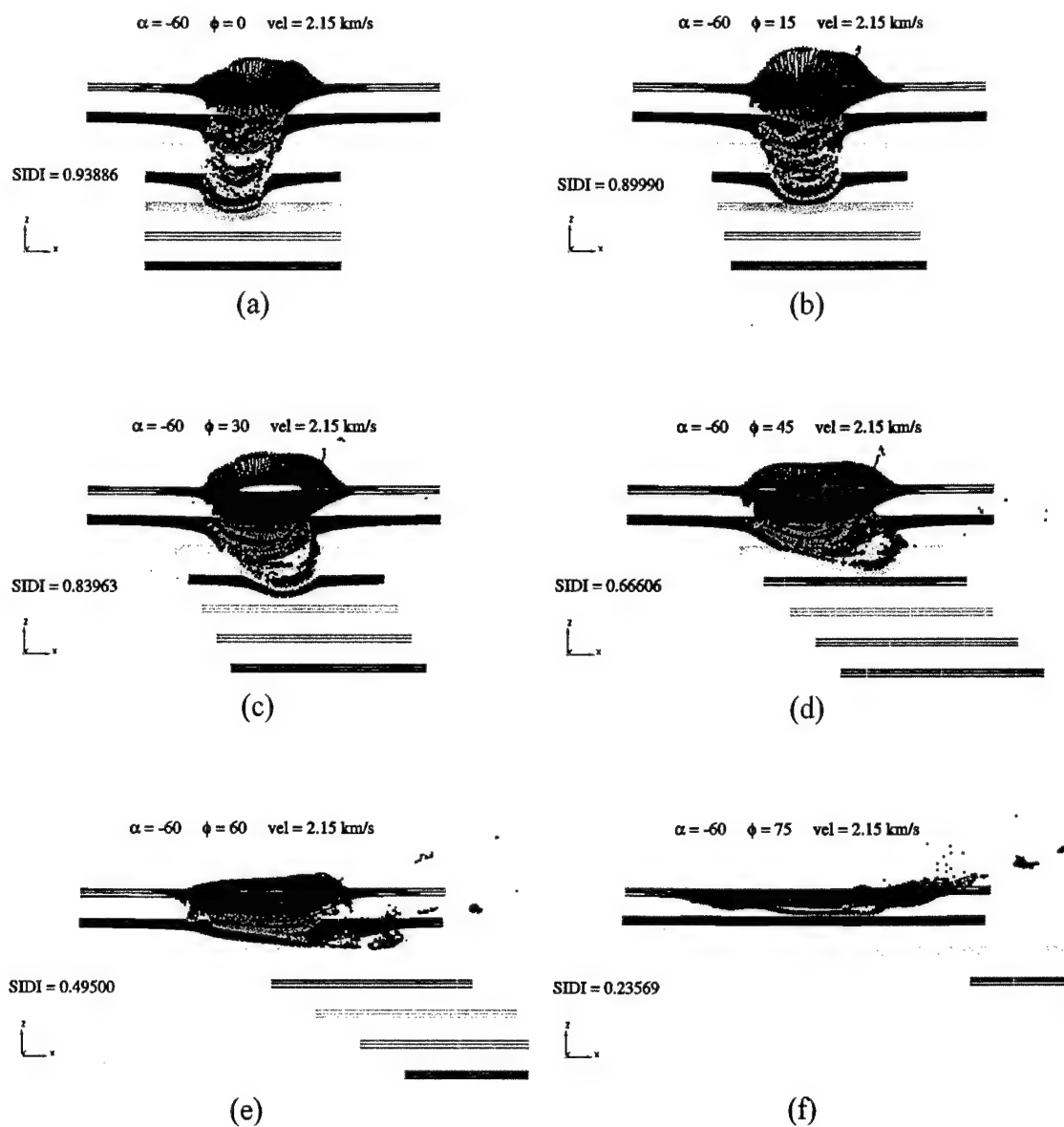


Figure 4.18. Impact Simulations for $LD = 4$ and $\alpha = -60$ at ϕ angles of 0, 15, 30, 45, 60, 75 (a, b, c, d, e, f respectively) at final time step.

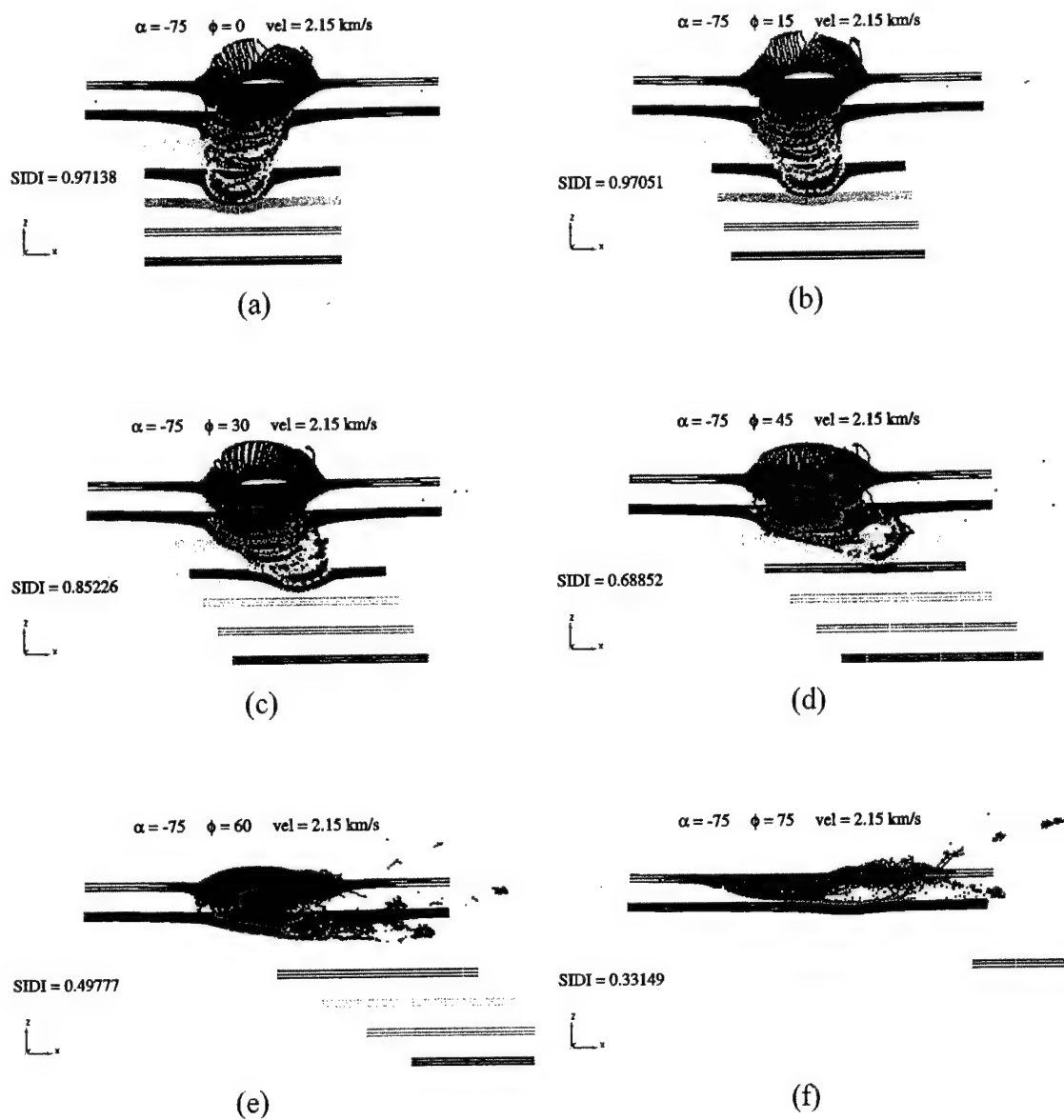


Figure 4.19. Impact Simulations for $LD = 4$ and $\alpha = -75$ at ϕ angles of 0, 15, 30, 45, 60, 75 (a, b, c, d, e, f respectively) at final time step.

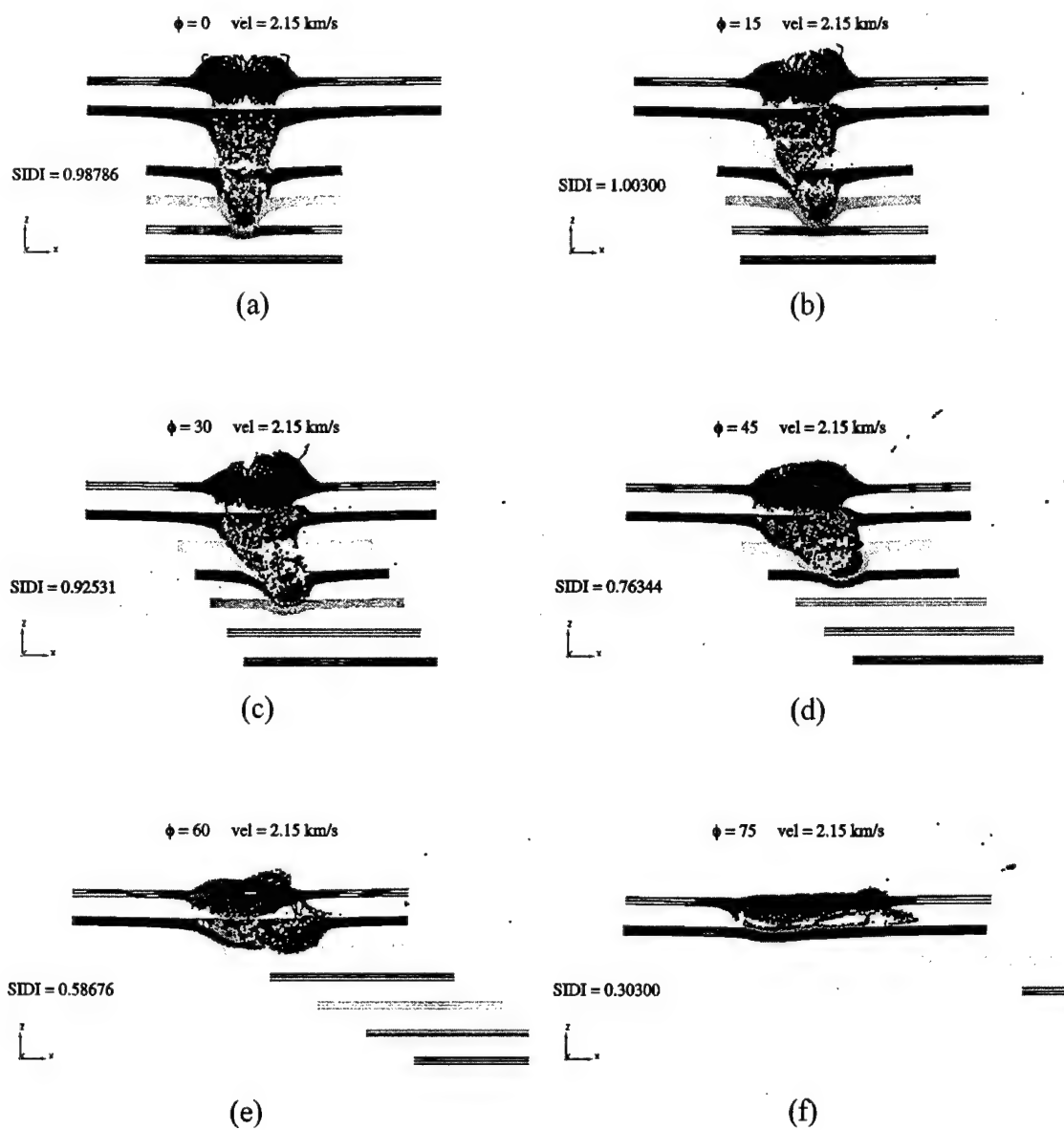


Figure 4.20. Impact Simulations for sphere projectile at α angles of 0, 15, 30, 45, 60, 75 (a, b, c, d, e, f respectively) at final time step.

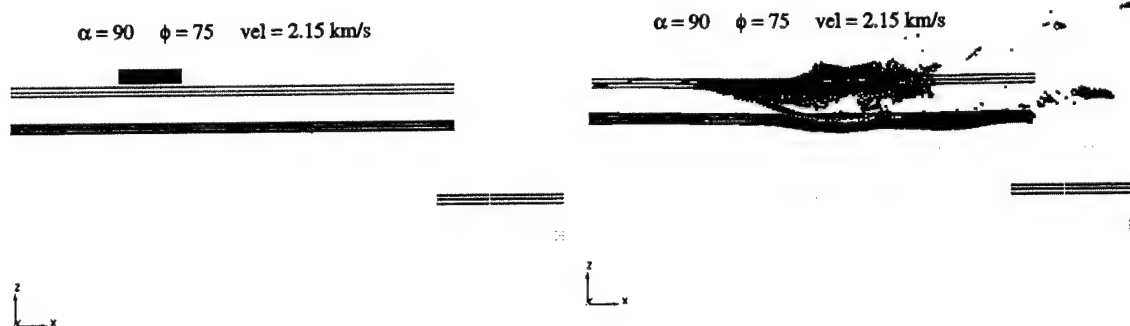


Figure 4.21. Case 1: Cylinder Impact $L/D = 4$, $\text{vel} = 2.15$, $\alpha = 90$, $\phi = 75$.

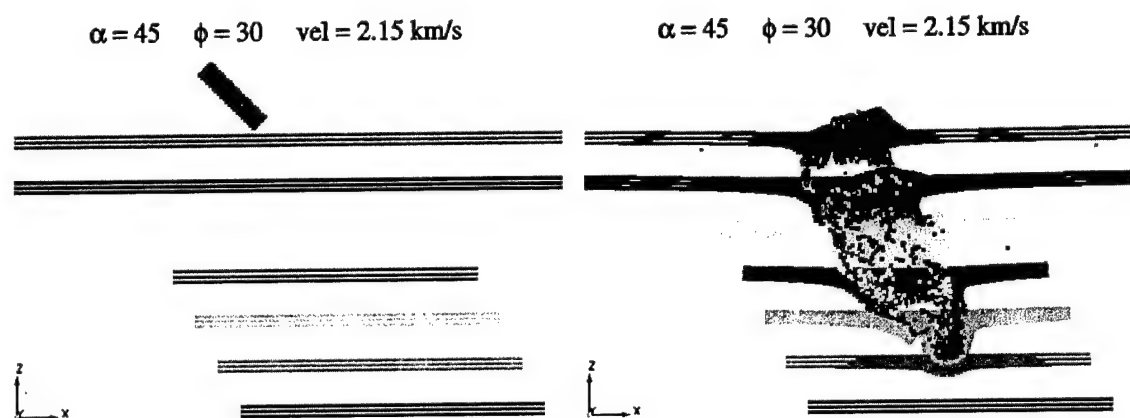


Figure 4.22. Case 2: Cylinder Impact $L/D = 4$, $\text{vel} = 2.15$, $\alpha = 45$, $\phi = 30$.

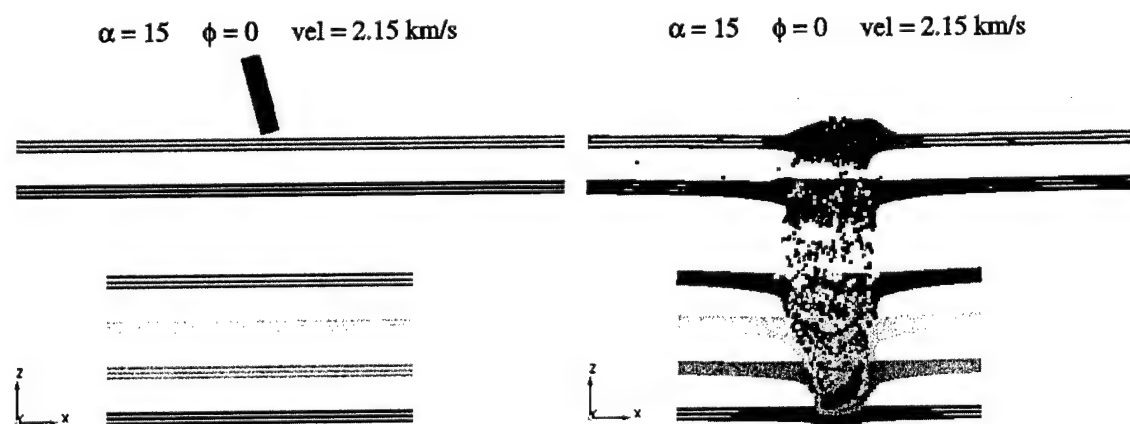


Figure 4.23. Case 3: Cylinder Impact $L/D = 4$, $\text{vel} = 2.15$, $\alpha = 15$, $\phi = 0$.

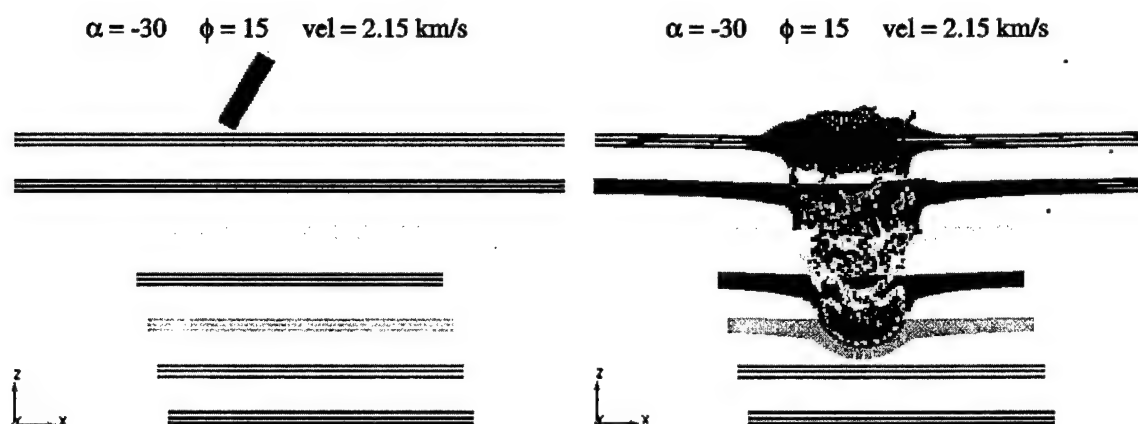


Figure 4.24. Case 4: Cylinder Impact $L/D = 4$, $\text{vel} = 2.15$, $\alpha = -30$, $\phi = 15$.

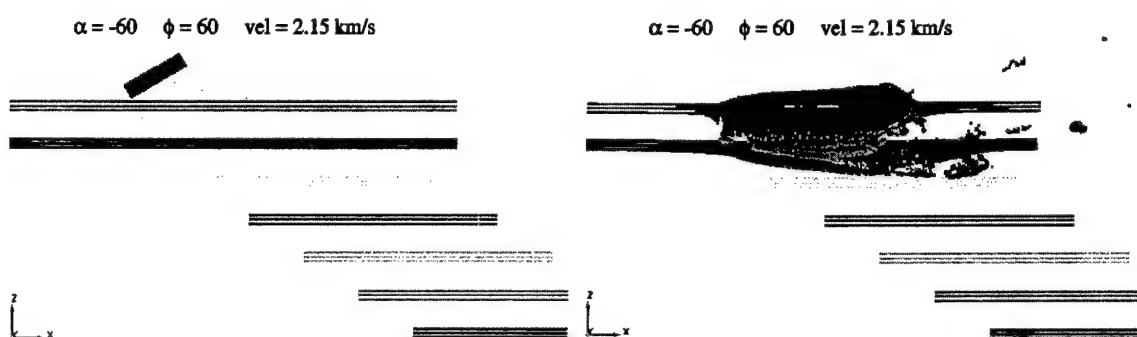


Figure 4.25. Case 5: Cylinder Impact $L/D = 4$, $\text{vel} = 2.15$, $\alpha = -60$, $\phi = 60$.

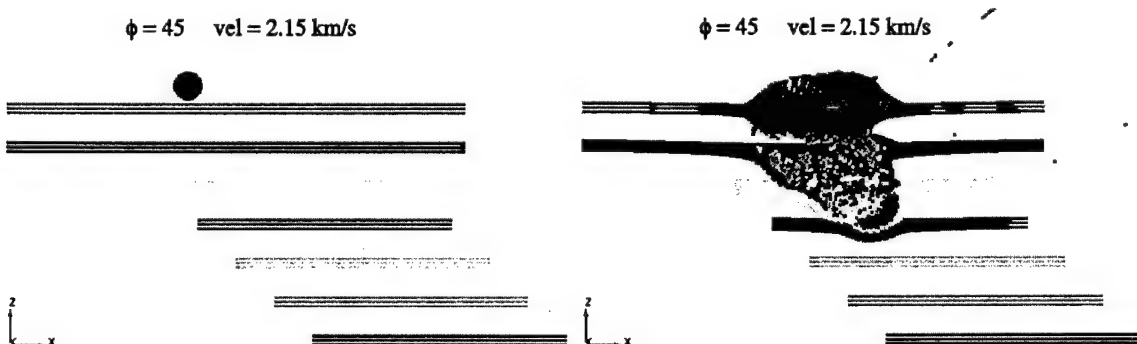


Figure 4.26. Case 6: Sphere Impact $\text{vel} = 2.15$, $\alpha = 90$.

Using the same graphical representation as in Figure 4.7 but now adding the SIDI values of L/D 's 1 and 2, a comparison between different L/D 's and the sphere, shown in Figure 4.27, shows the same shape of the curves per impact scenario of $L/D = 4$ and sphere. SIDI values of $L/D = 1$ for $\alpha = 90, 75, 60, 45, -45, -60, -75, -90$ and $\phi = 0$ are greater than SIDI values of $L/D = 4$ for the same cases whereas the SIDI values for $L/D = 4$ are greater for $\alpha = 30, 15, 0, -15, -30$ and $\phi = 0$ and 15.

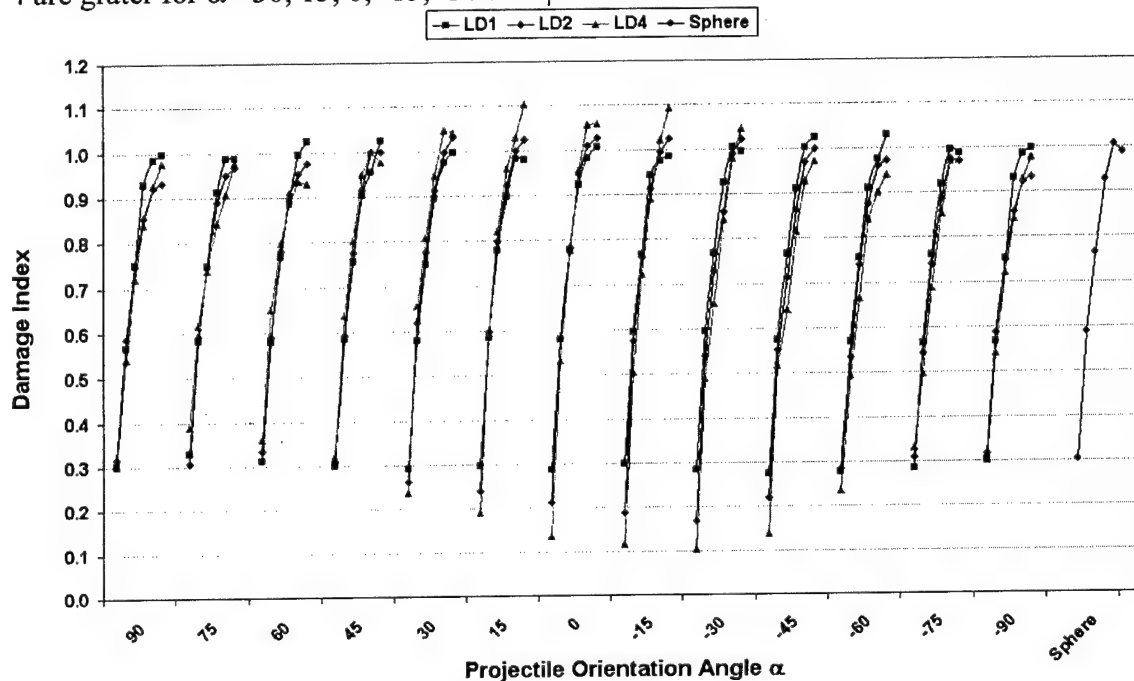


Figure 4.27. Comparison between L/D 's and sphere.

However, for some cases the SIDI differences among different L/D 's is minimum as it is illustrated in Figures 4.28-4.30 for projectile angles $\alpha = 0$ and $\phi = 15$. The figures show the same level of penetration and debris displaced for different L/D 's.

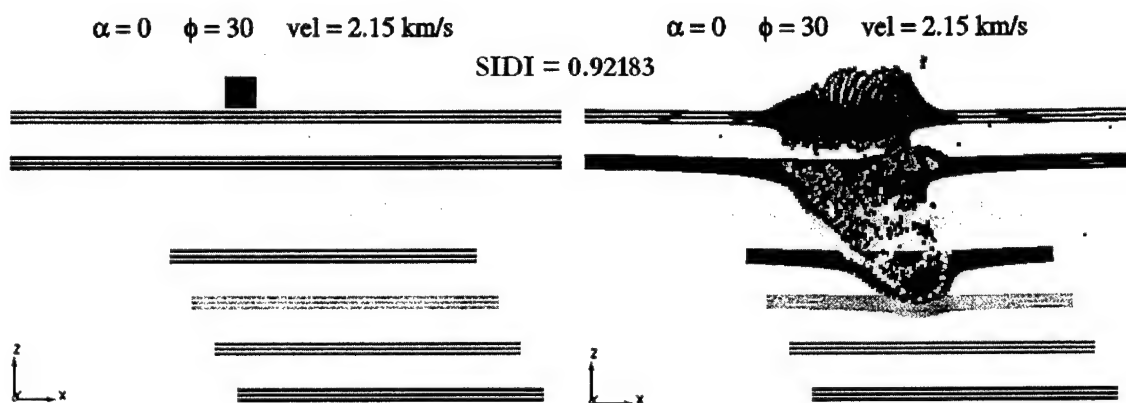


Figure 4.28. $L/D = 1$, $\text{vel} = 2.15$, $\alpha = 0$, $\phi = 15$.

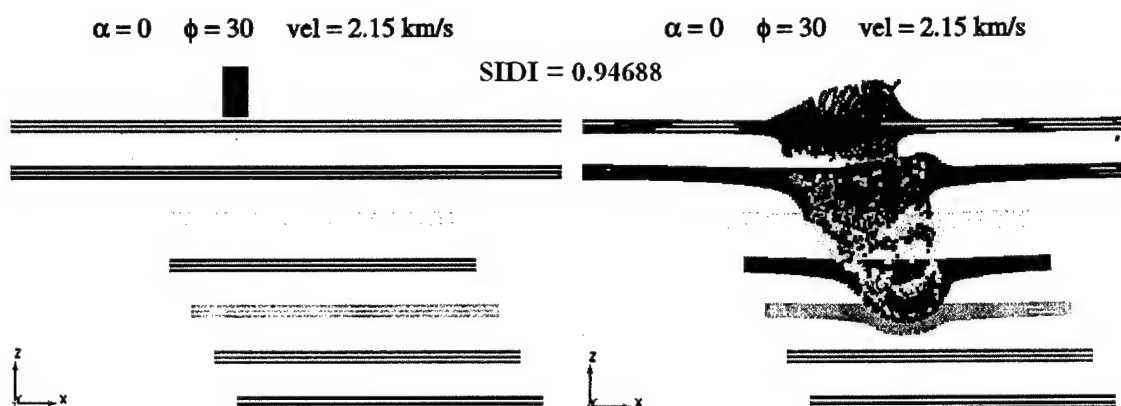


Figure 4.29. $L/D = 2$, $\text{vel} = 2.15$, $\alpha = 0$, $\phi = 15$.

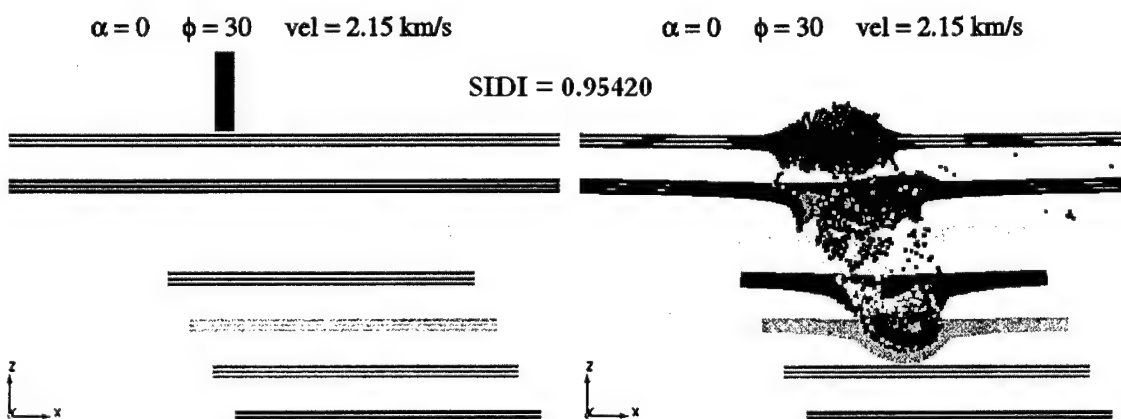


Figure 4.30. $L/D = 4$, $\text{vel} = 2.15$, $\alpha = 0$, $\phi = 15$.

A sensitivity analysis to validate the SIDI values for different materials and different projectile masses was performed in two schemes: varying the projectile material and varying the projectile mass. The simulations were run using a smoothing distance of 0.15 cm and for a $L/D = 4$, projectile velocity of 2.15 km/s, α values of 0, 45, and 90, and ϕ values of 0, 45, and 75. Figure 4.31 shows a comparison of SIDI values for projectiles with the same mass (15 gr) and different material. The materials used were tungsten (17.6 gr/cc), copper (8.93 gr/cc), steel (7.9 gr/cc), and aluminum (2.7 gr/cc).

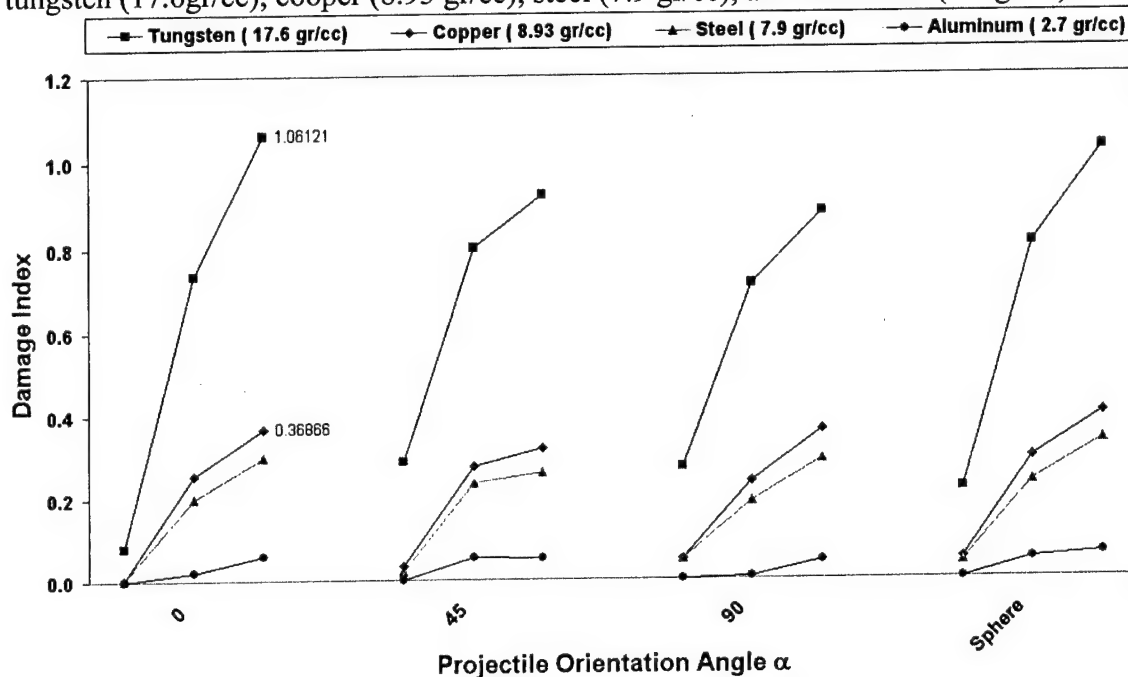


Figure 4.31. SIDI projectile material comparison with $h = 0.15$, $L/D = 4$ and Sphere, velocity = 02.15 km/s, $\alpha = 0, 45, 90$, and $\phi = 0, 45$, and 75.

The SIDI values for each material are plotted using the same scheme as for Figures 4.7 and 4.30 where each curve represents a fixed α angle and angle ϕ varies from 0 to 75 from up to down. The graph shows that as the density of the material increases, the SIDI increases. SIDI values of tungsten projectiles were more than twice the values of projectiles made of copper. Comparing the simulation final time step pictures, Figures 4.32-4.33, of those two projectiles at $\alpha = 0$ and $\phi = 0$, both the penetration and debris are considerable more for projectiles made of tungsten.

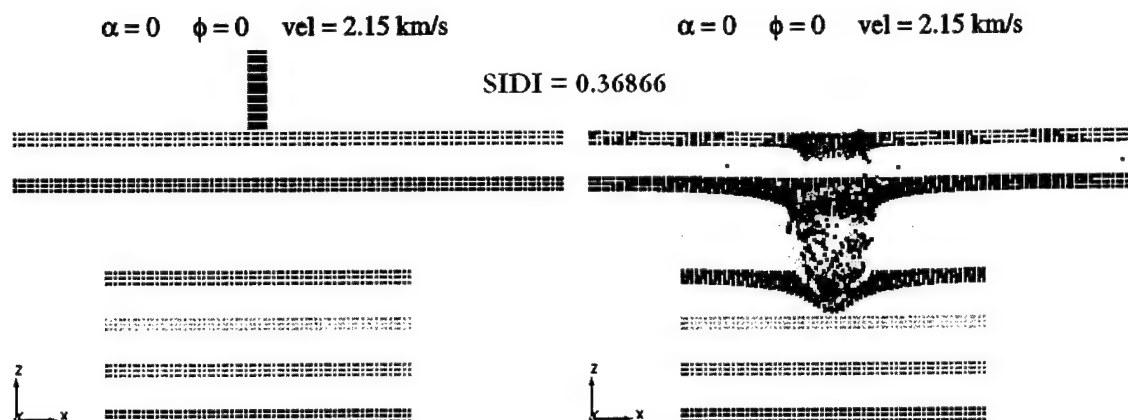


Figure 4.32. Copper projectile impact with mass of 15 gr, $L/D = 4$, $\text{vel} = 2.15 \text{ km/s}$, $\alpha = 0$, $\phi = 0$.

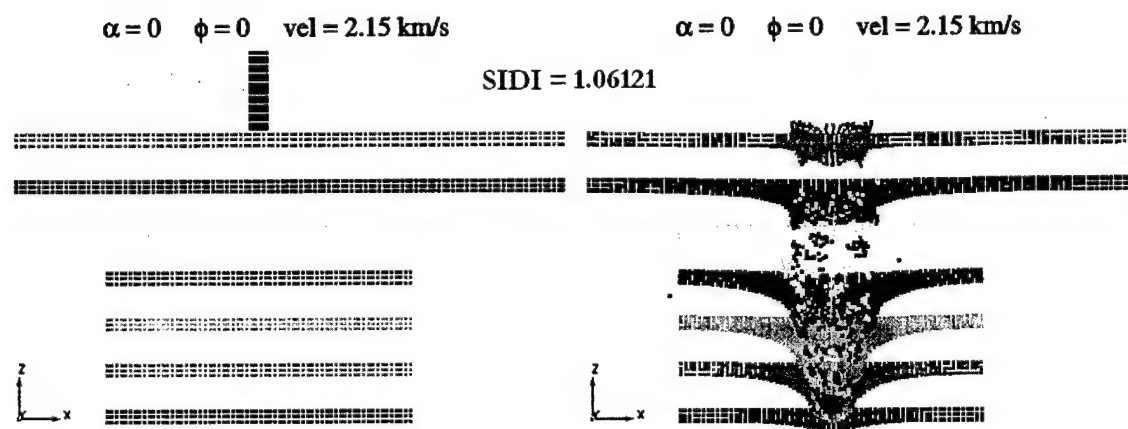


Figure 4.33. Tungsten projectile impact with mass of 15 gr, $L/D = 4$, $\text{vel} = 2.15 \text{ km/s}$, $\alpha = 0$, $\phi = 0$.

Figure 4.34 illustrates a graph with SIDI values of projectiles modeled with tungsten and different masses for the same scenario. It is observed that as the mass of the projectile increases, the SIDI values increases.

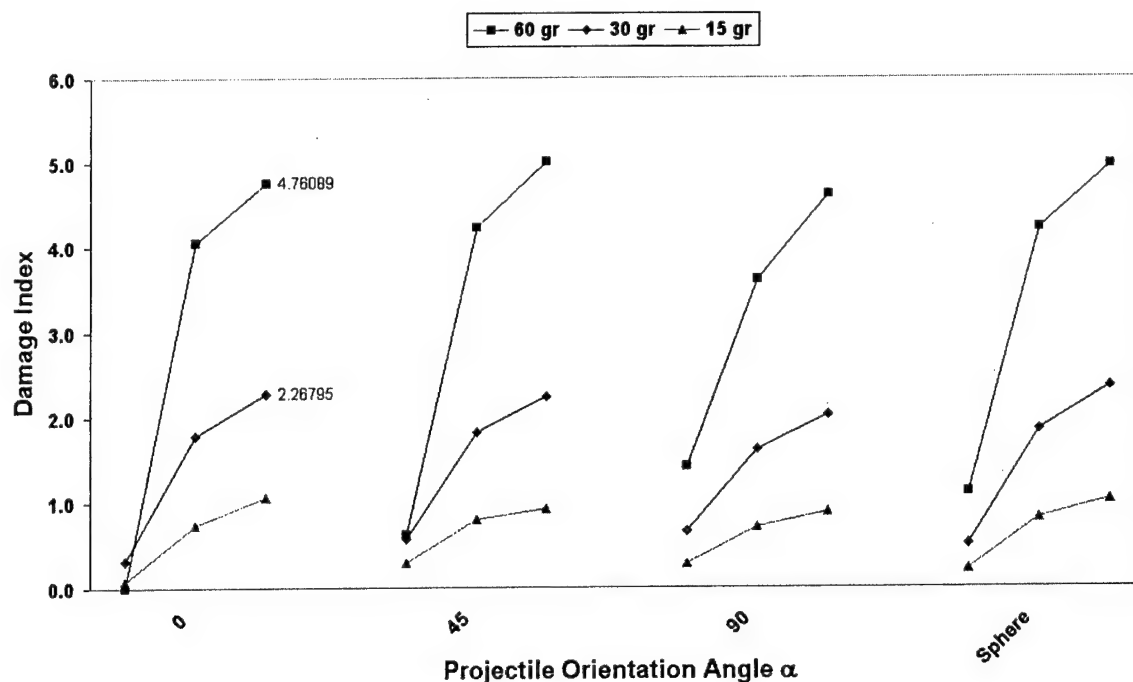


Figure 4.34. SIDI projectile mass comparison with $h = 0.15$, $L/D = 4$ and Sphere, velocity = 02.15 km/s, $\alpha = 0, 45, 90$, and $\phi = 0, 45$, and 75.

It is seen in Figures 4.32-4.33 and 4.35 that the SIDI value of the projectile with mass of 60 gr is greater than the SIDI of the projectile with mass of 15 gr for a case where $\alpha = 0$ and $\phi = 0$.

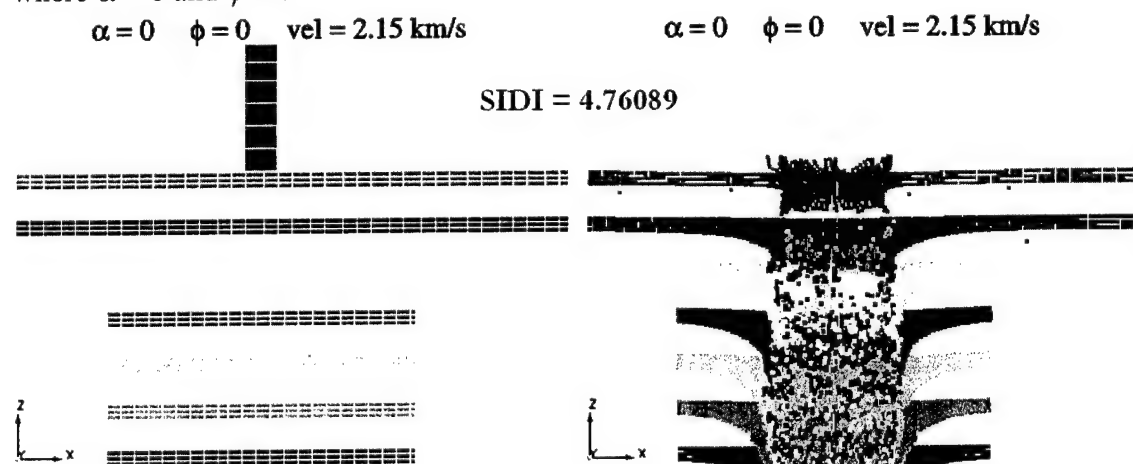


Figure 4.35. Tungsten projectile impact with mass of 60 gr, $L/D = 4$, $vel = 2.15$ km/s, $\alpha = 0$, $\phi = 0$.

An analysis involving two projectiles incrementing the distance between them was performed in order to observe the behavior of the proposed Damage Index for dual impacts. Each projectile is modeled with different impact parameters. The projectiles were separated in terms of its diameter distance. The Damage Index of those simulations (Multiple Impact Damage Index, MIDI) is compared with the aggregated values of the SIDI's of the same simulations. Figure 4.36 shows the MIDI values of simulations with diameter distances of 0, 1, 2, 4, 6, 8, and 10 for simulations with $h = 0.15$ cm, mass = 15 gr, and velocity of 2.15 km/s, $L/D = 4$ for the cylinder, and angles α and ϕ of 45 for both projectiles in the same simulation.

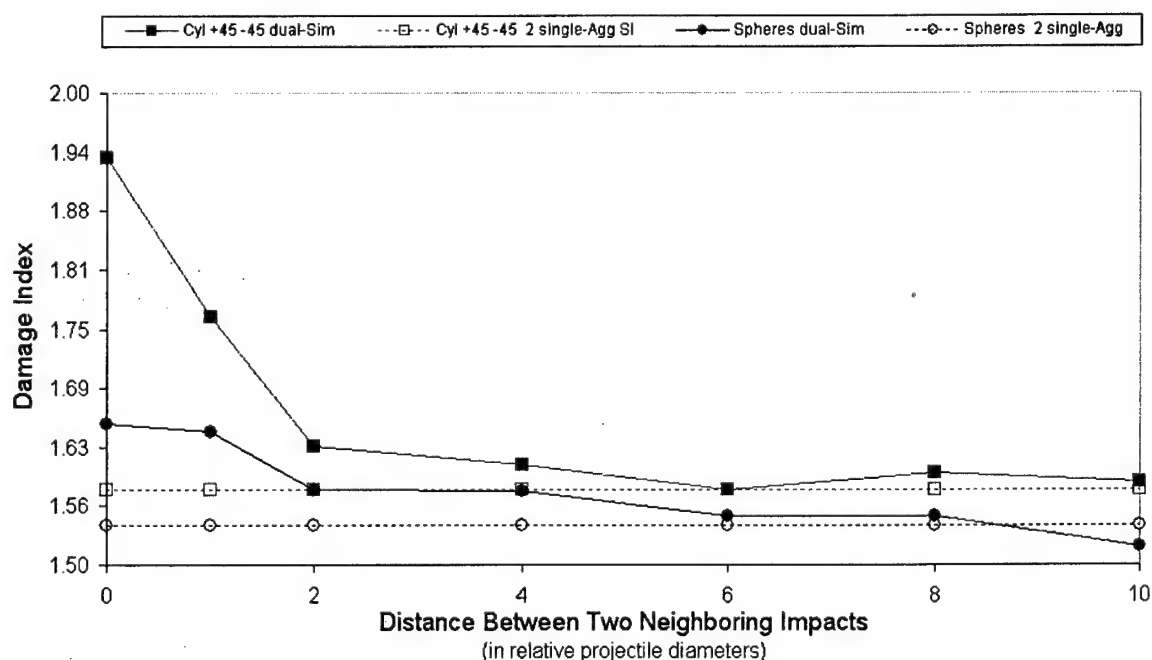


Figure 4.36. Dual impact comparison.

The graph shows that MIDI's of dual impacts with diameter distances of 0-2 of separation between projectiles is greater than the aggregated SIDI values of the same simulation. This is because the amount of debris displaced by both projectiles is more in comparison as that the ones displaced by a single impact. However, as the separation of between projectiles increases, the MIDI tends to become the aggregated SIDI of the impacts. Figure 4.37 depicts the impact of a single projectile for a case where $\alpha = 45$ and $\phi = 45$ whereas Figures 4.38-4.39 illustrates a dual impacts with the same impacts parameters for both projectiles at 0 and 10 diameters of distance between projectiles, respectively. The figures show that as the distance between projectiles increases, the impact approaches to two single projectiles impacts, and, consequently, the sum of the SIDI of each projectile.

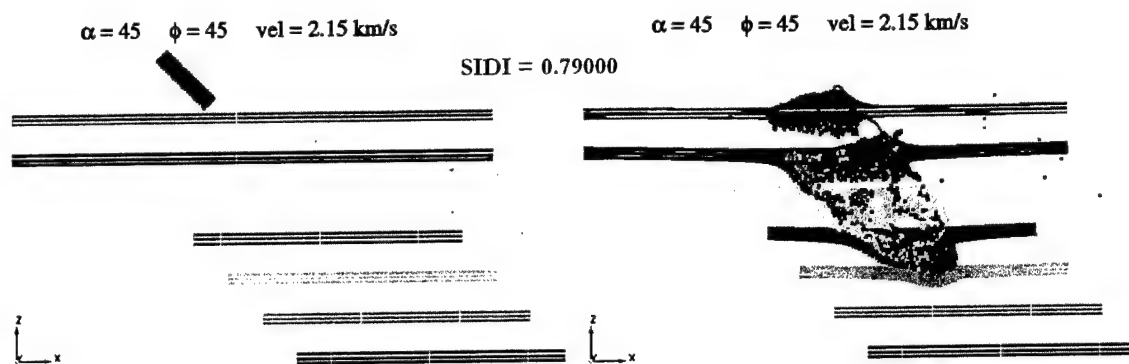


Figure 4.37. Single projectile impact with mass 15 gr, $L/D = 4$, $\text{vel} = 2.15 \text{ km/s}$, $\alpha = 0$, $\phi = 0$.

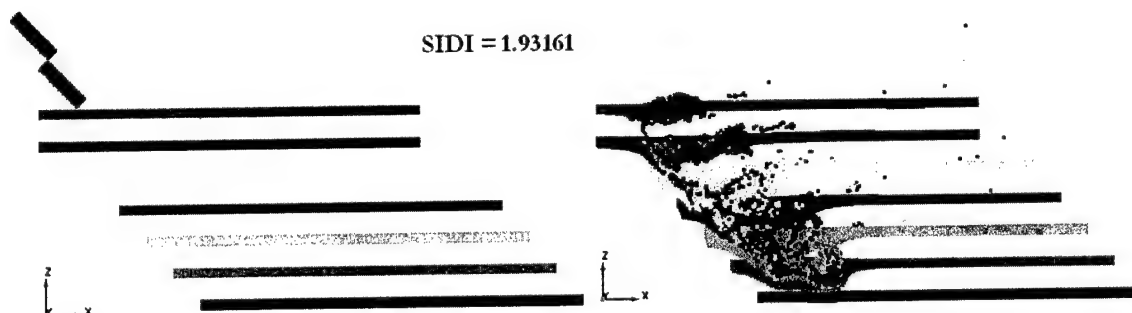


Figure 4.38. Dual projectile impact with mass 15 gr, $L/D = 4$, $\text{vel} = 2.15 \text{ km/s}$, $\alpha = 0$, $\phi = 0$ at relative distance of 0 diameters.

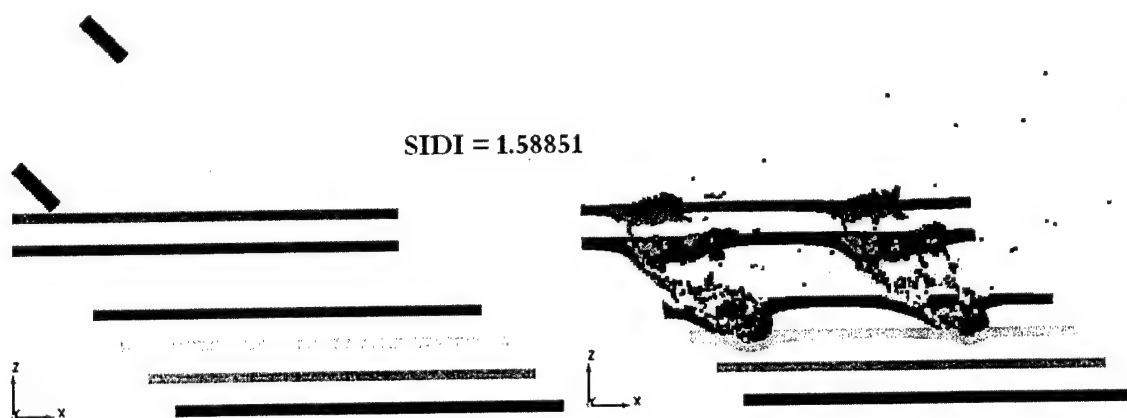


Figure 4.39. Dual projectile impact with mass 15 gr, $L/D = 4$, $\text{vel} = 2.15 \text{ km/s}$, $\alpha = 0$, $\phi = 0$ at relative distance of 10 diameters.

4.7 Lethality comparison between cylinders and spheres






In order to decide under which conditions the cylinder or the sphere is more lethal, based solely on the SIDI values of each simulation, a table in matrix form per L/D and velocity is created. The matrix have the α values on the columns, the ϕ values as the lines and the value of each element in the matrix is the value of the SIDI for that impact configuration. Figure 4.40 depicts a table for L/D 4 and velocity 1.80 km/s with SIDI values for each impact configuration. The SIDI values for sphere are located at the far right column of the table.

$L/D = 4$	Vel = 1.8 Km/s													
ϕ/α	90	75	60	45	30	15	0	-15	-30	-45	-60	-75	-90	Sphere
0	0.7521	0.7396	0.7367	0.7856	0.8265	0.8946	0.8905	0.8966	0.8293	0.7858	0.7414	0.7369	0.7521	0.7955
15	0.7175	0.6958	0.7428	0.7822	0.8751	0.8744	0.8727	0.8202	0.7759	0.7284	0.704	0.7328	0.7175	0.8009
30	0.6594	0.6662	0.7291	0.7854	0.7999	0.8077	0.7577	0.7051	0.6813	0.654	0.647	0.6509	0.6594	0.7363
45	0.5801	0.6097	0.6642	0.6925	0.684	0.6602	0.6328	0.5659	0.5451	0.5492	0.542	0.542	0.5801	0.6392
60	0.4643	0.514	0.5457	0.523	0.5263	0.4748	0.435	0.406	0.3973	0.4144	0.4178	0.4252	0.4643	0.4924
75	0.2541	0.2897	0.2969	0.2648	0.1859	0.1577	0.1138	0.0893	0.0849	0.1256	0.2229	0.2575	0.2541	0.2672

Figure 4.40. Table for $L/D = 4$ and Vel = 1.80 km/s and Sphere.

A ratio dividing the values of each cell in the α column of the cylinder by the values of each cell of the sphere column yields a parameter to measure which projectile shape is more lethal. Ratios Cylinder/Sphere less than one mean the sphere is more lethal for that impact configuration than the cylinder; cell values more than one mean the cylinder is more lethal than the sphere. Each cell is colored depending on the values shown in Table 4.4.

Table 4.4. Color Description for Ratios of Cylinder/Sphere.

Color	Ratio	Description Sphere is
	$0.50 > \text{Ratio}$	substantially more lethal than the Cylinder
	$0.66 > \text{Ratio} \geq 0.50$	more lethal than the Cylinder
	$0.80 > \text{Ratio} \geq 0.66$	moderately more lethal than the Cylinder
	$1.00 > \text{Ratio} \geq 0.80$	slightly more lethal than the Cylinder
	$\text{Ratio} > 1.00$	less lethal than Cylinder

Using the color code in Table 4.4, the ratios of the Table depicted in Figure 4.41 are colored developing the pattern in shown in Figure 4.42.

L/D= 4	Vel = 1.8 Km/s												
ϕ/α	90	75	60	45	30	15	0	-15	-30	-45	-60	-75	-90
0	0.9454	0.9297	0.9261	0.9876	1.0390	1.1246	1.1194	1.1271	1.0425	0.9878	0.9320	0.9263	0.9454
15	0.8959	0.8688	0.9275	0.9767	1.0926	1.0918	1.0896	1.0241	0.9688	0.9095	0.8790	0.9150	0.8959
30	0.8956	0.9048	0.9902	1.0667	1.0864	1.0970	1.0291	0.9576	0.9253	0.8882	0.8787	0.8840	0.8956
45	0.9075	0.9538	1.0391	1.0834	1.0701	1.0329	0.9900	0.8853	0.8528	0.8592	0.8479	0.8479	0.9075
60	0.9429	1.0439	1.1082	1.0621	1.0688	0.9643	0.8834	0.8245	0.8069	0.8416	0.8485	0.8635	0.9429
75	0.9510	1.0842	1.1112	0.9910	0.6957	0.5902	0.4259	0.3342	0.3177	0.4701	0.8342	0.9637	0.9510

Figure 4.41. Table for ratio of SIDI Cylinder/Sphere for $L/D = 4$ and velocity of 1.80 km/s.

L/D= 4	Vel = 1.8 Km/s												
ϕ/α	90	75	60	45	30	15	0	-15	-30	-45	-60	-75	-90
0	0.9454	0.9297	0.9261	0.9876	1.0390	1.1246	1.1194	1.1271	1.0425	0.9878	0.9320	0.9263	0.9454
15	0.8959	0.8688	0.9275	0.9767	1.0926	1.0918	1.0896	1.0241	0.9688	0.9095	0.8790	0.9150	0.8959
30	0.8956	0.9048	0.9902	1.0667	1.0864	1.0970	1.0291	0.9576	0.9253	0.8882	0.8787	0.8840	0.8956
45	0.9075	0.9538	1.0391	1.0834	1.0701	1.0329	0.9900	0.8853	0.8528	0.8592	0.8479	0.8479	0.9075
60	0.9429	1.0439	1.1082	1.0621	1.0688	0.9643	0.8834	0.8245	0.8069	0.8416	0.8485	0.8635	0.9429
75	0.9510	1.0842	1.1112	0.9910	0.6957	0.5902	0.4259	0.3342	0.3177	0.4701	0.8342	0.9637	0.9510

Figure 4.42. Colored table for ratio of SIDI Cylinder/Sphere for $L/D = 4$ and velocity of 1.80 km/s

Figure 4.42 shows a diagonal strip in white where the cylinder is more lethal than the sphere. The sphere is at least twice more lethal than the cylinder for cases where the cylinder impact the TBM in angles $\alpha = 0, -15, -30$, and -45 , and $\phi = 75$.

A comparison of those tables for $L/D = 4$ and all the velocities is illustrated in Figure 4.43. The lowest projectile velocity, 0.25 km/s, shows that the sphere is substantially more lethal for all α 's angles and $\phi = 45, 60$, and 75 and only in two cases the cylinder is more lethal than the sphere ($\alpha = 30 \phi = 30$ and $\alpha = 15$ and $\phi = 15$). However as the projectile velocity increases, the cylinder tends to increase the influence area where it is more lethal than the sphere.

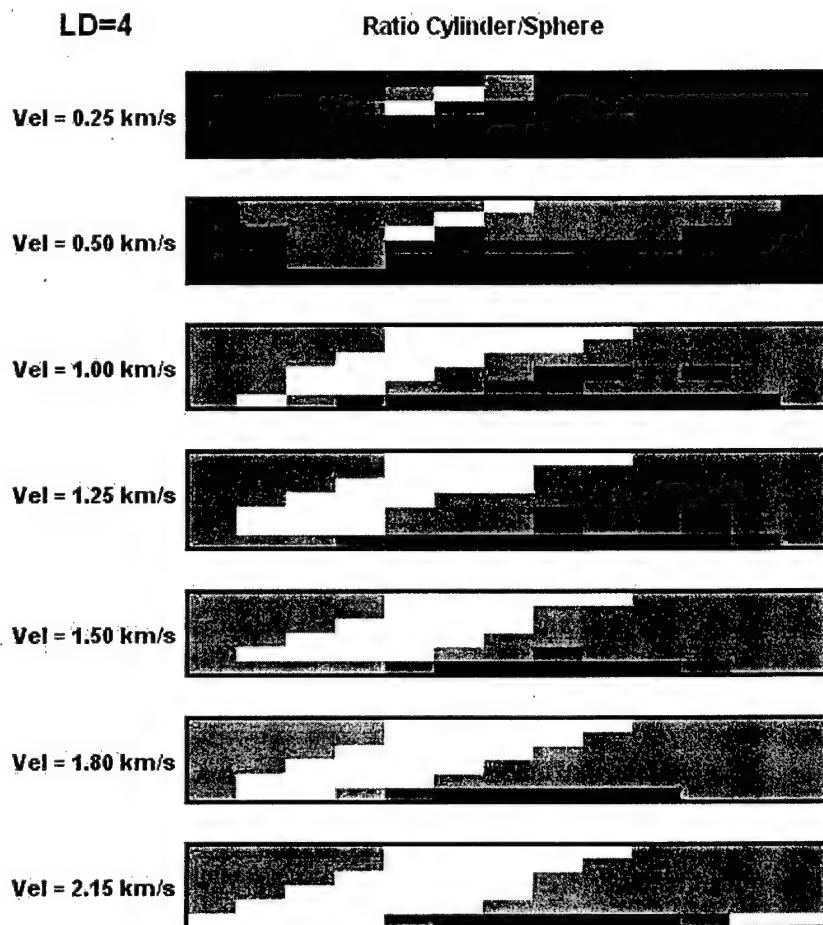


Figure 4.43. Tables of SIDI ratios Cylinder/ Sphere for $L/D = 4$ and all velocities.

The white area tends to be around the cylindrical simulations where the obliquity and orientation angles are aligned, this is for equal angle of α and ϕ . At the highest velocity, the sphere is as twice more lethal than the cylinder only in 4 cases ($\alpha = 0, -15, -30$, and -45 , and $\phi = 75$). A comparison of the ratios tables for a fixed velocity of 1.80 km/s and different L/D 's is shown in Figure 4.44

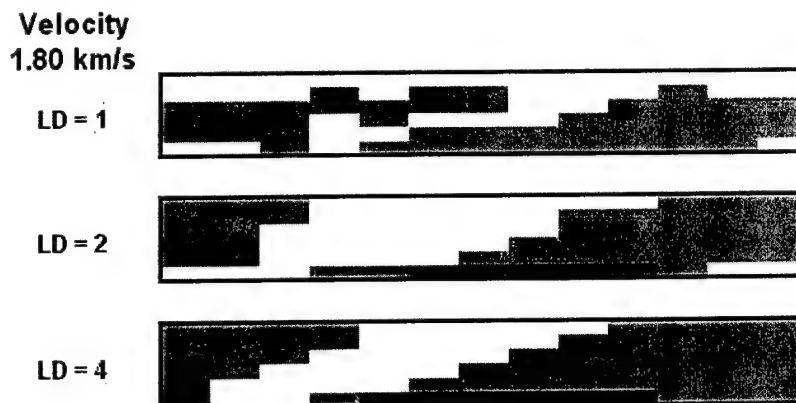


Figure 4.44. Tables of SIDI ratios Cylinder/Sphere for velocity 1.80 km/s and all L/D 's.

It is seen that the tendencies seen for the ratio table of $L/D = 4$ are presented in the table for $L/D = 2$. However, for $L/D = 1$ the influence area of the cylinder (white area) moves to all angles α and $\phi = 0, 15$ with all the other area being only slightly more lethal than the cylinder. This is due to the fact that as the diameter and length of the cylinder have equal dimensions, the cylindrical shape tends to become of the same dimensions as the sphere.

In general, the tables presented in Figures 4.43 and 4.44 show an increase in lethality for cylinder rods with L/D 's 2 and 4 when the orientation and velocity vector angle are aligned. Cylinder projectiles with L/D 's of 1 performed better at high yaw angles not only when the yaw angle is zero (α and ϕ aligned).

4.8 Summary

The development of an index for quantifying the damage made by hypervelocity impacts simulated using Smoothed Particles Hydrodynamics was presented. The damage index was based on the volume penetrated of the projectile and the volume displaced by its penetration. The developed damage index responded to changes in projectile material and mass giving good confidence to use as a level of lethality. Finally, the damage index provided an insight under which conditions the sphere is more lethal than the cylindrical projectiles

CHAPTER 5

ARTIFICIAL NEURAL NETWORKS MODEL

5.1 Introduction

Modeling of projectile's single impacts was performed using the previously selected hydrcode *MAGI*. However, considering that the projectiles from the EKV impacting the TBM in each near-miss encounter averages 200 and the number of possible near-miss configurations are over 1000, simulations of each individual impact for all the possible configurations would require 10 to 12 years to be completed. For that reason, a rapid solution model capable to predict the damage index for a wide range of impact scenarios is required instead of simulating each impact scenario given by the "Endgame" code. Successful research has been done in predicting the remaining life of flexible pavements (Abdallah I. *et al.* (1999)), the height of a wave at the time of its breaking and the depth of water in which it breaks (Deo M. C. *et al.* (2002)), and the strength of concrete (Lee S. C. (2002)) by using Artificial Neural Networks (ANNs). ANNs represent a new technology in computing science that tries to resemble the human brain in a rudimentary manner with the objective of predicting values and analyze data. These networks are trained to learn through experience using an historical data set to map relationships between inputs and outputs of problems. Furthermore, due to its nonlinear nature, ANNs are suitable to solve complex nonlinear problems. In this chapter, a brief introduction to Artificial Neural Networks theory is presented and an ANN model is developed and use to predict the SIDI values of a great number of projectile impact scenarios.

5.2 Artificial Neural Networks

Artificial Neural Networks (ANNs) were conceived as a computational method to resemble the highly complex, nonlinear, and parallel system in which the brain works. Haykin (1999) defines a neural network as "a machine that is designed to model the way in which the brain performs a particular task or function of interest; the network is usually implemented by using electronic components or is simulated in software on a digital computer." The basic component of a neural network is the neuron: information-processing units working in parallel which are called the Processing Elements (PEs). A graphical representation of a PE is illustrated in Figure 5.1. The set of connecting links between neurons are characterized by a weight or strength, w_i . Each connection receives an input signal, x_i that is multiplied by the connection weight, w_i , and added to the other weighted input signals. This sum, v_i , is used as the input in a transfer function $f(v_i)$ which limits the amplitude of the output of the PE and decides if other neurons have to be activated if a certain value is reached.

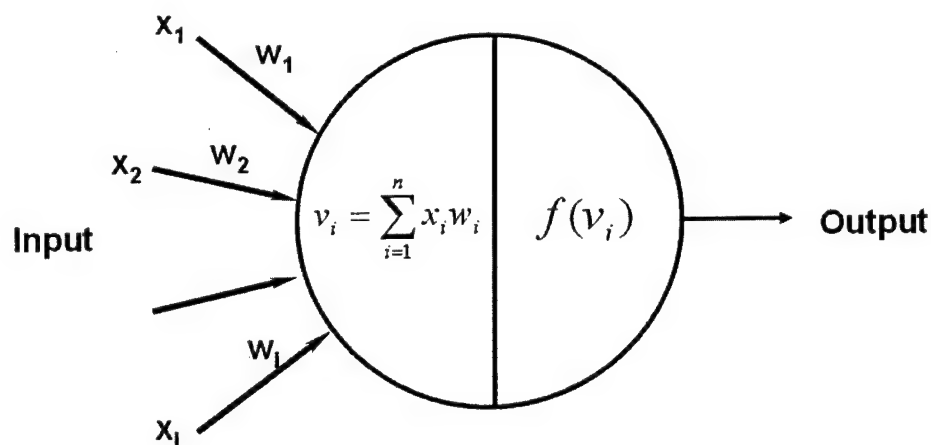


Figure 5.1. Schematic of a Processing Element

An ANN is a group of single interconnected PEs grouped in layers called the input, hidden, and output layers, as depicted in the neural network shown in Figure 5.2. The input layer consists of the neurons assigned to the each input variable. The output PEs represent the output layer of the network and are assigned to the parameters to be predicted. The remaining neurons may be arranged on one or several layers constituting the hidden layers of the network. This research uses a feedforward network, which means that the signal output flow of the neurons, depicted in Figure 5.2 in the direction of the arrows, is going from the input layer to the output layer and not vice versa. An ANN learns to improve its performance through a process called “training”. The training process consists in presenting examples of the input and modifying or adjusting the weights of each connection to match the desired output. Several learning algorithms, called also “learning rules”, have been developed since the conception of the first ANN. Hebbian, Boltzmann, and the Widrow-Hoff or error-correction training methods are encountered among the learning rule algorithms. The present work uses a learning rule based on the Widrow-Hoff (error-correction) training algorithm and generalized to multiple layer networks, the back propagation algorithm. The back-propagation algorithm calculates the error originated at the output PEs of the network propagating it backwards (layer by layer) and modifying the weights of each connecting link accordingly.

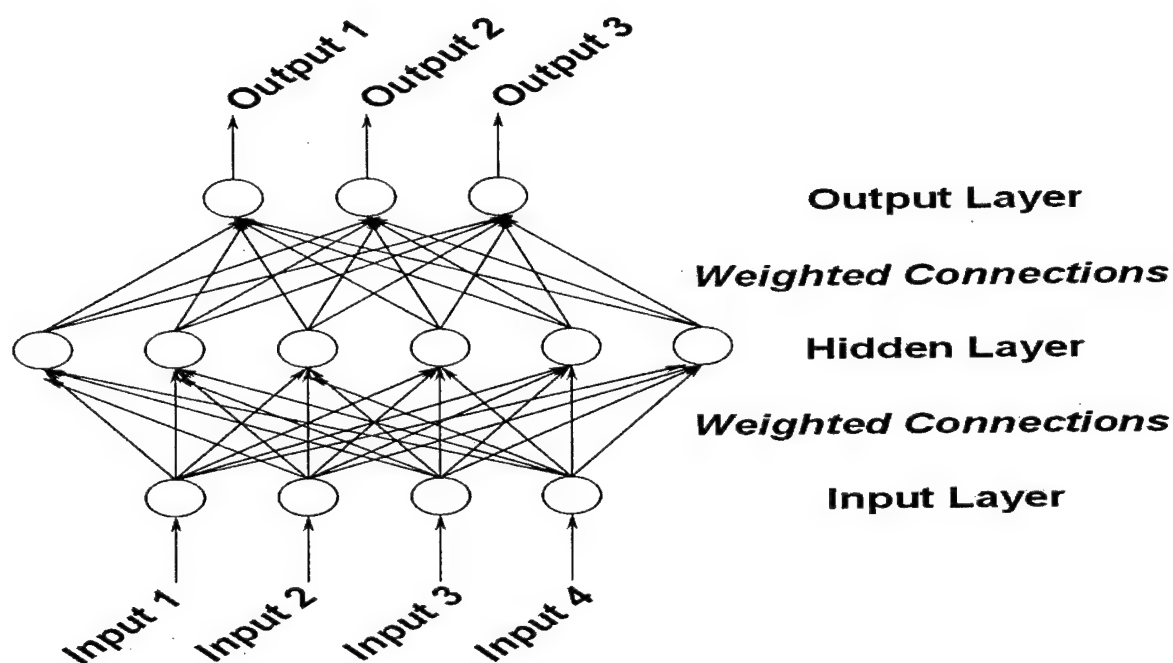


Figure 5.2. General structure of an Artificial Neural Network

5.3 Development of the Artificial Neural Network Model

Development of an ANN requires a database consisting of the input and output variables for each example. The ANN uses the database to train itself to map the relationships between the inputs and the outputs. In this research, a database of over 1500 impact cases was created by numerically simulating each impact using *MAGI* with a smoothing distance of 0.1255 cm. The inputs of each impact were the impact variables (L/D , velocity, α , ϕ) and the only output was the corresponding calculated SIDI. The numerical simulations were conducted for projectile LD ratios of 1, 2, and 4 and for spheres ($LD = 0$) with a mass of 15 grams at 7 different velocities, as illustrated in Table 5.1.

Table 5.1. Ranges of parameters used in ANN database

Shape	LD	Velocity	ϕ	α	Total per Shape
Sphere	N/A	0.25	0	N/A	
		0.50	15		
		1.00	30		
		1.25	45		
		1.50	60		
		1.80	75		
		2.15	90		
Combinations	1	7	7		49
Cylinder	1 2 4	0.25 0.50 1.00 1.25 1.50 1.80 2.15	0 15 30 45 60 75 90	-90	
				-75	
				-60	
				-45	
				-30	
				-15	
				0	
				15	
				30	
				45	
				60	
				75	
				90	
Combinations	3	7	7	13	1911
Database Total Cases					1960

The angles ϕ and α were varied at evenly spaced increments, from 0 to 75 for ϕ and from 75 to 90 for α both in increments of 15, for all LD's and velocities except for the sphere where the orientation angle α is not applicable. In addition to the cases simulated with *MAGI*, some cases were artificially built to have a comprehensive database which includes the whole range of the orientation angle α and velocity vector angle ϕ . The values of the variables that were synthetically assumed are shown bolded in Table 5.1. Taking advantage of symmetry, cylindrical impact cases with angle α of 90 were assumed to have same SIDI as impact cases with angle α of -90 degrees. Previous simulation experiments for the ϕ extra angle of 90 revealed that the corresponding SIDI values for these cases were extremely close to zero (from 0.00001 to 0.00003). Rounding to zero the SIDI's of these impacts forced the ANN to consider the cases with angles near $\phi = 90$ to be predicted as zero or close to zero. The final database, shown in Appendix D, consisted of 1960 cases. This same database was used as a training file to verify the ANN performance. In addition to this verification process, 31 impact cases given by the "Endgame" code were used to validate the ANN. These 31 cases had different impact variable values as compared to the ones contained in the database (Appendix D shows these cases with its corresponding SIDI values).

Development of the ANN was done using the Matlab™ Neural Network Toolbox. First attempts of ANN development did not provide good results because ANN development is based, most of the times, on a trial and error procedure. This trial and error procedure is due to the fact that every problem attempted to be modeled using ANNs is completely different in essence, even though the objectives (prediction or pattern recognition) are the same. Several ANN architectures, consisting of various combinations of training and transfer functions between layers along with different combinations in the number of processing elements in the hidden layers, were tested to find the best architecture predicting the SIDI. A computer code was programmed in Matlab™ to facilitate the task of finding the best possible combination of the number of neurons in each hidden layer. It was seen that no scaling problems were encountered and for that reason a pre-processing or post-processing of the raw data was unnecessary. ANN performance was first evaluated by using the root mean square (RMS) error and, secondly, by calculating the percentage of predictions within a $\pm 20\%$ error. The ANN with a RMS error lower than a threshold of 0.005 and the highest prediction percentage within the $\pm 20\%$ range was the one selected. A flowchart of this process is illustrated in Figure 5.3.

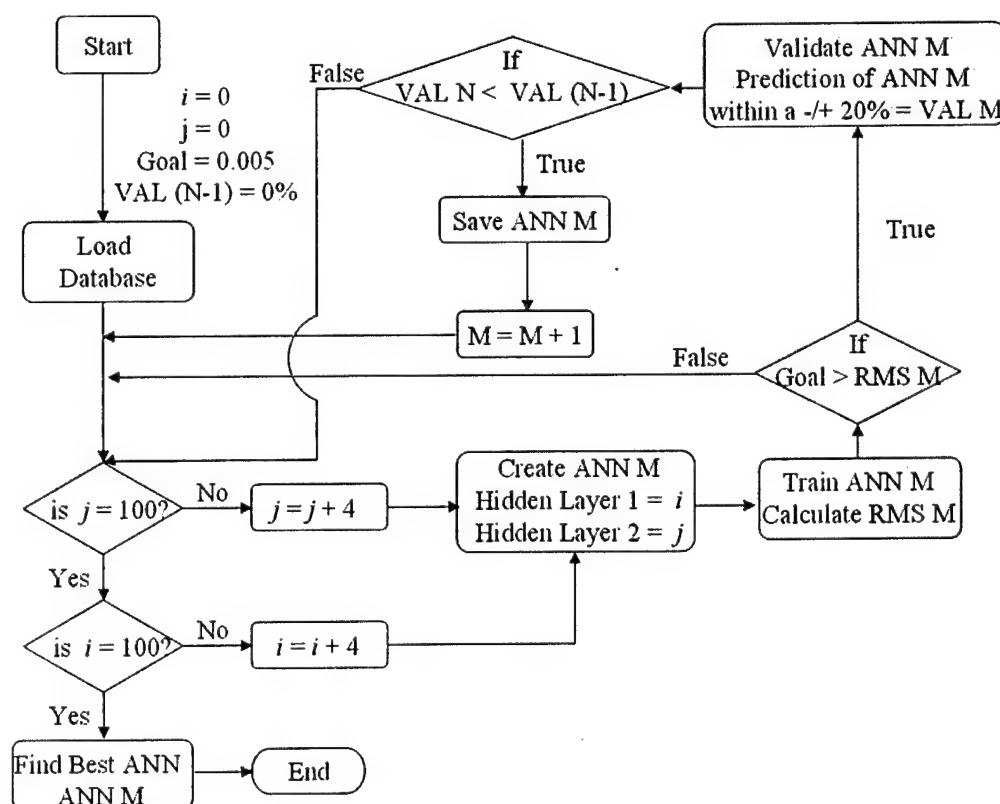


Figure 5.3. Matlab Code flowchart for optimum ANN architecture

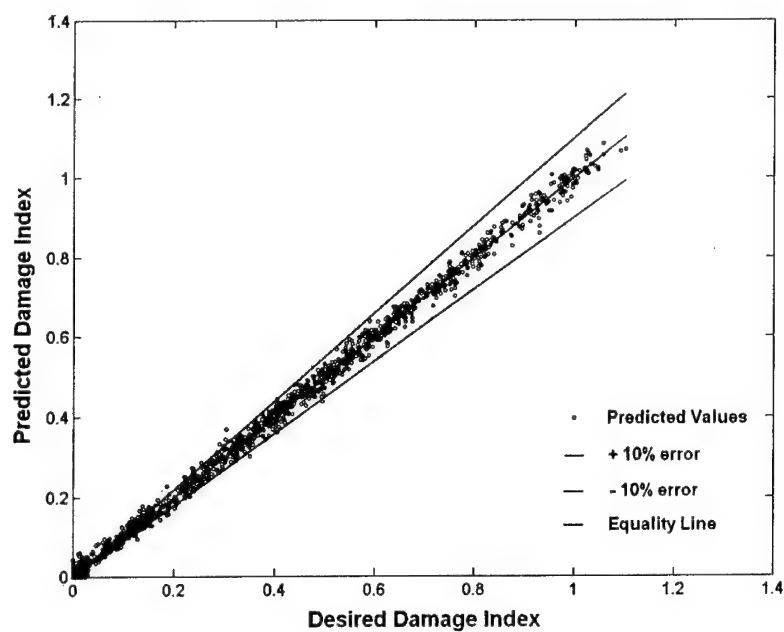


Figure 5.6. Results of ANN predicted DI values from training file

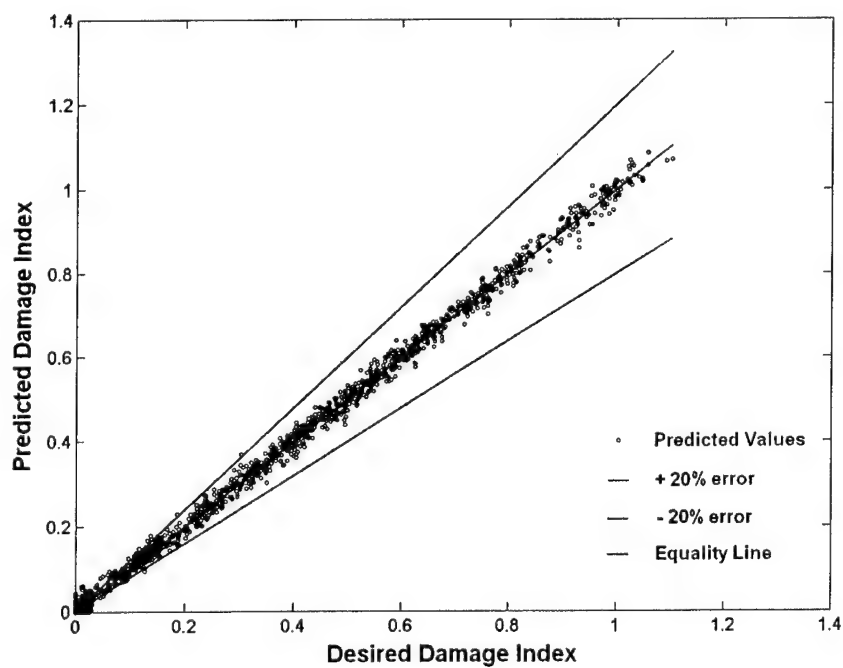


Figure 5.7. Results of ANN predicted DI values from training file

A new comparison between randomly selected actual SIDI values from the training file and its corresponding SIDI values predicted by the ANN are shown in Table 5.2. It is clearly seen that the error percentage from the twenty cases presented in this table, only three surpassed an error percentage of 10% and none surpassed a 20% error. Only 4 cases, cases 1, 2, 6, and 12, of the twenty cases had percentage errors above 5%. This case-to-case comparison shows that the ANN developed predicts in a reliable manner the SIDI values of cases that were previously presented for in the training file.

Table 5.2. Case comparison of actual SIDI and predicted SIDI.

Case Number	Input Parameters				Output Parameters		Error Percentage
	LD	Vel	α (degrees)	ϕ (degrees)	Actual SIDI	Predicted SIDI	
1	Sphere	0.25	0	45	0.01739	0.01579	9.20%
2	Sphere	1.00	0	75	0.15780	0.17564	11.31%
3	Sphere	1.25	0	30	0.49737	0.50032	0.59%
4	Sphere	1.80	0	0	0.79554	0.78199	1.70%
5	Sphere	2.15	0	15	1.00395	0.98685	1.62%
6	1	0.25	30	0	0.02718	0.02226	18.10%
7	1	1.00	-30	60	0.24264	0.25276	4.17%
8	1	1.25	-60	15	0.54238	0.52918	2.43%
9	1	1.50	-15	45	0.52031	0.53858	3.50%
10	1	1.80	0	30	0.73174	0.74976	2.46%
11	2	0.50	0	15	0.15796	0.16832	6.56%
12	2	1.00	60	75	0.11976	0.13581	13.40%
13	2	1.25	-45	30	0.45990	0.47466	3.21%
14	2	1.50	45	60	0.42800	0.42791	0.02%
15	2	2.15	-45	45	0.71493	0.73066	2.20%
16	4	0.25	45	0	0.02196	0.02096	4.55%
17	4	0.50	-60	75	0.01077	0.01028	4.55%
18	4	1.25	60	45	0.45249	0.45742	1.09%
19	4	1.50	-45	15	0.58858	0.57541	2.24%
20	4	2.15	45	30	0.94853	0.91578	3.45%

A set consisting of 31 verification cases (randomly extracted from the results of the "Endgame simulations" code) were simulated in MAGI to obtain its corresponding SIDI value. This set of data was passed through the ANN to verify that the network was reliable when presented to unknown cases. Figures 5.7 and 5.8 show that the ANN predicted high percentages within the margin error when presented to cases extracted from the "Endgame" code. An 84% and a 94% of the predicted values were within the +/-10% and +/-20% error margins respectively. Moreover, a curve comparison of the actual cases against the simulated cases, shown in Figure 5.9, demonstrates the model ability to predict.

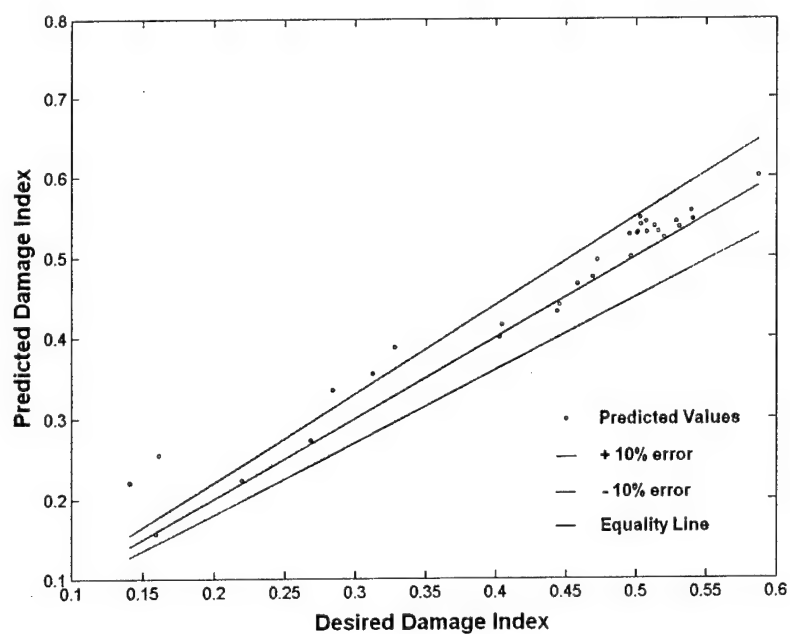


Figure 5.8. Results of ANN predicted DI values from validation cases

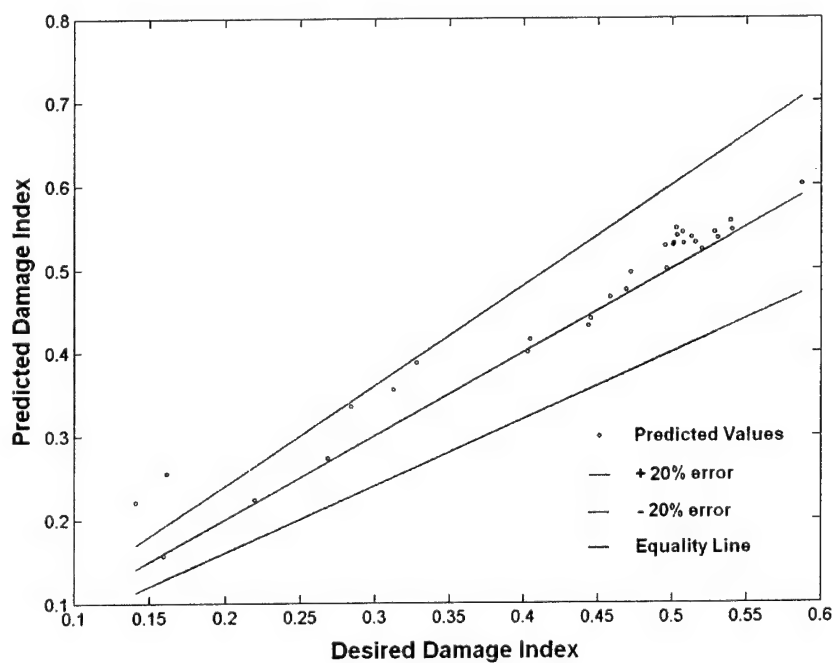


Figure 5.9. Results of ANN predicted DI values from validation cases

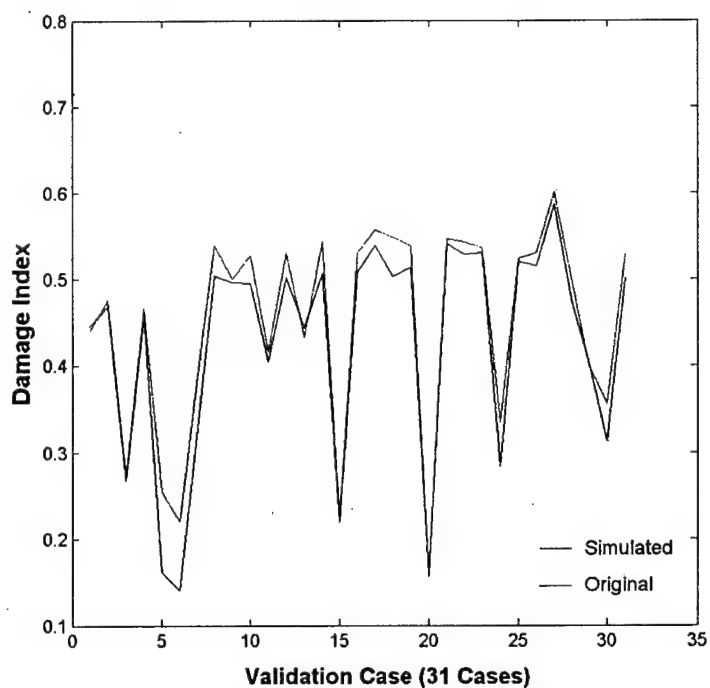


Figure 5.10. Curve comparison between the actual and predicted values

5.5 Lethality comparison between cylinders and spheres using ANNs

The values predicted by the developed ANN from the training file were sorted in tables in matrix form as the ones used for SIDs calculated from the *MAGI* simulations, as seen in Figure 4.7. Figure 5.11 shows a table with predicted values sorted by the same parameter in Figure 4.7 ($LD = 4$ and velocity 1.80 km/s).

L/D= 4	Vel = 1.8 km/s													
ϕ/α	90	75	60	45	30	15	0	-15	-30	-45	-60	-75	-90	Sphere
0	0.7585	0.7294	0.7241	0.7528	0.8066	0.8707	0.9021	0.8786	0.8244	0.7733	0.7411	0.7321	0.7418	0.7820
15	0.6775	0.7139	0.7521	0.7912	0.8270	0.8520	0.8547	0.8206	0.7608	0.7135	0.7003	0.7068	0.7050	0.8160
30	0.6235	0.6655	0.7170	0.7708	0.7948	0.7770	0.7450	0.7080	0.6711	0.6562	0.6580	0.6552	0.6428	0.7484
45	0.5706	0.6263	0.6832	0.7175	0.7002	0.6581	0.6178	0.5800	0.5568	0.5537	0.5545	0.5476	0.5451	0.6488
60	0.4918	0.5353	0.5631	0.5686	0.5438	0.5015	0.4555	0.4256	0.4110	0.3935	0.3951	0.4304	0.4677	0.4867
75	0.2878	0.3090	0.2972	0.2721	0.2278	0.1712	0.1270	0.0931	0.0811	0.1277	0.2088	0.2611	0.2455	0.2728

Figure 5.11. Table for ANN predicted values of $LD = 4$ and $Vel = 1.80$ km/s and Sphere.

The predicted values of the cylinder were divided by the corresponding values of the sphere (per ϕ value) and the resulted ratio Cylinder/ Sphere were colored according to Table 4.4 as seen in Figure 4.12.

$L/D = 4$ $Vel = 1.8 \text{ km/s}$

ϕ/α	90	75	60	45	30	15	0	-15	-30	-45	-60	-75	-90
0	0.9699	0.9327	0.9250	0.9327	1.0315	1.1134	1.1536	1.1235	1.0542	0.9869	0.9278	0.9363	0.9486
15	0.9607	0.8749	0.9218	0.9696	1.0135	1.0442	1.0474	1.0057	0.9324	0.8744	0.8552	0.8652	0.8640
30	0.8881	0.8892	0.9580	1.0299	1.0619	1.0382	0.9954	0.9460	0.8966	0.8768	0.8792	0.8754	0.8589
45	0.8795	0.9655	1.0531	1.1060	1.0794	1.0144	0.9523	0.8940	0.8566	0.8565	0.8647	0.8440	0.8408
60	1.0105	1.0999	1.1570	1.1682	1.1172	1.0303	0.9359	0.8744	0.8444	0.8085	0.8117	0.8842	0.9609
75	1.0549	1.1327	1.0892	0.9974	0.8348							0.9570	0.9000

Figure 5.12. Colored table for predicted ratio of SIDI Cylinder/Sphere for $LD = 4$ and velocity of 1.80 km/s.

It is seen that Figures 4.29 and 5.12 show the same trend. Both have the same cells where sphere is substantially more lethal than the cylinder. The area where cylinder is more lethal than the sphere appears in the same space in both tables.

New evenly spaced velocities (0.15375, 0.46125, 0.76875, 1.07625, 1.38375, 1.69125, 1.99875 km/s) were defined in place of the old velocity values and the SIDI values were re calculated using the ANN for the same α and ϕ values used before but with the new velocities. The re calculated values were sorted in tables as the ones shown in Figures 4.7 and 5.11, and the ratio Cylinder/Sphere was calculated and colored. Figures 5.13-5.15 show all the ratio tables per LD using the new values for the velocity.

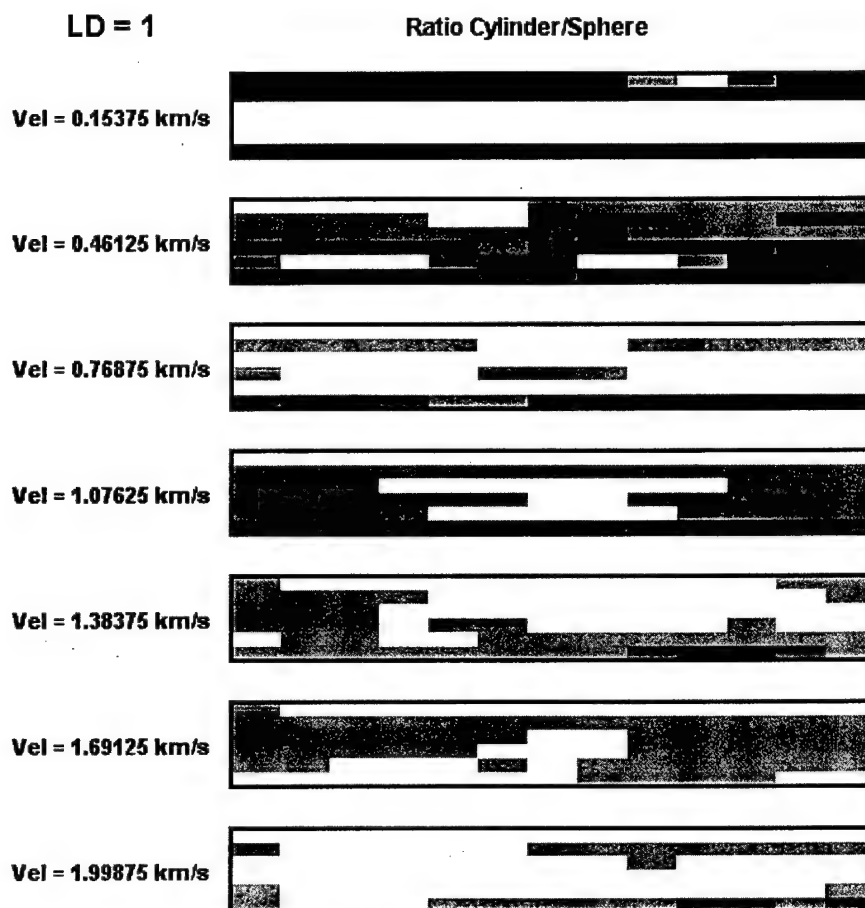


Figure 5.13. Tables of predicted SID ratios Cylinder/Sphere for $LD = 1$ and all new velocities.

In Figure 5.13, for ratios with cylinder having a LD of 1, it is observed that the sphere is substantially more or more lethal than the cylinder for all α 's and $\phi = 0, 15$, and 75 except for a single case where the cylinder is more lethal ($\alpha = -45, \phi = 0$). As the velocity increases, the area where the cylinder is more lethal than the sphere increases (white area) considerably.

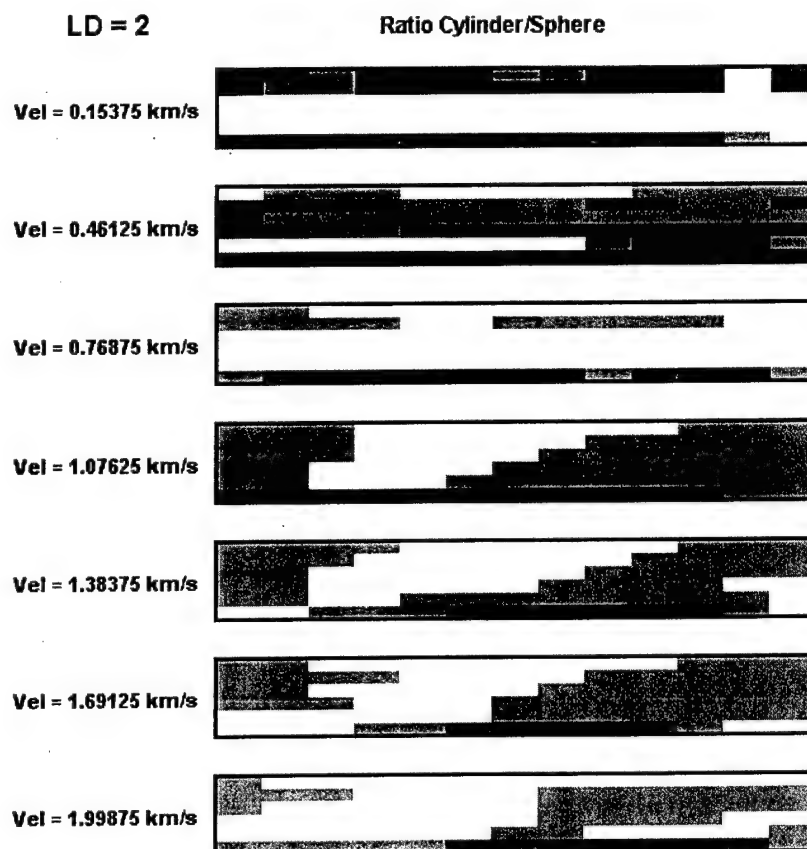


Figure 5.14. Tables of predicted SID ratios Cylinder/Sphere for LD = 2 and all new velocities.

In Figure 5.14, for ratios with cylinder having a *LD* of 2, a diagonal white strip trend appears as it appeared in the ratio tables with SIDIs calculated from *MAGI*. This trend means more lethality of the cylinder in cases where the velocity vector is aligned or slightly moved from the longitudinal axes of the cylinder.

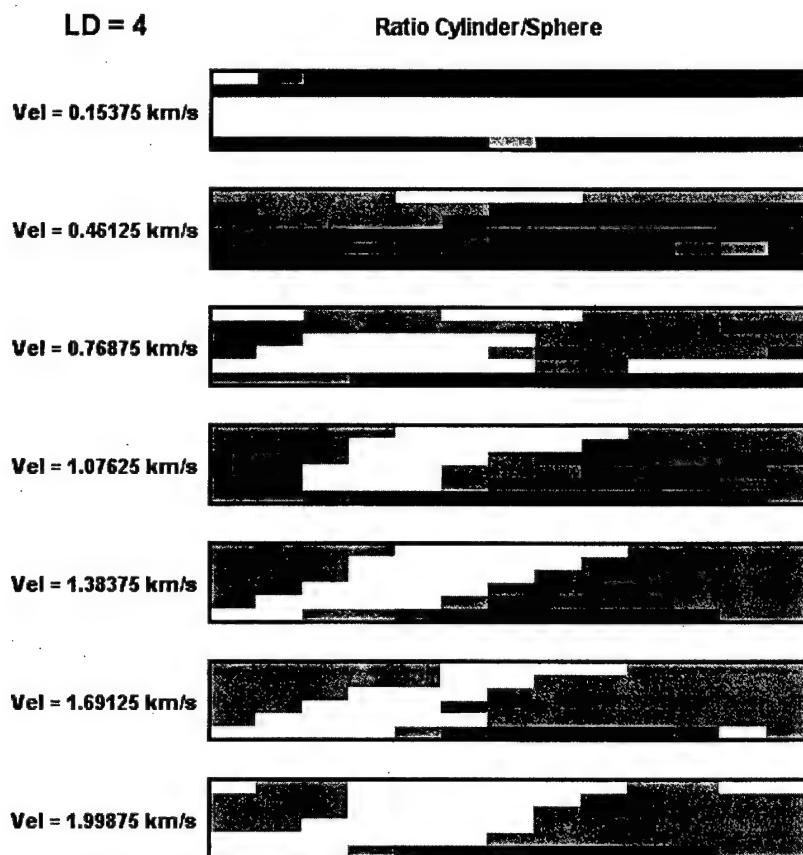


Figure 5.15. Tables of predicted SID ratios Cylinder/Sphere for $LD = 4$ and all new velocities.

Ratio tables with a cylinder with $LD = 4$ show the same tendency seen in Figure 5.14. The sphere is more lethal for lower velocities (0.15375 – 0.76875 km/s) and as the velocity increases the sphere increases its lethality especially where yaw angle have large values. On the contrary, cylinders with $LD = 1$ appear to be more effective in lethality terms for a wide range of cases, especially when the velocity increases. Spherical projectiles are more effective in comparison of any size of cylinder for lower velocities.

5.6 Summary

The description of the development of an ANN used to predict single impact DIs of several cases given by the “Endgame” code was presented. The ANN was trained and tested in its performance using a comprehensive database of 1960 cases. Validation of the ANN was performed using a set of 31 impact cases with unseen input variable values. The final ANN architecture consisted of an input layer (4 PEs), two hidden layers (76 and 72 PEs respectively) and an output layer (1 PE). The final ANN had a RMS error of 0.0002527 and predicted an 84% and a 94% of the validation cases within a $\pm 10\%$ and $\pm 20\%$ respectively.

CHAPTER 6

ENDGAME DAMAGE QUANTIFICATION ANALYSIS

6.1 Introduction

To determine whether a TBM warhead has been disabled or destructed at a certain encounter configuration scenario a quantitative measure of damage is required. Such a measure facilitates the assessment of relative lethality between encounter scenarios and moreover different projectile geometry/sizes. Chapter 4 described the development and justification of a Single Impact Damage Index (SIDI) associated to a preset number of possible impact configurations for different projectile geometry/sizes. Since the number of impacts to the TBM warhead per encounter scenario can be quite large and their individual configurations at the points of impact along the TBM warhead section are unique for each impact, an Artificial Neural Network was devised to accelerate the calculation of the SIDI associated to each impact. The development of the ANN is described in Chapter 5.

The ANN was integrated into the endgame code to immediately associate a SIDI to each warhead impact occurring at every encounter configuration scenario and automatically quantify the total damage inflicted to the TBM warhead, by aggregating the individual SIDIs. Figure 6.1 depicts the sequence in an Endgame simulation to quantify the total damage inflicted to the TBM warhead. For each encounter configuration scenario simulated, the number of impacts to the warhead is quantified. Each impact is characterized in terms of relative impact velocity, strike angle and spatial orientation (for cylindrical projectiles), which are fed to the ANN to automatically associate a SIDI. The individual SIDIs are aggregated and the total damage per encounter configuration scenario is quantified.

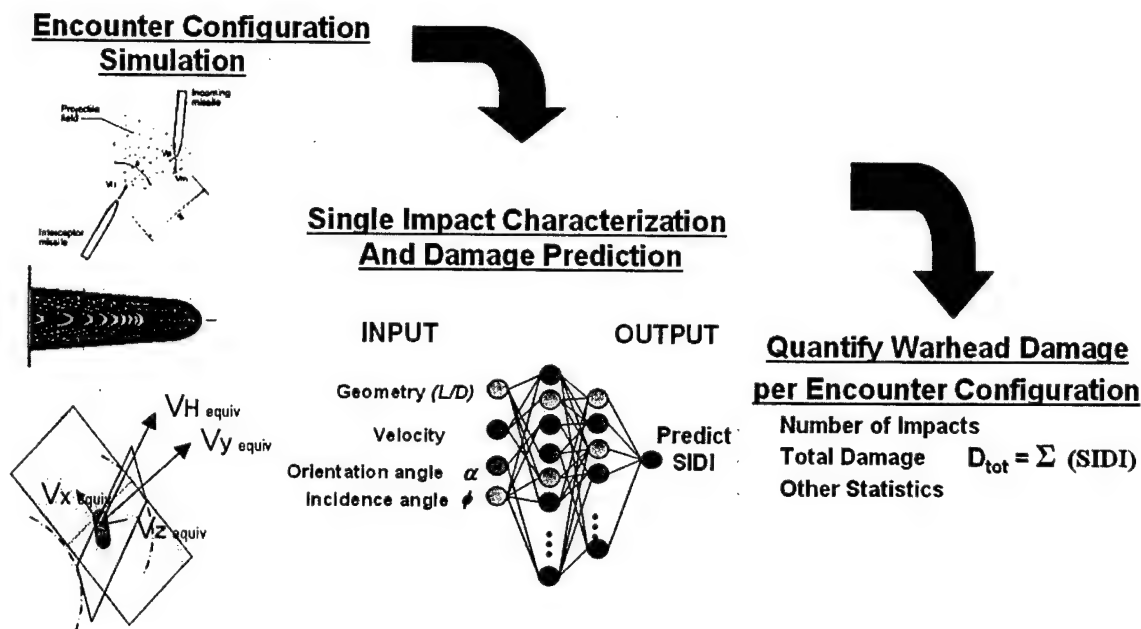


Figure 6.1. Damage Prediction and Quantification Sequence in an Endgame Simulation.

6.2 Total Damage Quantification per Encounter Configuration

For a comprehensive overview of the total damage inflicted to the TBM warhead throughout the entire encounter configuration scenario range, a set of tables were generated for each projectile geometry/size subjected to different deployment conditions per encounter configuration parameter. As for the impact quantification tables, the early-bird time (EBt) parameter was chosen as the first level of classification, reducing the number of tables per projectile geometry/size/condition, and showing the variation in total damage per crossing angle as the miss distance also varies. For reference purposes, the damage quantification tables presented below correspond to an early bird time of -0.006 seconds, same encounter configuration parameter under which the impact quantification tables were explained. Tables 6.1 through 6.4 illustrate the total damage, for the different projectile geometry/sizes, namely cylindrical projectiles with L/D of 4, 2 and 1, and for the spherical projectile of the same mass. These total damages were obtained from scenarios without tumbling effects and without variability in radial ejection velocity.

Table 6.1. Total Damage Quantification per Encounter Configuration for a Cylindrical Projectile with $L/D = 4$ @ $EBt = -0.006$ sec. Without Tumbling Effects and Without V_{rp} Variability.

L/D=4.00		Early Bird Time= -0.0060													Sum
MD/CA		0	15	30	45	60	75	90	105	120	135	150	165		
1	1	91.910	105.842	173.870	230.256	227.789	175.347	117.522	66.282	35.909	13.196	1.007	0.456	1239.388	
1.5	1	36.552	45.347	79.061	118.334	146.122	136.812	106.274	63.929	35.088	13.178	1.069	0.567	782.334	
2	1	17.506	26.600	42.998	72.261	89.367	94.396	78.841	56.822	33.133	11.117	1.163	0.217	524.420	
2.5	1	9.988	14.428	28.709	46.836	64.617	68.370	65.735	45.277	26.566	10.580	1.459	0.227	382.792	
3	1	7.032	11.303	18.757	31.335	47.285	51.697	51.237	40.662	24.796	10.749	1.647	0.254	296.754	
3.5	1	5.589	9.372	11.859	20.719	33.623	38.943	39.156	34.879	23.261	10.766	1.769	0.234	230.170	
4	1	3.847	7.342	9.787	15.431	24.844	30.261	31.379	26.940	21.536	10.690	1.861	0.167	184.084	
4.5	1	3.235	6.268	7.773	12.654	19.592	25.327	24.758	21.255	17.964	10.440	1.926	0.127	151.321	
5	1	2.399	5.074	7.059	10.418	16.375	22.065	20.844	18.145	13.958	9.946	1.795	0.141	128.218	
5.5	1	2.048	4.845	5.592	9.097	12.958	17.450	18.482	16.278	12.230	8.486	1.708	0.198	109.372	
6	1	0.972	4.355	5.255	8.002	12.191	14.610	16.613	14.220	11.109	7.716	1.432	0.242	96.718	
sum		181.078	240.777	390.721	575.342	694.764	675.276	570.841	404.690	255.551	116.865	16.835	2.831	4125.571	

Table 6.2. Total Damage Quantification per Encounter Configuration for a Cylindrical Projectile with $L/D = 2$ @ $EBt = -0.006$ sec. Without Tumbling Effects and Without V_{rp} Variability.

L/D=2.00		Early Bird Time= -0.0060													Sum
MD/CA		0	15	30	45	60	75	90	105	120	135	150	165		
1	1	58.198	71.786	148.523	209.942	213.897	173.844	120.170	75.181	38.468	15.709	1.679	0.027	1127.425	
1.5	1	22.959	30.935	67.692	108.746	136.404	134.086	108.223	71.937	37.794	15.337	1.750	0.112	735.975	
2	1	11.188	17.973	36.989	67.265	84.110	94.146	80.253	63.360	35.772	12.587	1.883	0.207	505.733	
2.5	1	6.278	9.890	24.271	42.981	60.255	67.371	66.432	50.513	28.655	11.962	2.067	0.255	370.929	
3	1	4.417	7.753	16.085	29.443	44.471	50.793	52.120	45.128	26.807	11.861	2.395	0.294	291.566	
3.5	1	3.506	6.407	10.546	19.351	31.626	39.219	39.373	38.716	25.376	11.953	2.457	0.254	228.785	
4	1	2.435	4.997	8.651	14.656	22.811	30.036	32.008	29.924	23.700	11.821	2.540	0.217	183.794	
4.5	1	2.056	4.279	6.827	11.987	18.281	24.772	25.047	23.847	19.841	11.333	2.564	0.197	151.030	
5	1	1.520	3.411	6.096	9.739	14.641	21.411	21.554	20.292	16.469	10.782	2.478	0.208	128.600	
5.5	1	1.355	3.250	4.810	8.420	12.346	16.933	18.619	18.026	14.206	9.131	2.151	0.233	109.479	
6	1	0.618	2.921	4.465	7.328	11.054	14.223	16.742	16.236	12.732	8.422	1.922	0.250	96.913	
sum		114.529	163.600	334.954	529.857	649.897	666.834	580.539	453.161	279.821	130.897	23.887	2.254	3930.230	

Table 6.3. Total Damage Quantification per Encounter Configuration for a Cylindrical Projectile with $L/D = 1$ @ $EBt = -0.006$ sec. Without Tumbling Effects and Without V_{rp} Variability.

L/D=1.00		Early Bird Time= -0.0060													Sum
MD/CA		0	15	30	45	60	75	90	105	120	135	150	165		
1	1	66.451	82.839	170.384	219.126	205.354	164.916	117.147	74.644	37.701	15.394	1.667	0.000	1155.621	
1.5	1	26.127	35.684	77.921	113.755	131.632	127.065	104.819	71.930	37.277	15.010	1.829	0.000	743.050	
2	1	12.371	20.453	42.080	70.605	81.149	89.696	78.500	62.520	35.277	12.466	1.917	0.000	507.035	
2.5	1	6.745	11.300	27.468	45.239	58.591	64.597	64.903	51.138	28.723	11.739	2.258	0.139	372.841	
3	1	4.775	8.581	18.195	31.022	43.184	48.884	50.739	45.408	26.711	11.904	2.435	0.081	291.919	
3.5	1	3.822	7.332	11.994	20.079	30.757	37.912	38.713	38.301	25.331	12.047	2.496	0.235	229.019	
4	1	2.620	5.719	9.876	15.318	21.946	28.957	31.180	30.204	23.339	11.693	2.528	0.267	183.648	
4.5	1	2.259	4.872	7.800	12.052	17.607	23.938	24.420	24.998	19.759	11.298	2.531	0.269	151.803	
5	1	1.660	3.925	6.982	9.727	14.147	20.799	20.919	20.618	16.679	10.637	2.556	0.272	128.920	
5.5	1	1.412	3.668	5.513	8.865	11.970	16.412	17.617	18.380	14.218	9.089	2.365	0.269	109.779	
6	1	0.721	3.328	5.113	7.729	10.747	13.717	16.180	16.466	12.865	8.244	1.951	0.269	97.330	
sum		128.963	187.701	383.327	553.518	627.085	636.893	565.137	454.606	277.879	129.521	24.533	1.801	3970.964	

Table 6.4. Total Damage Quantification per Encounter Configuration for a Spherical Projectile @ $EBt = -0.006$ sec. Without V_{rp} Variability.

L/D=Sphere Early Bird Time= -0.0060													Sum
MD/CA	0	15	30	45	60	75	90	105	120	135	150	165	
1	69.272	84.847	163.458	208.097	201.358	164.231	115.982	74.755	37.233	16.860	2.373	0.000	1138.464
1.5	27.550	36.732	75.139	108.349	128.632	126.251	103.822	71.991	36.743	16.452	2.560	0.000	734.221
2	13.247	21.126	40.847	67.570	78.719	89.339	77.705	62.954	34.700	13.507	2.721	0.000	502.435
2.5	7.414	11.759	26.958	43.479	56.815	64.275	64.796	50.916	28.436	12.559	2.753	0.000	370.160
3	5.221	9.010	17.858	29.849	42.050	48.537	50.346	45.281	26.558	12.694	3.385	0.000	290.788
3.5	4.149	7.433	11.180	19.401	29.804	37.616	38.612	38.094	24.814	12.438	3.523	0.064	227.129
4	2.880	5.959	9.517	14.732	21.458	28.858	31.075	30.103	23.093	12.136	3.691	0.072	183.573
4.5	2.443	5.099	7.532	11.639	17.217	23.790	24.338	24.543	19.644	11.635	3.563	0.083	151.526
5	1.802	4.095	6.783	9.425	13.852	20.590	20.882	20.205	16.825	10.925	3.319	0.109	128.813
5.5	1.608	3.916	5.359	8.564	11.725	16.252	17.545	18.122	14.262	9.221	3.130	0.079	109.783
6	0.742	3.519	5.007	7.464	10.522	13.630	16.084	16.130	12.902	8.481	2.785	0.051	97.317
sum	136.327	193.494	369.636	528.568	612.151	633.371	561.188	453.092	275.211	136.910	33.804	0.459	3934.210

The overall tendencies observed in these tables confirm that at smaller miss distances, the total damage inflicted increases substantially resembling a direct hit to the TBM warhead. The variation in total damage as the crossing angle varies is explained referring to Table 6.1 for an L/D of 4. For the miss distance of 1.0 meter as the crossing angle increases, the total damage starts at 91.910 increases to a maximum of 230.256 at 45° and thereon decreases at an increasing rate to a minimum occurring at 165° . For the miss distance of 2.0 meters the distribution of total damage behaves in a similar fashion, however, the maximum of 94.396 occurs at an angle of 75° . For miss distances of 3.5 and 6.0 meters, the distributions behave similarly, where the maximums of 39.156 and 16.613 respectively, occur at a crossing angle of 90° . The minimum damage at the different miss distances is inflicted at a crossing angle of 165° being less than 0.5. These parabolic tendencies are very similar to the ones observed in Figure 3.18 where impact frequencies are compared against crossing angle. Figures 6.2 to 6.4 depict total damage tendencies for selected early bird times at selected miss distances. Larger levels of damage are observed at late bird scenarios (-0.012 and -0.006 sec.) and low levels at early bird scenarios (0.0012 sec.). In late bird scenarios the variation in damage as miss distance increases is evident; however, in early bird scenarios the levels of damage are very similar regardless of miss distance. Similar tendencies are observed for the other projectile geometry/sizes and the remaining early bird times; however, these plots are not included in this report.

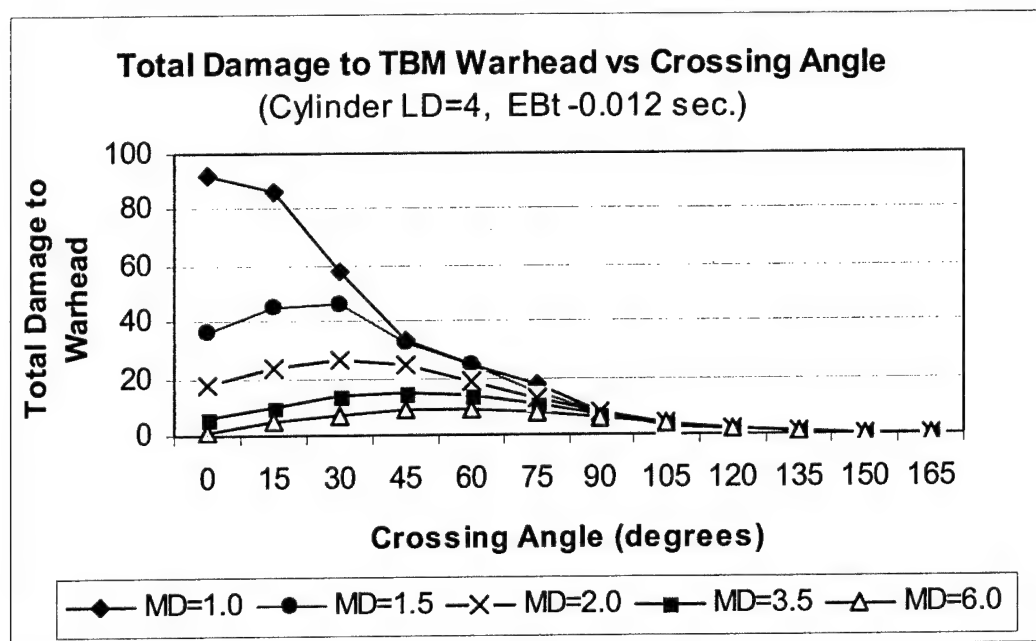


Figure 6.2. Cylinder L/D of 4 Total Damage vs. Crossing Angle @ EBt of -0.012 sec.

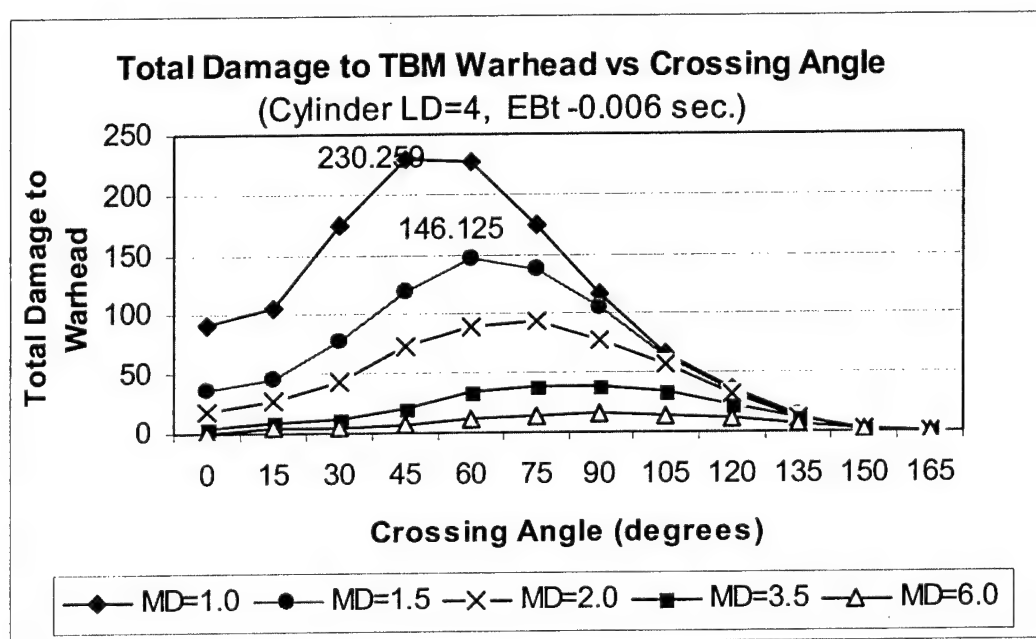


Figure 6.3. Cylinder L/D of 4 Total Damage vs. Crossing Angle @ EBt of -0.006 sec.

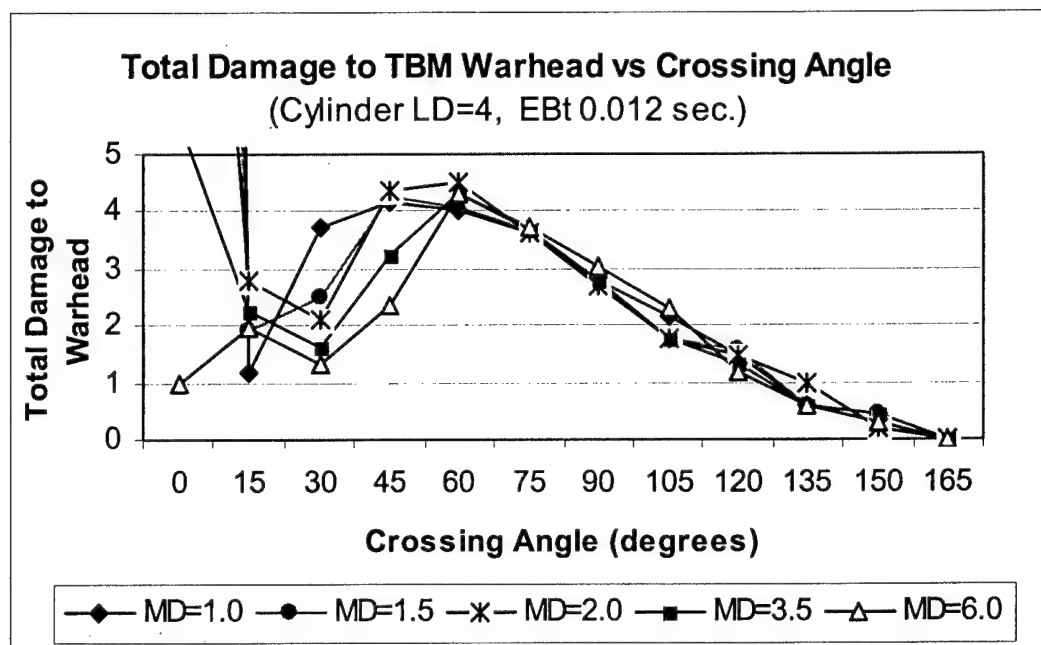


Figure 6.4. Cylinder L/D of 4 Total Damage vs. Crossing Angle @ EBt of 0.012 sec.

At the early bird time of -0.006 sec. the number of impacts is practically the same between the different geometry/sizes as observed in Tables 6.1 through 6.3. However, in some cases significant differences are observed in the level of total damage calculated for each encounter configuration scenario. Table 6.5 summarizes the total damage from five different encounter configuration scenarios from Tables 6.6 through 6.8 where the number of impacts is exactly the same regardless of projectile geometry/size.

Table 6.5. Total Damage Comparison among Projectile Geometry/Sizes of the Same Mass Without Tumbling Effects and Without V_{rp} Variability.

Scenario Case	Encounter Configuration $EBt = -0.006$ sec.	Number of Impacts	Cylinder Without Tumbling			Sphere
			$L/D=4$	$L/D=2$	$L/D=1$	
1	$CA = 0, MD = 1$	400	91.910	58.198	66.451	69.272
2	$CA = 0, MD = 6$	4	0.972	0.618	0.721	0.742
3	$CA = 165, MD = 1$	6	0.456	0.027	0.000	0.000
4	$CA = 165, MD = 6$	18	0.242	0.25	0.269	0.051
5	$CA = 75, MD = 3$	112	51.697	50.793	48.884	48.537

As observed for the first and second case scenarios, when the missiles are directly in front of each other with the least separation, the largest damage is inflicted when cylindrical shapes of L/D of 4 are deployed. Spherical projectiles generate more damage

than the other two cylindrical shapes. In contrast, for the third scenario, when the EKV is almost pursuing the TBM with the least separation, cylindrical shapes of $L/D = 4$ still inflict more damage than cylindrical shapes of $L/D = 2$; however, both the sphere and the cylindrical shape of $L/D = 1$ do not inflict any damage. For the fifth scenario, the damages are very similar, with the cylindrical shapes of $L/D = 4$ prevailing in lethality. Tables 6.6 to 6.8 summarize the total damage throughout the entire encounter configuration range for all three cylindrical projectiles at the same $EBt = -0.006$ sec. with tumbling effects and without variability in radial ejection velocity.

Table 6.6. Total Damage Quantification per Encounter Configuration for a Cylindrical Projectile with $L/D = 4$ @ $EBt = -0.006$ sec. With Tumbling Effects and Without V_{rp} Variability.

L/D=4.00 Early Bird Time=-0.0060													Sum
MD/CA	0	15	30	45	60	75	90	105	120	135	150	165	
1	87.086	98.825	162.940	213.238	207.609	161.132	105.769	63.765	35.090	13.549	1.218	0.473	1150.694
1.5	30.883	36.077	60.537	94.223	119.028	115.750	91.683	59.208	34.108	13.829	1.274	0.449	657.047
2	7.750	11.293	21.453	48.976	68.359	77.742	68.342	51.824	32.679	11.156	1.338	0.421	401.335
2.5	2.497	5.486	15.170	33.653	50.528	57.971	57.424	43.340	27.133	10.632	1.408	0.327	305.569
3	2.424	5.186	13.947	26.074	39.849	46.585	46.729	39.696	24.897	10.951	1.849	0.226	258.414
3.5	3.468	6.692	9.646	18.695	30.340	36.391	37.304	34.314	23.736	10.598	1.864	0.150	213.198
4	2.779	5.790	8.465	14.288	22.743	27.462	30.093	26.784	20.834	10.009	2.044	0.198	171.489
4.5	2.370	5.179	6.938	11.245	17.505	23.177	23.190	20.878	18.430	10.095	2.041	0.163	141.211
5	1.942	3.170	5.695	8.684	13.398	19.810	19.172	17.450	14.270	9.549	1.863	0.140	115.143
5.5	1.226	2.395	3.927	7.508	11.125	14.895	16.562	15.679	12.645	8.463	1.592	0.193	96.210
6	0.232	2.827	3.216	6.627	10.261	12.961	14.783	13.279	11.363	7.462	1.459	0.360	84.831
sum	142.659	182.919	311.936	483.209	590.745	593.878	511.052	386.217	255.185	116.292	17.950	3.101	3595.141

Table 6.7. Total Damage Quantification per Encounter Configuration for a Cylindrical Projectile with $L/D = 2$ @ $EBt = -0.006$ sec. With Tumbling Effects and Without V_{rp} Variability.

L/D=2.00 Early Bird Time=-0.0060													Sum
MD/CA	0	15	30	45	60	75	90	105	120	135	150	165	
1	59.071	69.333	142.958	206.773	204.357	160.500	111.845	70.065	40.020	15.795	1.503	0.066	1082.285
1.5	14.060	22.421	56.540	99.058	122.623	120.108	98.195	66.081	39.735	15.799	1.664	0.043	656.328
2	2.374	8.910	26.716	55.768	71.867	83.064	73.016	59.122	37.391	12.850	1.612	0.089	432.778
2.5	2.645	6.217	18.499	36.040	52.506	60.291	61.429	47.768	30.125	12.146	1.945	0.116	329.726
3	3.461	6.448	13.733	26.575	40.655	47.101	49.465	42.963	28.142	12.491	2.184	0.010	273.227
3.5	2.916	5.807	9.989	18.044	29.442	36.917	37.806	36.712	26.944	12.527	2.313	0.112	219.529
4	1.993	4.694	8.072	13.869	21.632	28.036	30.770	29.300	24.701	12.051	2.438	0.171	177.726
4.5	1.565	3.664	6.212	11.619	17.231	23.238	23.697	22.869	20.293	12.015	2.283	0.141	144.826
5	0.906	2.715	5.302	8.650	13.236	19.627	20.244	19.192	16.764	11.201	2.239	0.214	120.290
5.5	1.024	1.673	4.194	7.150	11.245	15.510	17.580	16.989	14.498	9.706	1.870	0.084	101.524
6	0.359	1.919	3.767	6.290	9.873	13.119	15.595	15.666	12.876	8.918	1.838	0.258	90.477
sum	90.373	133.801	295.983	489.835	594.666	607.511	539.641	426.728	291.489	135.500	21.886	1.305	3628.717

Table 6.8. Total Damage Quantification per Encounter Configuration for a Cylindrical Projectile with $L/D = 1$ @ $EBt = -0.006$ sec. With Tumbling Effects and Without V_{rp} Variability.

L/D=1.00		Early Bird Time=-0.0060													
MD/CA		0	15	30	45	60	75	90	105	120	135	150	165	Sum	
1		53.768	71.902	155.136	209.109	197.334	158.352	109.446	70.849	39.237	15.677	1.690	0.066	1082.565	
1.5		20.102	28.935	66.058	104.542	123.031	120.734	99.080	68.684	38.584	15.486	1.791	0.183	687.211	
2		10.380	17.948	35.124	62.182	75.379	85.874	75.142	60.374	36.428	12.669	1.834	0.057	473.392	
2.5		7.106	10.664	23.650	40.026	55.044	62.190	63.310	50.046	29.544	11.999	1.967	0.037	355.584	
3		5.107	8.338	16.192	28.163	41.379	47.769	50.319	44.569	27.176	11.993	2.360	0.035	283.400	
3.5		3.889	7.131	11.004	18.827	29.972	36.988	38.209	36.958	25.781	12.119	2.412	0.176	223.464	
4		2.705	5.641	9.069	14.668	21.647	28.553	30.401	29.385	24.009	11.670	2.648	0.005	180.400	
4.5		2.172	4.401	7.298	11.401	17.110	23.321	24.113	23.821	20.271	11.215	2.442	0.000	147.564	
5		1.438	3.539	6.205	9.177	13.668	19.984	20.520	19.599	16.937	10.919	2.298	0.122	124.406	
5.5		1.538	3.435	4.887	8.167	11.502	15.735	17.240	17.608	14.137	9.286	2.128	0.071	105.733	
6		0.572	3.106	4.722	7.342	10.523	13.342	15.832	15.832	13.108	8.520	1.944	0.073	94.914	
sum		108.776	165.038	339.345	513.602	596.588	612.843	543.611	437.726	285.213	131.553	23.514	0.823	3758.632	

When tumbling effects are added, the number of impacts remains the same as observed in Table 3.12; however, the total damage in all three projectile geometries is different than the damage generated without tumbling. The general tendencies in the variation of total damage throughout the encounter configuration scenarios are the same in all three tables as for the tables without tumbling. Similar tendencies are observed for other early bird times; therefore these tables are not included in this work. Table 6.9 shows the total damage observed when tumbling effects are added for the same five encounter configuration scenarios studied in Table 6.5.

Table 6.9. Total Damage Comparison among Projectile Geometry/Sizes of the Same Mass With Tumbling Effects and Without V_{rp} Variability.

Scenario	Encounter Configuration	Number of Impacts	Cylinder With Tumbling			Sphere
			L/D=4	L/D=2	L/D=1	
Case	EBt= -0.006 sec.					
1	CA = 0, MD = 1	400	87.086	59.071	53.768	69.272
2	CA = 0, MD = 6	4	0.232	0.359	0.572	0.742
3	CA = 165, MD = 1	6	0.473	0.066	0.066	0.000
4	CA = 165, MD = 6	18	0.360	0.258	0.073	0.051
5	CA = 75, MD = 3	112	46.585	47.101	47.769	48.537

Observing the first case, cylindrical shapes of L/D 4 still generate more damage than the other shapes; however, the damage is slightly lower than the damage without tumbling. The damages for L/D 2 and for L/D 1 are slightly higher and lower, respectively than without tumbling. For the second case, the cylinders always generate less damage than without tumbling; therefore, in this scenario, the sphere is more lethal than the cylinders. For the third scenario, the cylindrical shapes generate more damage than when they are not tumbling, prevailing over the sphere. Different tendencies are observed for the other cases, showing that when tumbling is considered in some cases the sphere is more lethal than the cylindrical shapes. These random fluctuations in total damage are due to the variation in the configuration of the impacts when tumbling is

added. Tables 6.10 and 6.11 compare the impact configurations and associated SIDI with and without tumbling for encounter scenario 2 for cylindrical shapes of L/D 4 and 1, respectively.

Table 6.10. Impact Configuration Comparison for Cylindrical Projectile with $L/D = 4$ With and Without Tumbling Effects and Without V_{rp} Variability for Encounter Scenario 2.

Impact Number	Tumbling case	Velocity Magnitude (km/s)	Strike Angle ϕ (degrees)	Orientation Angle α (degrees)	SIDI	
					Without	With
1	Without	2.015	81.35	88.24	0.2430	
	With	2.015	81.35	-3.28		0.0306
2	Without	2.015	81.35	88.24	0.2430	
	With	2.015	81.35	6.52		0.0394
3	Without	2.015	81.35	88.24	0.2430	
	With	2.015	81.35	21.01		0.0619
4	Without	2.015	81.35	88.24	0.2430	
	With	2.015	81.35	34.81		0.1003
Sum					0.972	0.232

Table 6.11. Impact Configuration Comparison for a Cylindrical Projectile with $L/D = 1$ With and Without Tumbling Effects and Without V_{rp} Variability for Encounter Scenario 2.

Impact Number	Tumbling case	Velocity Magnitude (km/s)	Strike Angle ϕ (degrees)	Orientation Angle α (degrees)	SIDI	
					Without	With
1	Without	2.015	81.35	88.24	0.1802	
	With	2.015	81.35	-59.71		0.1316
2	Without	2.015	81.35	88.24	0.1802	
	With	2.015	81.35	-56.23		0.1314
3	Without	2.015	81.35	88.24	0.1802	
	With	2.015	81.35	-52.05		0.1330
4	Without	2.015	81.35	88.24	0.1802	
	With	2.015	81.35	67.44		0.1759
Sum					0.721	0.572

When variability in radial ejection velocity is added both the number of impacts and the total damage calculated for each encounter scenario corresponds to the average of 30 simulations, such as shown in Tables 3.13 and 3.14. Tables 6.12 and 6.13 illustrate the total damage for a cylindrical projectile with $L/D = 4$ at the same EBt -0.006 sec. with 25% variability in radial ejection velocity, without and with tumbling effects, respectively.

Table 6.12. Total Damage Quantification per Encounter Configuration for a Cylindrical Projectile with $L/D = 4$ @ EBt -0.006 sec. Without Tumbling Effects and With a $COV V_{rp}$ of 25%.

L/D=4.00 MD/CA		Early Bird Time=-0.0060												Sum
		0	15	30	45	60	75	90	105	120	135	150	165	
1	82.464	98.930	156.732	194.182	188.117	147.746	99.994	55.962	28.097	9.860	0.998	0.125		1063.207
1.5	26.396	34.984	65.597	96.349	112.222	103.298	80.232	48.920	26.385	9.778	1.046	0.196		605.403
2	12.480	19.009	35.482	54.645	71.333	70.326	62.008	41.088	24.204	9.752	1.132	0.151		401.610
2.5	7.563	11.226	21.711	34.110	46.867	52.476	48.351	36.105	21.547	9.250	1.183	0.136		290.525
3	4.914	7.482	13.740	24.127	34.643	38.329	38.675	28.773	19.680	8.619	1.228	0.163		220.374
3.5	3.442	5.445	10.374	17.208	24.556	29.438	31.545	24.980	17.054	8.411	1.287	0.175		173.914
4	2.595	4.096	7.785	13.552	18.713	22.674	25.170	21.039	14.913	8.129	1.277	0.163		140.106
4.5	2.145	3.166	6.239	10.478	14.660	18.328	19.834	17.380	14.081	7.169	1.439	0.134		115.052
5	1.555	2.397	4.564	8.386	12.459	15.354	16.535	15.239	11.574	7.124	1.444	0.179		96.810
5.5	1.168	2.152	4.167	6.909	9.707	12.019	14.637	13.636	11.061	6.776	1.448	0.127		83.807
6	1.038	1.897	3.646	5.829	8.727	10.577	11.559	12.002	9.225	6.439	1.530	0.145		72.614
sum		145.759	190.784	330.037	465.775	542.004	520.565	448.540	315.124	197.820	91.307	14.013	1.695	3263.423

The total damages generated when variability is added are lower than without variability, except for a few isolated scenarios; however the general tendencies in the variation of total damage throughout the encounter configuration scenarios are the same. Similar tendencies are observed for other amounts of variability in radial ejection velocity and other projectile geometry/sizes.


Table 6.13. Total Damage Quantification per Encounter Configuration for a Cylindrical Projectile with $L/D = 4$ @ $EBt -0.006$ sec. With Tumbling Effects and With a COV_{V_p} of 25%.

L/D=4.00	Early Bird	Time=-0.0060											Sum
MD/CA	0	15	30	45	60	75	90	105	120	135	150	165	
1	85.801	101.732	160.482	204.398	200.265	156.248	106.003	60.687	32.262	12.037	1.352	0.144	1121.411
1.5	27.868	32.839	57.453	90.026	111.207	107.490	83.231	54.036	30.967	11.942	1.482	0.202	608.743
2	7.795	10.118	22.755	45.357	67.820	74.781	67.006	48.026	29.530	11.731	1.484	0.162	386.563
2.5	2.506	5.103	14.918	30.786	47.867	56.475	54.219	42.193	27.913	11.367	1.558	0.188	295.093
3	2.203	5.090	13.343	25.111	36.859	44.703	45.091	37.279	25.249	11.016	1.513	0.207	247.663
3.5	2.503	4.674	11.068	19.466	28.991	34.769	37.104	31.186	22.672	10.679	1.717	0.190	205.018
4	2.320	4.360	8.400	15.430	22.740	28.514	29.446	26.979	19.764	10.018	1.742	0.193	169.906
4.5	2.394	3.303	6.808	11.848	17.764	22.844	24.198	22.248	18.049	9.312	1.813	0.182	140.563
5	1.561	2.421	5.113	9.057	13.894	18.097	19.899	18.661	15.153	8.775	1.801	0.158	114.590
5.5	1.022	1.978	3.932	7.012	11.220	14.896	16.243	16.660	13.543	8.214	1.913	0.141	96.775
6	0.821	1.409	3.309	6.134	8.672	12.658	14.836	14.152	11.883	7.865	1.876	0.156	83.772
sum	136.794	173.026	307.381	464.626	567.299	571.475	497.276	372.108	246.985	112.955	18.251	1.922	3470.097

The combined effect of tumbling and added variability in radial ejection velocity is reflected in the total damages observed in Table 6.13. Compared to the cases without tumbling and without radial ejection velocity variability, the majority of the scenarios show an increase in the total damage, while for the remaining few the total damage decreases.

In the previous discussion, the tendencies in the absolute values of the total damages were compared among the selected deployment conditions. However, it would be cumbersome to study the variations in total damage among different projectile geometry/sizes subjected to the different deployment conditions by comparing absolute values. To facilitate the identification of encounter configuration scenarios with similar levels of total damage to the warhead, and subsequently identify ranges of encounter configuration scenarios where damage can be maximized, a five level total damage criterion was devised, similar to the criterion developed for impact frequencies. This criterion is summarized in Table 6.14.

Table 6.14. Total Damage Level Criterion.

Total Damage (absolute value)	Total Damage Level Descriptor	Associated Color
$D_{tot} < 1.0$	Very Low	
$1.0 \leq D_{tot} < 3.5$	Low	
$3.5 \leq D_{tot} < 7.5$	Moderate	
$7.5 \leq D_{tot} < 15$	High	
$15 \leq D_{tot}$	Very High	

Each damage level is defined by a range of total damage, based on a statistical analysis performed on the entire encounter configuration range, and has an associated damage level descriptor. To further facilitate the identification on the damage quantification tables, each level can be visually identified with a gray-scale based color. The higher the damage level the darker the color associated to that level. The criterion is applied to each cell in the total damage quantification tables per encounter configuration, and the scenarios with similar damage level become evident. Table 6.15 and 6.16

illustrate trends in the distribution of total damage throughout the encounter configuration range at an early bird time of -0.006 seconds, for a cylindrical projectile with L/D 4. Table 6.15 shows damage for scenarios without variability in radial ejection velocity and without tumbling effects. Table 6.16 shows damage for scenarios with 75% variability in the radial ejection velocity and with tumbling effects.

Table 6.15. Total Damage Quantification Trends per Encounter Configuration for a Cylindrical Projectile with $L/D = 4$ @ $EBt = -0.006$ sec. Without Tumbling Effects and Without $COV V_{rp}$.

L/D=4.00 Early Bird time=-0.0060															
MD/CA		0	15	30	45	60	75	90	105	120	135	150	165	Sum	
1												0.01	0.46	1239.39	
1.5												0.07	0.57	782.33	
2												0.06	0.22	524.42	
2.5												0.23	0.23	382.79	
3												0.25	0.25	296.75	
3.5												0.23	0.23	230.17	
4												0.17	0.17	184.08	
4.5												0.13	0.13	151.32	
5												0.14	0.14	128.22	
5.5												0.20	0.20	109.37	
6												0.24	0.24	96.72	
sum		181.08	240.78	390.72	575.34	694.76	675.28	570.84	404.69	255.55	116.86	16.83	2.83	4125.57	

Table 6.16. Total Damage Quantification Trends per Encounter Configuration for a Cylindrical Projectile with $L/D = 4$ @ $EBt = -0.006$ sec. With Tumbling Effects and With a $COV V_{rp}$ of 75%.

L/D=4.00 Early Bird Time=-0.0060															
MD/CA		0	15	30	45	60	75	90	105	120	135	150	165	Sum	
1												0.62	0.05	598.36	
1.5												0.66	0.06	279.33	
2												0.68	0.09	166.35	
2.5												0.69	0.08	122.61	
3												0.65	0.07	101.81	
3.5												0.71	0.05	84.41	
4												0.70	0.06	68.89	
4.5												0.78	0.07	55.94	
5												0.73	0.07	45.38	
5.5												0.69	0.06	38.30	
6												0.79	0.06	33.21	
sum		79.80	91.09	154.18	217.45	258.17	251.27	218.59	162.65	105.30	47.65	7.70	0.73	1594.59	

Five regions with different damage level are clearly identified in both tables. Scenarios without deployment conditions exhibit very high damage (darkest region) extending through the entire miss distance range as the crossing angle reaches 90° and continuing up to a crossing angle of 120° . A smaller number of scenarios with deployment conditions exhibit high levels of damage; the crossing angle range is the same; however, the scenarios extend half way the miss distance range at crossing angle 90° . A larger number of scenarios with deployment conditions are observed to have very low damage than scenarios without them.

Matrices of total damage quantification tables per encounter configuration scenarios and various deployment conditions were prepared for all projectile geometry/sizes. The format of the matrices is exactly the same as the format used for

impact quantification matrices (see Table 3.15). Tables 6.17 through 6.23 depict seven matrices for all three cylindrical projectiles and the sphere, without and with tumbling.

Table 6.17. Total Damage Quantification Matrix for a Cylindrical Projectile with $L/D = 4$ Without Tumbling Effects

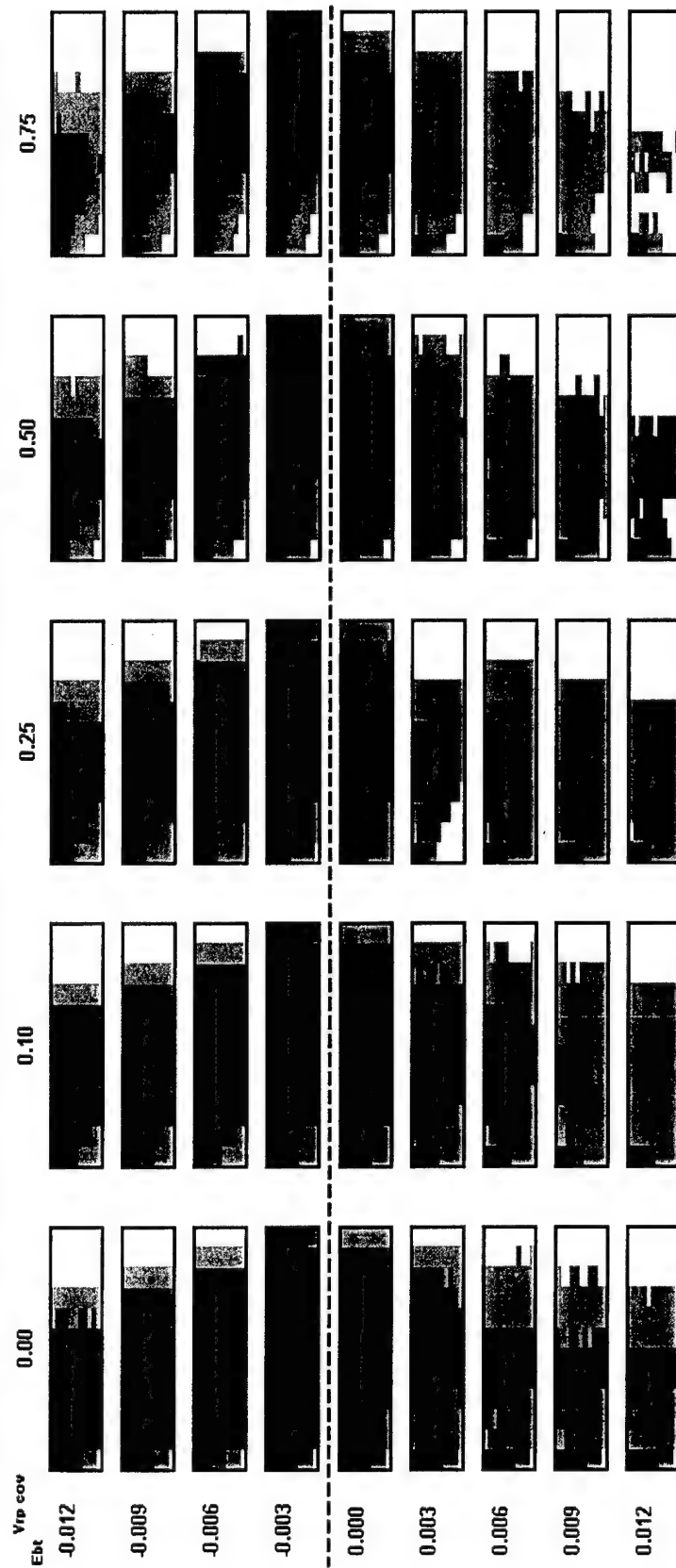


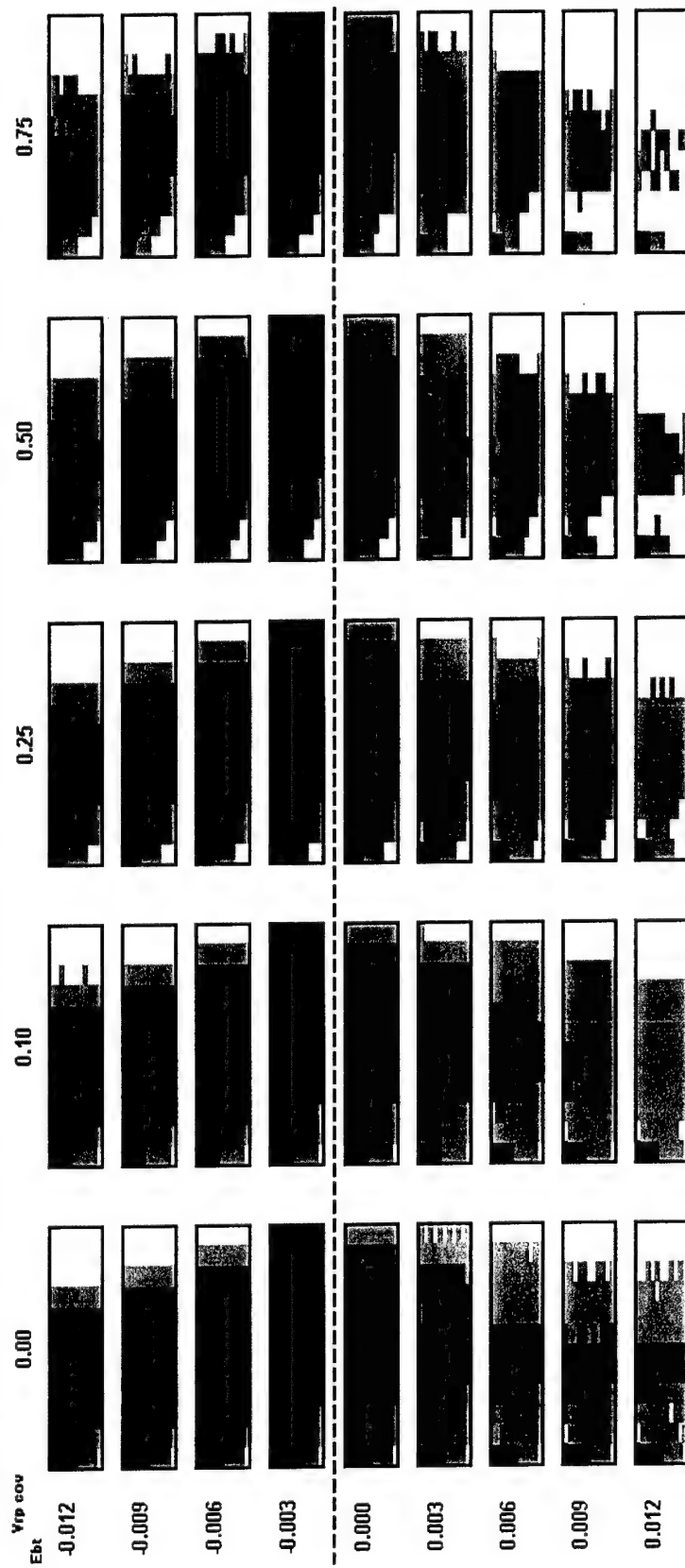
Table 6.18. Total Damage Quantification Matrix for a Cylindrical Projectile with $L/D = 2$ Without Tumbling Effects

Table 6.19. Total Damage Quantification Matrix for a Cylindrical Projectile with $L/D = 1$ Without Tumbling Effects

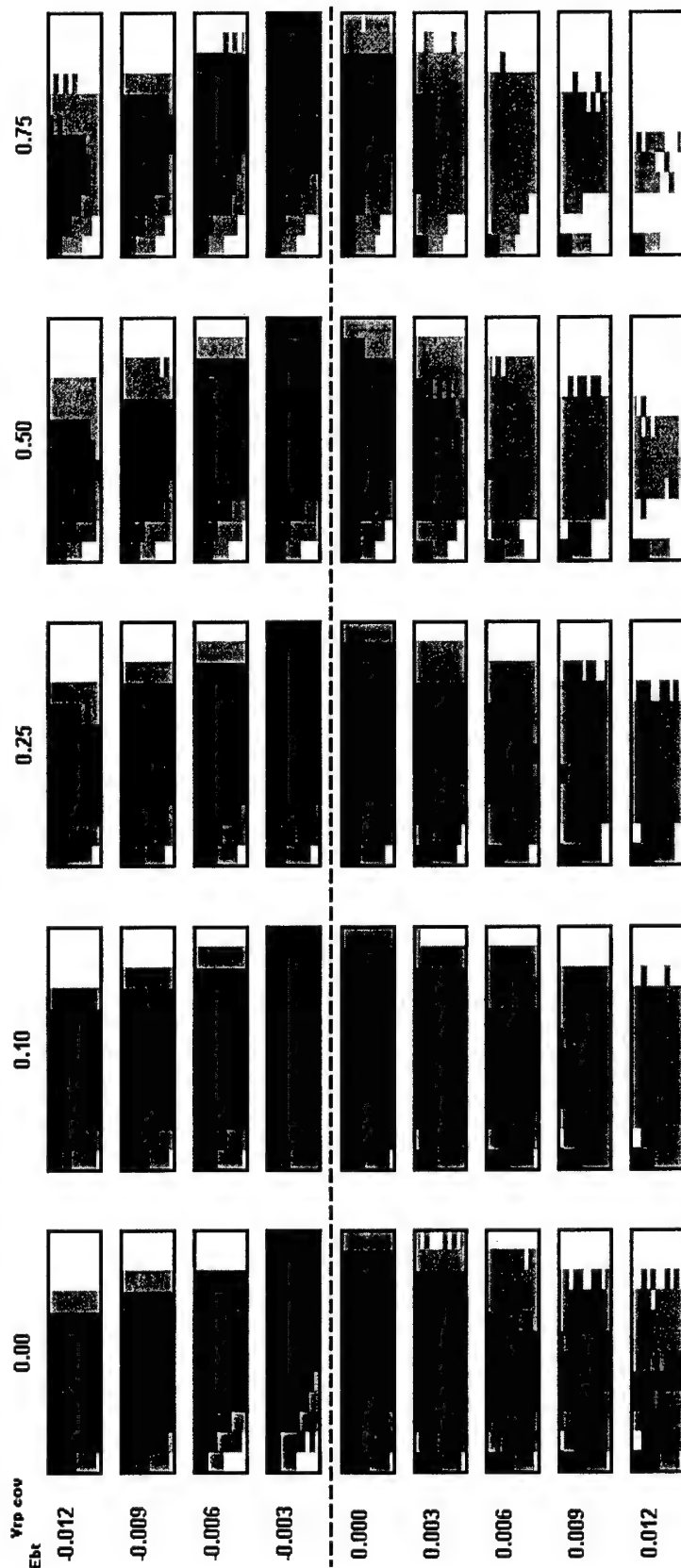


Table 6.20. Total Damage Quantification Matrix for a Spherical Projectile

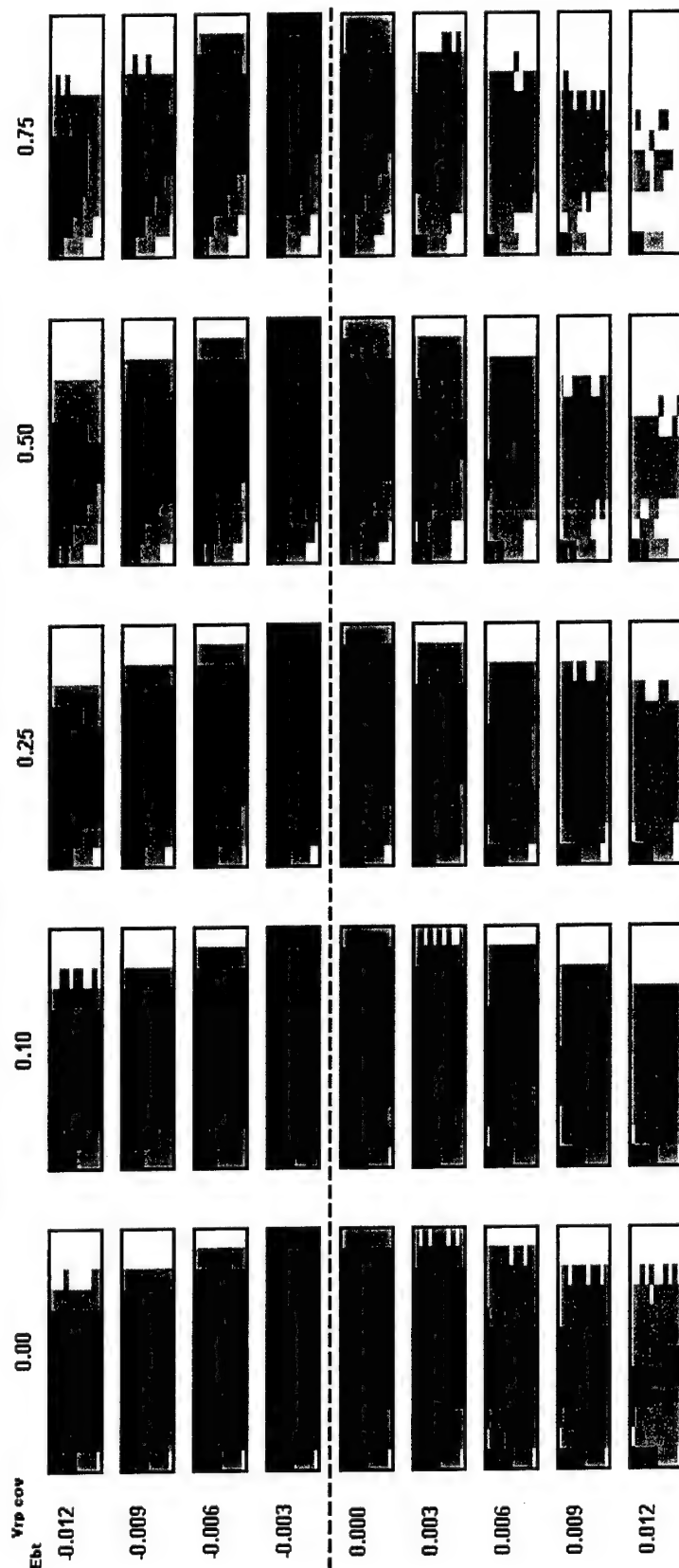


Table 6.21. Total Damage Quantification Matrix for a Cylindrical Projectile with $L/D = 4$ With Tumbling Effects

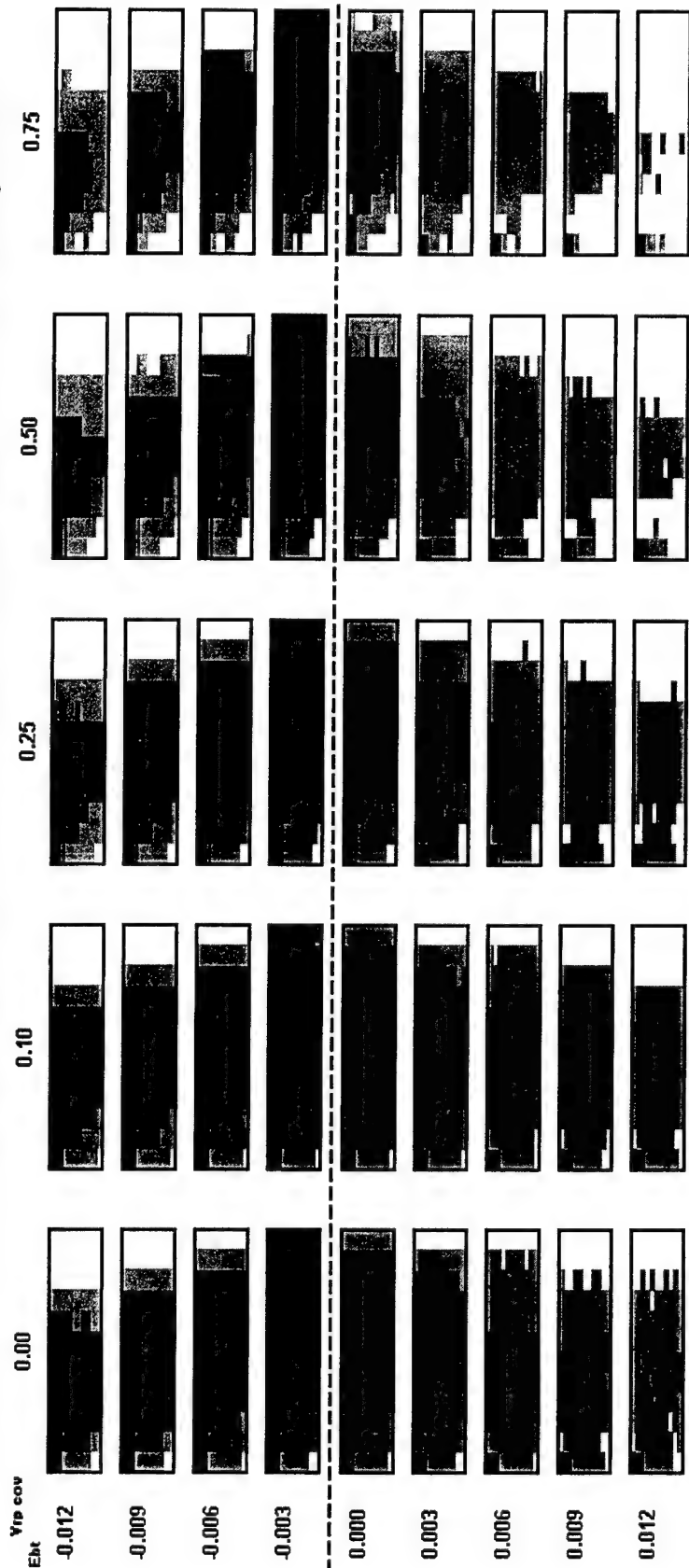


Table 6.22. Total Damage Quantification Matrix for a Cylindrical Projectile with $L/D = 2$ With Tumbling Effects

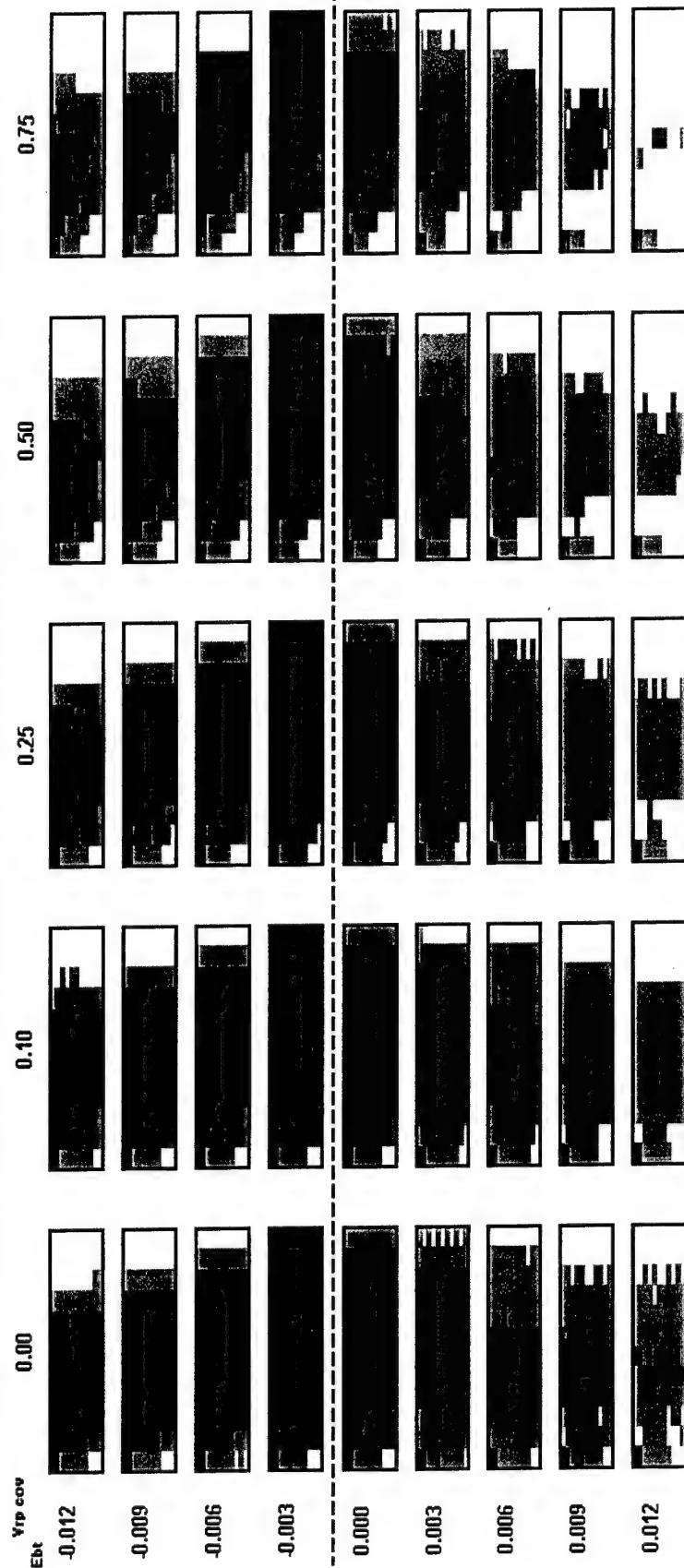
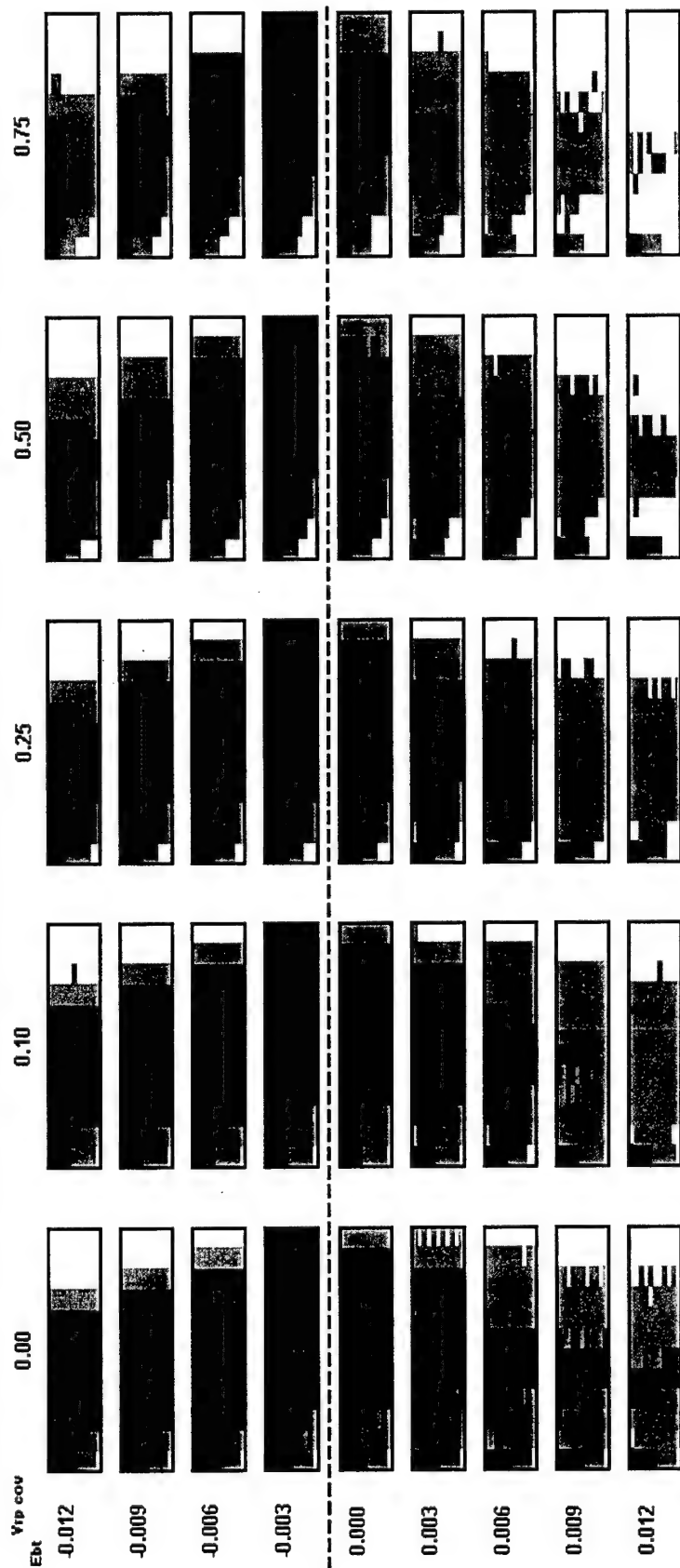


Table 6.23. Total Damage Quantification Matrix for a Cylindrical Projectile with $L/D = 1$ With Tumbling Effects



When comparing the cell-tables against the early bird parameter (vertical-wise) under a specific deployment variability case, it is observed that the total damage is maximized (dark color regions) over a larger scenario of encounter configurations at late-bird times, versus early bird times where the damage levels are low (light-color regions) for a large scenario of encounter configurations. The largest encounter configuration scenario range with a very high damage level is obtained at an early bird time of -0.003 sec. even when variability in the radial ejection velocity is included. Close to half or more of the entire encounter configuration range (upper triangle of each cell-table) show a very high damage level. As variability increases, this range of scenarios reduces, limiting in miss distance. The sphere is the only geometry that generates high levels of damage at scenarios with crossing angle of 165° between 1.0 and 2.0 meters. From the early bird time standpoint, and assuming a miss distance of zero, an early bird time of -0.003 sec. resembles a direct hit to the TBM warhead. As the early bird parameter moves away from this threshold, the encounter is considered a near-miss. A near-miss at a late bird time of -0.006 sec. shows a reduction in the encounter configuration scenarios with high damage levels compared to the threshold of -0.003; specifically up to approximately a crossing angle of 120° and a miss distance of 3.5 meters or less. As the late-bird time increases to -0.009 sec. and -0.012 sec. the high damage level regions are limited to crossing angles up to 90° and 30° respectively, and miss distances between 1.0 and 3.0 meters. For near-miss encounters at early bird times of 0.003 to 0.012 sec. the high impact frequency regions are concentrated around a crossing angle of 0° and miss distance of 1.0 meter. As the early bird time increases the regions of moderate to very low damage or no damage increase, and this is more noticeable as the variability in radial ejection velocity increases as well. Very similar patterns are observed for most projectile geometry/sizes with and without tumbling effects. Therefore, it is concluded that variability in radial ejection velocity does have an effect on the level of damage inversely proportional to the amount of variability.

In general, it is somewhat difficult to differentiate which projectile geometry/size is more lethal per encounter configuration scenario or per deployment condition, except that the sphere generates high levels of damage at scenarios with crossing angle of 165° between 1.0 and 2.0 meters. Observing these tables, it is also very difficult to differentiate between the levels of damage generated without and with tumbling. The section ahead presents a detailed analysis on tumbling effects.

6.3 Total Damage Ratio per Encounter Configuration

To identify the range of encounter configuration scenarios in which a certain cylindrical geometry/size projectile is more lethal than a spherical projectile, a total damage-ratio was computed as follows:

$$D_{rat} = \frac{\text{Total damage by Cylindrical geometry / size projectiles}}{\text{Total damage by Spherical projectiles}} \quad (6.1)$$

This total damage-ratio per encounter configuration scenario can take any positive values including zero when no impacts to the warhead are recorded; and therefore no damage inflicted. When the ratio is less than one (1.0), the spherical projectile inflicts

more damage to the warhead than the corresponding cylindrical projectile, for that particular encounter scenario. Conversely, when it's greater than one (1.0) the corresponding cylindrical projectile generated more damage than the sphere. For example, the total damage-ratio between a cylindrical projectile with $L/D = 4$ and the sphere at the encounter scenario with a crossing angle 0° , a miss distance of 1.0 meter and an early bird time of -0.006 sec. is computed by dividing the cylinder's total damage (see Table 6.1) by the sphere's total damage (see Table 6.4) as follows:

$$D_{rat} = \frac{91.910}{69.272} = 1.327$$


For simplicity, the total damage-ratios are presented in tables per encounter configuration maintaining the same format as utilized above for total damage quantification. Table 6.24 shows the damage ratios between a cylindrical projectile with L/D of 4 and the sphere at an early bird time of -0.006 sec. without tumbling effects and without variability in radial ejection velocity.

Table 6.24. Total Damage-Ratio per Encounter Configuration between a Cylindrical Projectile with $L/D = 4$ and a Sphere @ EBt -0.006 sec. Without Tumbling Effects and Without $COVV_{rp}$.

L/D=4.00 Early Bird Time=-0.0060													
MD/CA	0	15	30	45	60	75	90	105	120	135	150	165	Sum
1	1.327	1.247	1.064	1.106	1.131	1.068	1.013	0.887	0.964	0.783	0.424	Inf	11.015
1.5	1.327	1.235	1.052	1.092	1.136	1.084	1.024	0.888	0.955	0.801	0.418	Inf	11.011
2	1.322	1.259	1.053	1.069	1.135	1.057	1.015	0.903	0.955	0.823	0.427	Inf	11.017
2.5	1.347	1.227	1.065	1.077	1.137	1.064	1.014	0.889	0.934	0.842	0.530	Inf	11.128
3	1.347	1.254	1.050	1.050	1.124	1.065	1.018	0.898	0.934	0.847	0.487	Inf	11.074
3.5	1.347	1.261	1.061	1.068	1.128	1.035	1.014	0.916	0.937	0.866	0.502	3.636	14.770
4	1.336	1.232	1.028	1.047	1.158	1.049	1.010	0.895	0.933	0.881	0.504	2.308	13.381
4.5	1.324	1.229	1.032	1.087	1.138	1.065	1.017	0.866	0.914	0.897	0.540	1.530	12.641
5	1.331	1.239	1.041	1.105	1.182	1.072	0.998	0.898	0.830	0.910	0.541	1.296	12.443
5.5	1.274	1.237	1.044	1.062	1.105	1.074	1.053	0.898	0.858	0.920	0.546	2.501	13.572
6	1.310	1.238	1.050	1.072	1.159	1.072	1.033	0.882	0.861	0.910	0.514	4.754	15.854
sum	14.592	13.659	11.539	11.837	12.534	11.702	11.209	9.819	10.075	9.480	5.433	16.025	137.905

The smallest damage-ratio in this table is 0.418, which occurs at a crossing angle of 150° and a miss distance of 1.40 meters; and the largest ratio is 4.754, which occurs at 165° and a miss distance of 6.0 meters. Also notice that between crossing angles of 0° and 90° all the ratios are greater than one (1.0) except for a single case ($CA = 90^\circ$ and $MD = 5.0$ meters); and between crossing angles of 105° and 150° , the ratios are generally smaller than one (1.0). The exception occurs at a crossing angle of 165° where the ratios are significantly greater than 1.0 and even infinitely greater due to the occurrence of a low number of impacts or no impacts at all. For this reason excessively high ratios are considered statistically invalid. To facilitate the identification of encounter configuration scenarios with similar levels of total damage-ratios, and subsequently identify encounter configuration scenarios where a specific cylindrical geometry is more lethal than the sphere, a three level damage-ratio criterion summarized in Table 6.25 was used.

Table 6.25. Damage-Ratio Level Criterion.

Total Damage-Ratio Per Encounter Configuration Scenario	Descriptor Cylinder isthan the Sphere	Associated Color
$0 \leq D_{rat} < 1.00$	Less Lethal	
$1.00 \leq D_{rat} < 10.00$	Equally or More Lethal	
$10.00 \leq D_{rat}$ or 0/0 or #/0	Invalid	

To further facilitate the identification of the damage ratios on the tables, each level can be visually identified with a gray-scale based color. Ratios less than one (1.0) are gray-colored and ratios greater than one (1.0) are dark-colored. Occasionally, excessively high damage-ratios are computed at some encounter scenarios. The authors selected a limit of ten (10.0) to differentiate between possible high damage-ratios, those greater than one but less than ten, and invalid ones above ten. Undetermined damage-ratios are also possible, when no spherical impacts are simulated. These cases are also considered statistically invalid, and therefore, no color is associated to them. Each level has an associated descriptor. The criterion is applied to each cell in the total damage-ratio tables per encounter configuration, and the scenarios with similar ratio level are grouped. Tables 6.26 and 6.27 illustrate the distribution of lethality based on levels of damage-ratios throughout the entire encounter configuration range at an early bird time of -0.006 seconds for a cylindrical projectile with L/D 4. Table 6.26 corresponds to deployment without variability in radial ejection velocity and without tumbling effects; and Table 6.27 to cases with 75% variability in the radial ejection velocity and without tumbling effects.

Table 6.26. Damage-Ratio Levels per Encounter Configuration between a Cylindrical Projectile with $L/D = 4$ and a Sphere @ $EBt = -0.006$ sec. Without Tumbling Effects and Without $COV V_{rp}$.

L/D=4.00 Early Bird Time=-0.0060													
MD/CA	0	15	30	45	60	75	90	105	120	135	150	165	Sum
1								0.887	0.992	0.783	0.424	Inf	11.015
1.5								0.887	0.992	0.783	0.424	Inf	11.011
2								0.887	0.992	0.783	0.424	Inf	11.017
2.5								0.887	0.992	0.783	0.424	Inf	11.128
3								0.887	0.992	0.783	0.424	Inf	11.074
3.5								0.887	0.992	0.783	0.424	Inf	14.770
4								0.887	0.992	0.783	0.424	Inf	13.381
4.5								0.887	0.992	0.783	0.424	Inf	12.641
5								0.887	0.992	0.783	0.424	Inf	12.443
5.5								0.887	0.992	0.783	0.424	Inf	13.572
6								0.887	0.992	0.783	0.424	Inf	15.854
sum	14.592	13.659	11.539	11.837	12.534	11.702	11.209	9.819	10.075	9.480	5.433	16.025	137.905

Table 6.27. Damage-Ratio Levels per Encounter Configuration between a Cylindrical Projectile with $L/D = 4$ and a Sphere @ $EBt = -0.006$ sec. Without Tumbling Effects and With a $COVV_p$ of 75%.

L/D=4.00 Early Bird Time=-0.0060															Sum
MD/CA	0	15	30	45	60	75	90	105	120	135	150	165			
1	0.952		0.833	0.693			0.470	0.356	0.250	0.136	0.048		19.136		
1.5							0.490	0.355	0.250	0.136	0.048	10.499	20.912		
2							0.454	0.329	0.200	0.099	0.030	10.730	21.137		
2.5						0.421	0.297	0.190	0.090	0.049	0.010		17.835		
3						0.372			0.100	0.040	0.010		16.525		
3.5							0.305	0.180	0.090	0.040	0.010	10.010	20.865		
4								0.180	0.080	0.040	0.010		19.182		
4.5								0.180	0.080	0.040	0.010	16.254	27.308		
5						0.382	0.280	0.180	0.090	0.040	0.010		16.090		
5.5							0.380	0.280	0.180	0.090	0.010		14.122		
6								0.180	0.080	0.040	0.010		13.207		
sum	14.092	12.722	11.311	11.269	12.650	11.569	10.990	9.551	9.870	9.377	5.647	87.272	206.319		

When variability is included, some ratios slightly vary compared to the cases without variability, shifting the crossing angle range limit from 90° to 75° ; while the ratios at a crossing angle of 165° change substantially. Matrices of damage-ratio levels per encounter configuration scenarios at various deployment conditions were prepared for all cylindrical geometry/sizes. The format of the matrices is exactly the same as the format used for total damage quantification matrices (see Table 6.17). Tables 6.28 through 6.33 depict six matrices for all three cylindrical projectiles, without and with tumbling.

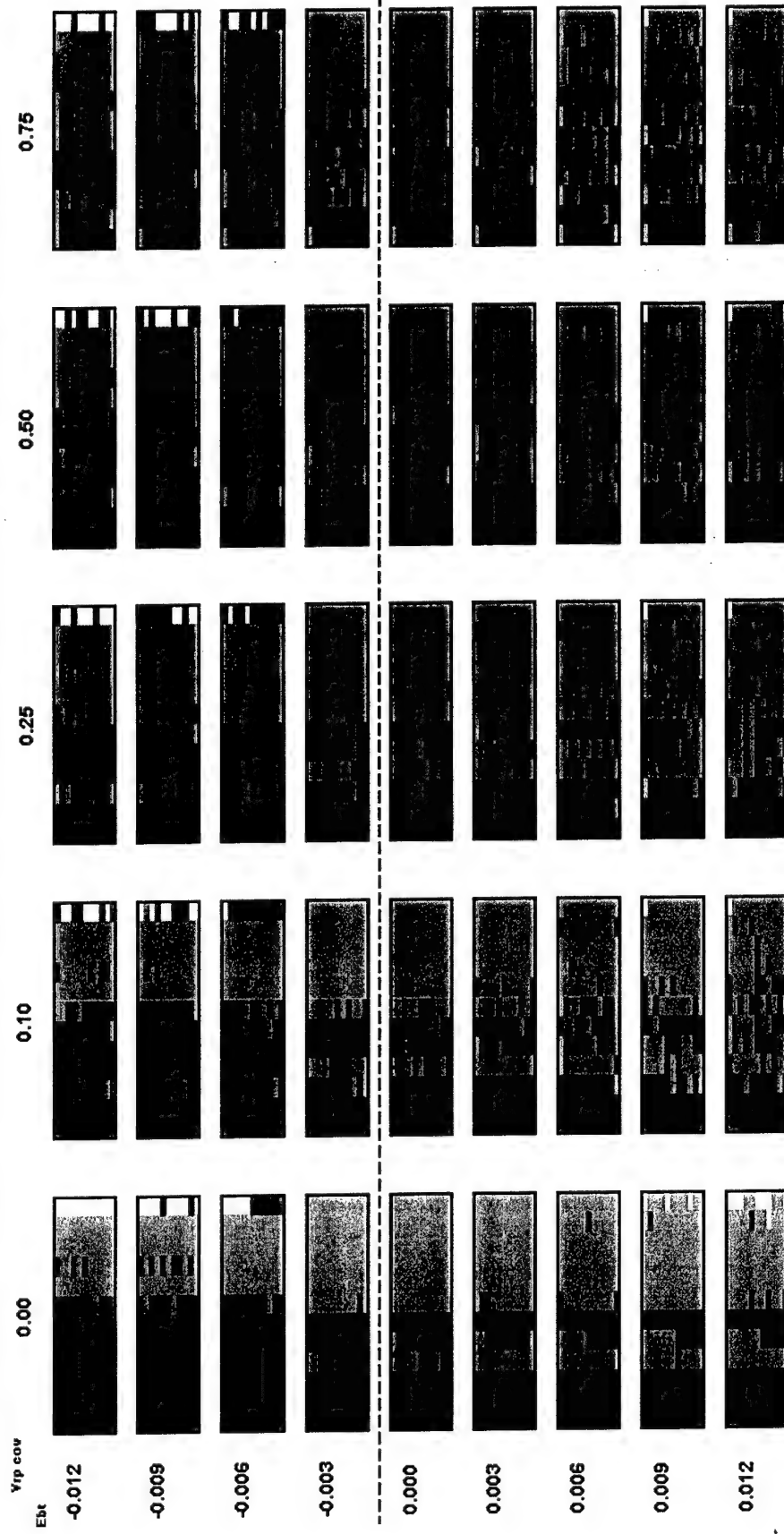
Table 6.28. Matrix of Damage-Ratio Levels for a Cylindrical Projectile with $L/D = 4$ Without Tumbling Effects

Table 6.29. Matrix of Damage-Ratio Levels for a Cylindrical Projectile with $L/D = 2$ Without Tumbling Effects

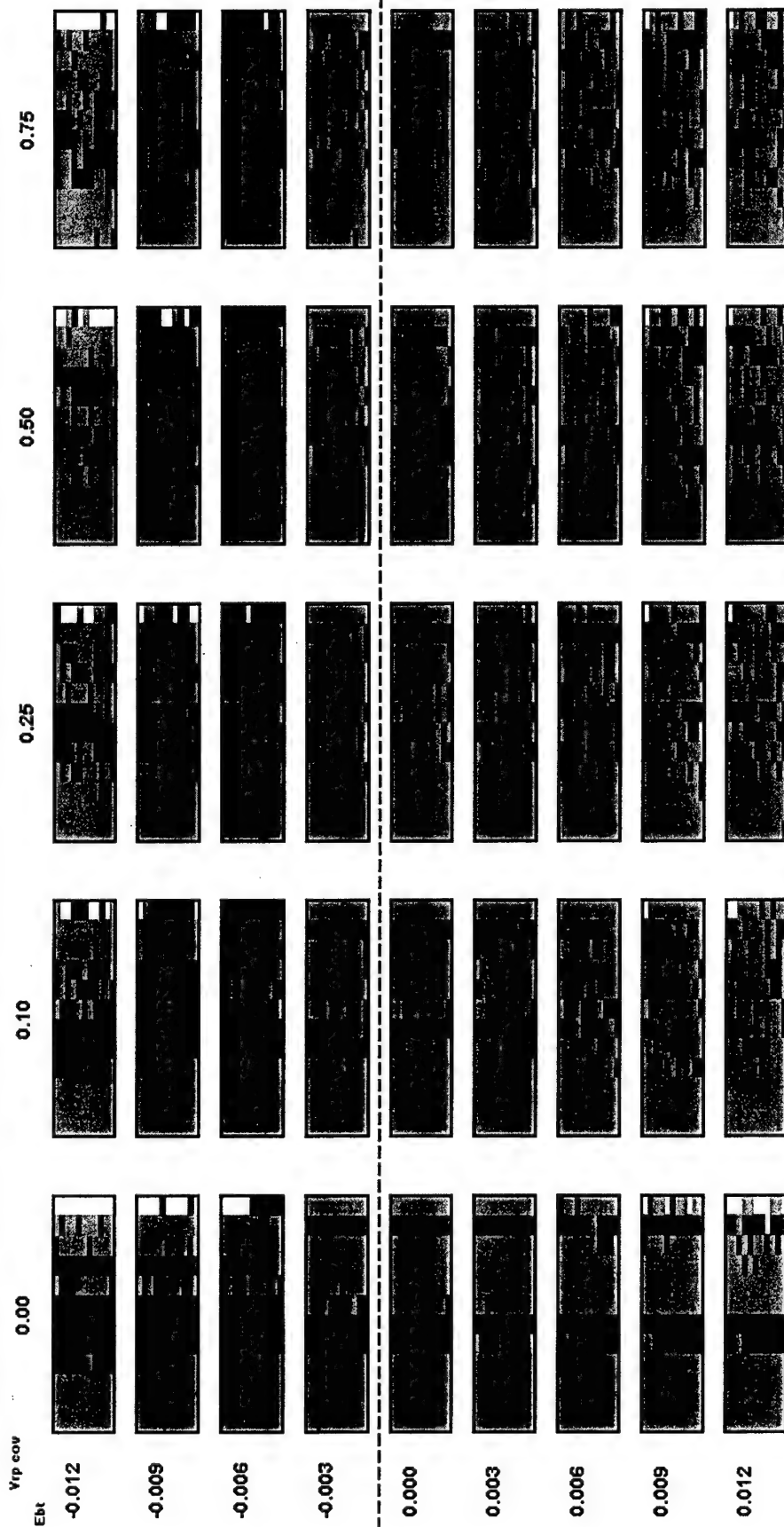


Table 6.30. Matrix of Damage-Ratio Levels for a Cylindrical Projectile with $L/D = 1$ Without Tumbling Effects

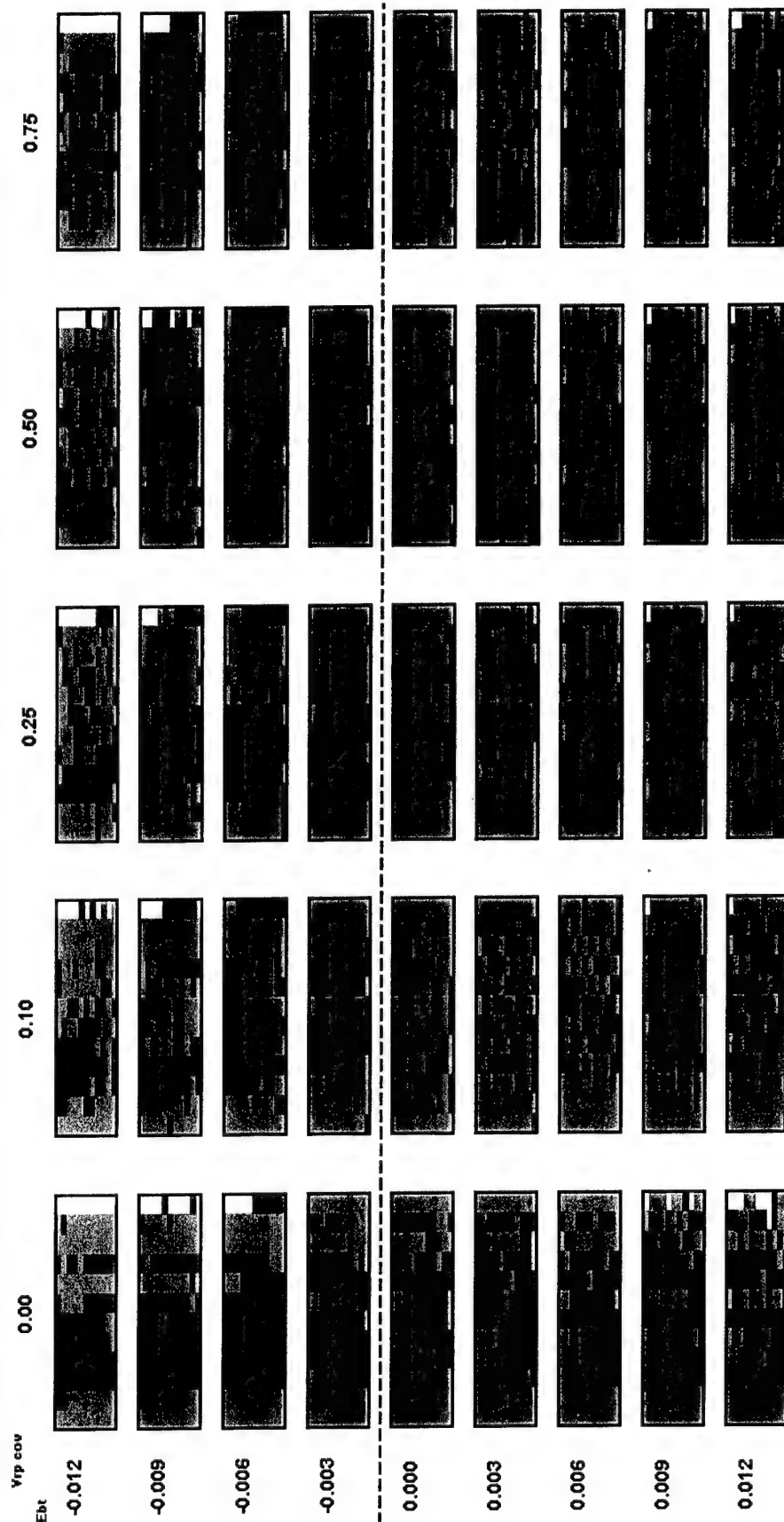


Table 6.31. Matrix of Damage-Ratio Levels for a Cylindrical Projectile with $L/D = 4$ With Tumbling Effects

$V_{ip} \text{ cov}$ Ebt	0.00	0.10	0.25	0.50	0.75
-0.012					
-0.009					
-0.006					
-0.003					
0.000					
0.003					
0.006					
0.009					
0.012					

Table 6.32. Matrix of Damage-Ratio Levels for a Cylindrical Projectile with $L/D = 2$ With Tumbling Effects

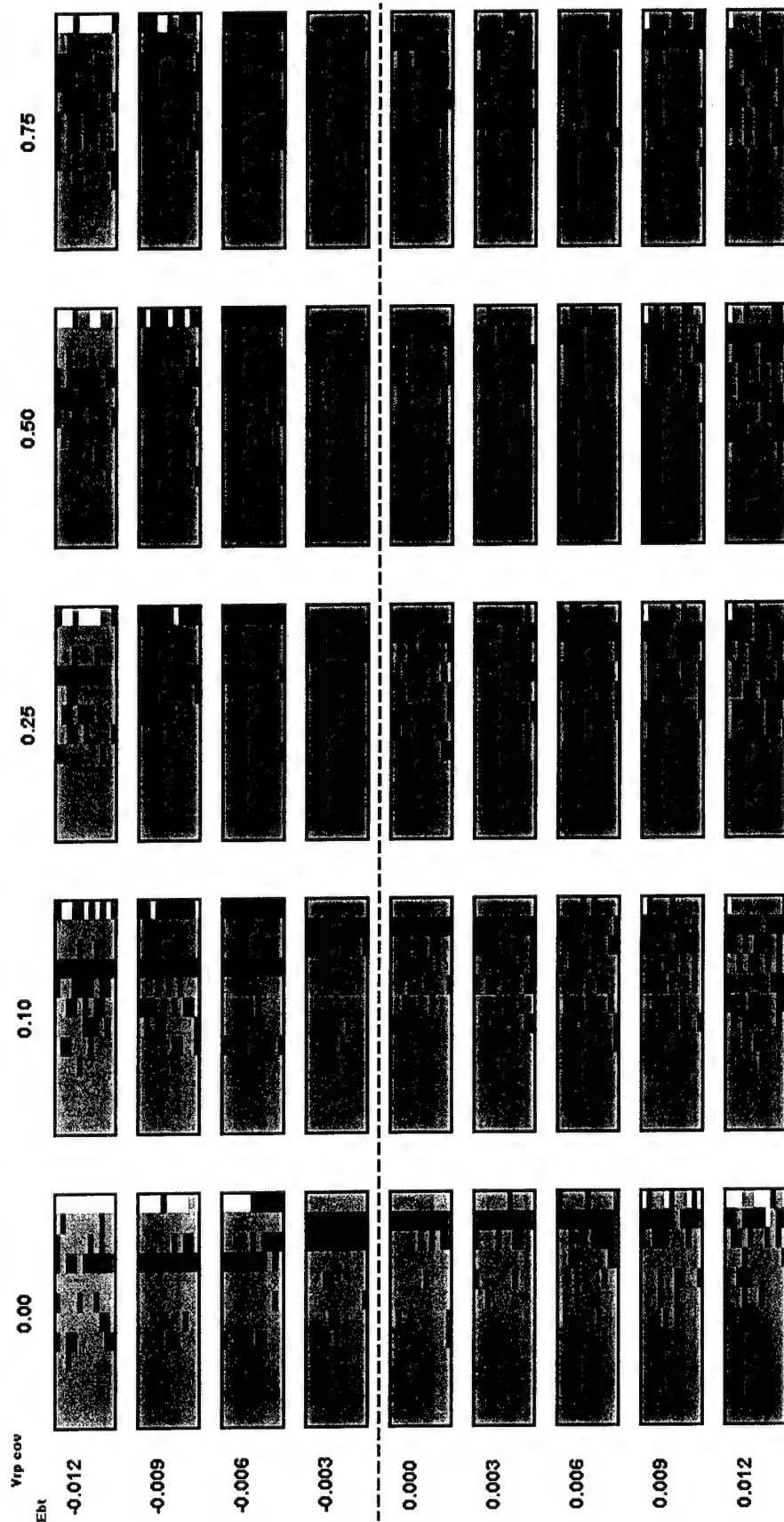
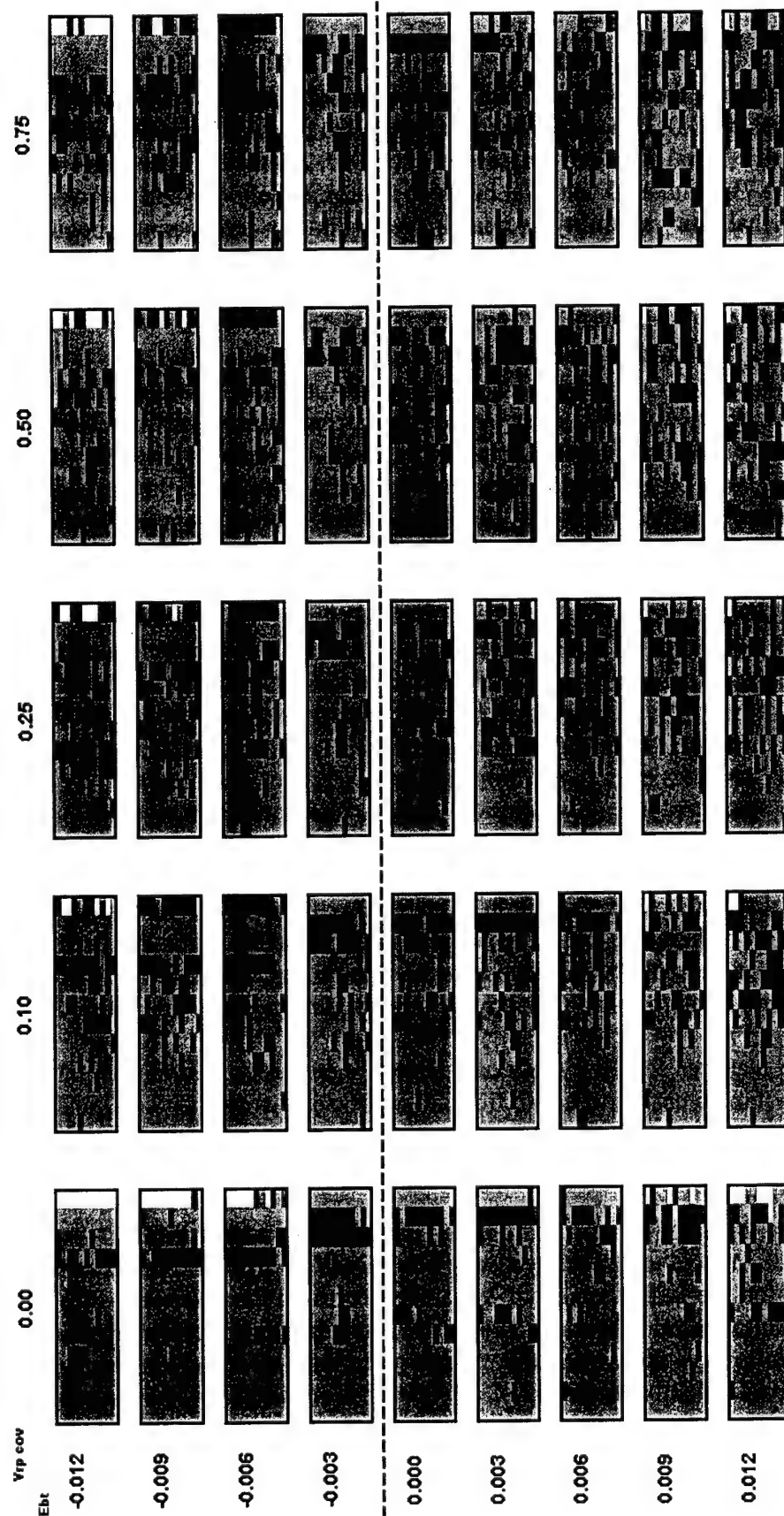


Table 6.33. Matrix of Damage-Ratio Levels for a Cylindrical Projectile with $L/D = 1$ With Tumbling Effects



The matrix for a cylinder with $L/D = 4$ without tumbling shows that for the early bird scenarios of -0.012 to -0.006 sec. without radial ejection variability, the cylinders are generally more lethal for a crossing angle up to 90° . Afterwards the crossing angle range is reduced to 75° with a 30° interval between approximately 45° and 60° where the spheres are more lethal. As variability is added, the cylinder's lethal range begins to slightly dissipate throughout the crossing angle range for all early bird scenarios, however, it seems that cylinders of $L/D = 4$ are always more lethal than spheres at small crossing angles approximately between 0° and 30° . The cylinders appear to be more lethal at a crossing angle of 165° for a wide range of miss distance scenarios.

The matrix for a cylinder $L/D = 2$ without tumbling shows that for the early bird scenarios of -0.003 to 0.012 sec. without radial ejection variability, the cylinders are generally more lethal within a crossing angle range between 60° and 90° , as well as for 150° . For the early bird scenarios between -0.012 and -0.006 sec. the crossing angle range is approximately within 45° and 120° except for a few scenarios around 105° . As variability is added the cylinder's lethal range begins to slightly dissipate throughout the crossing angle range for all early bird scenarios.

The matrix for a cylinder $L/D = 1$ without tumbling shows that for the early bird scenarios of -0.012 to 0.003 sec. without radial ejection variability, the cylinders are generally more lethal within a crossing angle range between 30° and 90° increasing to 120° . For the early bird scenarios beyond -0.003 sec. the cylinder's lethality starts dissipating throughout the crossing angle range. As variability is added the cylinder's lethal range dissipates even more throughout all early bird scenarios.

The matrices for all cylindrical shapes under tumbling effects show that the sphere is consistently more lethal than the cylinder of L/D of 4 throughout most of the encounter configuration scenarios including radial ejection variability. Similar patterns are observed for the cylinders of $L/D = 1$ and 2, except for a crossing angle range around 135° and 165° where the cylinders appear as more lethal for a few scenarios. These scenarios are more realistic than those without tumbling. Therefore, it can be concluded that the sphere is more lethal than any cylinder geometry/size under various deployment conditions.

The matrices for all cylindrical shapes, regardless of tumbling conditions, show that at early-bird times between -0.012 and -0.006 sec. as well as 0.009 and 0.012 sec. at a crossing angle of 165° , a number of miss distance scenarios, if not all, are invalid either because no impacts occurred or the damage ratio exceeds ten.

6.4 Total Damage Quantification per Impact Characterization

Total damage to the warhead was also classified from the impact characterization standpoint for the entire range of encounter configuration scenarios. Another set of damage quantification tables per projectile geometry/size/deployment conditions were generated following the same table format used for impact quantification, having the relative impact velocity as first level of classification, and then showing the variation in the total damage per spatial orientation angle range and strike angle range. For reference purposes, the damage quantification tables presented below correspond to an impact

velocity range of 0.615 to 0.9225 km/s, same impact configuration parameter under which the impact quantification tables were explained. Tables 6.34 through 6.36 illustrate the total damage, for the different projectile geometry/sizes, namely cylindrical projectiles with L/D of 4, 2 and 1, including the spherical projectile. These total damages were obtained from the scenarios without tumbling effects and without variability in radial ejection velocity. The total damage per $(\phi - \alpha)$ range scenario as well as the totals per strike angle range and per impact velocity range varies between cylindrical shapes and the sphere. These differences are due to the different damage indices (SIDIs) associated to each individual impact configuration. At this velocity range, it can be observed the sphere generates slightly more damage than the cylinder L/D of 4; however, smaller cylinders of L/D of 2 and 1 generate slightly more damage than the sphere. Projectiles impacting at a strike angle range (ϕ) between 22.5° and 37.5° generate the largest damage. Cylindrical tail impacts generate about twice as much more damage as tip impacts do. The most damage is generated when the cylinder orientation (α) is between -22.5° and -37.5° . The total damage distribution for other velocity ranges and other geometry/sizes can be explained in a similar fashion. Conversely, Tables 6.37 through 6.39 depict the distribution of total damage for cylindrical projectiles L/D of 4, 2 and 1 per relative impact velocity ranges, respectively.

The total damage per velocity range increases at higher impact velocity magnitudes. When comparing the total damage per velocity range between the sphere and the three cylindrical sizes, usually at velocities lower than 0.615 km/s the sphere generates more damage. In the middle velocity range up to 1.5375 km/s, the sphere is as damaging as the cylinders. When the velocity increases between 1.5375 and 1.8450 km/s the cylinders are slightly more lethal than the sphere. At higher velocities the cylinder of L/D of 4 generates more damage than the other geometry/sizes; however, the sphere generates more damage than the cylinders of L/D of 2 and 1.

Table 6.38. Total Damage Quantification per Impact Configuration for Cylindrical Projectiles $L/D = 2$

L/D=2.00		Velocity= 0.0000(km/s)- 0.3075(km/s)		Sphere		SumCyl	
phiAlpha	80.5>=a>82.5	82.5>=a>87.5	87.5>=a>90.0	0.0000	0.0000	0.0000	0.0000
0.0<phi<7.5	0	0	0	0	0	0	0
7.5<phi<22.5	0	0	0	0	0	0	0
22.5<phi<37.5	0	0	0	0	0	0	0
37.5<phi<52.5	0	0	0	0	0	0	0
52.5<phi<67.5	0	0	0	0	0	0	0
67.5<phi<90.0	0	0	0	0	0	0	0
sum rows	0.377	0.587	0.587	0.377	0.587	0.587	0.587
L/D=2.00		Velocity= 0.3075(km/s)- 0.6150(km/s)		Sphere		SumCyl	
phiAlpha	80.5>=a>82.5	82.5>=a>87.5	87.5>=a>90.0	0.0000	0.0000	0.0000	0.0000
0.0<phi<7.5	0	0	0	0	0	0	0
7.5<phi<22.5	0	0	0	0	0	0	0
22.5<phi<37.5	0	0	0	0	0	0	0
37.5<phi<52.5	0	0	0	0	0	0	0
52.5<phi<67.5	0	0	0	0	0	0	0
67.5<phi<90.0	0	0	0	0	0	0	0
sum rows	0.377	0.587	0.587	0.377	0.587	0.587	0.587
L/D=2.00		Velocity= 0.6150(km/s)- 0.9225(km/s)		Sphere		SumCyl	
phiAlpha	80.5>=a>82.5	82.5>=a>87.5	87.5>=a>90.0	0.0000	0.0000	0.0000	0.0000
0.0<phi<7.5	0	0	0	0	0	0	0
7.5<phi<22.5	0	0	0	0	0	0	0
22.5<phi<37.5	0	0	0	0	0	0	0
37.5<phi<52.5	0	0	0	0	0	0	0
52.5<phi<67.5	0	0	0	0	0	0	0
67.5<phi<90.0	0	0	0	0	0	0	0
sum rows	0.377	0.587	0.587	0.377	0.587	0.587	0.587
L/D=2.00		Velocity= 0.9225(km/s)- 1.2300(km/s)		Sphere		SumCyl	
phiAlpha	80.5>=a>82.5	82.5>=a>87.5	87.5>=a>90.0	0.0000	0.0000	0.0000	0.0000
0.0<phi<7.5	0	0	0	0	0	0	0
7.5<phi<22.5	0	0	0	0	0	0	0
22.5<phi<37.5	0	0	0	0	0	0	0
37.5<phi<52.5	0	0	0	0	0	0	0
52.5<phi<67.5	0	0	0	0	0	0	0
67.5<phi<90.0	0	0	0	0	0	0	0
sum rows	0.377	0.587	0.587	0.377	0.587	0.587	0.587
L/D=2.00		Velocity= 1.2300(km/s)- 1.5375(km/s)		Sphere		SumCyl	
phiAlpha	80.5>=a>82.5	82.5>=a>87.5	87.5>=a>90.0	0.0000	0.0000	0.0000	0.0000
0.0<phi<7.5	0	0	0	0	0	0	0
7.5<phi<22.5	0	0	0	0	0	0	0
22.5<phi<37.5	0	0	0	0	0	0	0
37.5<phi<52.5	0	0	0	0	0	0	0
52.5<phi<67.5	0	0	0	0	0	0	0
67.5<phi<90.0	0	0	0	0	0	0	0
sum rows	0.377	0.587	0.587	0.377	0.587	0.587	0.587
L/D=2.00		Velocity= 1.5375(km/s)- 1.8450(km/s)		Sphere		SumCyl	
phiAlpha	80.5>=a>82.5	82.5>=a>87.5	87.5>=a>90.0	0.0000	0.0000	0.0000	0.0000
0.0<phi<7.5	0	0	0	0	0	0	0
7.5<phi<22.5	0	0	0	0	0	0	0
22.5<phi<37.5	0	0	0	0	0	0	0
37.5<phi<52.5	0	0	0	0	0	0	0
52.5<phi<67.5	0	0	0	0	0	0	0
67.5<phi<90.0	0	0	0	0	0	0	0
sum rows	0.377	0.587	0.587	0.377	0.587	0.587	0.587
L/D=2.00		Velocity= 1.8450(km/s)- 2.1525(km/s)		Sphere		SumCyl	
phiAlpha	80.5>=a>82.5	82.5>=a>87.5	87.5>=a>90.0	0.0000	0.0000	0.0000	0.0000
0.0<phi<7.5	0	0	0	0	0	0	0
7.5<phi<22.5	0	0	0	0	0	0	0
22.5<phi<37.5	0	0	0	0	0	0	0
37.5<phi<52.5	0	0	0	0	0	0	0
52.5<phi<67.5	0	0	0	0	0	0	0
67.5<phi<90.0	0	0	0	0	0	0	0
sum rows	0.377	0.587	0.587	0.377	0.587	0.587	0.587

Tail impacts

Tip impacts

Table 6.39. Total Damage Quantification per Impact Configuration for Cylindrical Projectiles $L/D = 1$

L/D=1.00		0.3075(km/s)		0.6150(km/s)		1.2300(km/s)		1.5375(km/s)		1.8450(km/s)	
phi/alpha		90° => a=82.5		90° => a=82.5		90° => a=82.5		90° => a=82.5		90° => a=82.5	
0.0<phi<7.5	0	0	0.125	0.186	0.092	0.110	0.092	0.414	0.176	0.118	0
7.5<phi<22.5	0	0	0.480	0.447	1.240	0.708	0.247	0.241	0.008	0.259	0
22.5<phi<37.5	0	0	0.228	0.427	1.146	0.907	0.248	0.072	0.230	0.191	0
37.5<phi<52.5	0	0	0.021	0.385	0.710	0.286	0.285	0.444	0	0.558	0.022
52.5<phi<67.5	0	0.053	0.040	0.044	0.044	0.044	0.044	0	0	0.097	0.029
67.5<phi<90.0	0.050	0.403	0.040	0.040	0.040	0.040	0.040	0	0	0.487	0.114
sum rows			1.203	2.255	2.423	2.586	1.333	0.872	0.409	0.744	0.259
Sphere		0.000		0.000		0.000		0.000		0.000	
SumCyl		0.000		0.000		0.000		0.000		0.000	
SumCyl		0.000		0.000		0.000		0.000		0.000	
SumCyl		0.000		0.000		0.000		0.000		0.000	
SumCyl		0.000		0.000		0.000		0.000		0.000	
SumCyl		0.000		0.000		0.000		0.000		0.000	
SumCyl		0.000		0.000		0.000		0.000		0.000	
SumCyl		0.000		0.000		0.000		0.000		0.000	
SumCyl		0.000		0.000		0.000		0.000		0.000	
SumCyl		0.000		0.000		0.000		0.000		0.000	
SumCyl		0.000		0.000		0.000		0.000		0.000	
SumCyl		0.000		0.000		0.000		0.000		0.000	
SumCyl		0.000		0.000		0.000		0.000		0.000	
SumCyl		0.000		0.000		0.000		0.000		0.000	
SumCyl		0.000		0.000		0.000		0.000		0.000	
SumCyl		0.000		0.000		0.000		0.000		0.000	
SumCyl		0.000		0.000		0.000		0.000		0.000	
SumCyl		0.000		0.000		0.000		0.000		0.000	
SumCyl		0.000		0.000		0.000		0.000		0.000	
SumCyl		0.000		0.000		0.000		0.000		0.000	
SumCyl		0.000		0.000		0.000		0.000		0.000	
SumCyl		0.000		0.000		0.000		0.000		0.000	
SumCyl		0.000		0.000		0.000		0.000		0.000	
SumCyl		0.000		0.000		0.000		0.000		0.000	
SumCyl		0.000		0.000		0.000		0.000		0.000	
SumCyl		0.000		0.000		0.000		0.000		0.000	
SumCyl		0.000		0.000		0.000		0.000		0.000	
SumCyl		0.000		0.000		0.000		0.000		0.000	
SumCyl		0.000		0.000		0.000		0.000		0.000	
SumCyl		0.000		0.000		0.000		0.000		0.000	
SumCyl		0.000		0.000		0.000		0.000		0.000	
SumCyl		0.000		0.000		0.000		0.000		0.000	
SumCyl		0.000		0.000		0.000		0.000		0.000	
SumCyl		0.000		0.000		0.000		0.000		0.000	
SumCyl		0.000		0.000		0.000		0.000		0.000	
SumCyl		0.000		0.000		0.000		0.000		0.000	
SumCyl		0.000		0.000		0.000		0.000		0.000	
SumCyl		0.000		0.000		0.000		0.000		0.000	
SumCyl		0.000		0.000		0.000		0.000		0.000	
SumCyl		0.000		0.000		0.000		0.000		0.000	
SumCyl		0.000		0.000		0.000		0.000		0.000	
SumCyl		0.000		0.000		0.000		0.000		0.000	
SumCyl		0.000		0.000		0.000		0.000		0.000	
SumCyl		0.000		0.000		0.000		0.000		0.000	
SumCyl		0.000		0.000		0.000		0.000		0.000	
SumCyl		0.000		0.000		0.000		0.000		0.000	
SumCyl		0.000		0.000		0.000		0.000		0.000	
SumCyl		0.000		0.000		0.000		0.000		0.000	
SumCyl		0.000		0.000		0.000		0.000		0.000	
SumCyl		0.000		0.000		0.000		0.000		0.000	
SumCyl		0.000		0.000		0.000		0.000		0.000	
SumCyl		0.000		0.000		0.000		0.000		0.000	
SumCyl		0.000		0.000		0.000		0.000		0.000	
SumCyl		0.000		0.000		0.000		0.000		0.000	
SumCyl		0.000		0.000		0.000		0.000		0.000	
SumCyl		0.000		0.000		0.000		0.000		0.000	
SumCyl		0.000		0.000		0.000		0.000		0.000	
SumCyl		0.000		0.000		0.000		0.000		0.000	
SumCyl		0.000		0.000		0.000		0.000		0.000	
SumCyl		0.000		0.000		0.000		0.000		0.000	
SumCyl		0.000		0.000		0.000		0.000		0.000	
SumCyl		0.000		0.000		0.000		0.000		0.000	
SumCyl		0.000		0.000		0.000		0.000		0.000	
SumCyl		0.000		0.000		0.000		0.000		0.000	
SumCyl		0.000		0.000		0.000		0.000		0.000	
SumCyl		0.000		0.000		0.000		0.000		0.000	
SumCyl		0.000		0.000		0.000		0.000		0.000	
SumCyl		0.000		0.000		0.000		0.000		0.000	
SumCyl		0.000		0.000		0.000		0.000		0.000	
SumCyl		0.000		0.000		0.000		0.000		0.000	
SumCyl		0.000		0.000		0.000		0.000		0.000	
SumCyl		0.000		0.000		0.000		0.000		0.000	
SumCyl		0.000		0.000		0.000		0.000		0.000	
SumCyl		0.000		0.000		0.000		0.000		0.000	
SumCyl		0.000		0.000		0.000		0.000		0.000	
SumCyl		0.000		0.000		0.000		0.000		0.000	
SumCyl		0.000		0.000		0.000		0.000		0.000	
SumCyl		0.000		0.000		0.000		0.000		0.000	
SumCyl		0.000		0.000		0.000		0.000		0.000	
SumCyl		0.000		0.000		0.000		0.000		0.000	
SumCyl		0.000		0.000		0.000					

The damage ratio between tip impacts and tail impacts varies throughout the velocity range for all cylindrical sizes. For the lowest velocity range (0 – 0.3075 km/s) tip impacts damage twice as much more than tail impacts. For the second and third lowest velocity range (0.3075 – 0.6150 km/s, 0.6150 – 0.9225 km/s) the ratio inverts. For the fourth velocity range (0.9225 – 1.23 km/s) tail impacts generate 25 to 46% more damage than tip impacts. For the fifth velocity range (1.23 – 1.53 km/s) tip impacts generate between four and five times more damage than tail impacts. For the remaining high velocity ranges, tip impacts generate most of the damage.

Similar tables were generated for the cases when tumbling effects were added, as well as different scenarios of radial ejection velocity variability. These tables are not included in this report. The strike angle range under which the projectiles generate the most damage seems correlated with the magnitude of the impact velocity. The lower the velocity range the steeper the strike angle range. For low velocities between 0 and 0.6150 km/s the strike angle range varies between 7.5° and 22.5°. For the midrange velocities between 0.615 and 1.23 km/s the strike angle range varies between 22.5° and 37.5°. When the velocity varies between 1.23 and 1.5375 km/s the strike angle range varies between 37.5° and 52.5°. As the velocity increases to 1.845 km/s, the impacts strike between 52.5° and 67.5°. At higher velocities the projectiles impact at shallow strike angles between 67.5° and 90°. These tendencies are observed regardless of tumbling effects and radial ejection velocity variability.

Impact configuration regions with similar total damage levels were identified after applying the five-level impact frequency criterion described in Table 3.10 to each cell in the tables. Tables 6.40 through 6.45 depict matrices of total damage quantification per impact configuration for all three cylindrical projectiles. The top matrices correspond to the cases when tumbling is not considered and the bottom matrices when tumbling is considered for cylinders of L/D 4, 2 and 1. These matrices follow the same format as the matrices for impact quantification. The matrices of total damage without tumbling effects show the diagonal pattern of higher damage levels (dark color regions) in every cell table over the range of radial ejection variability. The range of $(\phi - \alpha)$ scenarios is practically the same; however, minor differences are observed in the level of damage, since these totals correspond to the average of 30 simulations. When comparing to the matrices with tumbling, a substantial change in the range and number of $(\phi - \alpha)$ scenarios with similar damage level is observed. When tumbling is considered, a wider range of $(\phi - \alpha)$ scenarios is observed, covering the entire range of orientation angles (α) for the same range of strike angles (ϕ) observed in the tables without tumbling.

Table 6.40. Total Damage Quantification Matrix for a Cylindrical Projectile with $L/D = 4$ Without Tumbling Effects per Impact Configuration

Vel Yrp cov	0.00	0.10	0.25	0.50	0.75
0.0000 -					
0.3075 -					
0.6150 -					
0.9225 -					
1.2300 -					
1.5375 -					
1.8450 -					

Table 6.41. Total Damage Quantification Matrix for a Cylindrical Projectile with $L/D = 4$ With Tumbling Effects per Impact Configuration

Vel Yrp cov	0.00	0.10	0.25	0.50	0.75
0.0000 -					
0.3075 -					
0.6150 -					
0.9225 -					
1.2300 -					
1.5375 -					
1.8450 -					

Table 6.42. Total Damage Quantification Matrix for a Cylindrical Projectile with $L/D = 2$ Without Tumbling Effects per Impact Configuration

Vel Vip cov	0.00	0.10	0.25	0.50	0.75
0.0000 - 0.3075					
0.3075 - 0.6150					
0.6150 - 0.9225					
0.9225 - 1.2300					
1.2300 - 1.5375					
1.5375 - 1.8450					
1.8450 -					

Table 6.43. Total Damage Quantification Matrix for a Cylindrical Projectile with $L/D = 2$ With Tumbling Effects per Impact Configuration

Vel Vip cov	0.00	0.10	0.25	0.50	0.75
0.0000 - 0.3075					
0.3075 - 0.6150					
0.6150 - 0.9225					
0.9225 - 1.2300					
1.2300 - 1.5375					
1.5375 - 1.8450					
1.8450 -					

Table 6.44. Total Damage Quantification Matrix for a Cylindrical Projectile with $L/D = 1$ Without Tumbling Effects per Impact Configuration

Vip cov Vel	0.00	0.10	0.25	0.50	0.75
0.0000 - 0.3075					
0.3075 - 0.6150					
0.6150 - 0.9225					
0.9225 - 1.2300					
1.2300 - 1.5375					
1.5375 - 1.8450					
1.8450 -					

Table 6.45. Total Damage Quantification Matrix for a Cylindrical Projectile with $L/D = 1$ With Tumbling Effects per Impact Configuration

Vip cov Vel	0.00	0.10	0.25	0.50	0.75
0.0000 - 0.3075					
0.3075 - 0.6150					
0.6150 - 0.9225					
0.9225 - 1.2300					
1.2300 - 1.5375					
1.5375 - 1.8450					
1.8450 -					

6.5 Damage Analysis per Impact Characterization

From the impact characterization standpoint, in general, number of impacts as well as total damage increase as the impact velocity magnitude increases. The strike angle range under which the projectiles generate the largest damage seems correlated with the magnitude of the impact velocity. The lower the velocity range the steeper the strike angle range. For low velocities between 0 and 0.6150 km/s the strike angle range varies between 7.5° and 22.5° . For the midrange velocities between 0.615 and 1.23 km/s the strike angle range varies between 22.5° and 37.5° . When the velocity varies between 1.23 and 1.5375 km/s the strike angle range varies between 37.5° and 52.5° . As the velocity increases to 1.845 km/s, the impacts strike between 52.5° and 67.5° . At higher velocities the projectiles impact at shallow strike angles between 67.5° and 90° . These tendencies are observed regardless of tumbling effects and radial ejection velocity variability. Figure 6.5 shows the most frequent strike angle ranges at which projectiles impact under a certain relative impact velocity range.

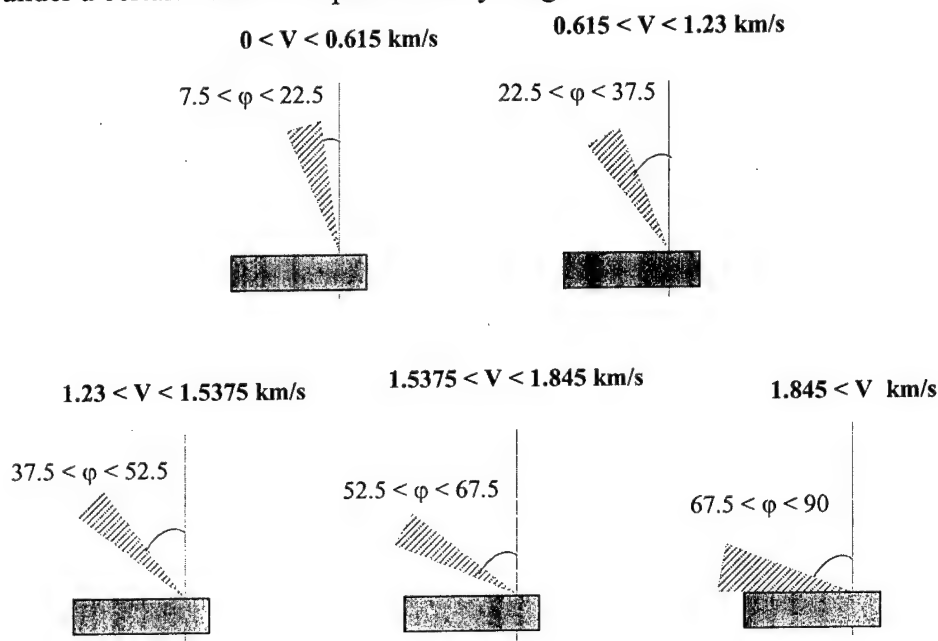


Figure 6.5. Most Frequent Strike Angle Ranges Under a Certain Impact Velocity Range.

Generally speaking, projectiles impact at steeper strike angles as the velocity reduces. As observed in figures 3.14 and 3.15 the impact velocity magnitude is inversely correlated to the crossing angle between the flight paths of the missiles, regardless of miss distance, early bird time, projectile geometry/size and deployment conditions. Cross referencing the later with total damage quantification per encounter configuration, it can be concluded that the largest damage is generated by shallow impacts for both cylindrical and spherical projectiles, occurring at low crossing angles.

In the case of cylindrical projectiles, as the relative impact velocity decreases the ratio of tip to tail impacts rapidly decreases, thus increasing the yaw angle range. When cylinders impact at low velocities with larger yaw angles, the total damage inflicted also decreases. These patterns are highly dependant on the relative speed between the missiles as well as the geometric shape of the TBM. Different patterns may be observed if either the missile speeds are different or the geometric shape of the TBM warhead section changes.

6.6 Damage Analysis per Near-Miss Encounter Configuration parameters

A damage analysis is presented to investigate the effects of each Near-Miss Encounter variable (*EBt*, *CA*, and *MD*).

6.6.1 Early Bird Time

Early bird time directly affects the frequency of impacts, thus the total damage inflicted to the TBM warhead. In late bird scenarios (-0.012 to -0.003 sec.) when the TBM warhead is after the point of closest approach (-0.003 sec.) to the EKV's nose, the frequency of impacts is much higher than in early bird scenarios (0.000 to -0.012 sec.), when the EKV missile flies in front of the TBM before the point of closest approach. The largest encounter configuration scenario range with high impact frequencies occurs at a late bird of -0.003 sec. Close to half of the entire encounter configuration range has high impact frequencies. This is because this late bird time closely resembles a direct hit to the TBM warhead. As the early bird time increases (between 0.003 to 0.012 sec.) the regions of very low frequency or no impact increase, and the high impact frequency regions are concentrated around a crossing angle of 0° and miss distance of 1.0 meter. Thus, larger levels of damage are observed at late bird scenarios (-0.012 to 0.000 sec.) with the highest occurring at -0.003 sec. Conversely, low damage levels are developed at early bird scenarios (0.003 to 0.0012 sec.). In late bird scenarios the variation in damage as miss distance increases is evident; however, in early bird scenarios the damage levels are very similar regardless of miss distance. It should be noted that since the number of impacts is very low in a large portion of most early bird scenarios, the observed damage levels may be treated as statistically invalid.

6.6.2 Crossing Angle and Miss Distance

Both impact frequencies and the total damage distributions resemble a shifted parabolic pattern as the crossing angle increases from 0° to 165° . The peaks of these parabolic tendencies shift towards larger crossing angles as early bird times range from late birds to early bird scenarios. At late bird scenarios the peak occurs between 0° and 45° . At times -0.003 and 0.000 sec. the peaks occur around 90° or 75° , respectively (these plots are not included in this report). In most early bird scenarios the maximum damage occurs at 0° followed by a substantial drop at 15° ; thereon, a flatter parabolic pattern develops as the crossing angle increases and the peaks occur at crossing angles between 45° and 60° . At -0.003 sec. the number of impacts is high at a crossing angle of 165° since the EKV is almost traveling along with the TBM for a longer period of time, and

therefore, when the EKV warhead is deployed, a fairly high number of projectiles impact the TBM warhead, even at large miss distances. As the miss distance increases from 1.0 to 6.0 meters the parabolic pattern flattens and the peaks also shifts towards larger crossing angles. The minimum impact frequencies and damage levels always occur at a crossing angle of 165° when the EKV is in pursuit course with the TBM. Again, in these cases the estimated damage levels may be treated as statistically invalid.

To further explain the total damage tendencies observed in the encounter configuration tables, six encounter scenarios without tumbling effects and without radial ejection velocity variability at an *EBt* of -0.006 sec. for a cylinder *L/D* of 4 were selected. The selected encounter scenarios are shown in Table 6.46 as follows.

Table 6.46. Selected Encounter Scenarios for Damage Tendencies

Scenario	Crossing Angle (degrees)	Miss Distance (meters)
1	0	1.0
2	45	1.0
3	90	1.0
4	90	2.0
5	90	6.0
6	165	1.0

Impact and the total damage quantification tables per impact configuration were generated for all six scenarios. For space optimization and paper reduction purposes, only those impact configuration scenarios that contain data are presented. Tables 6.47 through 6.52 list the impact configuration scenarios that contain the entire distribution of impacts of each selected encounter scenario. Tables 6.47 to 6.50 depict the impact distributions for a miss distance of 1.0 meter as the crossing angle increases from 0° to 45° to 90° and ends in 165° . Tables 6.51 and 6.52 complement the distribution of impacts for a crossing angle of 90° as the miss distance increases to 2.0 and 6.0 meters. Note that the total number of cylindrical impacts summarized under each of these tables matches the frequencies presented in table 3.7 under the corresponding encounter scenarios.

Table 6.49. Impact Quantification per Impact Configuration for Encounter Scenario 3 Without Tumbling Effects.

[illegible]

Table 6.50. Impact Quantification per Impact Configuration for Encounter Scenario 4 Without Tumbling Effects.

EBI=-0.0060		CA=165	MD=1.0	Velocity=0.0000 (km/s>=0.3075(km/s)														SumCyl
L/ID=4.00		90>=a>=82.5	82.5>=a>=67.5	67.5>=a>=52.5	52.5>=a>=37.5	37.5>=a>=22.5	22.5>=a>=7.5	7.5>=a>=-7.5	(-37.5>a>=-22.5	(-22.5>a>=-37.5	(-37.5>a>=-52.5	(-52.5>a>=-67.5	(-67.5>a>=-82.5	(-82.5>a>=-90	Sphere			
0.0<=phi<7.5		0	0	0	0	0	0	0	0	0	0	0	0	0	0	0		
7.5<=phi<22.5		0	0	0	0	0	0	0	0	0	0	0	0	0	0	0		
22.5<=phi<37.5		0	0	0	0	0	0	0	0	0	0	0	0	0	0	0		
37.5<=phi<52.5		0	0	0	0	0	0	0	0	0	0	0	0	0	0	0		
52.5<=phi<67.5		0	0	0	0	0	0	0	0	0	0	0	0	0	0	0		
67.5<=phi<90.0		0	0	0	0	0	0	0	0	0	0	0	0	0	0	0		
sum		0	6	0	0	0	0	0	0	0	0	0	0	0	6	6		
Total Impacts for Cylinder EC 6																		
Total Impacts for Sphere EC 6																		

[illegible][illegible]

Table 6.52. Impact Quantification per Impact Configuration for Encounter Scenario 6 Without Tumbling Effects.

[illegible][illegible]

Total Impacts	for Cylinder EC	38
Total Impacts	for Sphere EC	38

The distribution in impact velocity, strike angle and orientation angle for cylindrical projectiles are a function of a number of factors. The resultant velocity components of each projectile include the relative speed of the missiles, and the individual radial ejection velocities ($V_{rp} \leq 0.309$ km/s.). The missiles relative speed is also dependant on the crossing angle, and the radial ejection velocities are also a function of the position of each projectile in the EKV warhead arrangement. The variations in the strike angles of the impacts are due to the variations in radial deployment velocity and any variation in the target' surface slope. For cylindrical projectiles, the location where they hit on the TBM surface, and whether they hit with their tip or their tail, will contribute to variations in the impact orientation angle.

Table 6.47 shows that the 400 impacts generated in the crossing angle-miss distance scenario (*CA-MD*) of 0° -1.0 m. are tip impacts distributed within a very narrow range of impact velocities and $(\phi-\alpha)$ scenarios that are contained in a single $(\phi-\alpha)$ cell in the highest velocity range (1.845 km/s - ...) striking at shallow angles (67.5° to 90°). Table 6.48 shows that as the crossing angle increases to 45° at the same miss distance, the number of impacts increases to 502, mostly tip impacts; however they are distributed within a larger range of $(\phi-\alpha)$ scenarios than in 0° within a lower velocity range (1.5375 to 1.845 km/s). Most projectiles impact within 52.5° and 67.5° strike angles and shallower angles. Only very few of them impact with their tail and others impact at a higher velocity. Table 6.49 shows that as the crossing angle reaches 90° at the same miss distance, the number of impacts drops to 278, most of them striking at an even lower velocity range (1.23 to 1.5375 km/s) within an even larger range of $(\phi-\alpha)$ scenarios than at 45° , that fall within the mid range of strike angles (37.5° and 52.5°) and larger angles. Table 6.50 shows that when the crossing angle is 165° at the same miss distance, very few impacts are generated at the lowest velocity range (0.00 to 0.3075 km/s). This scenario can be considered statistically invalid. Tables 6.51 and 6.52 depict the distribution of impacts at a crossing angle of 90° as the miss distance increases to 2.0 and 6.0 meters, respectively. The number of impacts drop to 182 and 38, respectively; however, in both scenarios all of them strike in the same velocity range (1.23 to 1.5375 km/s) within approximately the same range of $(\phi-\alpha)$ scenarios.

These impact distribution patterns support the fact that as the crossing angle increases the relative impact velocity decreases. Therefore, it is expected that the total damage also decreases. To verify the later, Tables 6.53 through 6.58 present the corresponding damage distribution patterns for the selected encounter scenarios in the same impact configuration table format.

Table 6.53. Total Damage Quantification per Impact Configuration for Encounter Scenario 1 Without Tumbling Effects.

[illegible]

Table 6.54. Total Damage Quantification per Impact Configuration for Encounter Scenario 2 Without Tumbling Effects.

[illegible]

Table 6.55. Total Damage Quantification per Impact Configuration for Encounter Scenario 3 Without Tumbling Effects.

[illegible]

Table 6.56. Total Damage Quantification per Impact Configuration for Encounter Scenario 4 Without Tumbling Effects.

[illegible]

Table 6.57. Total Damage Quantification per Impact Configuration for Encounter Scenario 5 Without Tumbling Effects.

EBI=-0.0060		CA= 90 MD=2.0		Velocity= 1.2300(km/s)- 1.5375(km/s)																	
LD=4.00		90>=a>82.5		82.5>=a>67.5 67.5>=a>52.5 52.5>=a>37.5 37.5>=a>22.5 22.5>=a>7.5 7.5>=a>0 0 0 0 0 0 0 0 0 0 0 0 0 0 0 0																	
phi/alpha		0.0<=phi< 7.5		0 0																	
7.5<=phi<22.5		0 0		0 0																	
22.5<=phi<37.5		0 0		0 0																	
37.5<=phi<52.5		0 0		0 0																	
52.5<=phi<67.5		0 0		0 0																	
67.5<=phi<90.0		0 0		0 0																	
sum rows		0.166 1.125		3.337 7.567 10.041 18.988 37.618 0 0 0 0 0 0 0 0 0 0 0 0 0 0 0 0																	
Total DI		78.841																			
Total DI		77.705																			

Table 6.58. Total Damage Quantification per Impact Configuration for Encounter Scenario 6 Without Tumbling Effects.

EBI=-0.0060		CA= 90 MD=6.0		Velocity= 1.2300(km/s)- 1.5375(km/s)																	
LD=4.00		90>=a>82.5		82.5>=a>67.5 67.5>=a>52.5 52.5>=a>37.5 37.5>=a>22.5 22.5>=a>7.5 7.5>=a>0 0 0 0 0 0 0 0 0 0 0 0 0 0 0 0																	
phi/alpha		0.0<=phi< 7.5		0 0																	
7.5<=phi<22.5		0 0		0 0																	
22.5<=phi<37.5		0 0		0 0																	
37.5<=phi<52.5		0 0		0 0																	
52.5<=phi<67.5		0 0		0 0																	
67.5<=phi<90.0		0 0		0 0																	
sum rows		0 0.567		0.873 1.636 3.401 2.513 7.523 0 0 0 0 0 0 0 0 0 0 0 0 0 0 0 0																	
Total DI		16.613																			
Total DI		16.084																			

Table 6.53 shows that the 400 cylindrical impacts generated a total damage of 91.91 while the spheres generated less damage 69.272. Table 6.54 shows that as the crossing angle increased to 45° at the same miss distance, the total damage increased for both projectile geometries; to 230.256 for cylindrical projectiles versus 208.097 for spherical projectiles. In this table the levels of damage shown in a few $(\phi-\alpha)$ scenarios are analyzed. First, at the (1.5375 to 1.845 km/s) velocity range, within the 67.5° - 90° strike angle range, 60 cylinders impacted within an orientation angle range of 52.5° - 67.5° and generated a damage of 23.946. Conversely, 64 cylinders impacted within a shallower orientation angle range of 67.5° - 82.5° generating 19.089 of damage. Even though the number of impacts slightly increased less damage was inflicted. This is due to a reduction in the individual SIDs; a cylinder impacting at a shallower orientation angle than another, at the same velocity under the same strike angle has a lower SIDI (see Figure 4.7). Another example at the same velocity range, 231 cylinders impacting within a strike angle range of 52.5° - 67.5° , and within an orientation angle range of 37.5° to 52.5° generated a damage of 123.105. The number of impacts increase almost four times, however, the damage increased almost six times. This is also consistent with the fact that at steeper orientation and strike angles the individual SIDs become larger.

These scenarios prove that the total damage per encounter scenario is highly dependant on the frequency of impacts within certain impact characterization ranges of velocity, strike angles and orientation angles. Similar analyses on the damage levels shown in the different scenarios in Tables 6.55 through 6.58 confirm the later.

The total damage summarized under each of these tables matches the damage quantifications presented in table 6.1 for cylinders of L/D of 4 under the corresponding encounter scenarios. Therefore, for a given early bird time and regardless of projectile geometry/size, as the crossing angle increases:

- a) the frequency of impacts follows a parabolic trend;
- b) simultaneously the impact velocity decreases;
- c) projectiles impact the TBM surface at steeper strike angles.

Similarly, as the miss distance increases:

- a) the frequency of impacts reduces;
- b) the velocity range at which the projectiles impact remains approximately the same per crossing angle, as well as the range of strike angles and orientation angles.

All of the above support the fact that total damage to the TBM warhead decreases, which in turn is reflected in the colored damage level trends depicted in the total damage quantification matrices of all the projectiles. As illustrated in Table 6.14 the associated gray-scale color depends on the proposed damage range in which the estimated damage falls in.

6.7 Damage Analysis per Deployment Conditions

A damage analysis is presented to investigate the effects of the deployment conditions such as projectile tumbling and the variability in the radial ejection velocity of each projectile.

6.7.1 Tumbling

Tumbling does not seem to affect the number of projectiles impacting the TBM; however, the orientation in which cylindrical projectiles hit the target surface is affected by the number of rotations from the moment of deployment to impact and the slope of the target surface. The number of rotations about their centriodal axes depends on the angular velocity at which they travel and the time to impact.

To further explain this effect, impact and the total damage quantification tables per impact configuration were additionally generated for a few of the previously selected scenarios at an EBt of -0.006 sec. for a cylinder L/D of 4 with tumbling. Tables 6.59 through 6.62 list the impact configuration scenarios that contain the entire distribution of impacts when tumbling is considered for encounter scenarios 2, 3, 4, and 6. Note that the total number of cylindrical impacts summarized under each of these tables match the frequencies presented in table 3.5 under the corresponding encounter scenarios, which are the same as without tumbling. Table 6.59 shows that at a crossing angle of 45° , the impacts are distributed over a wider range of $(\phi-\alpha)$ scenarios than without tumbling. The number of tip impacts reduces from 499 to 352 and the number of tail impacts increases from 3 to 150. They still impact under the same velocity ranges and strike angle ranges, but the orientation angle range broadens up to the 7.5° to -7.5° range. Table 6.60 also shows that at a crossing angle of 90° , the impacts are distributed over the entire range of $(\phi-\alpha)$ scenarios under the same velocity ranges and strike angle ranges. The number of tip impacts reduces from 278 to 166 and the number of tail impacts increases from none to 112. Table 6.61 shows that even when the crossing angle is 165° , two of six impacts are tail impacts. However, this scenario is still considered statistically invalid. Table 6.62 depicts that at a crossing angle of 90° at a miss distance of 6.0 meters the impacts are distributed over almost the entire range of orientation angles, and still striking within the same velocity range and strike angle ranges.

When tumbling is added the distribution of the spatial orientation angle (α) for cylinders evens out compared to the distribution without tumbling; however, tumbling doesn't affect the strike angle or the magnitude of the velocity of impact, as observed in Figures 3.6 and 3.7. Nevertheless, the damage quantification tables per encounter configuration show similar damage level patterns regardless of whether tumbling is added or not.

To understand the effect tumbling has on the total damage per encounter scenario, Tables 6.63 through 6.66 present the corresponding damage distribution patterns for the selected encounter scenarios in the same impact configuration table format.

Table 6.59. Impact Quantification per Impact Configuration for Encounter Scenario 2 With Tumbling Effects.

EBI=0.0060		CA= 45		MD=1.0																															
L/D=4.00		Velocity= 1.53 75(km/s)		90°=a>82.5																															
phi/alpha		82.5°=a>67.5																																	
0.0°=phi< 7.5		67.5°=a>52.5																																	
7.5°=phi<22.5		52.5°=a>37.5																																	
22.5°=phi<37.5		37.5°=a>22.5																																	
37.5°=phi<52.5		22.5°=a>7.5																																	
52.5°=phi<67.5		7.5°=a>0																																	
67.5°=phi<90.0		0																																	
sum		70																																	
EBI=0.0060		CA= 45		MD=1.0																															
L/D=4.00		Velocity= 1.84 50(km/s)		90°=a>82.5																															
phi/alpha		82.5°=a>67.5																																	
0.0°=phi< 7.5		67.5°=a>52.5																																	
7.5°=phi<22.5		52.5°=a>37.5																																	
22.5°=phi<37.5		37.5°=a>22.5																																	
37.5°=phi<52.5		22.5°=a>7.5																																	
52.5°=phi<67.5		7.5°=a>0																																	
67.5°=phi<90.0		0																																	
sum		70																																	
Total Impacts		502																																	
Total Impacts		503																																	

EBI=0.0060		CA= 45		MD=1.0																															
L/D=4.00		Velocity= 1.53 75(km/s)		90°=a>82.5																															
phi/alpha		82.5°=a>67.5																																	
0.0°=phi< 7.5		67.5°=a>52.5																																	
7.5°=phi<22.5		52.5°=a>37.5																																	
22.5°=phi<37.5		37.5°=a>22.5																																	
37.5°=phi<52.5		22.5°=a>7.5																																	
52.5°=phi<67.5		7.5°=a>0																																	
67.5°=phi<90.0		0																																	
sum		70																																	
EBI=0.0060		CA= 45		MD=1.0																															
L/D=4.00		Velocity= 1.84 50(km/s)		90°=a>82.5																															
phi/alpha		82.5°=a>67.5																																	
0.0°=phi< 7.5		67.5°=a>52.5																																	
7.5°=phi<22.5		52.5°=a>37.5																																	
22.5°=phi<37.5		37.5°=a>22.5																																	
37.5°=phi<52.5		22.5°=a>7.5																																	
52.5°=phi<67.5		7.5°=a>0																																	
67.5°=phi<90.0		0																																	
sum		70																																	
Total Impacts		502																																	
Total Impacts		503																																	

EBI=0.0060		CA= 45		MD=1.0																															
L/D=4.00		Velocity= 1.53 75(km/s)		90°=a>82.5																															
phi/alpha		82.5°=a>67.5																																	
0.0°=phi< 7.5		67.5°=a>52.5																																	
7.5°=phi<22.5		52.5°=a>37.5																																	
22.5°=phi<37.5		37.5°=a>22.5																																	
37.5°=phi<52.5		22.5°=a>7.5																																	
52.5°=phi<67.5		7.5°=a>0																																	
67.5°=phi<90.0		0																																	
sum		70																																	
EBI=0.0060		CA= 45		MD=1.0																															
L/D=4.00		Velocity= 1.84 50(km/s)		90°=a>82.5																															
phi/alpha		82.5°=a>67.5																																	
0.0°=phi< 7.5		67.5°=a>52.5																																	
7.5°=phi<22.5		52.5°=a>37.5																																	
22.5°=phi<37.5		37.5°=a>22.5																																	
37.5°=phi<52.5		22.5°=a>7.5																																	
52.5°=phi<67.5		7.5°=a>0																																	
67.5°=phi<90.0		0																																	
sum		70																																	
Total Impacts		502																																	
Total Impacts		503																																	

EBI=0.0060		CA= 45		MD=1.0																															
L/D=4.00		Velocity= 1.53 75(km/s)		90°=a>82.5																															
phi/alpha		82.5°=a>67.5																																	
0.0°=phi< 7.5		67.5°=a>52.5																																	
7.5°=phi<22.5		52.5°=a>37.5																																	
22.5°=phi<37.5		37.5°=a>22.5																																	
37.5°=phi<52.5		22.5°=a>7.5																																	
52.5°=phi<67.5		7.5°=a>0																																	
67.5°=phi<90.0		0																																	
sum		70																																	
EBI=0.0060		CA= 45		MD=1.0																															
L/D=4.00		Velocity= 1.84 50(km/s)		90°=a>82.5																															
phi/alpha		82.5°=a>67.5																																	
0.0°=phi< 7.5		67.5°=a>52.5																																	
7.5°=phi<22.5		52.5°=a>37.5																																	
22.5°=phi<37.5		37.5°=a>22.5																																	
37.5°=phi<52.5		22.5°=a>7.5																																	
52.5°=phi<67.5		7.5°=a>0																																	
67.5°=phi<90.0		0																																	
sum		70																																	
Total Impacts		502																																	
Total Impacts		503																																	

EBI=0.0060		CA= 45		MD=1.0																															
L/D=4.00		Velocity= 1.53 75(km/s)		90°=a>82.5																															
phi/alpha		82.5°=a>67.5																																	
0.0°=phi< 7.5		67.5°=a>52.5																																	
7.5°=phi<22.5		52.5°=a>37.5																																	
22.5°=phi<37.5		37.5°=a>22.5																																	
37.5°=phi<52.5		22.5°=a>7.5																																	
52.5°=phi<67.5		7.5°=a>0																																	
67.5°=phi<90.0		0																																	
sum		70																																	
EBI=0.0060		CA= 45		MD=1.0																															
L/D=4.00		Velocity= 1.84 50(km/s)		90°=a>82.5																															
phi/alpha		82.5°=a>67.5																																	
0.0°=phi< 7.5		67.5°=a>52.5																																	
7.5°=phi<22.5		52.5°=a>37.5																																	
22.5°=phi<37.5		37.5°=a>22.5																																	
37.5°=phi<52.5		22.5°=a>7.5																																	
52.5°=phi<67.5		7.5°=a>0																																	
67.5°=phi<90.0		0																																	
sum		70																																	
Total Impacts		502																																	
Total Impacts		503																																	

EBI=0.0060		CA= 45		MD=1.0																															
L/D=4.00		Velocity= 1.53 75(km/s)		90°=a>82.5																															
phi/alpha		82.5°=a>67.5																																	
0.0°=phi< 7.5		67.5°=a>52.5																																	
7.5°=phi<22.5		52.5°=a>37.5																																	
22.5°=phi<37.5		37.5°=a>22.5																																	
37.5°=phi<52.5		22.5°=a>7.5																																	
52.5°=phi<67.5		7.5°=a>0																																	
67.5°=phi<90.0		0																																	
sum		70																																	
EBI=0.0060		CA= 45		MD=1.0																															
L/D=4.00		Velocity= 1.84 50(km/s)		90°=a>82.5																															
phi/alpha		82.5°=a>67.5																																	
0.0°=phi< 7.5		67.5°=a>52.5																																	
7.5°=phi<22.5		52.5°=a>37.5																																	
22.5°=phi<37.5		37.5°=a>22.5																																	
37.5°=phi<52.5		22.5°=a>7.5																																	
52.5°=phi<67.5		7.5°=a>0																																	
67.5°=phi<90.0		0																																	
sum		70																																	
Total Impacts		502																																	
Total Impacts		503																																	

EBI=0.0060		CA= 45		MD=1.0																															
L/D=4.00		Velocity= 1.53 75(km/s)		90°=a>82.5																															
phi/alpha		82.5°=a>67.5																																	
0.0°=phi< 7.5		67.5°=a>52.5																																	
7.5°=phi<22.5		52.5°=a>37.5																																	
22.5°=phi<37.5		37.5°=a>22.5																																	
37.5°=phi<52.5		22.5°=a>7.5																																	
52.5°=phi<67.5		7.5°=a>0																																	
67.5°=phi<90.0		0																																	
sum		70																																	
EBI=0.0060		CA= 45		MD=1.0																															
L/D=4.00		Velocity= 1.84 50(km/s)		90°=a>82.5																															
phi/alpha		82.5°=a>67.5																																	
0.0°=phi< 7.5		67.5°=a>52.5																																	
7.5°=phi<22.5		52.5°=a>37.5																																	
22.5°=phi<37.5		37.5°=a>22.5																																	
37.5°=phi<52.5		22.5°=a>7.5																																	
52.5°=phi<67.5		7.5°=a>0																																	
67.5°=phi<90.0		0																																	
sum		70																																	
Total Impacts		502																																	
Total Impacts		503																																	

EBI=0.0060		CA= 45		MD=1.0																															
L/D=4.00		Velocity= 1.53 75(km/s)		90°=a>82.5																															
phi/alpha		82.5°=a>67.5																																	
0.0°=phi< 7.5		67.5°=a>52.5																																	
7.5°=phi<22.5		52.5°=a>37.5																																	
22.5°=phi<37.5		37.5°=a>22.5																																	
37.5°=phi<52.5		22.5°=a>7.5																																	
52.5°=phi<67.5		7.5°=a>0																																	
67.5°=phi<90.0		0																																	
sum		70																																	
EBI=0.0060		CA= 45		MD=1.0																															
L/D=4.00		Velocity= 1.84 50(km/s)		90°=a>82.5																															
phi/alpha		82.5°=a>67.5																																	
0.0°=phi< 7.5		67.5°=a>52.5																																	
7.5°=phi<22.5		52.5°=a>37.5																																	
22.5°=phi<37.5		37.5°=a>22.5																																	
37.5°=phi<52.5		22.5°=a>7.5																																	
52.5°=phi<67.5		7.5°=a>0																																	
67.5°=phi<90.0		0																																	
sum		70																																	
Total Impacts		502																																	
Total Impacts		503																																	

EBI=0.0060		CA= 45		MD=1.0																															
L/D=4.00		Velocity= 1.53 75(km/s)		90°=a>82.5																															
phi/alpha		82.5°=a>67.5																																	
0.0°=phi< 7.5		67.5°=a>52.5																																	
7.5°=phi<22.5		52.5°=a>37.5																																	
22.5°=phi<37.5		37.5°=a>22.5																																	
37.5°=phi<52.5		22.5°=a>7.5																																	
52.5°=phi<67.5		7.5°=a>0																																	
67.5°=phi<90.0		0																																	
sum		70																																	
EBI=0.0060		CA= 45		MD=1.0																															
L/D=4.00		Velocity= 1.84 50(km/s)		90°=a>82.5																															
phi/alpha		82.5°=a>67.5																																	
0.0°=phi< 7.5		67.5°=a>52.5																																	
7.5°=phi<22.5		52.5°=a>37.5																																	
22.5°=phi<37.5		37.5°=a>22.5																																	
37.5°=phi<52.5		22.5°=a>7.5																																	
52.5°=phi<67.5		7.5°=a>0																																	
67.5°=phi<90.0		0																																	
sum		70																																	
Total Impacts		502																																	
Total Impacts		503																																	

EBI=0.0060		CA= 45		MD=1.0																															
L/D=4.00		Velocity= 1.53 75(km/s)		90°=a>82.5																															
phi/alpha		82.5°=a>67.5																																	
0.0°=phi< 7.5		67.5°=a>52.5																																	
7.5°=phi<22.5		52.5°=a>37.5																																	
22.5°=phi<37.5		37.5°=a>22.5																																	
37.5°=phi<52.5		22.5°=a>7.5																																	
52.5°=phi<67.5		7.5°=a>0																																	
67.5°=phi<90.0		0																																	
sum		70																																	
EBI=0.0060		CA= 45		MD=1.0																															
L/D=4.00		Velocity= 1.84 50(km/s)		90°=a>82.5																															
phi/alpha		82.5°=a>67.5																																	
0.0°=phi< 7.5		67.5°=a>52.5																																	
7.5°=phi<22.5		52.5°=a>37.5																																	
22.5°=phi<37.5		37.5°=a>22.5																																	
37.5°=phi<52.5		22.5°=a>7.5																																	
52.5°=phi<67.5		7.5°=a>0																																	
67.5°=phi<90.0		0																																	
sum		70																																	
Total Impacts		502																																	
Total Impacts		503																		</															

Table 6.60. Impact Quantification per Impact Configuration for Encounter Scenario 3 With Tumbling Effects.

EBI=0.0060		CA= 90		MD=1.0																															
L/D=4.00		Velocity= 0.92 25(km/s)		90°=a>82.5																															
phi/alpha		82.5°=a>67.5																																	
0.0°=phi< 7.5		67.5°=a>52.5																																	
7.5°=phi<22.5		52.5°=a>37.5																																	
22.5°=phi<37.5		37.5°=a>22.5																																	
37.5°=phi<52.5		22.5°=a>7.5																																	
52.5°=phi<67.5		7.5°=a>0																																	
67.5°=phi<90.0		0																																	
sum		2																																	
EBI=0.0060		CA= 90		MD=1.0																															
L/D=4.00		Velocity= 1.23 00(km/s)		90°=a>82.5																															
phi/alpha		82.5°=a>67.5																																	
0.0°=phi< 7.5		67.5°=a>52.5																																	
7.5°=phi<22.5		52.5°=a>37.5																																	
22.5°=phi<37.5		37.5°=a>22.5																																	
37.5°=phi<52.5		22.5°=a>7.5																																	
52.5°=phi<67.5		7.5°=a>0																																	
67.5°=phi<90.0		0																																	
sum		25																																	
Total Impacts		278																																	
Total Impacts		279																																	

EBI=0.0060		CA= 90		MD=1.0																															
L/D=4.00		Velocity= 0.92 25(km/s)		90°=a>82.5																															
phi/alpha		82.5°=a>67.5																																	
0.0°=phi< 7.5		67.5°=a>52.5																																	
7.5°=phi<22.5		52.5°=a>37.5																																	
22.5°=phi<37.5		37.5°=a>22.5																																	
37.5°=phi<52.5		22.5°=a>7.5																																	
52.5°=phi<67.5		7.5°=a>0																																	
67.5°=phi<90.0		0																																	
sum		2																																	
EBI=0.0060		CA= 90		MD=1.0																															
L/D=4.00		Velocity= 1.23 00(km/s)		90°=a>82.5																															
phi/alpha		82.5°=a>67.5																																	
0.0°=phi< 7.5		67.5°=a>52.5																																	
7.5°=phi<22.5		52.5°=a>37.5																																	
22.5°=phi<37.5		37.5°=a>22.5																																	
37.5°=phi<52.5		22.5°=a>7.5																																	
52.5°=phi<67.5		7.5°=a>0																																	
67.5°=phi<90.0		0																																	
sum		25																																	
Total Impacts		278																																	
Total Impacts		279																																	

EBI=0.0060		CA= 90		MD=1.0																															
L/D=4.00		Velocity= 0.92 25(km/s)		90°=a>82.5																															
phi/alpha		82.5°=a>67.5																																	
0.0°=phi< 7.5		67.5°=a>52.5																																	
7.5°=phi<22.5		52.5°=a>37.5																																	
22.5°=phi<37.5		37.5°=a>22.5																																	
37.5°=phi<52.5		22.5°=a>7.5																																	
52.5°=phi<67.5		7.5°=a>0																																	
67.5°=phi<90.0		0																																	
sum		2																																	
EBI=0.0060		CA= 90		MD=1.0																															
L/D=4.00		Velocity= 1.23 00(km/s)		90°=a>82.5																															
phi/alpha		82.5°=a>67.5																																	
0.0°=phi< 7.5		67.5°=a>52.5																																	
7.5°=phi<22.5		52.5°=a>37.5																																	
22.5°=phi<37.5		37.5°=a>22.5																																	
37.5°=phi<52.5		22.5°=a>7.5																																	
52.5°=phi<67.5		7.5°=a>0																																	
67.5°=phi<90.0		0																																	
sum		25																																	
Total Impacts		278																																	
Total Impacts		279																																	

EBI=0.0060		CA= 90		MD=1.0																															
L/D=4.00		Velocity= 0.92 25(km/s)		90°=a>82.5																															
phi/alpha		82.5°=a>67.5																																	
0.0°=phi< 7.5		67.5°=a>52.5																																	
7.5°=phi<22.5		52.5°=a>37.5																																	
22.5°=phi<37.5		37.5°=a>22.5																																	
37.5°=phi<52.5		22.5°=a>7.5																																	
52.5°=phi<67.5		7.5°=a>0																																	
67.5°=phi<90.0		0																																	
sum		2																																	
EBI=0.0060		CA= 90		MD=1.0																															
L/D=4.00		Velocity= 1.23 00(km/s)		90°=a>82.5																															
phi/alpha		82.5°=a>67.5																																	
0.0°=phi< 7.5		67.5°=a>52.5																																	
7.5°=phi<22.5		52.5°=a>37.5																																	
22.5°=phi<37.5		37.5°=a>22.5																																	
37.5°=phi<52.5		22.5°=a>7.5																																	
52.5°=phi<67.5		7.5°=a>0																																	
67.5°=phi<90.0		0																																	
sum		25																																	
Total Impacts		278																																	
Total Impacts		279																																	

EBI=0.0060		CA= 90		MD=1.0																															
L/D=4.00		Velocity= 0.92 25(km/s)		90°=a>82.5																															
phi/alpha		82.5°=a>67.5																																	
0.0°=phi< 7.5		67.5°=a>52.5																																	
7.5°=phi<22.5		52.5°=a>37.5																																	
22.5°=phi<37.5		37.5°=a>22.5																																	
37.5°=phi<52.5		22.5°=a>7.5																																	
52.5°=phi<67.5		7.5°=a>0																																	
67.5°=phi<90.0		0																																	
sum		2																																	
EBI=0.0060		CA= 90		MD=1.0																															
L/D=4.00		Velocity= 1.23 00(km/s)		90°=a>82.5																															
phi/alpha		82.5°=a>67.5																																	
0.0°=phi< 7.5		67.5°=a>52.5																																	
7.5°=phi<22.5		52.5°=a>37.5																																	
22.5°=phi<37.5		37.5°=a>22.5																																	
37.5°=phi<52.5		22.5°=a>7.5																																	
52.5°=phi<67.5		7.5°=a>0																																	
67.5°=phi<90.0		0																																	
sum		25																																	
Total Impacts		278																																	
Total Impacts		279																																	

EBI=0.0060		CA= 90		MD=1.0																															
L/D=4.00		Velocity= 0.92 25(km/s)		90°=a>82.5																															
phi/alpha		82.5°=a>67.5																																	
0.0°=phi< 7.5		67.5°=a>52.5																																	
7.5°=phi<22.5		52.5°=a>37.5																																	
22.5°=phi<37.5		37.5°=a>22.5																																	
37.5°=phi<52.5		22.5°=a>7.5																																	
52.5°=phi<67.5		7.5°=a>0																																	
67.5°=phi<90.0		0																																	
sum		2																																	
EBI=0.0060		CA= 90		MD=1.0																															
L/D=4.00		Velocity= 1.23 00(km/s)		90°=a>82.5																															
phi/alpha		82.5°=a>67.5																																	
0.0°=phi< 7.5		67.5°=a>52.5																																	
7.5°=phi<22.5		52.5°=a>37.5																																	
22.5°=phi<37.5		37.5°=a>22.5																																	
37.5°=phi<52.5		22.5°=a>7.5																																	
52.5°=phi<67.5		7.5°=a>0																																	
67.5°=phi<90.0		0																																	
sum		25																																	
Total Impacts		278																																	
Total Impacts		279																																	

EBI=0.0060		CA= 90		MD=1.0																															
L/D=4.00		Velocity= 0.92 25(km/s)		90°=a>82.5																															
phi/alpha		82.5°=a>67.5																																	
0.0°=phi< 7.5		67.5°=a>52.5																																	
7.5°=phi<22.5		52.5°=a>37.5																																	
22.5°=phi<37.5		37.5°=a>22.5																																	
37.5°=phi<52.5		22.5°=a>7.5																																	
52.5°=phi<67.5		7.5°=a>0																																	
67.5°=phi<90.0		0																																	
sum		2																																	
EBI=0.0060		CA= 90		MD=1.0																															
L/D=4.00		Velocity= 1.23 00(km/s)		90°=a>82.5																															
phi/alpha		82.5°=a>67.5																																	
0.0°=phi< 7.5		67.5°=a>52.5																																	
7.5°=phi<22.5		52.5°=a>37.5																																	
22.5°=phi<37.5		37.5°=a>22.5																																	
37.5°=phi<52.5		22.5°=a>7.5																																	
52.5°=phi<67.5		7.5°=a>0																																	
67.5°=phi<90.0		0																																	
sum		25																																	
Total Impacts		278																																	
Total Impacts		279																																	

EBI=0.0060		CA= 90		MD=1.0																															
L/D=4.00		Velocity= 0.92 25(km/s)		90°=a>82.5																															
phi/alpha		82.5°=a>67.5																																	
0.0°=phi< 7.5		67.5°=a>52.5																																	
7.5°=phi<22.5		52.5°=a>37.5																																	
22.5°=phi<37.5		37.5°=a>22.5																																	
37.5°=phi<52.5		22.5°=a>7.5																																	
52.5°=phi<67.5		7.5°=a>0																																	
67.5°=phi<90.0		0																																	
sum		2																																	
EBI=0.0060		CA= 90		MD=1.0																															
L/D=4.00		Velocity= 1.23 00(km/s)		90°=a>82.5																															
phi/alpha		82.5°=a>67.5																																	
0.0°=phi< 7.5		67.5°=a>52.5																																	
7.5°=phi<22.5		52.5°=a>37.5																																	
22.5°=phi<37.5		37.5°=a>22.5																																	
37.5°=phi<52.5		22.5°=a>7.5																																	
52.5°=phi<67.5		7.5°=a>0																																	
67.5°=phi<90.0		0																																	
sum		25																																	
Total Impacts		278																																	
Total Impacts		279																																	

EBI=0.0060		CA= 90		MD=1.0																															
L/D=4.00		Velocity= 0.92 25(km/s)		90°=a>82.5																															
phi/alpha		82.5°=a>67.5																																	
0.0°=phi< 7.5		67.5°=a>52.5																																	
7.5°=phi<22.5		52.5°=a>37.5																																	
22.5°=phi<37.5		37.5°=a>22.5																																	
37.5°=phi<52.5		22.5°=a>7.5																																	
52.5°=phi<67.5		7.5°=a>0																																	
67.5°=phi<90.0		0																																	
sum		2																																	
EBI=0.0060		CA= 90		MD=1.0																															
L/D=4.00		Velocity= 1.23 00(km/s)		90°=a>82.5																															
phi/alpha		82.5°=a>67.5																																	
0.0°=phi< 7.5		67.5°=a>52.5																																	
7.5°=phi<22.5		52.5°=a>37.5																																	
22.5°=phi<37.5		37.5°=a>22.5																																	
37.5°=phi<52.5		22.5°=a>7.5																																	
52.5°=phi<67.5		7.5°=a>0																																	
67.5°=phi<90.0		0																																	
sum		25																																	
Total Impacts		278																																	
Total Impacts		279																																	

EBI=0.0060		CA= 90		MD=1.0																															
L/D=4.00		Velocity= 0.92 25(km/s)		90°=a>82.5																															
phi/alpha		82.5°=a>67.5																																	
0.0°=phi< 7.5		67.5°=a>52.5																																	
7.5°=phi<22.5		52.5°=a>37.5																																	
22.5°=phi<37.5		37.5°=a>22.5																																	
37.5°=phi<52.5		22.5°=a>7.5																																	
52.5°=phi<67.5		7.5°=a>0																																	
67.5°=phi<90.0		0																																	
sum		2																																	
EBI=0.0060		CA= 90		MD=1.0																															
L/D=4.00		Velocity= 1.23 00(km/s)		90°=a>82.5																															
phi/alpha		82.5°=a>67.5																																	
0.0°=phi< 7.5		67.5°=a>52.5																																	
7.5°=phi<22.5		52.5°=a>37.5																																	
22.5°=phi<37.5		37.5°=a>22.5																																	
37.5°=phi<52.5		22.5°=a>7.5																																	
52.5°=phi<67.5		7.5°=a>0																																	
67.5°=phi<90.0		0																																	
sum		25																																	
Total Impacts		278																																	
Total Impacts		279																																	

||
||
||

Table 6.63. Total Damage Quantification per Impact Configuration for Encounter Scenario 2 With Tumbling Effects.

CA= 45		MD=1.0	1.8450(km/s)													SumCyl	
Velocity's 1.5375(km/s)-			82.5>=p<87.5	67.5>=p<62.5	52.5>=p<37.5	37.5>=p<22.5	22.5>=p<7.5	7.5>=p<-7.5	(-17.5>=p<-22.5	(-22.5>=p<-37.5	(-37.5>=p<-52.5	(-52.5>=p<-67.5	(-67.5>=p<-82.5	(-82.5>=p<-90	Sphere		
0	0	0	0	0	0	0	0	0	0	0	0	0	0	0	0	0	
0	0	0	0	0	0	0	0	0	0	0	0	0	0	0	0	0	
0	0	0	0	0	0	0	0	0	0	0	0	0	0	0	0	0	
22.632	47.264	35.070	13.435	5.854	1.375	0	0	0	0	0	0	0	5.252	13.962	134.620	142.845	
6.807	3.650	1.421	0.316	0	0	0	0	0	0	0	0	0	0	14.472	40.952	38.446	
29.439	50.815	34.492	13.750	5.854	1.375	0	0	0	0	0	0	0	0	2.299	175.573	181.291	
sum rows														19.725	23.543		

CA= 45		MD=1.0	1.8450(km/s)													SumCyl	
Velocity's 1.8450(km/s)-			82.5>=p<87.5	67.5>=p<62.5	52.5>=p<37.5	37.5>=p<22.5	22.5>=p<7.5	7.5>=p<-7.5	(-17.5>=p<-22.5	(-22.5>=p<-37.5	(-37.5>=p<-52.5	(-52.5>=p<-67.5	(-67.5>=p<-82.5	(-82.5>=p<-90	Sphere		
0	0	0	0	0	0	0	0	0	0	0	0	0	0	0	0	0	
0	0	0	0	0	0	0	0	0	0	0	0	0	0	0	0	0	
0	0	0	0	0	0	0	0	0	0	0	0	0	0	0	0	0	
1.410	1.488	9.447	7.438	3.648	1.600	0.383	0	0	0	0	0	0	0	0	24.384	24.391	
0	0	1.306	2.441	2.887	0.992	0	0	0	0	0	0	0	0	0	8.140	7.556	
1.410	1.466	9.753	9.879	6.535	2.522	0.383	0	0	0	0	0	0	0	0	32.524	31.947	
sum rows																	

EBI=-0.0060		Total DI	
J/D=4.00		for Cylinder	
shh/shl/alpha		for Sphere	
0.0<=p<7.5	213.238	Total DI	208.097
7.5<=p<22.5			
22.5<=p<37.5			
37.5<=p<52.5			
52.5<=p<67.5			
67.5<=p<82.5			
82.5<=p<90.0			
sum rows			

Table 6.64. Total Damage Quantification per Impact Configuration for Encounter Scenario 3 With Tumbling Effects.

[illegible]

Table 6.63 shows that the 502 cylindrical impacts tumbling generated a total damage of 213.238 while the without tumbling generated more damage 230.256. At the (1.5375 to 1.845 km/s) velocity range, the number of tip impacts reduced from 428 to 281, however, their orientation angle range increased. This reduced the total tip impact damage from 197.277 to 135.725. Conversely, the number of tail impacts increased from 3 to 150 and their orientation angle range also increased. This increased the total tail impact damage from 0.112 to 45.567. The redistribution of impacts over a broader range of orientation angles reduced the total damage at that velocity range from 197.389 to 181.291. In the (1.845 km/s or higher) velocity range, the 71 impacts were also redistributed over a broader range of orientation angles that reduced the total damage from 32.867 to 31.947. Overall, tumbling reduced the total damage at this encounter scenario.

Similar analyses on the damage levels shown in the different scenarios in Tables 6.64 and 6.66 confirm the later. The total damage under tumbling for scenario 4 where the crossing angle is 165° is a bit higher than without tumbling; however this case is considered statistically invalid. The total damage summarized under each of these tables matches the damage quantifications presented in table 6.6 for cylinders of L/D of 4 under the corresponding encounter scenarios. These examples demonstrate that when tumbling is considered, the total damage is highly dependant on the frequency of impacts within a certain range of orientation angles. However, the effect that tumbling has on the total damage per encounter scenario is less evident when the impact frequencies are high. The higher the number of cylindrical impacts to be redistributed over a broader range of orientation angles, for example at steeper orientation angles and/or larger number of tail impacts (see Figures 3.6 and 3.7), the larger the redistribution of individual damages towards smaller levels. In statistical terms, the mean value of individual damage per encounter scenario is slightly smaller than in cases without tumbling, but the standard deviation is larger. This is the reason for which the color levels in the matrices of total damage-per encounter configuration scenarios are very similar between cases without and with tumbling.

6.7.2 Radial Ejection Velocity Variability

Variability in the radial ejection velocity of projectiles of any geometry/size was accounted for by conducting 30 EKV deployment simulations per encounter scenario based on an outer radial velocity with a normal distribution with mean of 0.309 km/s. and preset coefficients of variation. The number of impacts on the TBM varied in each simulation, as well as their location on the TBM and their strike angles, thus varying the total damage per simulation. Impact and total damage averages were computed from the 30 simulations and presented in the corresponding tables.

To further explain the effect of variability in radial velocity, impact and the total damage quantification tables per impact configuration were generated for encounter scenarios 2, 4 and 6 at an *EBt* of -0.006 sec. for a cylinder L/D of 4 without tumbling. Tables 6.67 and 6.72 list the impact configuration scenarios that contain the entire distribution of impacts for encounter scenarios 2, 4 and 6. For each encounter scenario

pairs of tables are presented contiguously corresponding to 25% and 75% variability conditions. Table 6.67 corresponds to scenario 2 with 25% variability and Table 6.68 corresponds to the same scenario with 75% variability, and so on so forth. Note that the total number of cylindrical impacts summarized under the 25% tables match the frequencies presented in table 3.7. Overall, when variability in radial velocity is considered the average number of cylindrical and spherical impacts per encounter scenario drops with respect to the total impacts obtained without variability, as shown in tables 6.48, 6.50 and 6.52. As variability increases from 25% to 75% the average impacts drop even more.

To clarify this effect, Figures 6.6 *a* through *d* depict snapshots of endgame simulations where projectiles are launched straight ahead to the TBM (crossing angle of 0°) and the variability in radial ejection velocity increases from 0% to 75% in increments of 25%. Since the simulations are symmetric, only half of the TBM is shown.

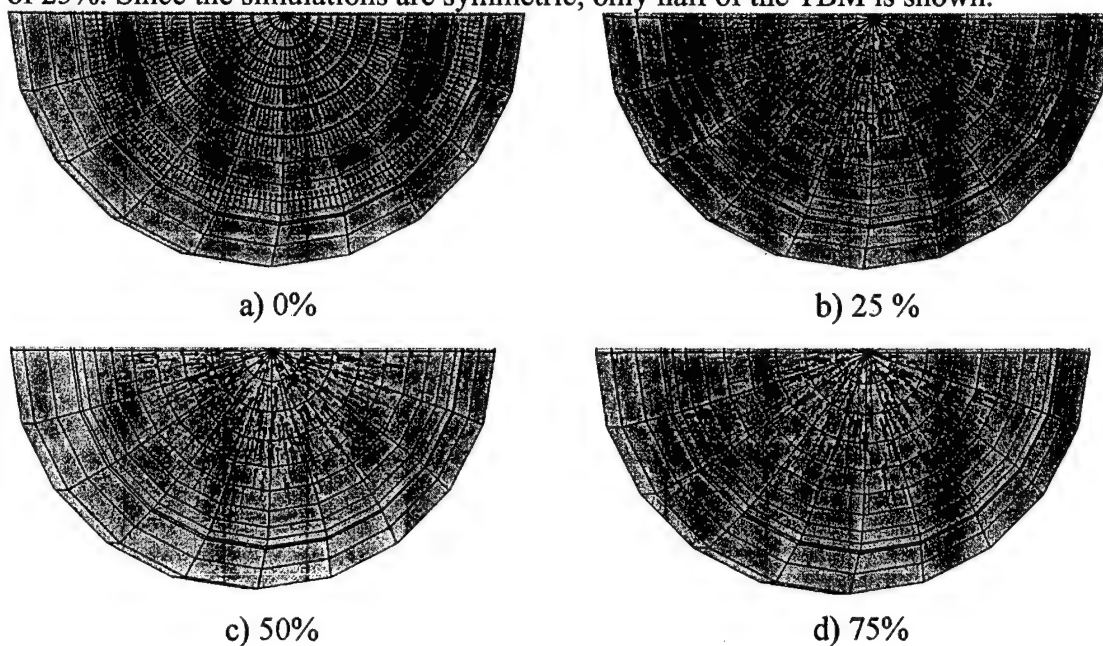


Figure 6.6. Impact Frequencies at Various Variability Levels.

Table 6.69. Impact Quantification per Impact Configuration for Encounter Scenario 4 With 25% Variability Without Tumbling Effects.

EBI=0.0060		CA=165		MD=1.0	
LD=4.00		Velocity= 0.0000 (km/s)		0.3075(km/s)	
phi/alpha		90>=a>=82.5		82.5>a>=67.5	
0.0<=phi< 7.5		0		0	
7.5<=phi<22.5		0		0	
22.5<=phi<37.5		0		0	
37.5<=phi<52.5		0		0.667	
52.5<=phi<67.5		0.2		0.667	
67.5<=phi<90.0		0.4		0.367	
sum		0.6		1.700	
Total Impacts		for Cylinder EC		2.367	
Total Impacts		for Sphere EC		2.433	
				Sphere	
				0	
				0	
				0	
				0.767	
				1.033	
				0.867	
				0.833	
				2.433	
				SumCyl	
				0	
				0	
				0	
				0.667	
				0.667	
				0.367	
				2.367	

Table 6.70. Impact Quantification per Impact Configuration for Encounter Scenario 4 With 75% Variability Without Tumbling Effects.

EBI=0.0060		CA=165		MD=1.0	
LD=4.00		Velocity= 0.0000 (km/s)		0.3075(km/s)	
phi/alpha		90>=a>=82.5		82.5>a>=67.5	
0.0<=phi< 7.5		0		0	
7.5<=phi<22.5		0		0	
22.5<=phi<37.5		0		0	
37.5<=phi<52.5		0		0.367	
52.5<=phi<67.5		0.167		0.467	
67.5<=phi<90.0		0.333		0.167	
sum		0.333		1.000	
Total Impacts		for Cylinder EC		1.367	
Total Impacts		for Sphere EC		1.300	
				Sphere	
				0	
				0	
				0	
				0.300	
				0.767	
				0.633	
				0.233	
				1.300	
				SumCyl	
				0	
				0	
				0	
				0.367	
				0.633	
				0.367	
				1.367	

Table 6.71. Impact Quantification per Impact Configuration for Encounter Scenario 6 With 25% Variability Without Tumbling Effects.

[illegible]

Table 6.72. Impact Quantification per Impact Configuration for Encounter Scenario 6 With 75% Variability Without Tumbling Effects.

[illegible]

Figure 6.6a shows the impact frequency without variability ($\text{COV } V_{rp} 0\%$), meaning that each ring of projectiles has the same radial velocity; therefore, the circular patterns are clearly defined. Figure 6.6.b shows less number of impacts at 25% variability and the circular patterns are lost. Figures 6.6.b through 6.6.d, show that less number of projectiles impact the TBM each time the variability in radial velocity increases to 25%, 50% and 75%, respectively. The reason for this is that some of the projectiles assembled in the outer-rings of the EKV warhead reached higher radial velocities and missed the TBM. This is the reason for which the colored patterns in the matrices of total damage-per encounter configuration scenarios change as variability increases.

Impact velocity ranges and strike angle ranges practically do not seem to change from the ones without variability for this early bird time, except when the crossing angle gets closer to 165° or the miss distance increases towards 6.0 meters. However, comparing Figures 3.6 and 3.8 slight variations are observed in the velocity distribution as well as the orientation angle distribution. The range of orientation angles do seem to show that they vary as variability increases. These slight changes in the ranges may be due to the fact that the variability is being applied to the radial velocity component of the resultant impact velocity, which only contributes about 15% of the resultant velocity as the crossing angles are closer to 0° , but up to 55% as the crossing angles reach 165° .

Tables 6.73 to 6.78 present the corresponding damage distribution patterns in impact configuration table format for the same encounter scenarios. In all cases the computed damage averages are lower than the damages without variability without tumbling, as shown in tables 6.54, 6.56 and 6.58. This trend is consistent with the corresponding impact patterns previously observed. This is the reason for which the color levels in the matrices of total damage-per encounter configuration scenarios vary as variability in radial ejection velocity increases. Therefore, it is concluded that variability in radial ejection velocity does have an effect on the impact frequencies, thus in the level of damage inversely proportional to the amount of variability. Low impact frequencies and low damage averages are moreover considered statistically invalid.

It is expected that the larger the number of simulations per encounter scenario, the computed averages for impact frequencies and total damage will be closer to the actual means of the distributions corresponding to each coefficient of variation. It should be noted that the totals computed without variability are not the distribution means.

Table 6.76. Total Damage Quantification per Impact Configuration for Encounter Scenario 4 With 75% Variability Without Tumbling Effects.

[illegible]

6.8 Damage Analysis per Projectile Geometry/Size

A damage analysis is presented to investigate the effects of the projectile geometry and the projectile size.

6.8.1 Impact Configuration

When comparing the total damage per velocity range between the sphere and the three cylindrical sizes, usually at velocities lower than 0.615 km/s the sphere generates more damage. In the middle velocity range up to 1.5375 km/s, the sphere is as damaging as the cylinders. When the velocity increases between 1.5375 and 1.8450 km/s the cylinders are slightly more lethal than the sphere. At higher velocities the cylinder of L/D of 4 generates more damage than the other geometry/sizes; however, the sphere generates more damage than the cylinders of L/D of 2 and 1.

6.8.2 Encounter Configuration

A cylinder with L/D of 4 without tumbling effects is generally more lethal than a sphere within crossing angles up to 75° or 90°, with the exception a small range of scenarios where between approximately 45° and 60° in early bird scenarios were the spheres are more lethal. As variability is added, the cylinder' lethal range begins to slightly dissipate throughout the crossing angle range, where in early bird scenarios is more noticeable. However, it seems that cylinders of L/D of 4 are always more lethal than spheres at small crossing angles approximately between 0° and 30°. The cylinders appear to be more lethal at a crossing angle of 165° for a wide range of miss distance scenarios.

A cylinder with L/D of 2 without tumbling effects is generally more lethal within a crossing angle range between 60° and 90°, as well as at a crossing angle of 150° regardless of early bird scenario. This range increases between 45° and 120° at early bird scenarios. As variability is added the cylinder' lethal range begins to slightly dissipate throughout the crossing angle range for all early bird scenarios.

A cylinder with L/D of 1 without tumbling effects is clearly more lethal within a crossing angle range between 30° and 90° and occasionally up to 120° in late bird scenarios, and as the encounters become early bird scenarios the cylinder' lethality starts dissipating throughout the crossing angle range. As variability is added the cylinder' lethal range dissipates even more throughout all early bird scenarios.

Under tumbling effects the sphere is consistently more lethal than the cylinder of L/D of 4 throughout most of the encounter configuration scenarios even with variability. Similar patterns are observed for the cylinders of L/D of 1 and 2, except at a crossing angle range around 135° and 165°, where the cylinders appear as more lethal for a few scenarios. These scenarios are more realistic than those without tumbling. It can be concluded that the sphere is more lethal than any cylinder geometry/size under various deployment conditions.

CHAPTER 7

SUMMARY, CONCLUSIONS AND RECOMMENDATIONS

7.1 Introduction

The increasing ballistic missile production and research by other nations demonstrates the necessity to study the possible countermeasures against such threats. One possible countermeasure, given the low probabilities of a direct impact of the TBM due to the high closing velocities that appear in missile encounters, is the use of KE-rod warheads in an Exo-atmospheric Kill Vehicle (EKV) that would track the TBM trajectory. For that reason, the main objective of this research work was to provide guidelines that would improve the EKV design in order to inflict maximum damage to the TBM in near miss encounter where KE-rod warheads can be employed.

7.2 Summary

A general background of the problem and a review of the literature of articles concerning the study of lethality of projectile under diverse impact circumstances were presented in Chapter 1.

An overview of ballistic missiles including the description of the TBM's currently employed and produced, the characteristics of the different EKV KE-rod warhead deployment systems, and the shapes and materials of projectiles used as KE-rod warheads were introduced in Chapter 2. Based on the TMB, EKV, and projectile characteristics, a computer coded was developed to simulate and study the interactions of different variables of the terminal encounter kinematics between the TBM and the EKV. The development of the computer code is described in Chapter 3.

The necessity to quantify the damage inflicted by each projectile impact lead to the development of a damage index using a code capable to model large material deformations and fracture appearing in hypervelocity impacts. Smoothed Particles Hydrodynamics was the code used to model each projectile impact. Chapter 4 presents the development of the index used to quantify impact damage.

To predict damage indexes of impacts given by the results of the impact characterization of the Endgame Simulations not modeled using Smoothed Particles Hydrodynamics, a rapid solution model using Artificial Neural Networks was developed employing a database of projectile impacts at predetermined parameters. The ANN model developed is described in Chapter 5.

The Endgame Simulations code was coupled with the ANN model to accelerate the calculation of the damage indexes of projectile impacts under different encounter variables (*EBt*, *CA*, *MD*). A detailed description of the results and preliminary conclusions are given in Chapter 6.

7.3 Conclusions

The following conclusions can be reached from the impact quantification results given by the "Endgame Simulations":

- a) Impact frequencies resemble a shifted parabolic pattern as the crossing angle increases from 0° to 165° . The peaks of these parabolic tendencies shift towards larger crossing angles as early bird times range from late birds to early bird scenarios.
- b) There exist a relationship between the crossing angle and the projectile impact velocity. As the crossing angle increases, the relative impact velocity decreases.
- c) In general, the number of impacts increases as the impact velocity magnitude increases. As the early bird time increases (between 0.003 to 0.012 sec.) the regions of very low frequency or no impact, and the high impact frequency regions are concentrated around a crossing angle of 0° and miss distance of 1.0 meter.
- e) The general tendencies mentioned above are observed for any cylindrical geometry or size at any early bird time.

From the developed Single Impact Damage Index results the subsequent conclusions can be stated:

- a) Smoothed Particles Hydrodynamics provided a good tool to model hypervelocity impacts of projectiles where large material displacements and deformations are present.
- b) The single impacts damage index (SIDI) represents a more general approach to quantify damage inflicted by projectiles. It is based on the projectile depth of penetration and volume displaced by the projectile.
- c) The SIDI gave good visual correlation results to changes in the projectile's material, mass and impact conditions. The SIDI is strongly correlated to the magnitude of the projectile's velocity and mass.
- d) In general, using the SIDI calculated values for a wide range of values for the impact parameters, cylindrical projectiles are more lethal than spherical projectiles when both the vector angle (strike angle, ϕ) and the orientation angle (α) of the projectile are aligned or the yaw angle is ± 30 . On the contrary, the sphere proved to be more lethal than the cylinder for all the other cases.
- e) The tendencies of the calculated SIDI values between different sizes of cylindrical projectiles (L/D s of 1, 2, and 4) keeping the same amount of mass are the same and the differences are minimal. Therefore, the penetration and displaced debris of different L/D s are of the same order.

The conclusions of the damage quantification analysis discussed in Chapter 6 are as follows:

- a) Total damage tendencies, in the same manner as the impact frequencies, resemble a shifted parabolic pattern as the crossing angle increases from 0° to 165° . The peaks of these parabolic tendencies shift towards larger crossing angles as early bird range from late birds (EBt negative values) to early bird times (EBt positive values). Larger levels of damage are observed at late bird scenarios compared to early bird scenarios. It is also noted for increasing values of CA that the impact velocity decreases and the projectile impact the TBM surface at steeper strike angles.

- b) As the miss distance increases from 1.0 to 6.0 meters, the parabolic pattern flattens and the peaks also shift towards larger crossing angles. The overall tendencies observed confirm that at smaller distances, the total damage inflicted increases substantially resembling a direct hit to the TBM warhead.
- c) The minimum impact frequencies and damage levels occur at a crossing angle of 165° , regardless of miss distance. This scenario is when the EKV is in pursuit course towards the TBM.
- d) The general tendencies in the variation of total damage throughout the encounter configuration scenarios are the same between cylindrical geometry/sizes without tumbling although when tumbling effects are added, the total damage generated by the three cylindrical geometries is different than the damage generated without tumbling.
- e) Total damages generated when variability to the projectile ejection velocity is added are lower than without variability, except for a few isolated scenarios; however, the general tendencies in the variation of total damage throughout the encounter configuration scenarios are the same. Therefore, it is concluded that variability does have an effect on the level of damage inversely proportional to the amount of variability.
- f) The combined effect of tumbling and variability in radial ejection velocity is reflected in the total damages.
- g) The total damage per velocity range increases at higher impact velocity magnitudes.
- h) The strike angle under which the projectiles generate the most damage seems correlated with the magnitude of the impact velocity. The lower the velocity range the steeper the strike angle range. These tendencies are observed regardless of tumbling and radial ejection velocity variability.
- i) The matrices of total damage without tumbling effects show the diagonal pattern of higher damage levels (darker color regions) in every cell table over the range of radial ejection variability.
- j) From the impact characterization standpoint, in general, the total damage increases as the impact velocity increases.

7.4 Recommendations

The following recommendations are made:

- a) The study reported here was made using a fixed amount of warhead mass, projectile mass regardless of the size or shape, and a unique shape and dimensions of the TBM. Therefore, a tradeoff analysis between EKV warhead mass, projectile-mass, and projectile geometry, could be performed along with different sizes and shapes of TBMs. This will provide more insight in how these parameters influence lethality.

REFERENCES

- Allahdadi F.A., Medina F.D., Olson E.T. and Jeffers S. R., (1998) "Simulation of Impact Induced Detonation of AIM-120. A Novel Approach." Final Report AFSC-TR-2000-0002, Weapons, Space, and Nuclear Safety Division, AIR FORCE SAFETY CENTER, KIRTLAND AIR FORCE BASE, NM 87117-5670, August 1998.
- Anderson C. E., Orphal D. L., Franzen R. R., and Walker J. D., (1999) "On the hydrodynamic approximation for long-rod penetration." *International Journal of Impact Engineering*, Vol. 22, pp.23-43.
- Anderson C. E., Walker J. D., Bless S. J., and Partom .Y, (1996) "On the L/D effect for long-rod penetrators." *International Journal of Impact Engineering*, Vol. 18, pp.247-264.
- Beer F. P., and Johnston E. R., (1996) *Vector Mechanics for Engineers*, 6th Edition, McGraw-Hill Companies, Inc, New York.
- Birkhoff G., MacDougall DP, Pugh E. M., Taylor G., (1948) "Explosives with lined cavities." *Journal of Applied Phys*, Vol. 19, pp563-582.
- Bjerke T. W., Silsby G. F., Scheffler D. R., and Mudd R. M., (1992) "Yawed long-rod armor penetration." *International Journal of Impact Engineering*, Vol. 12, pp. 281-292.
- BMDO Fact Sheet, (1998) U.S. Department of Defense, Ballistic Missile Defense Organization, External Affairs.
- Campbell J., Vignjevic R., and Libersky L., (2000) "A contact algorithm for smoothed particle hydrodynamics." *Computer Methods in Applied Mechanics and Engineering*, Vol. 184, pp. 49-65.
- Carrasco C. J., (2000) "Development of a Constitutive Microdamage Model for Simulation of Damage and Fracture of Metallic Plates Caused by Hypervelocity Impact." Ph. D. Dissertation, The University of Texas at El Paso.-
- Carrasco C., Eftis J., and. Osegueda R. A, (2001) "Constitutive Modeling Of Spall-Fracture On 1100 Aluminum After Hypervelocity Impact," *Proceedings of EXPLOMET 2000 International Conference on Fundamental Issues and Applications of Shock -Wave and High-Strain-Rate Phenomena*, pp.467-474.

Carrasco C. J., and Osegueda R. A., (2001) "Modeling Hypervelocity Impact for Kill Enhancement of Ballistic Missile Warheads." Proposal for a Ballistic Research Grant BMDO.

Chocron S., Anderson C. E., Walker J. D. and Ravid M., (2003) "A unified model for long-rod penetration in multiple metallic plates." *International Journal of Impact Engineering*, Vol. 28, pp.391-411.

Christiansen E. L., Cykowski E., and Ortega J., (1993) "Highly oblique impacts into thick and thin plates." *International Journal of Impact Engineering*, Vol. 14, pp. 157-168.

Christiansen E. L., and Kerr J. H., (1997) "Projectile shape effects on shielding performance." *International Journal of Impact Engineering*, Vol. 20, pp. 165-172.

Christiansen E. L., and Kerr J. H., (2001) "Ballistic limit equations for spacecraft shielding." *International Journal of Impact Engineering*, Vol. 26, pp. 93-104.

Cour-Palais B. G., (2001) "The shape effect of non-spherical projectiles in hypervelocity impacts." *International Journal of Impact Engineering*, Vol. 26, pp. 129-143.

Deo M. C., and Jagdale S. S., (2003) "Prediction of breaking waves with neural networks." Vol. 30, pp. 1163-1178.

Dickinson D. L., and Wilson L. T., (1997) "The effect of impact orientation on the critical velocity needed to initiate a covered explosive charge." *International Journal of Impact Engineering*, Vol. 20, pp. 223-233.

Dickinson D. L., and Wilson L. T., (1999) "The impact of long rods into spaced-plate arrays." *International Journal of Impact Engineering*, Vol. 23, pp. 193-204.

Dvorak B. D., (1999) "Hypervelocity impact testing of the pressurized mating adapters for the International Space Station." *International Journal of Impact Engineering*, Vol. 23, pp. 215-224.

Eftis J., Carrasco C., and Osegueda R.A., (2003) "A Constitutive-Microdamage Model to Simulate Hypervelocity Projectile-Target Impact, Material Damage and Fracture." *International Journal of Plasticity*, Vol. 19 pp.132 -1354.

Eftis J., Carrasco C., and. Osegueda R.A., (2001) "Simulations of hypervelocity impact damage and fracture of aluminum targets using a constitutive-microdamage material model." *International Journal of Impact Engineering*, Volume 26, pp.157-168.

Espinosa H. D., Brar N. S., Yuan G., Xu Y., and Arrieta V., (2000) "Enhanced ballistic performance of confined multi-layered ceramic targets against long rod penetrators through interface defeat." *International Journal of Solids and Structures*, Vol. 37, pp. 4893-4913.

Gee D. J., and Littlefield D. L., (2001)"Yaw impact of rod projectiles." *International Journal of Impact Engineering*, Vol. 26, pp.211-220.

Gingold R. A., and Monaghan J. J., (1977) "Smoothed Particle Hydrodynamics: Theory and Application to non-spherical stars." *Monthly Notices of the Royal Astronomical Society*, Vol. 181, pp. 375-398.

Hagan M. T., Demuth H.B., and Beale M. H., *Neural Network Design*, Campus Publishing Service of the University of Colorado at Boulder, Boulder, Colorado.

Hayhurst C. J., Livingston I. H., Clegg R. A., Fairlie G. E., Hiermair S. J., and Lamber, M., (1998) "Numerical simulation of hypervelocity impacts on aluminum and Nextel/Kevlar Whipple shields." Presented at the *Hypervelocity Shielding Workshop* Galveston, Texas.

Haykin S. (1998) *Neural Networks: A comprehensive Foundation*, 2nd Edition, Prentice Hall, New York.

Holsapple K.A., (1993) "Hypervelocity impact experiments in surrogated materials." *International Journal of Impact Engineering*, Vol. 14, pp.335-345.

Hörz F., Bernhard R. P., and See T. H., (1995) "Hypervelocity Penetration in Aluminum 6061 and 1100 Alloys." *Metallurgical and Materials Applications of Shock-Wave and High-Strain-Rate Phenomena* (34), Murr L.E., Staudhammer K.P., and Meyers M.A. (Editors), Elsevier Science, pp. 273-283,

Johnson G.R., and Cook W.H. (1983) "A Constitutive Model and Data for Metals Subjected to Large Strains, High Strain Rates and High Temperatures." Presented at the Seventh International Symposium on Ballistics, The Hague, The Netherlands, April 1983.

Johnson G. R., and Cook W. H., (1993) "Lagrangian EPIC code computations for oblique, yawed-rod impacts onto thin-plates and spaced-plate targets at various velocities." *International Journal of Impact Engineering*, Vol. 14, pp. 373-383.

Jolly W. H., and Williamsen J. E., (1993) "Statistical ballistic limit curve regression for space station freedom meteoroid/orbital debris shielding." *International Journal of Impact Engineering*, Vol. 14, pp. 395-406.

Lee S. C., (2003) "Prediction of concrete strength using artificial neural networks." *Engineering Structures*, Vol. 25, pp. 849-857.

Lloyd R. M., (1998) *Conventional Warhead Systems Physics and Engineering Design*,. Progress in Astronautics and Aeronautics Vol. 179, American Institute of Aeronautics and Astronautics Inc, Reston, Virginia.

Lloyd R. M., (2000) *Lethality of Rod Warheads against Ballistic Missiles. Raytheon Final Technical Report BR-27007*, Raytheon Electronic Systems, Tewksbury, Massachusetts.

Li K., and Goldsmith W., (1997) "Perforation of steel and polycarbonate plates by tumbling projectiles." *International Journal of Solids Structures*, Vol. 34/35-36, pp. 4581-4596.

Li K., and Goldsmith W., (1996) "Impact on aluminum plates by tumbling projectiles: Experimental Study." *International Journal of Impact Engineering*, Vol. 18/1, pp. 23-43.

Libersky L. D., Petschek A. G., Theodore C. C., Hipp J. R., and Allahdadi F. A., (1993) "High Strain Lagrangian Hydrodynamics." *Journal of Computational Physics*, Vol. 109, pp. 67-75.

Lucy L.B., (1977) "A numerical approach to the testing of the fission hypothesis." *The Astronomical Journal*, Vol. 82, pp. 1013-1024.

Malvern L. E., (1969) *Introduction to the Mechanics of a Continuous Medium*, Prentice-Hall, Inc., Englewood Cliffs, New Jersey.

Mase G. E., (1970) *Schaum's Outline of Theory and Problems of Continuum Mechanics*, Mc Graw Hill, New York.

Matlab Documentation, Matlab 6.5 software, The Mathworks Inc.

Monaghan J. J., (1988) "An Introduction to SPH." *Computer Physics Communications*, Vol. 48, pp. 89-96.

Monaghan J. J., (1992) "Smoothed Particle Hydrodynamics." *Annual Reviews of Astronomical Astrophysics*, Vol. 30, pp. 543-574.

Nazarian S., Abdallah I., Ferregut C. M., and Melchor-Lucero O., (1999) "Prediction of remaining life of flexible pavements with Artificial Neural Networks." *Nondestructive Testing of Pavements and Backcalculation of Moduli: Vol. 3, ASTM STP 1735*, pp. 484-498.

Osegueda R. A., Carrasco C. J., Orozco M., Eftis J., Reynolds E., and Sholar T.G., (2001) "CONTOUR Dust Shield Performance," *ASCE J. Aerospace Engineering*, Vol. 14/4, pp. 147-157.

Randles P. W., and Libersky L. D., (2000) "Normalized SPH with stress points." *Journal of Numerical Methods in Engineering*, Vol. 148, pp. 1445-1462.

Rosenberg Z., Bless S. J., Gallagher J. P., (1987) "A model for hydrodynamic ram failure based on fracture mechanics analysis." *International Journal of Impact Engineering*, Vol. 6, pp. 51-61.

Rosenberg Z. and Dekel E., (1994) "The relation between the penetration capability of long rods and their length to diameter ratio." *International Journal of Impact Engineering*, Vol. 15, pp.125-129.

Rosenberg Z. and Dekel E., (2000) "Further examination of long rod penetration: the role penetrator strength at hypervelocity impacts." *International Journal of Impact Engineering*, Vol. 24, pp.85-102.

Segletes S. B., and Walters W. P., (2003) "Extensions to the exact solution of the long-rod penetration/erosion equations." Vol 28, pp. 363-376.

Spiegel M.R., (1991) *Schaum's Outline of Theory and Problems of Vector Analysis and an Introduction to Tensor Analysis*, 27th Printing, McGraw-Hill, New York.

Swift H. F., (1982) Impact Dynamics, 1st Edition, "Chapter 6: Hypervelocity Impact Mechanics." Zukas J. A., Nicholas T., Swift H. F., Greszczuk L. B., and Curran D. R. (Editors), pp. 215 – 239, Wiley Publications, New York.

Tate A., (1967) "A theory for the deceleration of long rods after impact." *Journal of the Mechanics and Physics of Solids*, Vo. 15, pp.387-399.

Tate A., (1969) "Further results is the theory of long rod penetration." *Journal of the Mechanics and Physics of Solids*, Vo. 17, pp.141-150.

Tate A., (1986) "Long rod penetration models-Part II Extensions to the hydrodynamic theory of penetration." *International Journal of Mechanical Sciences*, Vol. 28, pp.599-612.

Walker J. D. and Anderson CE, (1995) "A time-dependent model for long-rod penetration." *International Journal of Impact Engineering*, Vol. 16, pp.19-48.

Zukas J. A., (1982) Impact Dynamics, 1st Edition, "Chapter 10: Numerical Simulation of Impact Phenomena." Zukas J. A., Nicholas T., Swift H. F., Greszczuk L. B., and Curran D. R. (Editors), pp. 367 – 417, Wiley Publications, New York.

Zukas J. A., (1993) "Some common problems in the numerical modeling of impact phenomena." *Computing Systems in Engineering*, Vol. 4, No. 1, pp. 43-58.

Zukas J. A., and Scheffler D. R., (2001) "Impact effects in multilayered plates." *International Journal of Solids and Structures*, Vol. 38, pp. 3321-3328.

Zukas J. A., and Segletes S. B., (1992) "Numerical modeling of hypervelocity impact phenomena with desktop computers." *Advances in Engineering Software*, Vol. 14, pp. 77-84.

APPENDIX A

IMPACT DISTRIBUTION TABLES

Table A.1. Impact Distribution per Encounter Configuration for a Spherical Projectile Without Radial Ejection Velocity
Variability @ $EBt = -0.0012$

L/D=Sphere MD/CA	Early 0	15	30	45	60	75	90	105	120	135	150	165	Sum
1	400	262	145	74	50	36	20	12	8	4	4	0	1015
1.5	168	146	114	72	52	30	20	12	8	6	4	0	632
2	86	78	70	55	38	26	20	12	8	6	2	0	401
2.5	52	58	54	43	32	26	16	11	8	6	4	0	310
3	36	43	43	38	29	26	19	12	8	6	4	0	264
3.5	28	34	36	32	27	24	16	12	8	6	4	0	227
4	20	28	30	29	24	20	16	12	8	4	4	0	195
4.5	16	24	28	26	24	18	16	12	8	6	2	0	180
5	12	22	26	26	22	20	16	12	8	6	4	0	174
5.5	12	18	24	20	20	16	14	12	8	6	4	0	154
6	4	18	20	21	19	16	12	10	8	6	4	0	138
sum	834	731	590	436	337	258	185	129	88	62	40	0	3690

Table A.2. Impact Distribution per Encounter Configuration for a Spherical Projectile Without Radial Ejection Velocity
Variability @ $EBt = -0.0090$

L/D=Sphere MD/CA	Early 0	15	30	45	60	75	90	105	120	135	150	165	Sum
1	400	372	255	181	123	85	58	40	24	18	4	0	1560
1.5	168	163	169	146	108	77	58	39	26	16	6	0	976
2	86	98	112	110	94	76	52	35	24	15	6	2	710
2.5	52	60	78	77	72	66	45	32	24	14	6	0	526
3	36	46	51	54	54	49	46	34	24	10	6	2	412
3.5	28	38	42	46	44	40	34	34	26	12	4	1	349
4	20	28	34	40	38	36	32	27	20	12	6	0	293
4.5	16	26	30	34	34	32	28	26	17	9	6	2	260
5	12	24	28	30	31	29	26	24	18	12	6	0	240
5.5	12	18	22	26	28	26	26	22	16	10	6	2	214
6	4	16	18	24	24	24	23	20	16	8	6	2	185
sum	834	889	839	768	650	540	428	333	235	136	62	11	5725

Table A.3. Impact Distribution per Encounter Configuration for a Spherical Projectile Without Radial Ejection Velocity
Variability @ $EBt = 0.0000$

L/D=Sphere MD/CA	Early	Bird Time= 0.0000	45	60	75	90	105	120	135	150	165	Sum
1	400	114	98	94	84	85	70	60	39	32	20	1146
1.5	168	75	69	77	76	71	70	60	38	36	18	806
2	86	67	58	66	73	64	63	58	40	34	16	673
2.5	52	39	40	58	59	61	56	54	41	32	18	558
3	36	28	40	50	47	52	48	52	37	29	16	483
3.5	28	18	38	46	42	50	48	45	34	32	18	441
4	20	18	20	36	31	38	43	40	32	32	18	368
4.5	16	14	18	25	21	31	40	38	32	28	18	319
5	12	16	14	14	18	22	37	36	32	32	18	287
5.5	12	12	14	10	14	20	31	32	32	30	18	257
6	4	12	10	10	12	16	26	30	32	28	18	228
sum	834	413	419	486	477	510	532	505	389	345	196	5566

Table A.4. Impact Distribution per Encounter Configuration for a Spherical Projectile Without Radial Ejection Velocity
Variability @ $EBt = 0.0030$

L/D=Sphere MD/CA	Early	Bird Time= 0.0030	45	60	75	90	105	120	135	150	165	Sum
1	400	50	31	34	28	20	16	16	15	12	8	646
1.5	168	46	38	35	28	20	18	16	16	12	6	424
2	86	57	44	28	27	22	18	16	16	12	8	352
2.5	52	38	37	22	30	22	16	14	15	12	6	279
3	36	21	32	19	28	23	16	19	12	12	6	240
3.5	28	19	30	16	25	20	17	16	16	10	6	217
4	20	15	26	16	18	20	16	14	14	12	8	193
4.5	16	12	16	12	16	20	16	13	11	14	6	164
5	12	13	15	8	14	20	16	15	14	12	8	159
5.5	12	13	14	8	14	18	14	12	14	12	6	149
6	4	12	6	8	12	17	14	14	11	14	8	134
sum	834	296	289	206	240	222	177	164	154	134	76	2957

Table A.5. Impact Distribution per Encounter Configuration for a Spherical Projectile Without Radial Ejection Velocity Variability @ $EBt + 0.006$

L/D=Sphere	Early	Bird Time= 0.0060													Sum
MD/CA	0	15	30	45	60	75	90	105	120	135	150	165			
1	400	30	33	22	16	14	12	8	6	6	4	2	553		
1.5	168	33	17	24	20	12	10	8	6	4	4	5	311		
2	86	42	14	24	16	14	10	8	6	4	6	6	236		
2.5	52	32	14	22	20	16	10	8	6	4	4	2	190		
3	36	21	14	14	16	12	10	8	6	4	4	6	151		
3.5	28	14	10	12	16	14	10	8	6	4	5	5	132		
4	20	12	13	10	16	12	10	8	6	4	4	2	117		
4.5	16	12	6	12	18	16	10	8	6	4	6	4	118		
5	12	12	6	8	10	14	10	8	6	4	2	5	97		
5.5	12	8	6	8	10	14	10	8	6	4	4	2	92		
6	4	10	6	8	10	14	12	8	6	4	6	4	92		
sum	834	226	139	164	168	152	114	88	66	46	49	43	2089		

Table A.6. Impact Distribution per Encounter Configuration for a Spherical Projectile Without Radial Ejection Velocity Variability @ $EBt + 0.009$

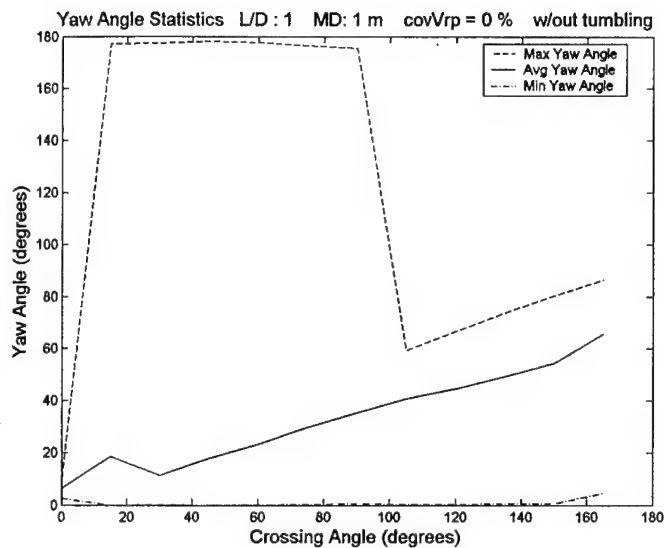
L/D=Sphere MD/CA	Early	Bird Time= 0.0090														Sum
	0	15	30	45	60	75	90	105	120	135	150	165				
1	400	22	24	18	14	12	8	6	6	4	2	0	516			
1.5	168	22	16	18	14	10	8	6	6	4	2	2	276			
2	86	29	10	16	12	10	8	6	6	2	2	4	191			
2.5	52	26	10	16	12	10	8	6	6	4	2	4	156			
3	36	16	10	14	14	10	8	6	6	4	2	0	126			
3.5	28	12	10	12	12	10	8	6	6	4	2	2	112			
4	20	10	8	8	14	10	8	6	6	2	2	4	98			
4.5	16	10	6	8	12	10	8	6	6	4	2	3	91			
5	12	10	4	6	12	10	8	6	6	4	2	0	80			
5.5	12	10	6	6	12	10	8	6	6	2	2	2	82			
6	4	12	6	6	10	11	8	6	6	4	2	4	79			
sum	834	179	110	128	138	113	88	66	66	38	22	25	1807			

Table A.7. Impact Distribution per Encounter Configuration for a Spherical Projectile Without Radial Ejection Velocity
 Variability @ $EBt + 0.012$

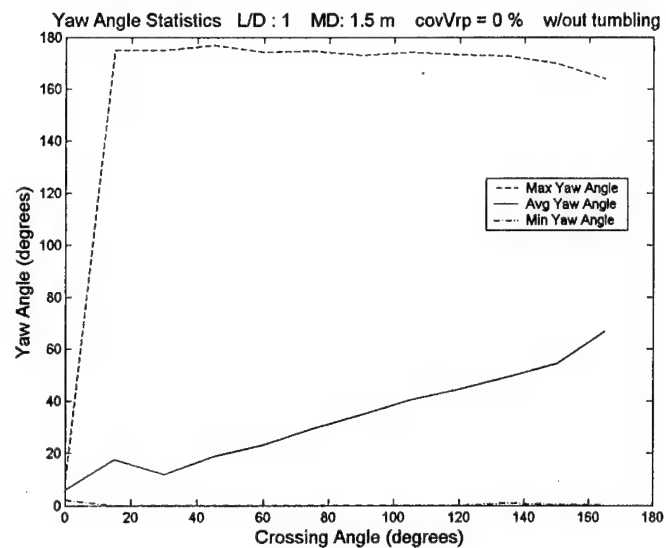
L/D=Sphere MD/CA	Bird Time= 0.0120												Sum
	0	15	30	45	60	75	90	105	120	135	150	165	
1	400	14	20	14	10	8	6	6	4	2	2	0	486
1.5	168	17	12	14	10	8	6	4	4	2	2	0	247
2	86	23	11	14	12	8	6	4	4	4	2	0	174
2.5	52	19	10	14	10	10	6	4	4	2	2	2	135
3	36	10	8	14	10	8	8	4	2	4	2	2	108
3.5	28	11	7	10	12	8	6	4	4	2	2	0	94
4	20	10	6	8	12	8	6	6	4	2	2	0	84
4.5	16	10	4	8	12	10	8	6	4	4	0	0	82
5	12	10	5	8	12	8	6	6	4	2	2	2	77
5.5	12	8	4	6	12	10	6	6	4	4	2	2	76
6	4	9	4	6	10	8	8	6	4	2	2	0	63
sum	834	141	91	116	122	94	72	56	42	30	20	8	1626

APPENDIX B

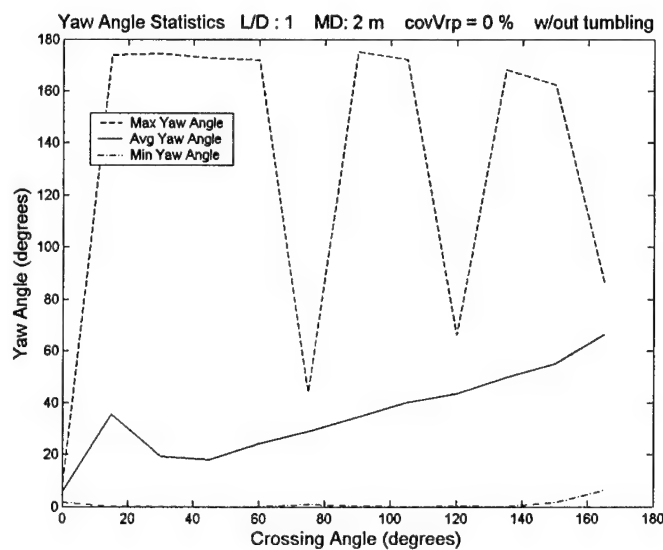
YAW ANGLE STATISTICS CHARTS



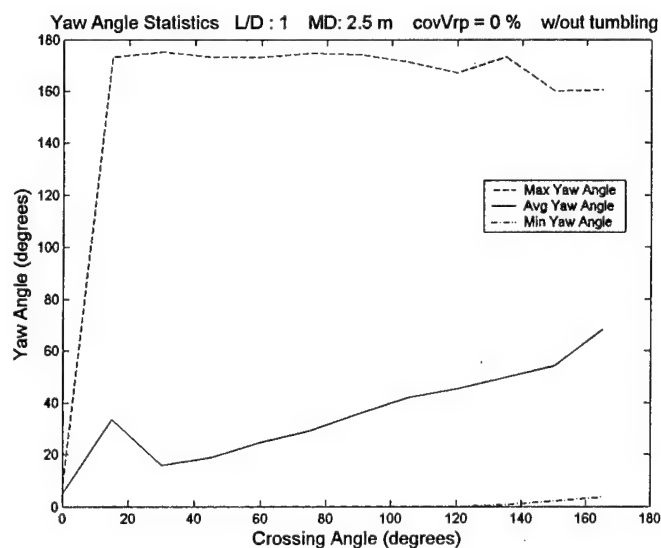
a)



b)

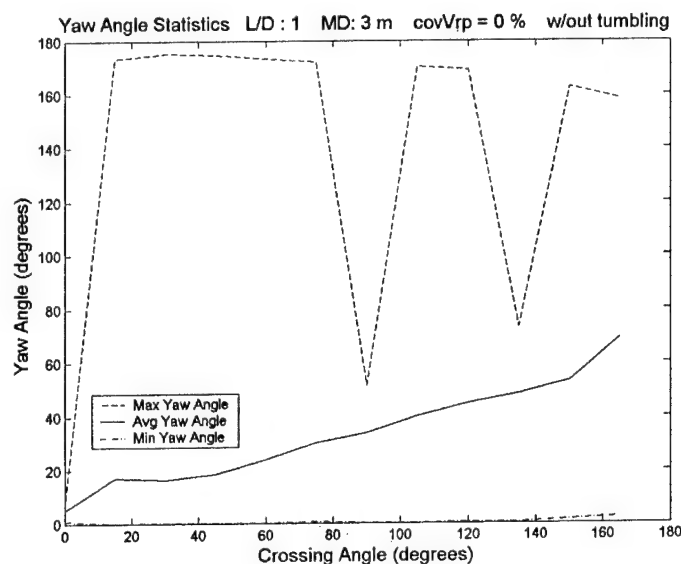


c)

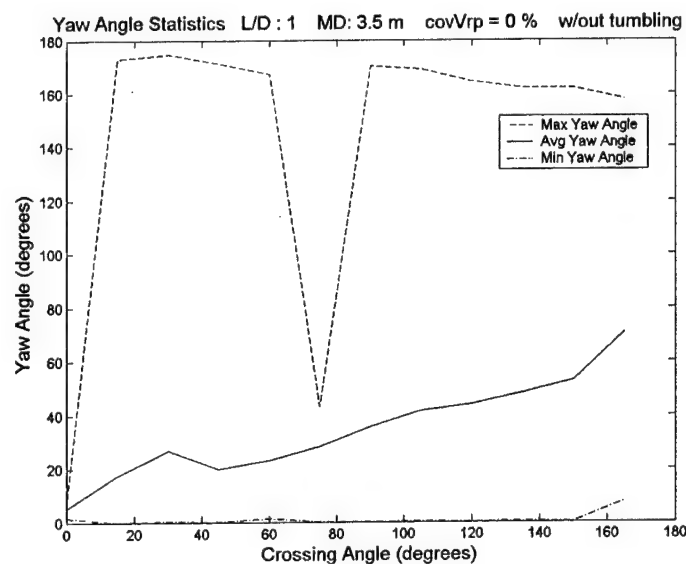


d)

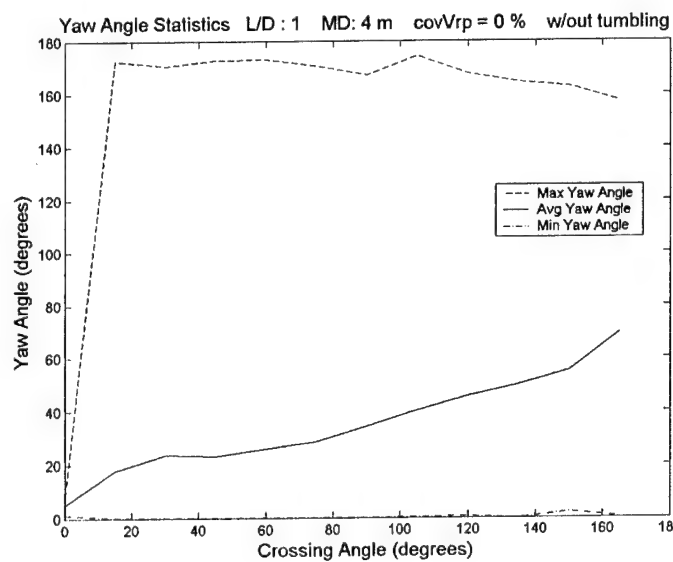
Figure B.1. Yaw Angle Statistics for Cylindrical Projectiles $L/D = 1$ vs. Crossing Angle at miss distances of 1m, 1.5m, 2m, 2.5m (a, b, c, d, respectively).



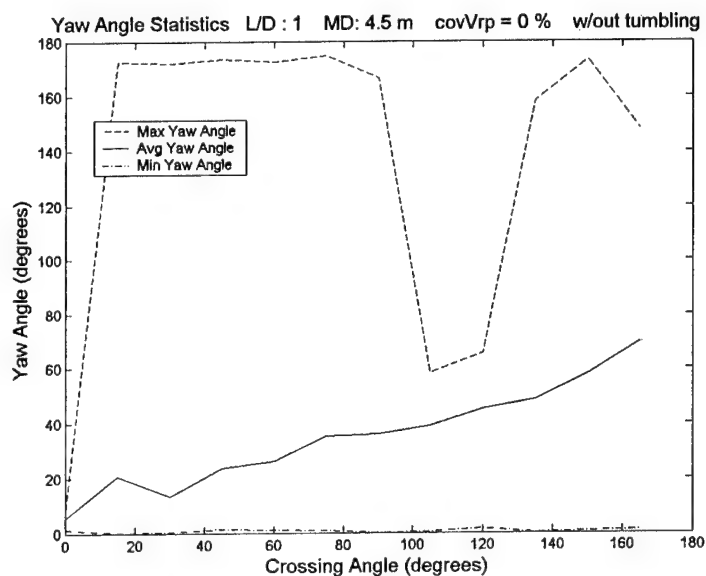
a)



b)

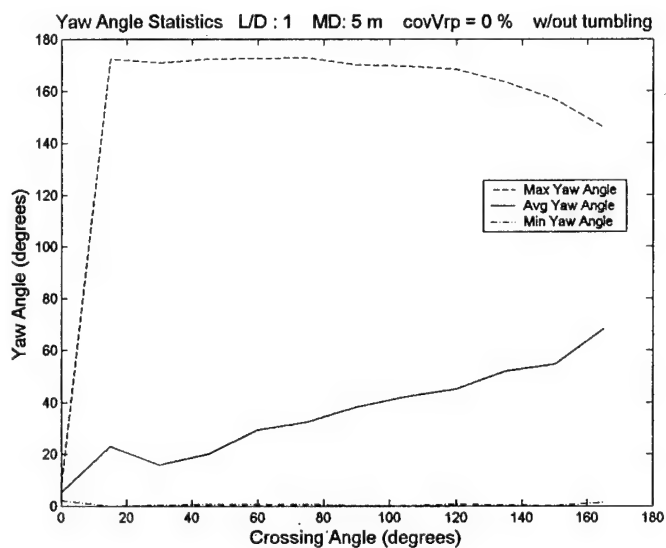


c)

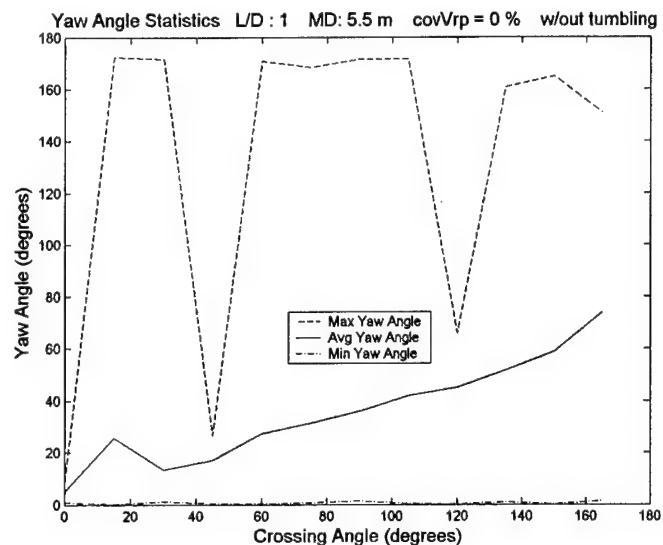


d)

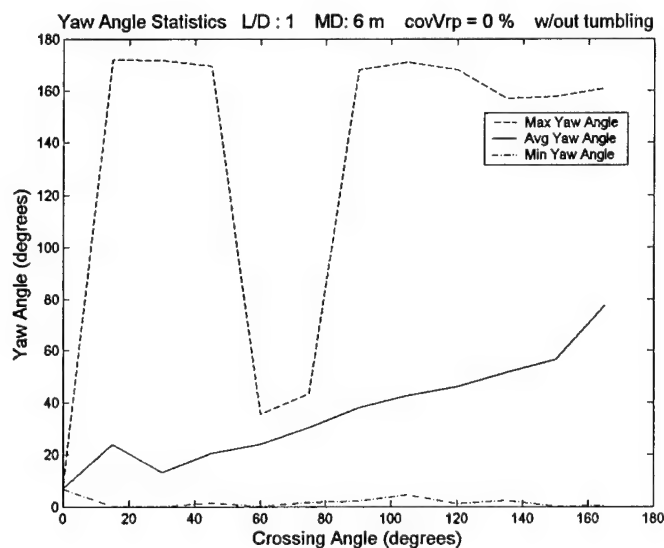
Figure B.2. Yaw Angle Statistics for Cylindrical Projectiles $L/D = 1$ vs. Crossing Angle at miss distances of 3m, 3.5m, 4m, 4.5m (a, b, c, d, respectively).



a)

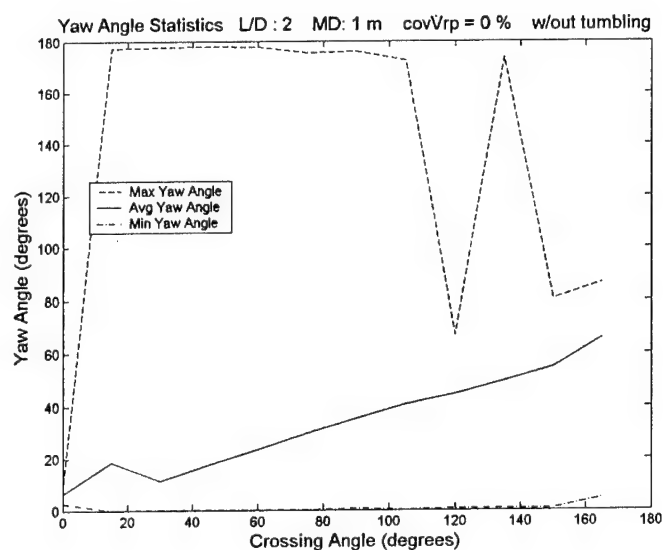


b)

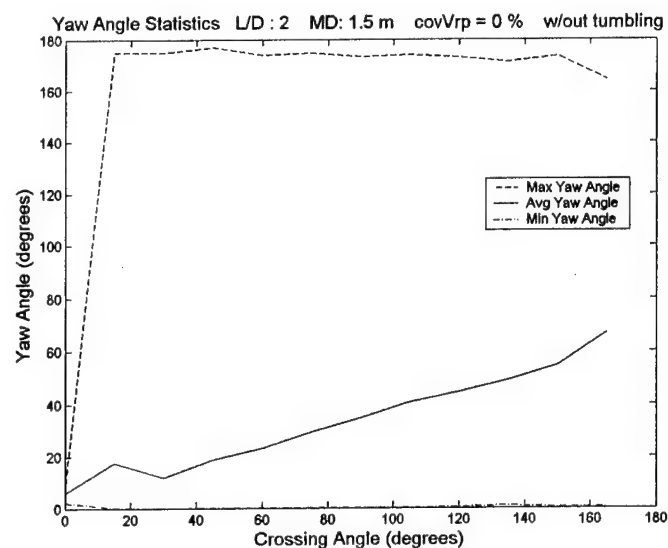


c)

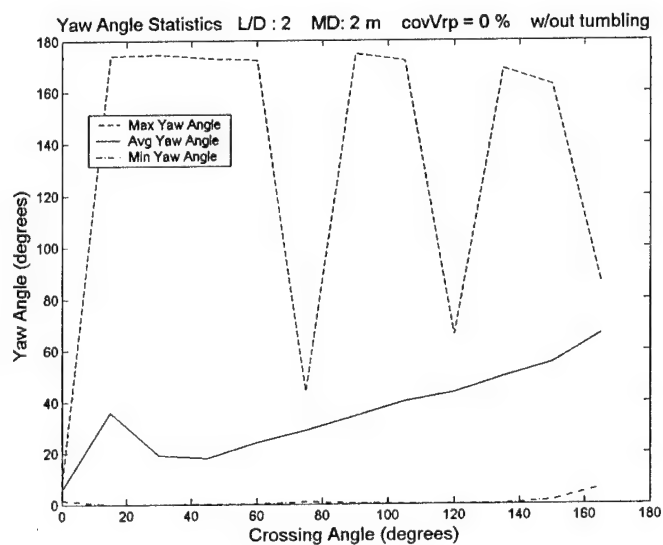
Figure B.3. Yaw Angle Statistics for Cylindrical Projectiles $L/D = 1$ vs. Crossing Angle at miss distances of 5m, 5.5m, 6m (a, b, c, respectively)



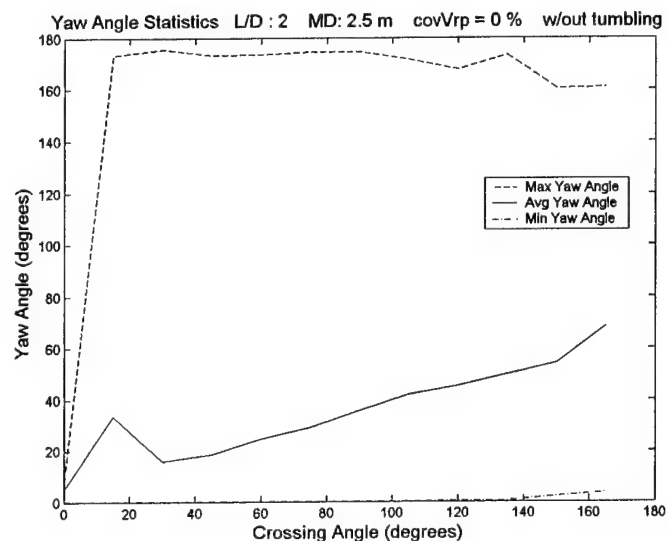
a)



b)

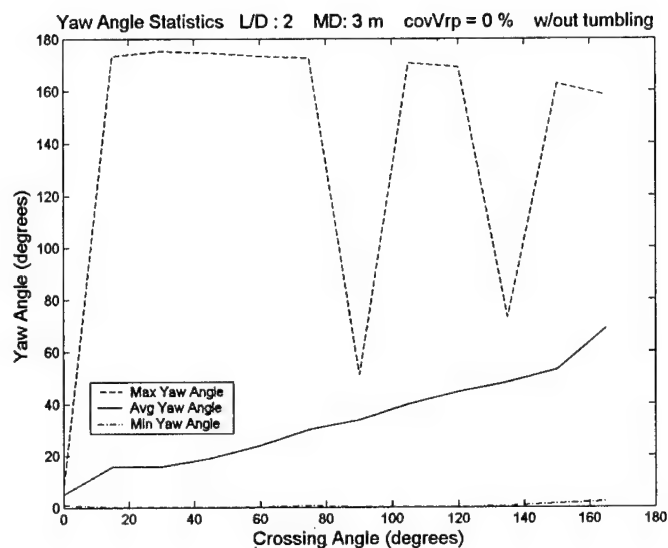


c)

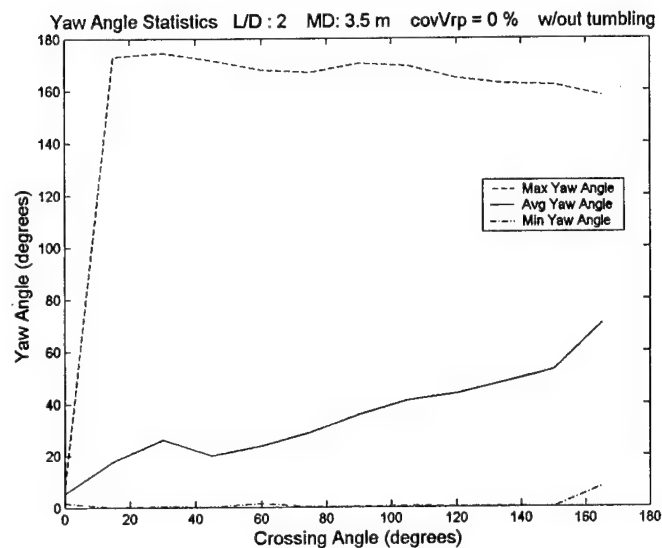


d)

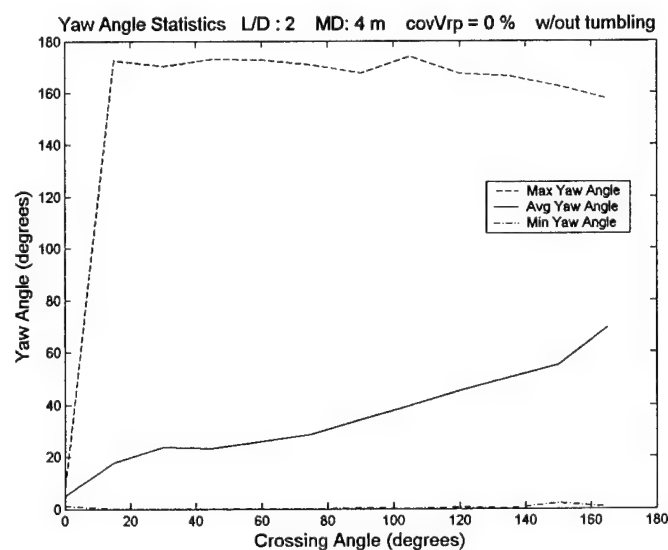
Figure B.4. Yaw Angle Statistics for Cylindrical Projectiles $L/D = 2$ vs. Crossing Angle at miss distances of 1m, 1.5m, 2m, 2.5m (a, b, c, d, respectively).



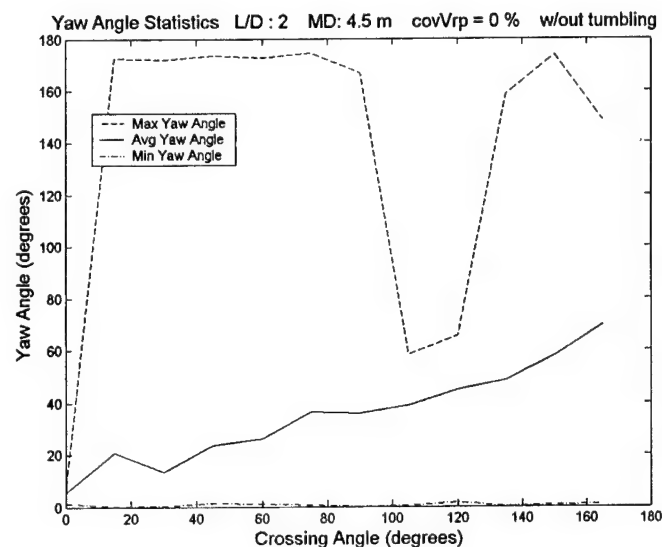
a)



b)

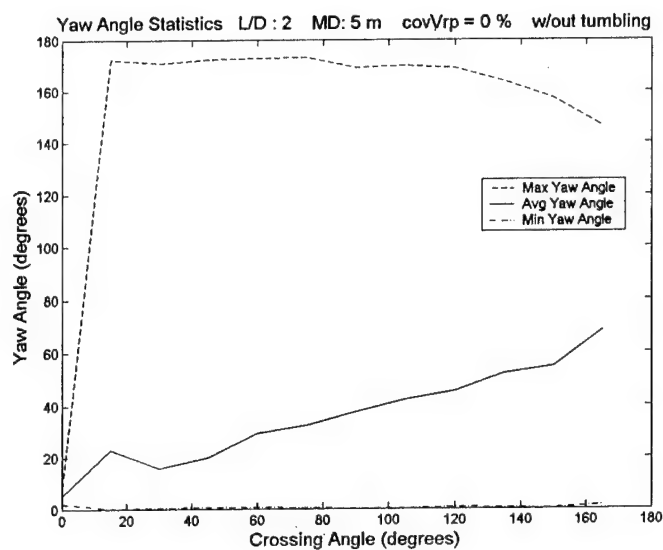


c)

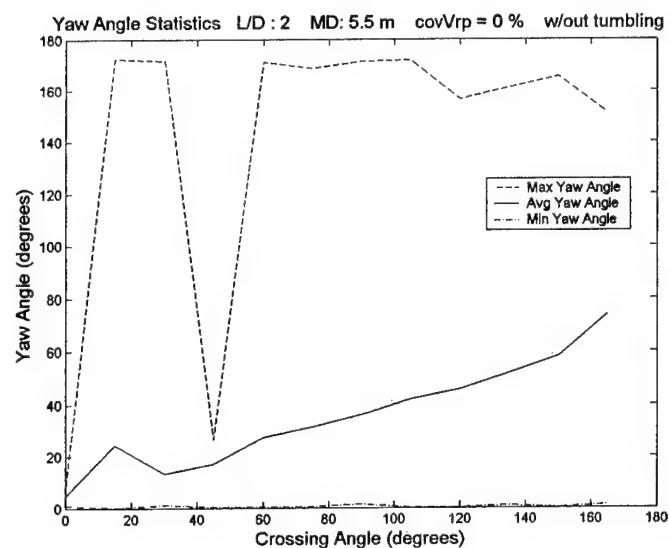


d)

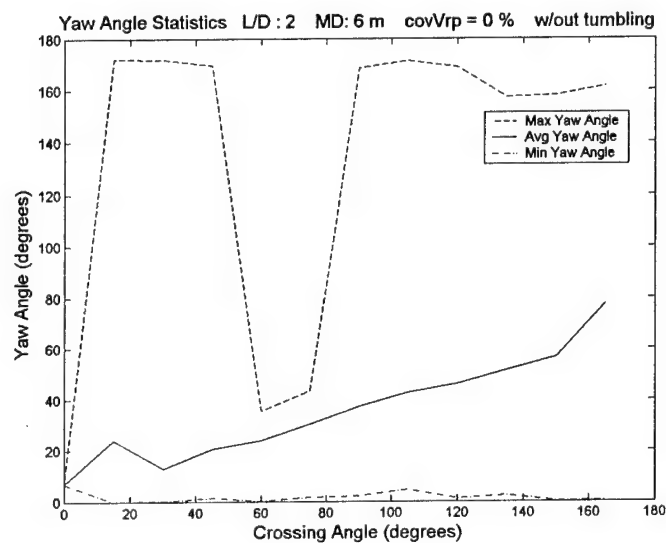
Figure B.5 Yaw Angle Statistics for Cylindrical Projectiles $L/D = 2$ vs. Crossing Angle at miss distances of 3m, 3.5m, 4m, 4.5m (a, b, c, d, respectively).



a)

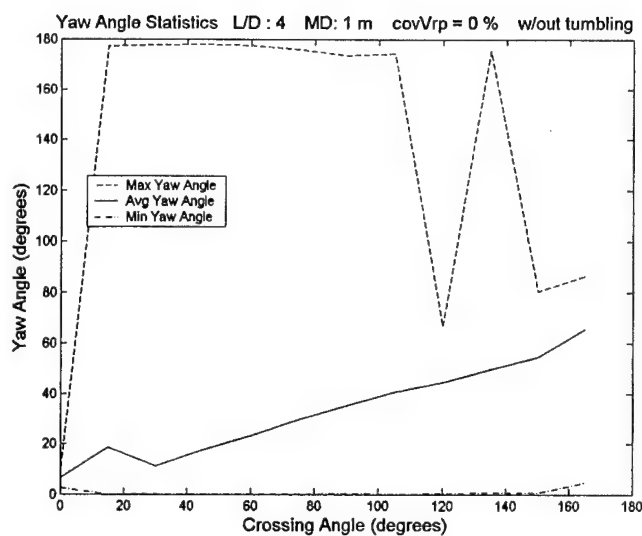


b)

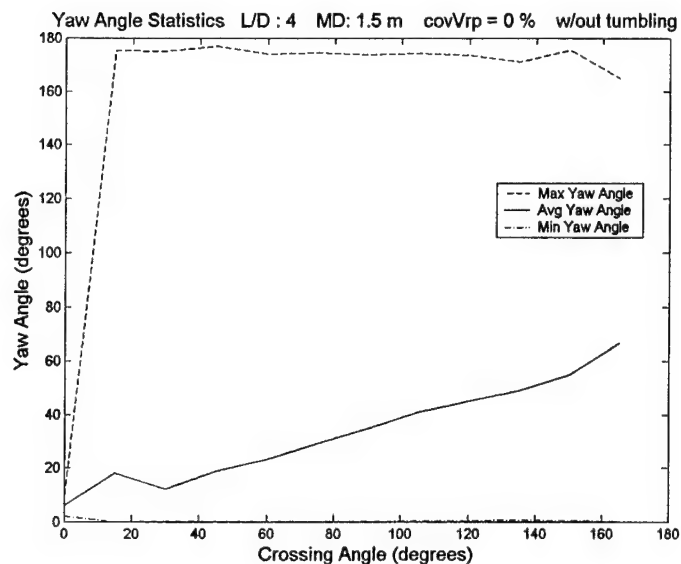


c)

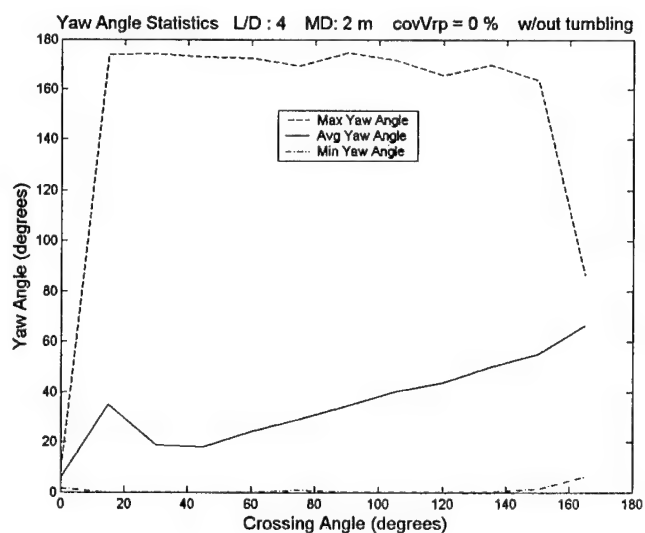
Figure B.6. Yaw Angle Statistics for Cylindrical Projectiles $L/D = 2$ vs. Crossing Angle at miss distances of 5m, 5.5m, 6m (a, b, c, respectively).



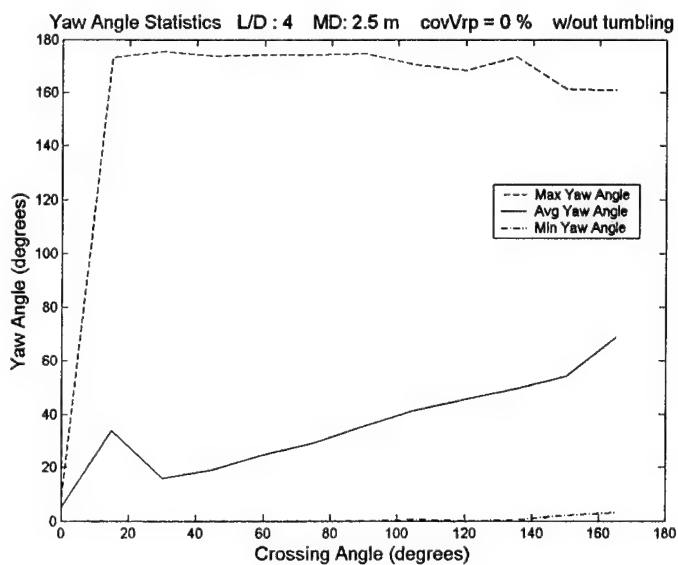
a)



b)

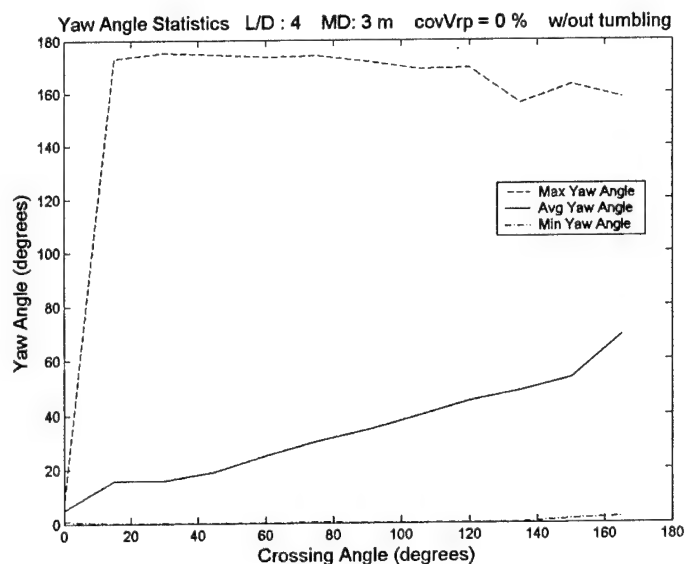


c)

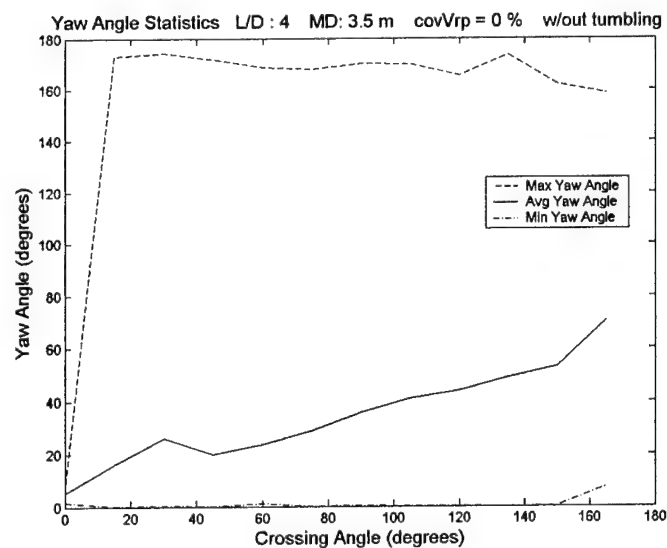


d)

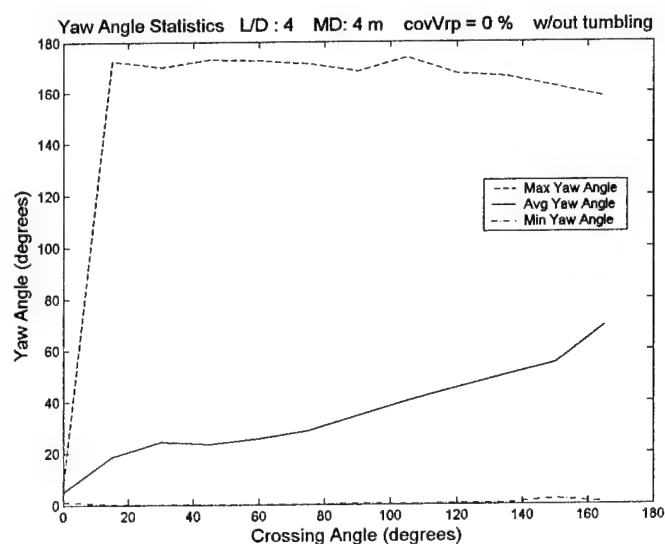
Figure B.7. Yaw Angle Statistics for Cylindrical Projectiles $L/D = 4$ vs. Crossing Angle at miss distances of 1m, 1.5m, 2m, 2.5m (a, b, c, d, respectively).



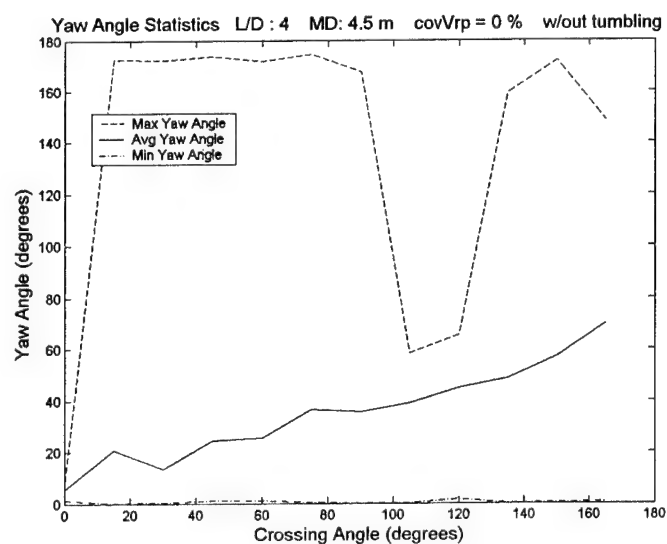
a)



b)

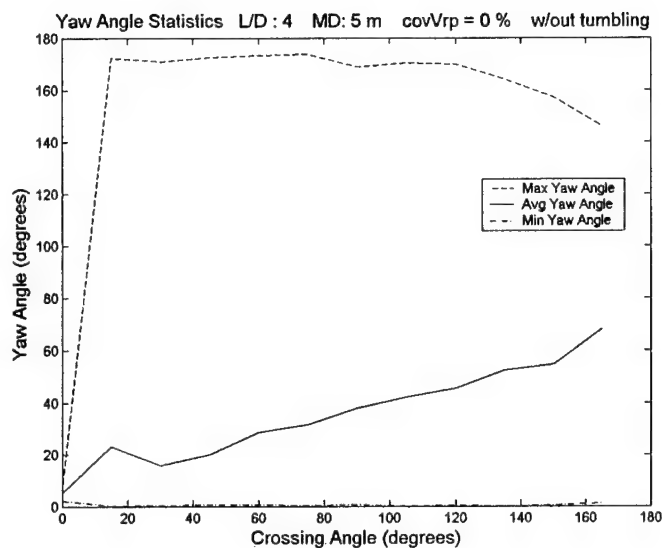


c)

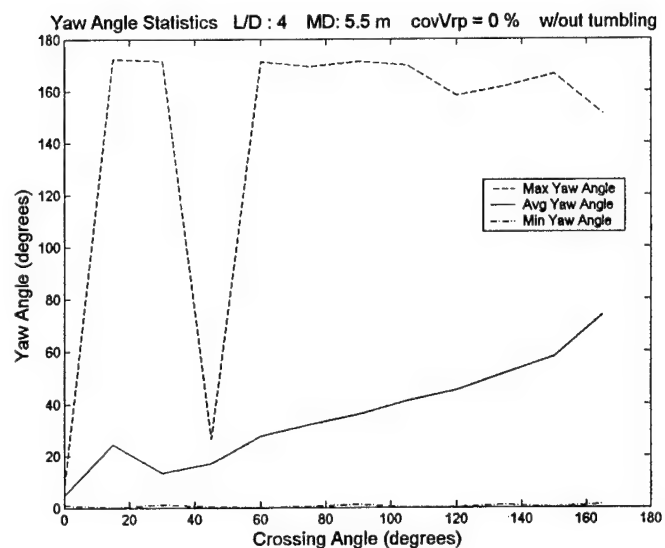


d)

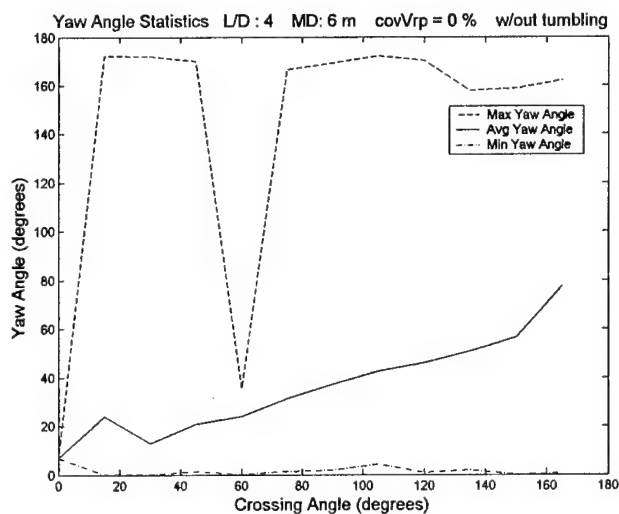
Figure B.8. Yaw Angle Statistics for Cylindrical Projectiles $L/D = 4$ vs. Crossing Angle at miss distances of 3m, 3.5m, 4m, 4.5m (a, b, c, d, respectively).



a)



b)



c)

Figure B.9. Yaw Angle Statistics for Cylindrical Projectiles $L/D = 4$ vs. Crossing Angle at miss distances of 5m, 5.5m, 6m (a, b, c, respectively).

APPENDIX C

YAW ANGLE FREQUENCY DISTRIBUTION CHARTS

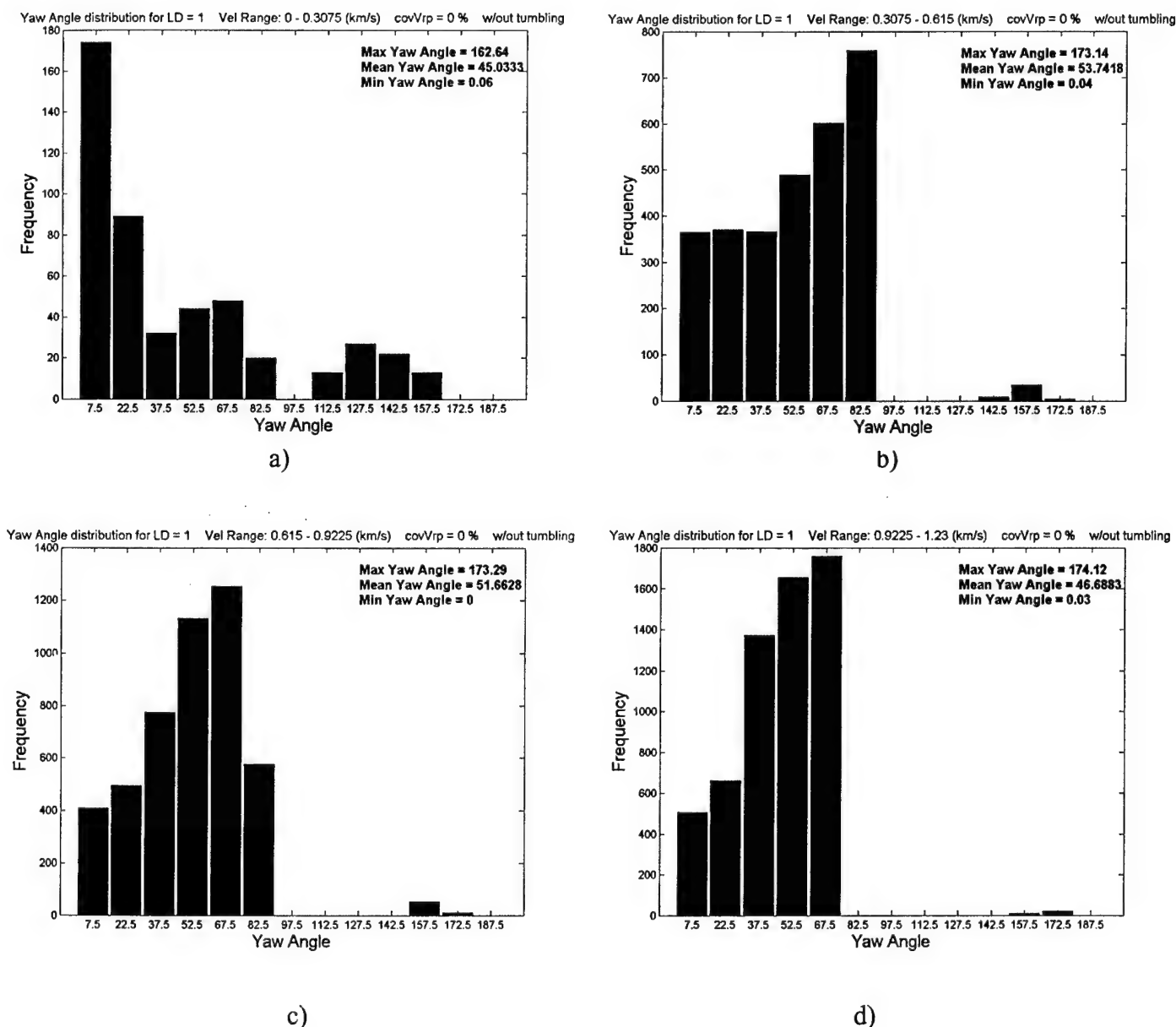
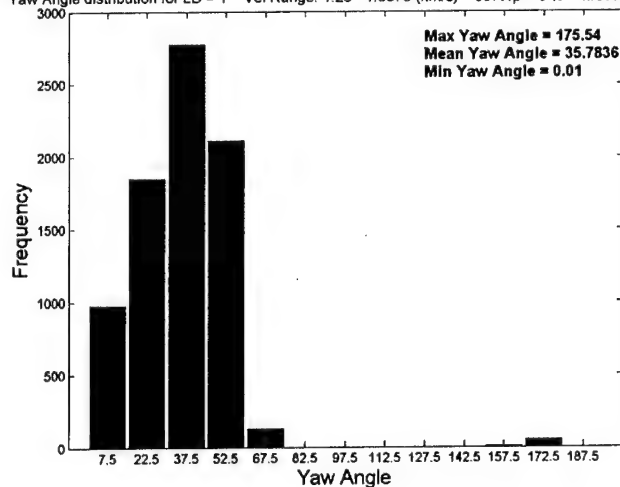


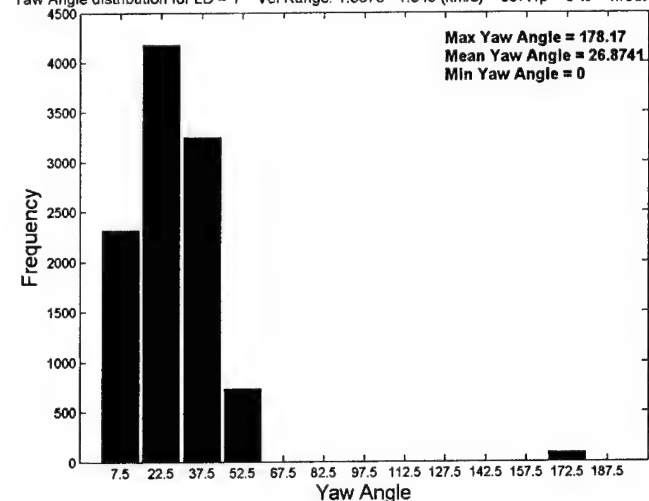
Figure C.1. Yaw Angle Frequency Distribution per Impact Velocity Ranges of 0-0.3075 km/s, 0.3075-0.615 km/s, 0.615-0.9225 km/s, 0.9225-1.23 km/s (a, b, c, d respectively) for Cylindrical Projectiles $L/D = 1$, Without Radial Ejection Velocity Variability.

Yaw Angle distribution for LD = 1 Vel Range: 1.23 - 1.5375 (km/s) covVrp = 0 % w/out tumbling



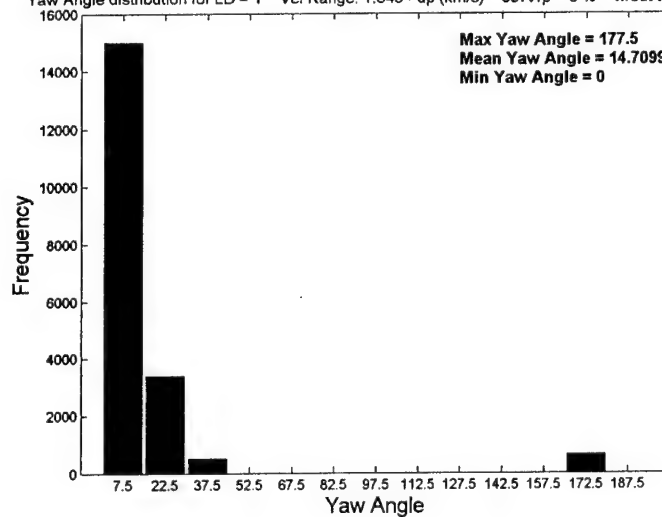
a)

Yaw Angle distribution for LD = 1 Vel Range: 1.5375 - 1.845 (km/s) covVrp = 0 % w/out tumbling



b)

Yaw Angle distribution for LD = 1 Vel Range: 1.845 - up (km/s) covVrp = 0 % w/out tumbling



c)

Figure C.2. Yaw Angle Frequency Distribution per Impact Velocity Ranges of 1.23-1.5375 km/s, 1.5375-1.845 km/s, 1.845-up km/s (a, b, c respectively) for Cylindrical Projectiles $L/D = 1$, Without Radial Ejection Velocity Variability.

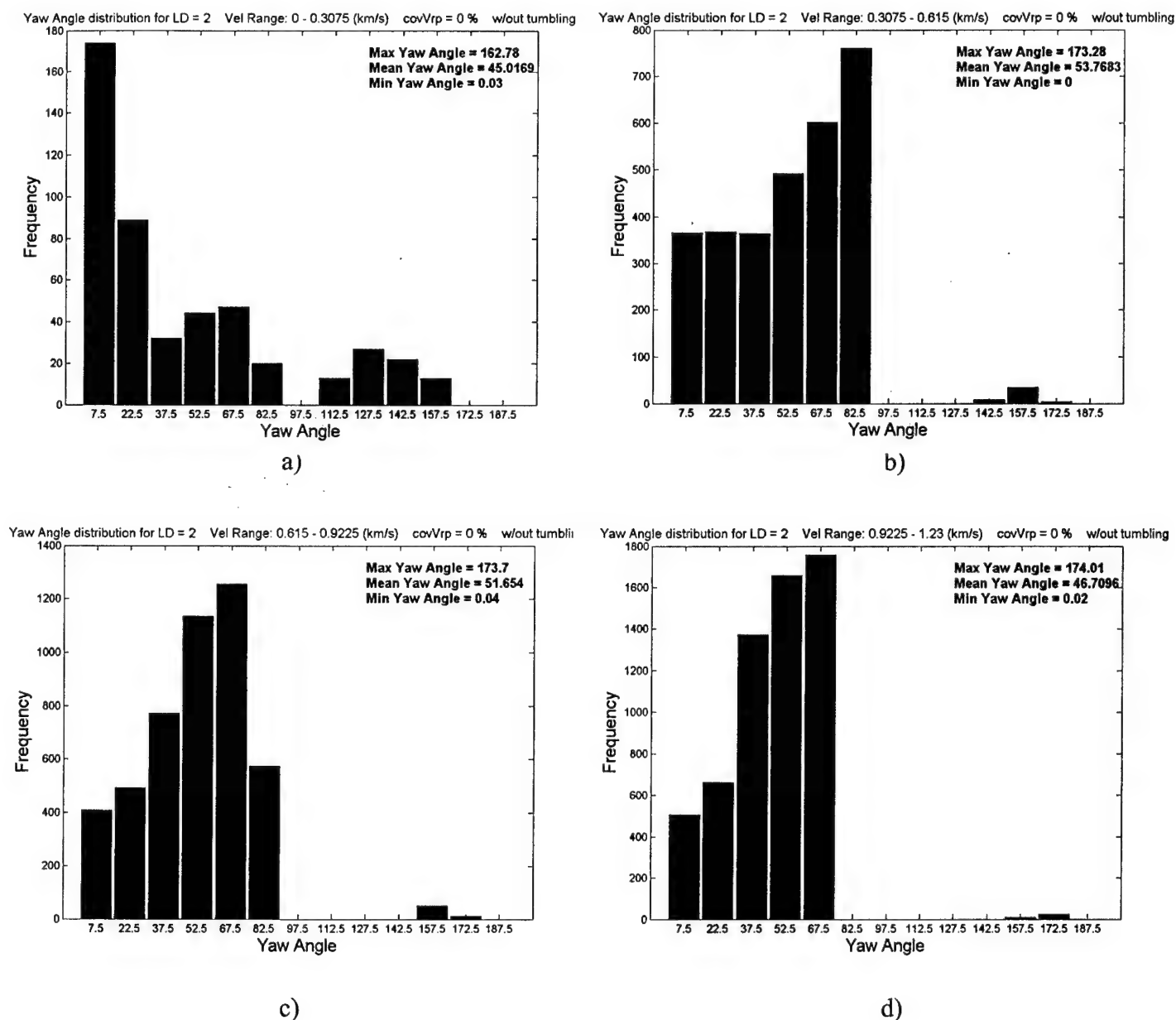


Figure C.3. Yaw Angle Frequency Distribution per Impact Velocity Ranges of 0-0.3075 km/s, 0.3075-0.615 km/s, 0.615-0.9225 km/s, 0.9225-1.23 km/s (a, b, c, d respectively) for Cylindrical Projectiles $L/D = 2$, Without Radial Ejection Velocity Variability.

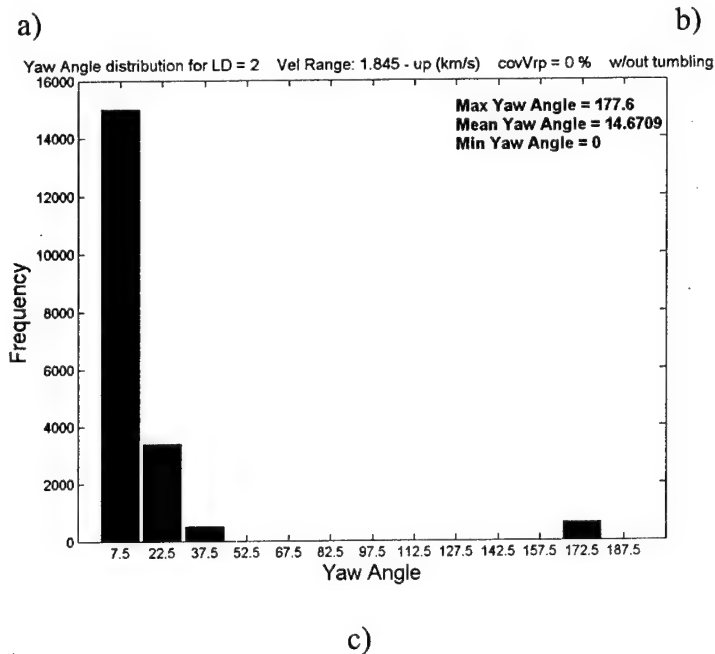
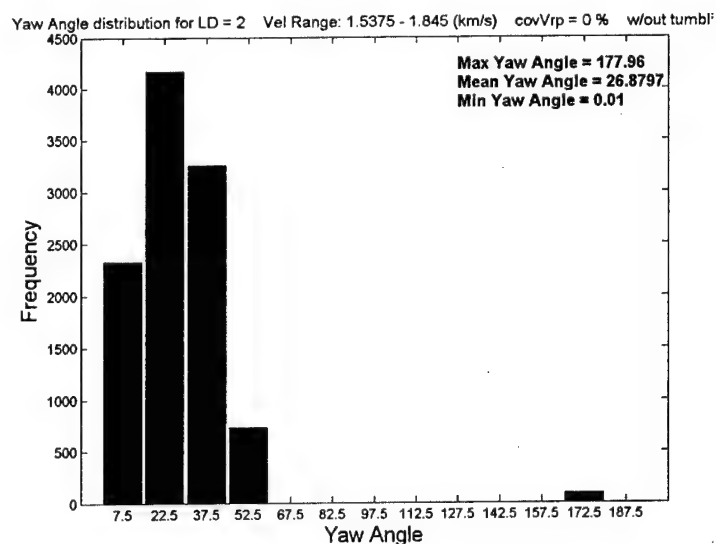
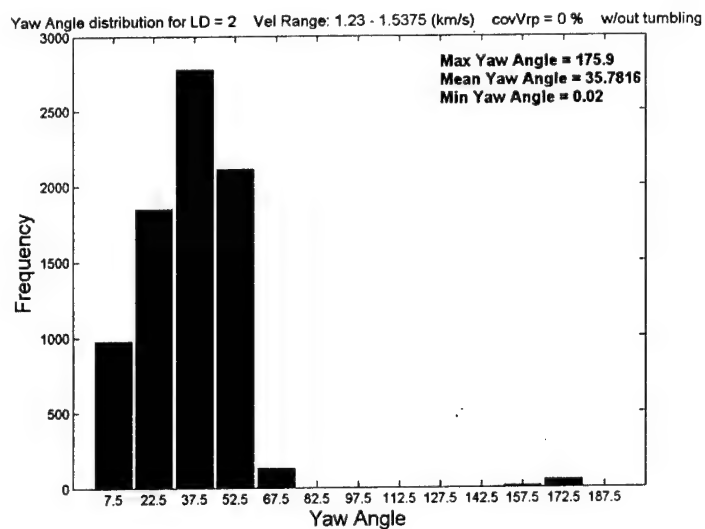


Figure C.4. Yaw Angle Frequency Distribution per Impact Velocity Ranges of 1.23-1.5375 km/s, 1.5375-1.845 km/s, 1.845-up km/s (a, b, c respectively) for Cylindrical Projectiles $L/D = 2$, Without Radial Ejection Velocity Variability.

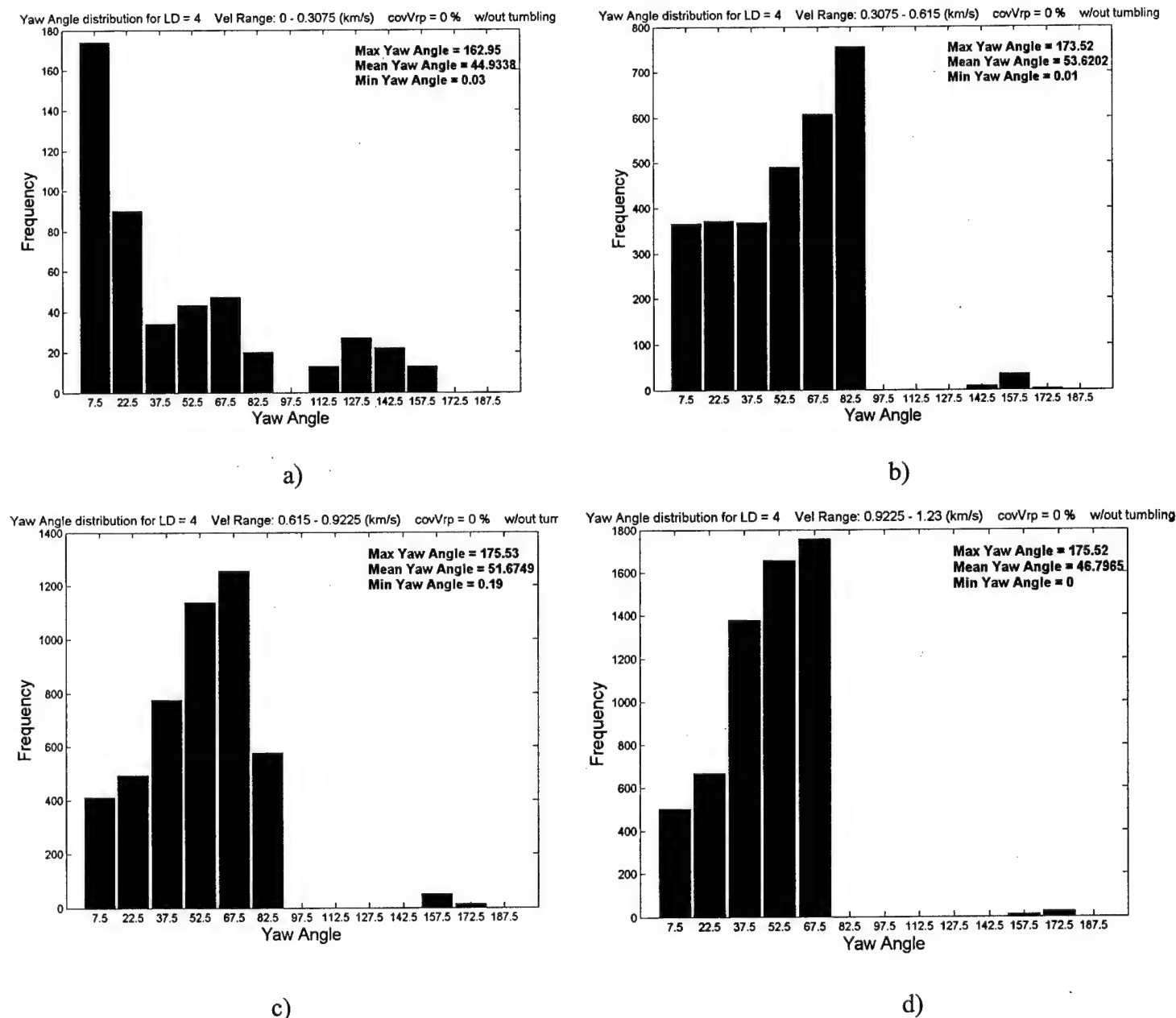


Figure C.5. Yaw Angle Frequency Distribution per Impact Velocity Ranges of 0-0.3075 km/s, 0.3075-0.615 km/s, 0.615-0.9225 km/s, 0.9225-1.23 km/s (a, b, c, d respectively) for Cylindrical Projectiles $L/D = 4$, Without Radial Ejection Velocity Variability.

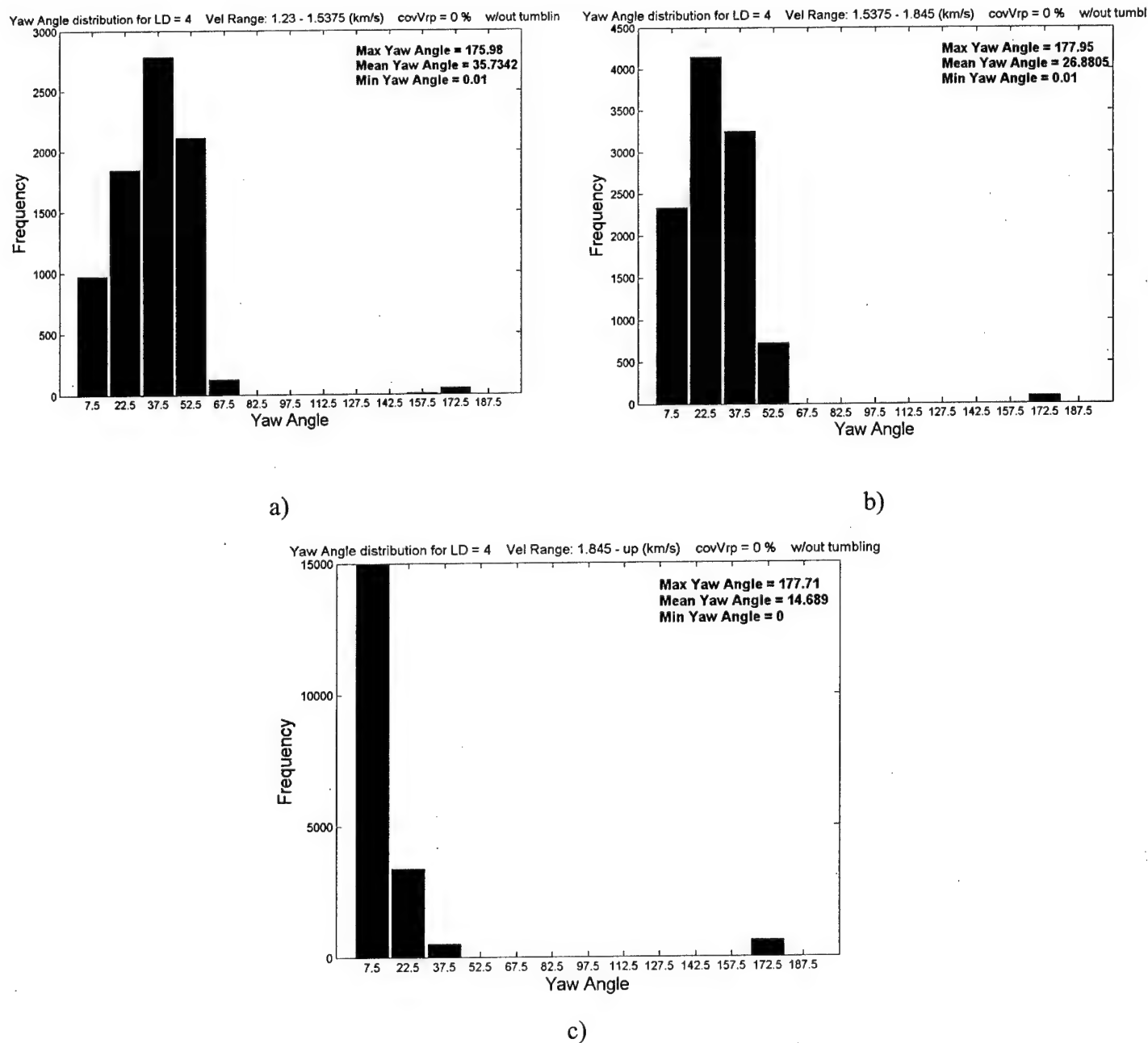


Figure C.6. Yaw Angle Frequency Distribution per Impact Velocity Ranges of 1.23-1.5375 km/s, 1.5375-1.845 km/s, 1.845-up km/s (a, b, c respectively) for Cylindrical Projectiles $L/D = 4$, Without Radial Ejection Velocity Variability.

APPENDIX D

SIDI VALUES DATABASE

Table D.1. SIDI values of the spherical projectiles for all velocities.

LD	Velocity (km/s)	α (degrees)	ϕ (degrees)	DI
Sphere	0.25	N/A	75	0.00603
Sphere	0.25	N/A	60	0.01097
Sphere	0.25	N/A	45	0.01739
Sphere	0.25	N/A	30	0.02424
Sphere	0.25	N/A	15	0.02964
Sphere	0.25	N/A	0	0.03698
Sphere	0.50	N/A	75	0.04009
Sphere	0.50	N/A	60	0.08826
Sphere	0.50	N/A	45	0.13190
Sphere	0.50	N/A	30	0.15064
Sphere	0.50	N/A	15	0.15229
Sphere	0.50	N/A	0	0.15306
Sphere	1.00	N/A	75	0.15780
Sphere	1.00	N/A	60	0.25203
Sphere	1.00	N/A	45	0.32957
Sphere	1.00	N/A	30	0.38198
Sphere	1.00	N/A	15	0.40045
Sphere	1.00	N/A	0	0.40314
Sphere	1.25	N/A	75	0.22041
Sphere	1.25	N/A	60	0.33297
Sphere	1.25	N/A	45	0.43270
Sphere	1.25	N/A	30	0.49737
Sphere	1.25	N/A	15	0.53758
Sphere	1.25	N/A	0	0.52787
Sphere	1.50	N/A	75	0.24273
Sphere	1.50	N/A	60	0.39898
Sphere	1.50	N/A	45	0.50971
Sphere	1.50	N/A	30	0.60858
Sphere	1.50	N/A	15	0.66853
Sphere	1.50	N/A	0	0.66022
Sphere	1.80	N/A	75	0.26725
Sphere	1.80	N/A	60	0.49241
Sphere	1.80	N/A	45	0.63918

Sphere	1.80	N/A	30	0.73627
Sphere	1.80	N/A	15	0.80091
Sphere	1.80	N/A	0	0.79554
Sphere	2.15	N/A	75	0.30237
Sphere	2.15	N/A	60	0.58676
Sphere	2.15	N/A	45	0.76344
Sphere	2.15	N/A	30	0.92531
Sphere	2.15	N/A	15	1.00305
Sphere	2.15	N/A	0	0.98786

Table D.2. SIDI values for cylindrical projectile with $L/D = 1$ for all velocities.

LD	Velocity (km/s)	α (degrees)	ϕ (degrees)	DI
1	0.25	90	75	0.00007
1	0.25	90	60	0.00580
1	0.25	90	45	0.01259
1	0.25	90	30	0.02086
1	0.25	90	15	0.02278
1	0.25	90	0	0.02489
1	0.25	75	75	0.00047
1	0.25	75	60	0.00792
1	0.25	75	45	0.01477
1	0.25	75	30	0.02229
1	0.25	75	15	0.02518
1	0.25	75	0	0.02897
1	0.25	60	75	0.00009
1	0.25	60	60	0.00413
1	0.25	60	45	0.01310
1	0.25	60	30	0.02070
1	0.25	60	15	0.02687
1	0.25	60	0	0.02858
1	0.25	45	75	0.00004
1	0.25	45	60	0.00108
1	0.25	45	45	0.00761
1	0.25	45	30	0.01842
1	0.25	45	15	0.02641
1	0.25	45	0	0.03002
1	0.25	30	75	0.00000
1	0.25	30	60	0.00129
1	0.25	30	45	0.00667
1	0.25	30	30	0.01515
1	0.25	30	15	0.02341
1	0.25	30	0	0.02718
1	0.25	15	75	0.00000
1	0.25	15	60	0.00184
1	0.25	15	45	0.01069

1	0.25	15	30	0.01829
1	0.25	15	15	0.02119
1	0.25	15	0	0.02343
1	0.25	0	75	0.00000
1	0.25	0	60	0.00655
1	0.25	0	45	0.01424
1	0.25	0	30	0.02094
1	0.25	0	15	0.02575
1	0.25	0	0	0.02408
1	0.25	-15	75	0.00120
1	0.25	-15	60	0.00691
1	0.25	-15	45	0.01423
1	0.25	-15	30	0.02206
1	0.25	-15	15	0.02579
1	0.25	-15	0	0.02401
1	0.25	-30	75	0.00014
1	0.25	-30	60	0.00256
1	0.25	-30	45	0.01378
1	0.25	-30	30	0.02402
1	0.25	-30	15	0.02809
1	0.25	-30	0	0.02607
1	0.25	-45	75	0.00013
1	0.25	-45	60	0.00103
1	0.25	-45	45	0.00738
1	0.25	-45	30	0.01930
1	0.25	-45	15	0.02908
1	0.25	-45	0	0.02840
1	0.25	-60	75	0.00003
1	0.25	-60	60	0.00202
1	0.25	-60	45	0.00753
1	0.25	-60	30	0.01625
1	0.25	-60	15	0.02597
1	0.25	-60	0	0.02881
1	0.25	-75	75	0.00000
1	0.25	-75	60	0.00249
1	0.25	-75	45	0.01039

1	0.25	-75	30	0.01813
1	0.25	-75	15	0.02333
1	0.25	-75	0	0.02708
1	0.25	-90	75	0.00007
1	0.25	-90	60	0.00580
1	0.25	-90	45	0.01259
1	0.25	-90	30	0.02086
1	0.25	-90	15	0.02278
1	0.25	-90	0	0.02489
1	0.50	90	75	0.02148
1	0.50	90	60	0.06410
1	0.50	90	45	0.11010
1	0.50	90	30	0.13665
1	0.50	90	15	0.15189
1	0.50	90	0	0.14974
1	0.50	75	75	0.02227
1	0.50	75	60	0.07588
1	0.50	75	45	0.11822
1	0.50	75	30	0.13664
1	0.50	75	15	0.14343
1	0.50	75	0	0.15017
1	0.50	60	75	0.01792
1	0.50	60	60	0.07401
1	0.50	60	45	0.12749
1	0.50	60	30	0.13349
1	0.50	60	15	0.14494
1	0.50	60	0	0.14724
1	0.50	45	75	0.02062
1	0.50	45	60	0.06896
1	0.50	45	45	0.12566
1	0.50	45	30	0.14521
1	0.50	45	15	0.14581
1	0.50	45	0	0.14619
1	0.50	30	75	0.02286
1	0.50	30	60	0.06525
1	0.50	30	45	0.11698

1	0.50	30	30	0.14383
1	0.50	30	15	0.14855
1	0.50	30	0	0.14867
1	0.50	15	75	0.01801
1	0.50	15	60	0.06717
1	0.50	15	45	0.10998
1	0.50	15	30	0.13818
1	0.50	15	15	0.15035
1	0.50	15	0	0.14917
1	0.50	0	75	0.01773
1	0.50	0	60	0.07245
1	0.50	0	45	0.11080
1	0.50	0	30	0.13666
1	0.50	0	15	0.14761
1	0.50	0	0	0.15593
1	0.50	-15	75	0.01790
1	0.50	-15	60	0.06996
1	0.50	-15	45	0.11901
1	0.50	-15	30	0.14084
1	0.50	-15	15	0.14793
1	0.50	-15	0	0.14988
1	0.50	-30	75	0.00761
1	0.50	-30	60	0.07431
1	0.50	-30	45	0.12374
1	0.50	-30	30	0.14555
1	0.50	-30	15	0.14813
1	0.50	-30	0	0.14670
1	0.50	-45	75	0.00113
1	0.50	-45	60	0.05995
1	0.50	-45	45	0.12475
1	0.50	-45	30	0.14796
1	0.50	-45	15	0.14571
1	0.50	-45	0	0.14839
1	0.50	-60	75	0.00978
1	0.50	-60	60	0.05167
1	0.50	-60	45	0.11670

1	0.50	-60	30	0.14469
1	0.50	-60	15	0.15048
1	0.50	-60	0	0.14812
1	0.50	-75	75	0.01884
1	0.50	-75	60	0.06031
1	0.50	-75	45	0.11034
1	0.50	-75	30	0.13732
1	0.50	-75	15	0.14875
1	0.50	-75	0	0.15047
1	0.50	-90	75	0.02148
1	0.50	-90	60	0.06410
1	0.50	-90	45	0.11010
1	0.50	-90	30	0.13665
1	0.50	-90	15	0.15189
1	0.50	-90	0	0.14974
1	1.00	90	75	0.13059
1	1.00	90	60	0.23942
1	1.00	90	45	0.32582
1	1.00	90	30	0.38054
1	1.00	90	15	0.40661
1	1.00	90	0	0.41578
1	1.00	75	75	0.12676
1	1.00	75	60	0.23932
1	1.00	75	45	0.33908
1	1.00	75	30	0.37557
1	1.00	75	15	0.40141
1	1.00	75	0	0.41651
1	1.00	60	75	0.12245
1	1.00	60	60	0.24940
1	1.00	60	45	0.34854
1	1.00	60	30	0.38460
1	1.00	60	15	0.39794
1	1.00	60	0	0.40935
1	1.00	45	75	0.13410
1	1.00	45	60	0.24291
1	1.00	45	45	0.34964

1	1.00	45	30	0.39552
1	1.00	45	15	0.40425
1	1.00	45	0	0.40744
1	1.00	30	75	0.14348
1	1.00	30	60	0.24180
1	1.00	30	45	0.34754
1	1.00	30	30	0.39569
1	1.00	30	15	0.42616
1	1.00	30	0	0.41688
1	1.00	15	75	0.13732
1	1.00	15	60	0.23978
1	1.00	15	45	0.33683
1	1.00	15	30	0.39139
1	1.00	15	15	0.42213
1	1.00	15	0	0.43667
1	1.00	0	75	0.12319
1	1.00	0	60	0.23485
1	1.00	0	45	0.33947
1	1.00	0	30	0.38735
1	1.00	0	15	0.41939
1	1.00	0	0	0.43333
1	1.00	-15	75	0.10434
1	1.00	-15	60	0.23934
1	1.00	-15	45	0.34655
1	1.00	-15	30	0.39006
1	1.00	-15	15	0.41099
1	1.00	-15	0	0.43927
1	1.00	-30	75	0.07146
1	1.00	-30	60	0.24264
1	1.00	-30	45	0.33389
1	1.00	-30	30	0.38360
1	1.00	-30	15	0.40689
1	1.00	-30	0	0.42152
1	1.00	-45	75	0.06227
1	1.00	-45	60	0.24260
1	1.00	-45	45	0.33279

1	1.00	-45	30	0.39125
1	1.00	-45	15	0.40526
1	1.00	-45	0	0.40913
1	1.00	-60	75	0.09494
1	1.00	-60	60	0.23967
1	1.00	-60	45	0.32679
1	1.00	-60	30	0.38884
1	1.00	-60	15	0.41070
1	1.00	-60	0	0.41420
1	1.00	-75	75	0.12154
1	1.00	-75	60	0.23513
1	1.00	-75	45	0.32161
1	1.00	-75	30	0.38037
1	1.00	-75	15	0.40749
1	1.00	-75	0	0.41845
1	1.00	-90	75	0.13059
1	1.00	-90	60	0.23942
1	1.00	-90	45	0.32582
1	1.00	-90	30	0.38054
1	1.00	-90	15	0.40661
1	1.00	-90	0	0.41578
1	1.25	90	75	0.18942
1	1.25	90	60	0.32509
1	1.25	90	45	0.41133
1	1.25	90	30	0.49316
1	1.25	90	15	0.52938
1	1.25	90	0	0.54926
1	1.25	75	75	0.19084
1	1.25	75	60	0.32716
1	1.25	75	45	0.41685
1	1.25	75	30	0.49510
1	1.25	75	15	0.53368
1	1.25	75	0	0.54824
1	1.25	60	75	0.16817
1	1.25	60	60	0.33136
1	1.25	60	45	0.42450

1	1.25	60	30	0.49342
1	1.25	60	15	0.53681
1	1.25	60	0	0.54668
1	1.25	45	75	0.17196
1	1.25	45	60	0.33400
1	1.25	45	45	0.43178
1	1.25	45	30	0.50719
1	1.25	45	15	0.53521
1	1.25	45	0	0.54012
1	1.25	30	75	0.18204
1	1.25	30	60	0.33487
1	1.25	30	45	0.42933
1	1.25	30	30	0.50682
1	1.25	30	15	0.54349
1	1.25	30	0	0.55341
1	1.25	15	75	0.17855
1	1.25	15	60	0.33388
1	1.25	15	45	0.43235
1	1.25	15	30	0.51259
1	1.25	15	15	0.54329
1	1.25	15	0	0.56289
1	1.25	0	75	0.18408
1	1.25	0	60	0.32701
1	1.25	0	45	0.42735
1	1.25	0	30	0.50650
1	1.25	0	15	0.54532
1	1.25	0	0	0.55252
1	1.25	-15	75	0.17798
1	1.25	-15	60	0.32518
1	1.25	-15	45	0.43313
1	1.25	-15	30	0.51169
1	1.25	-15	15	0.54159
1	1.25	-15	0	0.55427
1	1.25	-30	75	0.13361
1	1.25	-30	60	0.32524
1	1.25	-30	45	0.42650

1	1.25	-30	30	0.49957
1	1.25	-30	15	0.53040
1	1.25	-30	0	0.55617
1	1.25	-45	75	0.10229
1	1.25	-45	60	0.31678
1	1.25	-45	45	0.42486
1	1.25	-45	30	0.50846
1	1.25	-45	15	0.53402
1	1.25	-45	0	0.54604
1	1.25	-60	75	0.12179
1	1.25	-60	60	0.31667
1	1.25	-60	45	0.42018
1	1.25	-60	30	0.48547
1	1.25	-60	15	0.54238
1	1.25	-60	0	0.54772
1	1.25	-75	75	0.16590
1	1.25	-75	60	0.31019
1	1.25	-75	45	0.41413
1	1.25	-75	30	0.49358
1	1.25	-75	15	0.53310
1	1.25	-75	0	0.54589
1	1.25	-90	75	0.18942
1	1.25	-90	60	0.32509
1	1.25	-90	45	0.41133
1	1.25	-90	30	0.49316
1	1.25	-90	15	0.52938
1	1.25	-90	0	0.54926
1	1.50	90	75	0.22893
1	1.50	90	60	0.40439
1	1.50	90	45	0.50248
1	1.50	90	30	0.60418
1	1.50	90	15	0.64850
1	1.50	90	0	0.67502
1	1.50	75	75	0.24906
1	1.50	75	60	0.41225
1	1.50	75	45	0.50937

1	1.50	75	30	0.60184
1	1.50	75	15	0.64743
1	1.50	75	0	0.65972
1	1.50	60	75	0.22038
1	1.50	60	60	0.40340
1	1.50	60	45	0.50365
1	1.50	60	30	0.59931
1	1.50	60	15	0.66178
1	1.50	60	0	0.67384
1	1.50	45	75	0.20665
1	1.50	45	60	0.40529
1	1.50	45	45	0.51224
1	1.50	45	30	0.61215
1	1.50	45	15	0.63936
1	1.50	45	0	0.67802
1	1.50	30	75	0.22269
1	1.50	30	60	0.42092
1	1.50	30	45	0.51171
1	1.50	30	30	0.60529
1	1.50	30	15	0.64535
1	1.50	30	0	0.67618
1	1.50	15	75	0.21546
1	1.50	15	60	0.40734
1	1.50	15	45	0.52643
1	1.50	15	30	0.60459
1	1.50	15	15	0.65074
1	1.50	15	0	0.66551
1	1.50	0	75	0.21311
1	1.50	0	60	0.40422
1	1.50	0	45	0.52268
1	1.50	0	30	0.62110
1	1.50	0	15	0.64141
1	1.50	0	0	0.65030
1	1.50	-15	75	0.22137
1	1.50	-15	60	0.39735
1	1.50	-15	45	0.52031

1	1.50	-15	30	0.61990
1	1.50	-15	15	0.65939
1	1.50	-15	0	0.66405
1	1.50	-30	75	0.20172
1	1.50	-30	60	0.39660
1	1.50	-30	45	0.53174
1	1.50	-30	30	0.60716
1	1.50	-30	15	0.67019
1	1.50	-30	0	0.67533
1	1.50	-45	75	0.15062
1	1.50	-45	60	0.38942
1	1.50	-45	45	0.50568
1	1.50	-45	30	0.60824
1	1.50	-45	15	0.64630
1	1.50	-45	0	0.68340
1	1.50	-60	75	0.15333
1	1.50	-60	60	0.38315
1	1.50	-60	45	0.50221
1	1.50	-60	30	0.60601
1	1.50	-60	15	0.64806
1	1.50	-60	0	0.67663
1	1.50	-75	75	0.20895
1	1.50	-75	60	0.39988
1	1.50	-75	45	0.50487
1	1.50	-75	30	0.60079
1	1.50	-75	15	0.65017
1	1.50	-75	0	0.67328
1	1.50	-90	75	0.22893
1	1.50	-90	60	0.40439
1	1.50	-90	45	0.50248
1	1.50	-90	30	0.60418
1	1.50	-90	15	0.64850
1	1.50	-90	0	0.67502
1	1.81	90	75	0.26855
1	1.81	90	60	0.48660
1	1.81	90	45	0.62548

1	1.81	90	30	0.72338
1	1.81	90	15	0.80716
1	1.81	90	0	0.81403
1	1.81	75	75	0.27854
1	1.81	75	60	0.48708
1	1.81	75	45	0.62013
1	1.81	75	30	0.73098
1	1.81	75	15	0.80978
1	1.81	75	0	0.81916
1	1.81	60	75	0.25872
1	1.81	60	60	0.48720
1	1.81	60	45	0.63205
1	1.81	60	30	0.72284
1	1.81	60	15	0.81260
1	1.81	60	0	0.82334
1	1.81	45	75	0.26977
1	1.81	45	60	0.49750
1	1.81	45	45	0.64050
1	1.81	45	30	0.73346
1	1.81	45	15	0.79565
1	1.81	45	0	0.82083
1	1.81	30	75	0.26342
1	1.81	30	60	0.49730
1	1.81	30	45	0.62070
1	1.81	30	30	0.71930
1	1.81	30	15	0.80338
1	1.81	30	0	0.81889
1	1.81	15	75	0.25424
1	1.81	15	60	0.48813
1	1.81	15	45	0.64889
1	1.81	15	30	0.72069
1	1.81	15	15	0.79496
1	1.81	15	0	0.81232
1	1.81	0	75	0.24691
1	1.81	0	60	0.49161
1	1.81	0	45	0.64242

1	1.81	0	30	0.73174
1	1.81	0	15	0.79529
1	1.81	0	0	0.80348
1	1.81	-15	75	0.26570
1	1.81	-15	60	0.48952
1	1.81	-15	45	0.64451
1	1.81	-15	30	0.75849
1	1.81	-15	15	0.80590
1	1.81	-15	0	0.81818
1	1.81	-30	75	0.25169
1	1.81	-30	60	0.47932
1	1.81	-30	45	0.63816
1	1.81	-30	30	0.75082
1	1.81	-30	15	0.82209
1	1.81	-30	0	0.82317
1	1.81	-45	75	0.22669
1	1.81	-45	60	0.46716
1	1.81	-45	45	0.62345
1	1.81	-45	30	0.72731
1	1.81	-45	15	0.81011
1	1.81	-45	0	0.83214
1	1.81	-60	75	0.21702
1	1.81	-60	60	0.47825
1	1.81	-60	45	0.61211
1	1.81	-60	30	0.72082
1	1.81	-60	15	0.79095
1	1.81	-60	0	0.83122
1	1.81	-75	75	0.25059
1	1.81	-75	60	0.48857
1	1.81	-75	45	0.62350
1	1.81	-75	30	0.71653
1	1.81	-75	15	0.80994
1	1.81	-75	0	0.82189
1	1.81	-90	75	0.26855
1	1.81	-90	60	0.48660
1	1.81	-90	45	0.62548

1	1.81	-90	30	0.72338
1	1.81	-90	15	0.80716
1	1.81	-90	0	0.81403
1	2.15	90	75	0.30161
1	2.15	90	60	0.56859
1	2.15	90	45	0.75091
1	2.15	90	30	0.92972
1	2.15	90	15	0.98524
1	2.15	90	0	0.99567
1	2.15	75	75	0.33099
1	2.15	75	60	0.58173
1	2.15	75	45	0.74954
1	2.15	75	30	0.91151
1	2.15	75	15	0.98681
1	2.15	75	0	0.98692
1	2.15	60	75	0.31178
1	2.15	60	60	0.58066
1	2.15	60	45	0.76922
1	2.15	60	30	0.89185
1	2.15	60	15	0.99531
1	2.15	60	0	1.02322
1	2.15	45	75	0.30037
1	2.15	45	60	0.58455
1	2.15	45	45	0.75682
1	2.15	45	30	0.90294
1	2.15	45	15	0.95387
1	2.15	45	0	1.02366
1	2.15	30	75	0.29359
1	2.15	30	60	0.58031
1	2.15	30	45	0.74881
1	2.15	30	30	0.89450
1	2.15	30	15	0.97436
1	2.15	30	0	0.99580
1	2.15	15	75	0.29792
1	2.15	15	60	0.58563
1	2.15	15	45	0.77833

1	2.15	15	30	0.89762
1	2.15	15	15	0.98169
1	2.15	15	0	0.97961
1	2.15	0	75	0.28686
1	2.15	0	60	0.57935
1	2.15	0	45	0.77941
1	2.15	0	30	0.92183
1	2.15	0	15	0.98294
1	2.15	0	0	1.00639
1	2.15	-15	75	0.29988
1	2.15	-15	60	0.59402
1	2.15	-15	45	0.76727
1	2.15	-15	30	0.94243
1	2.15	-15	15	0.97479
1	2.15	-15	0	0.98312
1	2.15	-30	75	0.28517
1	2.15	-30	60	0.59412
1	2.15	-30	45	0.76834
1	2.15	-30	30	0.92386
1	2.15	-30	15	1.00292
1	2.15	-30	0	0.99382
1	2.15	-45	75	0.27420
1	2.15	-45	60	0.57638
1	2.15	-45	45	0.76518
1	2.15	-45	30	0.90944
1	2.15	-45	15	1.00055
1	2.15	-45	0	1.02311
1	2.15	-60	75	0.27830
1	2.15	-60	60	0.57057
1	2.15	-60	45	0.75583
1	2.15	-60	30	0.90938
1	2.15	-60	15	0.97341
1	2.15	-60	0	1.02777
1	2.15	-75	75	0.28607
1	2.15	-75	60	0.56516
1	2.15	-75	45	0.76076

1	2.15	-75	30	0.91750
1	2.15	-75	15	0.99298
1	2.15	-75	0	0.98692
1	2.15	-90	75	0.30161
1	2.15	-90	60	0.56859
1	2.15	-90	45	0.75091
1	2.15	-90	30	0.92972
1	2.15	-90	15	0.98524
1	2.15	-90	0	0.99567

Table D.3 SIDI values for cylindrical projectile with $L/D = 2$ for all velocities.

LD	Velocity (km/s)	α (degrees)	ϕ (degrees)	DI
2	0.25	90	75	0.00000
2	0.25	90	60	0.00649
2	0.25	90	45	0.01109
2	0.25	90	30	0.01821
2	0.25	90	15	0.02181
2	0.25	90	0	0.02317
2	0.25	75	75	0.00040
2	0.25	75	60	0.00727
2	0.25	75	45	0.01242
2	0.25	75	30	0.01853
2	0.25	75	15	0.02250
2	0.25	75	0	0.02250
2	0.25	60	75	0.00007
2	0.25	60	60	0.00798
2	0.25	60	45	0.01357
2	0.25	60	30	0.01910
2	0.25	60	15	0.02218
2	0.25	60	0	0.02331
2	0.25	45	75	0.00004
2	0.25	45	60	0.00306
2	0.25	45	45	0.01138
2	0.25	45	30	0.02272
2	0.25	45	15	0.02383
2	0.25	45	0	0.02576
2	0.25	30	75	0.00001
2	0.25	30	60	0.00323
2	0.25	30	45	0.01288
2	0.25	30	30	0.01930
2	0.25	30	15	0.02774
2	0.25	30	0	0.02845
2	0.25	15	75	0.00000
2	0.25	15	60	0.00320

2	0.25	15	45	0.01171
2	0.25	15	30	0.02072
2	0.25	15	15	0.02840
2	0.25	15	0	0.02830
2	0.25	0	75	0.00004
2	0.25	0	60	0.00475
2	0.25	0	45	0.01055
2	0.25	0	30	0.02207
2	0.25	0	15	0.02685
2	0.25	0	0	0.03048
2	0.25	-15	75	0.00066
2	0.25	-15	60	0.00463
2	0.25	-15	45	0.01059
2	0.25	-15	30	0.02006
2	0.25	-15	15	0.02687
2	0.25	-15	0	0.02966
2	0.25	-30	75	0.00009
2	0.25	-30	60	0.00183
2	0.25	-30	45	0.00988
2	0.25	-30	30	0.01876
2	0.25	-30	15	0.02666
2	0.25	-30	0	0.03067
2	0.25	-45	75	0.00006
2	0.25	-45	60	0.00081
2	0.25	-45	45	0.00596
2	0.25	-45	30	0.01415
2	0.25	-45	15	0.02189
2	0.25	-45	0	0.02561
2	0.25	-60	75	0.00000
2	0.25	-60	60	0.00200
2	0.25	-60	45	0.00605
2	0.25	-60	30	0.01296
2	0.25	-60	15	0.01982
2	0.25	-60	0	0.02281
2	0.25	-75	75	0.00000
2	0.25	-75	60	0.00307

2	0.25	-75	45	0.00950
2	0.25	-75	30	0.01518
2	0.25	-75	15	0.01970
2	0.25	-75	0	0.02250
2	0.25	-90	75	0.00000
2	0.25	-90	60	0.00649
2	0.25	-90	45	0.01109
2	0.25	-90	30	0.01821
2	0.25	-90	15	0.02181
2	0.25	-90	0	0.02317
2	0.50	90	75	0.02046
2	0.50	90	60	0.07121
2	0.50	90	45	0.10805
2	0.50	90	30	0.12635
2	0.50	90	15	0.13174
2	0.50	90	0	0.12890
2	0.50	75	75	0.02015
2	0.50	75	60	0.07840
2	0.50	75	45	0.11399
2	0.50	75	30	0.13432
2	0.50	75	15	0.13617
2	0.50	75	0	0.13428
2	0.50	60	75	0.02340
2	0.50	60	60	0.08909
2	0.50	60	45	0.12459
2	0.50	60	30	0.13789
2	0.50	60	15	0.14001
2	0.50	60	0	0.13661
2	0.50	45	75	0.01652
2	0.50	45	60	0.07370
2	0.50	45	45	0.12889
2	0.50	45	30	0.14050
2	0.50	45	15	0.14776
2	0.50	45	0	0.14369
2	0.50	30	75	0.01457
2	0.50	30	60	0.06227

2	0.50	30	45	0.11579
2	0.50	30	30	0.14563
2	0.50	30	15	0.15365
2	0.50	30	0	0.14872
2	0.50	15	75	0.01475
2	0.50	15	60	0.05006
2	0.50	15	45	0.11541
2	0.50	15	30	0.14458
2	0.50	15	15	0.15668
2	0.50	15	0	0.15632
2	0.50	0	75	0.01698
2	0.50	0	60	0.06441
2	0.50	0	45	0.11147
2	0.50	0	30	0.14328
2	0.50	0	15	0.15796
2	0.50	0	0	0.17152
2	0.50	-15	75	0.01540
2	0.50	-15	60	0.06292
2	0.50	-15	45	0.10890
2	0.50	-15	30	0.13457
2	0.50	-15	15	0.15124
2	0.50	-15	0	0.15415
2	0.50	-30	75	0.00811
2	0.50	-30	60	0.05937
2	0.50	-30	45	0.11416
2	0.50	-30	30	0.13357
2	0.50	-30	15	0.14494
2	0.50	-30	0	0.14721
2	0.50	-45	75	0.00872
2	0.50	-45	60	0.05186
2	0.50	-45	45	0.11527
2	0.50	-45	30	0.13458
2	0.50	-45	15	0.14072
2	0.50	-45	0	0.14292
2	0.50	-60	75	0.01336
2	0.50	-60	60	0.05419

2	0.50	-60	45	0.10495
2	0.50	-60	30	0.13058
2	0.50	-60	15	0.13972
2	0.50	-60	0	0.13926
2	0.50	-75	75	0.01416
2	0.50	-75	60	0.05972
2	0.50	-75	45	0.10412
2	0.50	-75	30	0.12818
2	0.50	-75	15	0.13609
2	0.50	-75	0	0.13567
2	0.50	-90	75	0.02046
2	0.50	-90	60	0.07121
2	0.50	-90	45	0.10805
2	0.50	-90	30	0.12635
2	0.50	-90	15	0.13174
2	0.50	-90	0	0.12890
2	1.00	90	75	0.15229
2	1.00	90	60	0.24168
2	1.00	90	45	0.31553
2	1.00	90	30	0.36276
2	1.00	90	15	0.38718
2	1.00	90	0	0.39596
2	1.00	75	75	0.15534
2	1.00	75	60	0.24026
2	1.00	75	45	0.33948
2	1.00	75	30	0.37604
2	1.00	75	15	0.38144
2	1.00	75	0	0.38717
2	1.00	60	75	0.11976
2	1.00	60	60	0.26232
2	1.00	60	45	0.35752
2	1.00	60	30	0.38034
2	1.00	60	15	0.38768
2	1.00	60	0	0.39200
2	1.00	45	75	0.12721
2	1.00	45	60	0.25814

2	1.00	45	45	0.35986
2	1.00	45	30	0.41111
2	1.00	45	15	0.41014
2	1.00	45	0	0.39691
2	1.00	30	75	0.10956
2	1.00	30	60	0.23974
2	1.00	30	45	0.36257
2	1.00	30	30	0.43351
2	1.00	30	15	0.45234
2	1.00	30	0	0.42518
2	1.00	15	75	0.09847
2	1.00	15	60	0.24090
2	1.00	15	45	0.34642
2	1.00	15	30	0.41522
2	1.00	15	15	0.46186
2	1.00	15	0	0.47327
2	1.00	0	75	0.08133
2	1.00	0	60	0.23683
2	1.00	0	45	0.33629
2	1.00	0	30	0.39144
2	1.00	0	15	0.46258
2	1.00	0	0	0.46091
2	1.00	-15	75	0.08119
2	1.00	-15	60	0.22775
2	1.00	-15	45	0.32568
2	1.00	-15	30	0.38084
2	1.00	-15	15	0.42270
2	1.00	-15	0	0.46618
2	1.00	-30	75	0.07208
2	1.00	-30	60	0.23299
2	1.00	-30	45	0.29880
2	1.00	-30	30	0.36993
2	1.00	-30	15	0.40299
2	1.00	-30	0	0.43205
2	1.00	-45	75	0.07892
2	1.00	-45	60	0.23888

2	1.00	-45	45	0.30383
2	1.00	-45	30	0.36700
2	1.00	-45	15	0.39565
2	1.00	-45	0	0.40221
2	1.00	-60	75	0.08852
2	1.00	-60	60	0.23330
2	1.00	-60	45	0.29414
2	1.00	-60	30	0.35900
2	1.00	-60	15	0.38573
2	1.00	-60	0	0.39080
2	1.00	-75	75	0.11998
2	1.00	-75	60	0.23333
2	1.00	-75	45	0.28955
2	1.00	-75	30	0.35449
2	1.00	-75	15	0.37477
2	1.00	-75	0	0.38925
2	1.00	-90	75	0.15229
2	1.00	-90	60	0.24168
2	1.00	-90	45	0.31553
2	1.00	-90	30	0.36276
2	1.00	-90	15	0.38718
2	1.00	-90	0	0.39596
2	1.25	90	75	0.21055
2	1.25	90	60	0.32192
2	1.25	90	45	0.40437
2	1.25	90	30	0.45242
2	1.25	90	15	0.49666
2	1.25	90	0	0.50058
2	1.25	75	75	0.22384
2	1.25	75	60	0.34836
2	1.25	75	45	0.41963
2	1.25	75	30	0.47539
2	1.25	75	15	0.49691
2	1.25	75	0	0.51688
2	1.25	60	75	0.20085
2	1.25	60	60	0.36594

2	1.25	60	45	0.43875
2	1.25	60	30	0.50510
2	1.25	60	15	0.52043
2	1.25	60	0	0.51237
2	1.25	45	75	0.17308
2	1.25	45	60	0.36624
2	1.25	45	45	0.46251
2	1.25	45	30	0.53299
2	1.25	45	15	0.54107
2	1.25	45	0	0.52857
2	1.25	30	75	0.15094
2	1.25	30	60	0.35085
2	1.25	30	45	0.44740
2	1.25	30	30	0.54308
2	1.25	30	15	0.57173
2	1.25	30	0	0.55258
2	1.25	15	75	0.11669
2	1.25	15	60	0.31303
2	1.25	15	45	0.44034
2	1.25	15	30	0.53398
2	1.25	15	15	0.58029
2	1.25	15	0	0.59974
2	1.25	0	75	0.10688
2	1.25	0	60	0.28568
2	1.25	0	45	0.43149
2	1.25	0	30	0.52406
2	1.25	0	15	0.57766
2	1.25	0	0	0.60334
2	1.25	-15	75	0.09310
2	1.25	-15	60	0.28415
2	1.25	-15	45	0.42151
2	1.25	-15	30	0.49217
2	1.25	-15	15	0.55342
2	1.25	-15	0	0.59479
2	1.25	-30	75	0.09409
2	1.25	-30	60	0.28208

2	1.25	-30	45	0.40056
2	1.25	-30	30	0.46519
2	1.25	-30	15	0.52892
2	1.25	-30	0	0.55350
2	1.25	-45	75	0.10232
2	1.25	-45	60	0.29448
2	1.25	-45	45	0.40862
2	1.25	-45	30	0.45990
2	1.25	-45	15	0.51261
2	1.25	-45	0	0.53082
2	1.25	-60	75	0.13250
2	1.25	-60	60	0.28930
2	1.25	-60	45	0.40162
2	1.25	-60	30	0.44896
2	1.25	-60	15	0.48803
2	1.25	-60	0	0.51005
2	1.25	-75	75	0.18430
2	1.25	-75	60	0.30303
2	1.25	-75	45	0.40437
2	1.25	-75	30	0.45097
2	1.25	-75	15	0.48483
2	1.25	-75	0	0.52097
2	1.25	-90	75	0.21055
2	1.25	-90	60	0.32192
2	1.25	-90	45	0.40437
2	1.25	-90	30	0.45242
2	1.25	-90	15	0.49666
2	1.25	-90	0	0.50058
2	1.50	90	75	0.23650
2	1.50	90	60	0.40724
2	1.50	90	45	0.47767
2	1.50	90	30	0.57375
2	1.50	90	15	0.62575
2	1.50	90	0	0.62946
2	1.50	75	75	0.25749
2	1.50	75	60	0.41948

2	1.50	75	45	0.51853
2	1.50	75	30	0.59123
2	1.50	75	15	0.61957
2	1.50	75	0	0.62541
2	1.50	60	75	0.24031
2	1.50	60	60	0.42120
2	1.50	60	45	0.54498
2	1.50	60	30	0.60618
2	1.50	60	15	0.62390
2	1.50	60	0	0.62842
2	1.50	45	75	0.22936
2	1.50	45	60	0.42800
2	1.50	45	45	0.55209
2	1.50	45	30	0.63784
2	1.50	45	15	0.65280
2	1.50	45	0	0.64912
2	1.50	30	75	0.19113
2	1.50	30	60	0.42728
2	1.50	30	45	0.55490
2	1.50	30	30	0.64605
2	1.50	30	15	0.70332
2	1.50	30	0	0.68517
2	1.50	15	75	0.17207
2	1.50	15	60	0.40216
2	1.50	15	45	0.53916
2	1.50	15	30	0.63266
2	1.50	15	15	0.69013
2	1.50	15	0	0.72180
2	1.50	0	75	0.14200
2	1.50	0	60	0.38100
2	1.50	0	45	0.51693
2	1.50	0	30	0.62175
2	1.50	0	15	0.70347
2	1.50	0	0	0.70593
2	1.50	-15	75	0.11752
2	1.50	-15	60	0.36493

2	1.50	-15	45	0.49915
2	1.50	-15	30	0.61359
2	1.50	-15	15	0.67356
2	1.50	-15	0	0.70898
2	1.50	-30	75	0.11485
2	1.50	-30	60	0.35528
2	1.50	-30	45	0.47941
2	1.50	-30	30	0.59144
2	1.50	-30	15	0.64014
2	1.50	-30	0	0.69309
2	1.50	-45	75	0.14185
2	1.50	-45	60	0.36915
2	1.50	-45	45	0.48882
2	1.50	-45	30	0.56969
2	1.50	-45	15	0.62796
2	1.50	-45	0	0.65153
2	1.50	-60	75	0.17796
2	1.50	-60	60	0.36760
2	1.50	-60	45	0.48289
2	1.50	-60	30	0.56743
2	1.50	-60	15	0.61703
2	1.50	-60	0	0.62572
2	1.50	-75	75	0.23493
2	1.50	-75	60	0.37829
2	1.50	-75	45	0.47628
2	1.50	-75	30	0.56902
2	1.50	-75	15	0.62421
2	1.50	-75	0	0.62968
2	1.50	-90	75	0.23650
2	1.50	-90	60	0.40724
2	1.50	-90	45	0.47767
2	1.50	-90	30	0.57375
2	1.50	-90	15	0.62575
2	1.50	-90	0	0.62946
2	1.81	90	75	0.26807
2	1.81	90	60	0.47779

2	1.81	90	45	0.60855
2	1.81	90	30	0.68933
2	1.81	90	15	0.76080
2	1.81	90	0	0.78483
2	1.81	75	75	0.28497
2	1.81	75	60	0.48321
2	1.81	75	45	0.61854
2	1.81	75	30	0.70523
2	1.81	75	15	0.76471
2	1.81	75	0	0.77291
2	1.81	60	75	0.29538
2	1.81	60	60	0.49331
2	1.81	60	45	0.64674
2	1.81	60	30	0.75257
2	1.81	60	15	0.77891
2	1.81	60	0	0.78605
2	1.81	45	75	0.26517
2	1.81	45	60	0.49854
2	1.81	45	45	0.64315
2	1.81	45	30	0.76490
2	1.81	45	15	0.81902
2	1.81	45	0	0.81530
2	1.81	30	75	0.22261
2	1.81	30	60	0.50577
2	1.81	30	45	0.65607
2	1.81	30	30	0.75267
2	1.81	30	15	0.83159
2	1.81	30	0	0.83304
2	1.81	15	75	0.20369
2	1.81	15	60	0.49771
2	1.81	15	45	0.65905
2	1.81	15	30	0.75455
2	1.81	15	15	0.82643
2	1.81	15	0	0.85536
2	1.81	0	75	0.18701
2	1.81	0	60	0.46632

2	1.81	0	45	0.64830
2	1.81	0	30	0.76794
2	1.81	0	15	0.82359
2	1.81	0	0	0.85498
2	1.81	-15	75	0.16049
2	1.81	-15	60	0.45623
2	1.81	-15	45	0.61800
2	1.81	-15	30	0.73667
2	1.81	-15	15	0.82264
2	1.81	-15	0	0.85261
2	1.81	-30	75	0.13510
2	1.81	-30	60	0.46084
2	1.81	-30	45	0.60718
2	1.81	-30	30	0.71577
2	1.81	-30	15	0.79545
2	1.81	-30	0	0.83628
2	1.81	-45	75	0.18590
2	1.81	-45	60	0.45418
2	1.81	-45	45	0.58831
2	1.81	-45	30	0.70239
2	1.81	-45	15	0.78106
2	1.81	-45	0	0.80996
2	1.81	-60	75	0.23859
2	1.81	-60	60	0.44708
2	1.81	-60	45	0.58674
2	1.81	-60	30	0.69754
2	1.81	-60	15	0.75513
2	1.81	-60	0	0.78396
2	1.81	-75	75	0.27418
2	1.81	-75	60	0.46637
2	1.81	-75	45	0.59401
2	1.81	-75	30	0.70545
2	1.81	-75	15	0.76147
2	1.81	-75	0	0.76857
2	1.81	-90	75	0.26807
2	1.81	-90	60	0.47779

2	1.81	-90	45	0.60855
2	1.81	-90	30	0.68933
2	1.81	-90	15	0.76080
2	1.81	-90	0	0.78483
2	2.15	90	75	0.31657
2	2.15	90	60	0.58758
2	2.15	90	45	0.74793
2	2.15	90	30	0.85507
2	2.15	90	15	0.92311
2	2.15	90	0	0.93314
2	2.15	75	75	0.30702
2	2.15	75	60	0.59224
2	2.15	75	45	0.74970
2	2.15	75	30	0.88983
2	2.15	75	15	0.94838
2	2.15	75	0	0.96814
2	2.15	60	75	0.33566
2	2.15	60	60	0.58917
2	2.15	60	45	0.78182
2	2.15	60	30	0.90786
2	2.15	60	15	0.95250
2	2.15	60	0	0.97414
2	2.15	45	75	0.31111
2	2.15	45	60	0.59289
2	2.15	45	45	0.77504
2	2.15	45	30	0.91418
2	2.15	45	15	0.99869
2	2.15	45	0	0.99862
2	2.15	30	75	0.26224
2	2.15	30	60	0.62036
2	2.15	30	45	0.77519
2	2.15	30	30	0.91315
2	2.15	30	15	0.99735
2	2.15	30	0	1.03259
2	2.15	15	75	0.23932
2	2.15	15	60	0.59787

2	2.15	15	45	0.79857
2	2.15	15	30	0.92154
2	2.15	15	15	1.00031
2	2.15	15	0	1.02329
2	2.15	0	75	0.21230
2	2.15	0	60	0.58282
2	2.15	0	45	0.78395
2	2.15	0	30	0.94688
2	2.15	0	15	1.00895
2	2.15	0	0	1.02760
2	2.15	-15	75	0.18789
2	2.15	-15	60	0.57627
2	2.15	-15	45	0.76215
2	2.15	-15	30	0.91287
2	2.15	-15	15	0.99439
2	2.15	-15	0	1.02446
2	2.15	-30	75	0.16817
2	2.15	-30	60	0.54167
2	2.15	-30	45	0.73002
2	2.15	-30	30	0.86107
2	2.15	-30	15	0.98888
2	2.15	-30	0	1.02200
2	2.15	-45	75	0.21989
2	2.15	-45	60	0.55269
2	2.15	-45	45	0.71493
2	2.15	-45	30	0.86315
2	2.15	-45	15	0.97062
2	2.15	-45	0	0.99808
2	2.15	-60	75	0.28603
2	2.15	-60	60	0.53598
2	2.15	-60	45	0.74105
2	2.15	-60	30	0.87564
2	2.15	-60	15	0.95891
2	2.15	-60	0	0.97253
2	2.15	-75	75	0.31020
2	2.15	-75	60	0.54184

2	2.15	-75	45	0.74177
2	2.15	-75	30	0.88416
2	2.15	-75	15	0.97320
2	2.15	-75	0	0.97030
2	2.15	-90	75	0.31657
2	2.15	-90	60	0.58758
2	2.15	-90	45	0.74793
2	2.15	-90	30	0.85507
2	2.15	-90	15	0.92311
2	2.15	-90	0	0.93314

Table D.4. SIDI values for cylindrical projectile with $L/D = 4$ for all velocities.

LD	Velocity (km/s)	α (degrees)	ϕ (degrees)	DI
4	0.25	90	75	0.00000
4	0.25	90	60	0.00143
4	0.25	90	45	0.00766
4	0.25	90	30	0.01312
4	0.25	90	15	0.01763
4	0.25	90	0	0.01896
4	0.25	75	75	0.00003
4	0.25	75	60	0.00234
4	0.25	75	45	0.00693
4	0.25	75	30	0.01235
4	0.25	75	15	0.01695
4	0.25	75	0	0.01928
4	0.25	60	75	0.00003
4	0.25	60	60	0.00434
4	0.25	60	45	0.00915
4	0.25	60	30	0.01328
4	0.25	60	15	0.01774
4	0.25	60	0	0.01989
4	0.25	45	75	0.00002
4	0.25	45	60	0.00555
4	0.25	45	45	0.01252
4	0.25	45	30	0.01963
4	0.25	45	15	0.02208
4	0.25	45	0	0.02196
4	0.25	30	75	0.00000
4	0.25	30	60	0.00292
4	0.25	30	45	0.01023
4	0.25	30	30	0.02486
4	0.25	30	15	0.02811
4	0.25	30	0	0.02589
4	0.25	15	75	0.00000
4	0.25	15	60	0.00227
4	0.25	15	45	0.00641

4	0.25	15	30	0.01911
4	0.25	15	15	0.03086
4	0.25	15	0	0.02937
4	0.25	0	75	0.00004
4	0.25	0	60	0.00419
4	0.25	0	45	0.00769
4	0.25	0	30	0.01560
4	0.25	0	15	0.02688
4	0.25	0	0	0.03437
4	0.25	-15	75	0.00008
4	0.25	-15	60	0.00288
4	0.25	-15	45	0.00922
4	0.25	-15	30	0.01748
4	0.25	-15	15	0.02335
4	0.25	-15	0	0.02824
4	0.25	-30	75	0.00007
4	0.25	-30	60	0.00268
4	0.25	-30	45	0.00851
4	0.25	-30	30	0.01847
4	0.25	-30	15	0.02288
4	0.25	-30	0	0.02591
4	0.25	-45	75	0.00005
4	0.25	-45	60	0.00247
4	0.25	-45	45	0.00634
4	0.25	-45	30	0.01403
4	0.25	-45	15	0.01938
4	0.25	-45	0	0.02226
4	0.25	-60	75	0.00017
4	0.25	-60	60	0.00227
4	0.25	-60	45	0.00556
4	0.25	-60	30	0.01271
4	0.25	-60	15	0.01823
4	0.25	-60	0	0.01962
4	0.25	-75	75	0.00062
4	0.25	-75	60	0.00253
4	0.25	-75	45	0.00637

4	0.25	-75	30	0.01255
4	0.25	-75	15	0.01707
4	0.25	-75	0	0.01966
4	0.25	-90	75	0.00000
4	0.25	-90	60	0.00143
4	0.25	-90	45	0.00766
4	0.25	-90	30	0.01312
4	0.25	-90	15	0.01763
4	0.25	-90	0	0.01896
4	0.50	90	75	0.00519
4	0.50	90	60	0.05142
4	0.50	90	45	0.09100
4	0.50	90	30	0.10755
4	0.50	90	15	0.11392
4	0.50	90	0	0.11601
4	0.50	75	75	0.01108
4	0.50	75	60	0.05580
4	0.50	75	45	0.10544
4	0.50	75	30	0.11814
4	0.50	75	15	0.12614
4	0.50	75	0	0.12478
4	0.50	60	75	0.00789
4	0.50	60	60	0.07246
4	0.50	60	45	0.11757
4	0.50	60	30	0.12853
4	0.50	60	15	0.13417
4	0.50	60	0	0.13026
4	0.50	45	75	0.01683
4	0.50	45	60	0.07668
4	0.50	45	45	0.12761
4	0.50	45	30	0.13476
4	0.50	45	15	0.13772
4	0.50	45	0	0.13387
4	0.50	30	75	0.01008
4	0.50	30	60	0.04223
4	0.50	30	45	0.09894

4	0.50	30	30	0.15266
4	0.50	30	15	0.14652
4	0.50	30	0	0.13621
4	0.50	15	75	0.00668
4	0.50	15	60	0.03226
4	0.50	15	45	0.08673
4	0.50	15	30	0.11706
4	0.50	15	15	0.17218
4	0.50	15	0	0.15244
4	0.50	0	75	0.00737
4	0.50	0	60	0.03756
4	0.50	0	45	0.08924
4	0.50	0	30	0.12051
4	0.50	0	15	0.13990
4	0.50	0	0	0.18887
4	0.50	-15	75	0.00531
4	0.50	-15	60	0.04291
4	0.50	-15	45	0.09100
4	0.50	-15	30	0.12415
4	0.50	-15	15	0.13456
4	0.50	-15	0	0.14880
4	0.50	-30	75	0.00869
4	0.50	-30	60	0.04520
4	0.50	-30	45	0.09885
4	0.50	-30	30	0.12533
4	0.50	-30	15	0.13627
4	0.50	-30	0	0.13931
4	0.50	-45	75	0.00932
4	0.50	-45	60	0.04217
4	0.50	-45	45	0.09818
4	0.50	-45	30	0.12387
4	0.50	-45	15	0.13447
4	0.50	-45	0	0.13362
4	0.50	-60	75	0.01077
4	0.50	-60	60	0.04020
4	0.50	-60	45	0.08253

4	0.50	-60	30	0.11495
4	0.50	-60	15	0.12954
4	0.50	-60	0	0.12953
4	0.50	-75	75	0.00850
4	0.50	-75	60	0.04634
4	0.50	-75	45	0.08630
4	0.50	-75	30	0.10990
4	0.50	-75	15	0.12081
4	0.50	-75	0	0.12494
4	0.50	-90	75	0.00519
4	0.50	-90	60	0.05142
4	0.50	-90	45	0.09100
4	0.50	-90	30	0.10755
4	0.50	-90	15	0.11392
4	0.50	-90	0	0.11601
4	1.00	90	75	0.13955
4	1.00	90	60	0.22296
4	1.00	90	45	0.26757
4	1.00	90	30	0.32060
4	1.00	90	15	0.34558
4	1.00	90	0	0.35602
4	1.00	75	75	0.16120
4	1.00	75	60	0.23030
4	1.00	75	45	0.30459
4	1.00	75	30	0.32856
4	1.00	75	15	0.35031
4	1.00	75	0	0.35853
4	1.00	60	75	0.14273
4	1.00	60	60	0.29574
4	1.00	60	45	0.34743
4	1.00	60	30	0.35894
4	1.00	60	15	0.37239
4	1.00	60	0	0.36435
4	1.00	45	75	0.10926
4	1.00	45	60	0.26303
4	1.00	45	45	0.39620

4	1.00	45	30	0.41943
4	1.00	45	15	0.38730
4	1.00	45	0	0.37690
4	1.00	30	75	0.06948
4	1.00	30	60	0.23709
4	1.00	30	45	0.34872
4	1.00	30	30	0.46441
4	1.00	30	15	0.46032
4	1.00	30	0	0.40332
4	1.00	15	75	0.07343
4	1.00	15	60	0.21743
4	1.00	15	45	0.32477
4	1.00	15	30	0.43079
4	1.00	15	15	0.49943
4	1.00	15	0	0.46440
4	1.00	0	75	0.06342
4	1.00	0	60	0.19610
4	1.00	0	45	0.28365
4	1.00	0	30	0.37680
4	1.00	0	15	0.46929
4	1.00	0	0	0.51507
4	1.00	-15	75	0.05885
4	1.00	-15	60	0.18744
4	1.00	-15	45	0.26260
4	1.00	-15	30	0.35006
4	1.00	-15	15	0.40649
4	1.00	-15	0	0.47372
4	1.00	-30	75	0.07286
4	1.00	-30	60	0.20336
4	1.00	-30	45	0.25636
4	1.00	-30	30	0.32212
4	1.00	-30	15	0.38059
4	1.00	-30	0	0.40345
4	1.00	-45	75	0.07352
4	1.00	-45	60	0.23152
4	1.00	-45	45	0.26765

4	1.00	-45	30	0.30764
4	1.00	-45	15	0.35881
4	1.00	-45	0	0.37795
4	1.00	-60	75	0.06668
4	1.00	-60	60	0.21738
4	1.00	-60	45	0.26298
4	1.00	-60	30	0.30995
4	1.00	-60	15	0.34555
4	1.00	-60	0	0.36357
4	1.00	-75	75	0.09782
4	1.00	-75	60	0.22230
4	1.00	-75	45	0.26473
4	1.00	-75	30	0.30932
4	1.00	-75	15	0.34954
4	1.00	-75	0	0.36056
4	1.00	-90	75	0.13955
4	1.00	-90	60	0.22296
4	1.00	-90	45	0.26757
4	1.00	-90	30	0.32060
4	1.00	-90	15	0.34558
4	1.00	-90	0	0.35602
4	1.25	90	75	0.19908
4	1.25	90	60	0.29460
4	1.25	90	45	0.39495
4	1.25	90	30	0.43447
4	1.25	90	15	0.45945
4	1.25	90	0	0.45403
4	1.25	75	75	0.20575
4	1.25	75	60	0.34951
4	1.25	75	45	0.40858
4	1.25	75	30	0.44225
4	1.25	75	15	0.46395
4	1.25	75	0	0.47950
4	1.25	60	75	0.20407
4	1.25	60	60	0.36664
4	1.25	60	45	0.45249

4	1.25	60	30	0.47828
4	1.25	60	15	0.48146
4	1.25	60	0	0.47774
4	1.25	45	75	0.16823
4	1.25	45	60	0.38363
4	1.25	45	45	0.49544
4	1.25	45	30	0.54490
4	1.25	45	15	0.52500
4	1.25	45	0	0.49878
4	1.25	30	75	0.11090
4	1.25	30	60	0.33207
4	1.25	30	45	0.47794
4	1.25	30	30	0.58341
4	1.25	30	15	0.62548
4	1.25	30	0	0.53585
4	1.25	15	75	0.09714
4	1.25	15	60	0.27554
4	1.25	15	45	0.43197
4	1.25	15	30	0.55351
4	1.25	15	15	0.62857
4	1.25	15	0	0.63356
4	1.25	0	75	0.10015
4	1.25	0	60	0.26889
4	1.25	0	45	0.40005
4	1.25	0	30	0.50655
4	1.25	0	15	0.61840
4	1.25	0	0	0.64251
4	1.25	-15	75	0.09600
4	1.25	-15	60	0.25753
4	1.25	-15	45	0.37397
4	1.25	-15	30	0.45302
4	1.25	-15	15	0.52821
4	1.25	-15	0	0.62148
4	1.25	-30	75	0.08671
4	1.25	-30	60	0.26697
4	1.25	-30	45	0.36259

4	1.25	-30	30	0.43712
4	1.25	-30	15	0.49487
4	1.25	-30	0	0.54142
4	1.25	-45	75	0.08615
4	1.25	-45	60	0.28621
4	1.25	-45	45	0.34952
4	1.25	-45	30	0.42309
4	1.25	-45	15	0.45928
4	1.25	-45	0	0.49486
4	1.25	-60	75	0.10805
4	1.25	-60	60	0.26377
4	1.25	-60	45	0.35767
4	1.25	-60	30	0.42059
4	1.25	-60	15	0.45276
4	1.25	-60	0	0.47858
4	1.25	-75	75	0.16815
4	1.25	-75	60	0.27739
4	1.25	-75	45	0.37314
4	1.25	-75	30	0.42343
4	1.25	-75	15	0.45329
4	1.25	-75	0	0.47583
4	1.25	-90	75	0.19908
4	1.25	-90	60	0.29460
4	1.25	-90	45	0.39495
4	1.25	-90	30	0.43447
4	1.25	-90	15	0.45945
4	1.25	-90	0	0.45403
4	1.50	90	75	0.21983
4	1.50	90	60	0.39095
4	1.50	90	45	0.46517
4	1.50	90	30	0.52555
4	1.50	90	15	0.56189
4	1.50	90	0	0.58251
4	1.50	75	75	0.22244
4	1.50	75	60	0.40157
4	1.50	75	45	0.49415

4	1.50	75	30	0.55413
4	1.50	75	15	0.58240
4	1.50	75	0	0.58575
4	1.50	60	75	0.24120
4	1.50	60	60	0.45146
4	1.50	60	45	0.54897
4	1.50	60	30	0.58136
4	1.50	60	15	0.58850
4	1.50	60	0	0.59357
4	1.50	45	75	0.21805
4	1.50	45	60	0.43815
4	1.50	45	45	0.58909
4	1.50	45	30	0.66183
4	1.50	45	15	0.64101
4	1.50	45	0	0.61382
4	1.50	30	75	0.16336
4	1.50	30	60	0.43263
4	1.50	30	45	0.57709
4	1.50	30	30	0.67824
4	1.50	30	15	0.72178
4	1.50	30	0	0.67868
4	1.50	15	75	0.11212
4	1.50	15	60	0.36464
4	1.50	15	45	0.54165
4	1.50	15	30	0.66962
4	1.50	15	15	0.75388
4	1.50	15	0	0.76062
4	1.50	0	75	0.10933
4	1.50	0	60	0.32430
4	1.50	0	45	0.48852
4	1.50	0	30	0.62702
4	1.50	0	15	0.72083
4	1.50	0	0	0.76324
4	1.50	-15	75	0.09526
4	1.50	-15	60	0.31179
4	1.50	-15	45	0.44728

4	1.50	-15	30	0.57187
4	1.50	-15	15	0.66084
4	1.50	-15	0	0.75219
4	1.50	-30	75	0.07710
4	1.50	-30	60	0.32100
4	1.50	-30	45	0.45805
4	1.50	-30	30	0.54668
4	1.50	-30	15	0.61294
4	1.50	-30	0	0.66837
4	1.50	-45	75	0.10108
4	1.50	-45	60	0.32037
4	1.50	-45	45	0.45159
4	1.50	-45	30	0.52159
4	1.50	-45	15	0.58858
4	1.50	-45	0	0.61238
4	1.50	-60	75	0.16081
4	1.50	-60	60	0.33957
4	1.50	-60	45	0.43872
4	1.50	-60	30	0.50469
4	1.50	-60	15	0.56913
4	1.50	-60	0	0.59555
4	1.50	-75	75	0.22072
4	1.50	-75	60	0.35454
4	1.50	-75	45	0.46662
4	1.50	-75	30	0.51306
4	1.50	-75	15	0.56629
4	1.50	-75	0	0.58573
4	1.50	-90	75	0.21983
4	1.50	-90	60	0.39095
4	1.50	-90	45	0.46517
4	1.50	-90	30	0.52555
4	1.50	-90	15	0.56189
4	1.50	-90	0	0.58251
4	1.81	90	75	0.25409
4	1.81	90	60	0.46432
4	1.81	90	45	0.58010

4	1.81	90	30	0.65940
4	1.81	90	15	0.71745
4	1.81	90	0	0.75207
4	1.81	75	75	0.28974
4	1.81	75	60	0.51397
4	1.81	75	45	0.60970
4	1.81	75	30	0.66622
4	1.81	75	15	0.69577
4	1.81	75	0	0.73958
4	1.81	60	75	0.29694
4	1.81	60	60	0.54573
4	1.81	60	45	0.66422
4	1.81	60	30	0.72915
4	1.81	60	15	0.74280
4	1.81	60	0	0.73669
4	1.81	45	75	0.26479
4	1.81	45	60	0.52300
4	1.81	45	45	0.69254
4	1.81	45	30	0.78544
4	1.81	45	15	0.78217
4	1.81	45	0	0.78560
4	1.81	30	75	0.18586
4	1.81	30	60	0.52632
4	1.81	30	45	0.68397
4	1.81	30	30	0.79988
4	1.81	30	15	0.87511
4	1.81	30	0	0.82649
4	1.81	15	75	0.15767
4	1.81	15	60	0.47478
4	1.81	15	45	0.66016
4	1.81	15	30	0.80771
4	1.81	15	15	0.87437
4	1.81	15	0	0.89461
4	1.81	0	75	0.11384
4	1.81	0	60	0.43498
4	1.81	0	45	0.63278

4	1.81	0	30	0.75773
4	1.81	0	15	0.87267
4	1.81	0	0	0.89054
4	1.81	-15	75	0.08929
4	1.81	-15	60	0.40596
4	1.81	-15	45	0.56594
4	1.81	-15	30	0.70507
4	1.81	-15	15	0.82021
4	1.81	-15	0	0.89660
4	1.81	-30	75	0.08489
4	1.81	-30	60	0.39735
4	1.81	-30	45	0.54514
4	1.81	-30	30	0.68126
4	1.81	-30	15	0.77588
4	1.81	-30	0	0.82928
4	1.81	-45	75	0.12557
4	1.81	-45	60	0.41443
4	1.81	-45	45	0.54920
4	1.81	-45	30	0.65401
4	1.81	-45	15	0.72839
4	1.81	-45	0	0.78583
4	1.81	-60	75	0.22289
4	1.81	-60	60	0.41784
4	1.81	-60	45	0.54199
4	1.81	-60	30	0.64700
4	1.81	-60	15	0.70397
4	1.81	-60	0	0.74143
4	1.81	-75	75	0.25746
4	1.81	-75	60	0.42519
4	1.81	-75	45	0.54201
4	1.81	-75	30	0.65092
4	1.81	-75	15	0.73275
4	1.81	-75	0	0.73692
4	1.81	-90	75	0.25409
4	1.81	-90	60	0.46432
4	1.81	-90	45	0.58010

4	1.81	-90	30	0.65940
4	1.81	-90	15	0.71745
4	1.81	-90	0	0.75207
4	2.15	90	75	0.30280
4	2.15	90	60	0.54222
4	2.15	90	45	0.72227
4	2.15	90	30	0.83957
4	2.15	90	15	0.92741
4	2.15	90	0	0.97590
4	2.15	75	75	0.38838
4	2.15	75	60	0.61711
4	2.15	75	45	0.73982
4	2.15	75	30	0.84202
4	2.15	75	15	0.90763
4	2.15	75	0	0.97645
4	2.15	60	75	0.36083
4	2.15	60	60	0.65209
4	2.15	60	45	0.79759
4	2.15	60	30	0.88845
4	2.15	60	15	0.93454
4	2.15	60	0	0.92991
4	2.15	45	75	0.31934
4	2.15	45	60	0.63776
4	2.15	45	45	0.80265
4	2.15	45	30	0.94853
4	2.15	45	15	0.99809
4	2.15	45	0	0.97753
4	2.15	30	75	0.23890
4	2.15	30	60	0.65662
4	2.15	30	45	0.80903
4	2.15	30	30	0.94346
4	2.15	30	15	1.04654
4	2.15	30	0	1.04027
4	2.15	15	75	0.19064
4	2.15	15	60	0.59692
4	2.15	15	45	0.82183

4	2.15	15	30	0.95881
4	2.15	15	15	1.02985
4	2.15	15	0	1.10300
4	2.15	0	75	0.13629
4	2.15	0	60	0.53413
4	2.15	0	45	0.77948
4	2.15	0	30	0.95420
4	2.15	0	15	1.05718
4	2.15	0	0	1.05821
4	2.15	-15	75	0.11549
4	2.15	-15	60	0.50675
4	2.15	-15	45	0.72327
4	2.15	-15	30	0.89077
4	2.15	-15	15	1.02036
4	2.15	-15	0	1.09289
4	2.15	-30	75	0.10521
4	2.15	-30	60	0.49097
4	2.15	-30	45	0.65788
4	2.15	-30	30	0.84327
4	2.15	-30	15	0.98048
4	2.15	-30	0	1.04720
4	2.15	-45	75	0.13836
4	2.15	-45	60	0.51739
4	2.15	-45	45	0.64115
4	2.15	-45	30	0.81578
4	2.15	-45	15	0.92728
4	2.15	-45	0	0.97249
4	2.15	-60	75	0.23569
4	2.15	-60	60	0.49500
4	2.15	-60	45	0.66606
4	2.15	-60	30	0.83963
4	2.15	-60	15	0.89990
4	2.15	-60	0	0.93886
4	2.15	-75	75	0.33149
4	2.15	-75	60	0.49777
4	2.15	-75	45	0.68852

4	2.15	-75	30	0.85226
4	2.15	-75	15	0.97051
4	2.15	-75	0	0.97138
4	2.15	-90	75	0.30280
4	2.15	-90	60	0.54222
4	2.15	-90	45	0.72227
4	2.15	-90	30	0.83957
4	2.15	-90	15	0.92741
4	2.15	-90	0	0.97590

Table D.5. SIDI Values of verification cases used for ANN.

LD	Velocity (km/s)	α (degrees)	ϕ (degrees)	DI
Sphere	1.704	0.00	61.33	0.44545
Sphere	1.811	0.00	61.68	0.46886
Sphere	1.799	0.00	74.95	0.26852
Sphere	1.562	0.00	56.38	0.45846
Sphere	1.93	0.00	78.24	0.16165
1	2.025	88.24	79.81	0.14100
1	1.981	42.99	73.09	0.32829
1	1.644	2.16	51.33	0.50350
1	1.786	13.25	58.43	0.49669
1	1.647	0.35	52.46	0.49557
1	1.703	30.37	64.02	0.40469
1	1.627	4.28	51.49	0.50160
1	1.651	15.43	60.92	0.44369
1	1.65	2.91	51.14	0.50699
2	1.719	33.01	74.85	0.21985
2	1.76	18.81	57.09	0.50797
2	1.752	-2.71	51.34	0.53928
2	1.703	10.84	53.15	0.50291
2	1.714	13.35	54.73	0.51324
2	2.053	88.21	81.33	0.15965
2	1.76	2.35	53.55	0.54085
2	1.755	-2.35	52.88	0.52875
2	1.875	11.98	58.66	0.53071
4	2.039	88.24	77.11	0.28428
4	1.819	40.30	62.53	0.51994
4	1.952	-0.83	58.24	0.51571
4	1.908	24.18	57.4	0.58724
4	1.943	13.04	62.61	0.47244
4	2.122	38.80	71.45	0.40289
4	1.943	14.66	68.71	0.31287
4	1.906	-0.48	57.73	0.50091